

The Gravity Collective: A Search for the Electromagnetic Counterpart to the Neutron Star-Black Hole Merger GW190814

CHARLES D. KILPATRICK,¹ DAVID A. COULTER,² IAIR ARCAVI,^{3,4} THOMAS G. BRINK,⁵ GEORGIOS DIMITRIADIS,² ALEXEI V. FILIPPENKO,^{5,6} RYAN J. FOLEY,² D. ANDREW HOWELL,^{7,8} DAVID O. JONES,² MARTIN MAKLER,^{9,10} ANTHONY L. PIRO,¹¹ CÉSAR ROJAS-BRAVO,² DAVID J. SAND,¹² JONATHAN J. SWIFT,¹³ DOUGLAS TUCKER,¹⁴ WEIKANG ZHENG,⁵ SAHAR S. ALLAM,¹⁴ JAMES T. ANNIS,¹⁴ JUANITA ANTILEN,¹⁵ TRISTAN G. BACHMANN,¹⁶ JOSHUA S. BLOOM,¹⁷ CLECIO R. BOM,^{10,18} K. AZALEE BOSTROEM,¹⁹ DILLON BROUT,²⁰ JAMISON BURKE,^{7,8} ROBERT E. BUTLER,²¹ MELISSA BUTNER,²² ABDO CAMPILLAY,²³ KAROLI E. CLEVER,² CHRISTOPHER J. CONSELICE,²⁴ JEFF COOKE,^{25,26} KRISTEN C. DAGE,^{27,28,29} REINALDO R. DE CARVALHO,³⁰ THOMAS DE JAEGER,^{5,31} SHANTANU DESAI,³² ALYSSA GARCIA,³³ JUAN GARCIA-BELLIDO,³⁴ MANDEEP S. S. GILL,³⁵ NACHIKET GIRISH,⁵ NA'AMA HALLAKOUN,^{36,3} KENNETH HERNER,¹⁴ DAICHI HIRAMATSU,^{7,8} DANIEL E. HOLZ,³⁷ GRACE HUBER,¹³ ADAM M. KAWASH,²⁹ CURTIS MCCULLY,^{7,8} SOPHIA A. MEDALLON,² BRIAN D. METZGER,^{38,39} SHAUNAK MODAK,⁵ ROBERT MORGAN,⁴⁰ RICARDO R. MUÑOZ,¹⁵ NAHIR MUÑOZ-ELGUETA,⁴¹ YUKEI S. MURAKAMI,⁵ FELIPE OLIVARES E.,⁴² ANTONELLA PALMESE,¹⁴ KISHORE PATRA,⁵ MARIA E. S. PEREIRA,³³ THALLIS L. PESSI,^{43,44} J. PINEDA-GARCIA,⁴⁵ JONATHAN QUIROLA-VÁSQUEZ,^{46,47} ENRICO RAMIREZ-RUIZ,² SANDRO BARBOZA REMBOLD,⁴³ ARMIN REST,^{48,49} ÓSMAR RODRÍGUEZ,³ LUIDHY SANTANA-SILVA,³⁰ NORA F. SHERMAN,³³ MATTHEW R. SIEBERT,² CARLI SMITH,² J. ALLYN SMITH,⁵⁰ MARCELLE SOARES-SANTOS,³³ HOLLAND STACEY,¹³ BENJAMIN E. STAHL,⁵ JAY STRADER,²⁹ ERIKA STRASBURGER,⁵ JAMES SUNSERI,⁵ SAMAPORN TINYANONT,² BRAD E. TUCKER,^{51,52,53} NATALIE ULLOA,²³ STEFANO VALENTI,¹⁹ SERGIY VASYLYEV,⁵ MATTHEW P. WIESNER,⁵⁴ AND KETO D. ZHANG⁵

¹Center for Interdisciplinary Exploration and Research in Astrophysics (CIERA), Northwestern University, Evanston, IL 60208, USA

²Department of Astronomy and Astrophysics, University of California, Santa Cruz, CA 95064, USA

³The School of Physics and Astronomy, Tel Aviv University, Tel Aviv 69978, Israel

⁴CIFAR Azrieli Global Scholars program, CIFAR, Toronto, Canada

⁵Department of Astronomy, University of California, Berkeley, CA 94720-3411, USA

⁶Miller Institute for Basic Research in Science, University of California, Berkeley, CA 94720, USA

⁷Department of Physics, University of California, Santa Barbara, CA 93106-9530, USA

⁸Las Cumbres Observatory, 6740 Cortona Dr, Suite 102, Goleta, CA 93117-5575, USA

⁹International Center for Advanced Studies & Instituto de Ciencias Físicas, ECyT-UNSAM & CONICET, 1650, Buenos Aires, Argentina

¹⁰Centro Brasileiro de Pesquisas Físicas, Rua Dr. Xavier Sigaud 150, CEP 22290-180, Rio de Janeiro, RJ, Brazil

¹¹The Observatories of the Carnegie Institution for Science, 813 Santa Barbara St., Pasadena, CA 91101, USA

¹²Steward Observatory, University of Arizona, 933 North Cherry Avenue, Tucson, AZ 85721-0065, USA

¹³Thacher Observatory, Thacher School, 5025 Thacher Rd. Ojai, CA 93023, USA

¹⁴Fermi National Accelerator Laboratory, P. O. Box 500, Batavia, IL 60510, USA

¹⁵Departamento de Astronomía, Universidad de Chile, Camino El Observatorio 1515, Las Condes, Santiago, Chile

¹⁶Department of Astronomy and Astrophysics, University of Chicago, Chicago, IL 60637, USA

¹⁷Lawrence Berkeley National Laboratory, 1 Cyclotron Road, MS 50B-4206, Berkeley, CA 94720-3411, USA

¹⁸Centro Federal de Educação Tecnológica Celso Suckow da Fonseca, Rodovia Mário Covas, lote J2, quadra J, CEP 23810-000, Itaguaí, RJ, Brazil

¹⁹Department of Physics and Astronomy, University of California, Davis, CA, 95616

²⁰Center for Astrophysics, Harvard & Smithsonian, 60 Garden St, Cambridge, MA 02138, USA*

²¹Department of Astronomy, Indiana University, 727 E. Third St., Bloomington, IN 47405

²²Department of Physics and Astronomy, East Tennessee State University, Johnson City, TN 37614, USA

²³Carnegie Observatories, Las Campanas Observatory, Casilla 601, La Serena, Chile

²⁴Jodrell Bank Centre for Astrophysics, University of Manchester, Oxford Road, Manchester; UK

²⁵Centre for Astrophysics and Supercomputing, Swinburne University of Technology, PO Box 218, H29, Hawthorn, VIC, 3122, Australia

²⁶Australian Research Council Centre of Excellence for Gravitational Wave Discovery, Swinburne University of Technology, Hawthorn, VIC, 3122, Australia

²⁷Department of Physics, McGill University, 3600 University Street, Montréal, QC H3A 2T8, Canada

²⁸McGill Space Institute, McGill University, 3550 University Street, Montréal, QC H3A 2A7, Canada

²⁹Center for Data Intensive and Time Domain Astronomy, Department of Physics and Astronomy, Michigan State University, East Lansing, MI 48824, USA

³⁰NAT-Universidade Cruzeiro do Sul / Universidade Cidade de São Paulo, Rua Galvão Bueno, 868, 01506-000, São Paulo, SP, Brazil

³¹Institute for Astronomy, University of Hawaii, 2680 Woodlawn Drive, Honolulu, HI 96822, USA

³²Indian Institute of Technology, Hyderabad, Kandi Telangana 502285 India

³³Department of Physics, University of Michigan, Ann Arbor, MI 48109, USA

³⁴Instituto de Física Teórica UAM/CSIC, Universidad Autónoma de Madrid, 28049 Madrid, Spain

³⁵Kavli Institute for Particle Astrophysics & Cosmology, P. O. Box 2450, Stanford University, Stanford, CA 94305, USA

³⁶Department of Particle Physics and Astrophysics, Weizmann Institute of Science, Rehovot, 7610001, Israel

³⁷*Enrico Fermi Institute, Department of Physics, Department of Astronomy and Astrophysics, and Kavli Institute for Cosmological Physics, University of Chicago, Chicago, IL 60637, USA*

³⁸*Columbia Astrophysics Laboratory, Columbia University, New York, NY 10027, USA*

³⁹*Center for Computational Astrophysics, Flatiron Institute, 162 W. 5th Avenue, New York, NY 10011, USA*

⁴⁰*Physics Department, University of Wisconsin-Madison, Madison, WI 53706, USA*

⁴¹*Max-Planck-Institut für Astrophysik, Karl-Schwarzschild-Str 1, D-85748 Garching bei München, Germany*

⁴²*Instituto de Astronomía y Ciencias Planetarias, Universidad de Atacama, Copayapu 485, Copiapó, Chile*

⁴³*Departamento de Física, Centro de Ciências Naturais e Exatas, Universidade Federal de Santa Maria, 97105-900, Santa Maria, RS, Brazil*

⁴⁴*Núcleo de Astronomía, Universidad Diego Portales, Av. Ejército 441, Santiago, Chile*

⁴⁵*Departamento de Ciencias Físicas, Universidad Andres Bello, Avda. Republica 252, Santiago, Chile*

⁴⁶*Instituto de Astrofísica, Pontificia Universidad Católica de Chile, Casilla 306, Santiago 22, Chile*

⁴⁷*Millennium Institute of Astrophysics (MAS), Nuncio Monseñor Sótero Sanz 100, Providencia, Santiago, Chile*

⁴⁸*Department of Physics and Astronomy, Johns Hopkins University, 3400 North Charles Street, Baltimore, MD 21218, USA*

⁴⁹*Space Telescope Science Institute, 3700 San Martin Drive, Baltimore, MD 21218, USA*

⁵⁰*Austin Peay State University, Dept. Physics, Engineering and Astronomy, P.O. Box 4608, Clarksville, TN 37044, USA*

⁵¹*Mt Stromlo Observatory, The Research School of Astronomy and Astrophysics, Australian National University, ACT 2601, Australia*

⁵²*National Centre for the Public Awareness of Science, Australian National University, Canberra, ACT 2611, Australia*

⁵³*The ARC Centre of Excellence for All-Sky Astrophysics in 3 Dimensions (ASTRO 3D), Australia*

⁵⁴*Benedictine University, Department of Physics, 5700 College Road, Lisle, IL, 60532, USA*

ABSTRACT

We present optical follow-up imaging obtained with the Katzman Automatic Imaging Telescope, Las Cumbres Observatory Global Telescope Network, Nickel Telescope, Swope Telescope, and Thacher Telescope of the LIGO/Virgo gravitational wave (GW) signal from the neutron star–black hole (NSBH) merger GW190814. We searched the GW190814 localization region (19 deg² for the 90th percentile best localization), covering a total of 51 deg² and 94.6% of the two-dimensional localization region. Analyzing the properties of 189 transients that we consider as candidate counterparts to the NSBH merger, including their localizations, discovery times from merger, optical spectra, likely host-galaxy redshifts, and photometric evolution, we conclude that none of these objects are likely to be associated with GW190814. Based on this finding, we consider the likely optical properties of an electromagnetic counterpart to GW190814, including possible kilonovae and short gamma-ray burst afterglows. Using the joint limits from our follow-up imaging, we conclude that a counterpart with an r -band decline rate of 0.68 mag day^{−1}, similar to the kilonova AT 2017gfo, could peak at an absolute magnitude of at most -17.8 mag (50% confidence). Our data are not constraining for “red” kilonovae and rule out “blue” kilonovae with $M > 0.5 M_{\odot}$ (30% confidence). We strongly rule out all known types of short gamma-ray burst afterglows with viewing angles $< 17^{\circ}$ assuming an initial jet opening angle of $\sim 5.2^{\circ}$ and explosion energies and circumburst densities similar to afterglows explored in the literature. Finally, we explore the possibility that GW190814 merged in the disk of an active galactic nucleus, of which we find four in the localization region, but we do not find any candidate counterparts among these sources.

Keywords: gravitational waves — merger: black holes, neutron stars

1. INTRODUCTION

Neutron star (NS) and black hole (BH) mergers are among the strongest gravitational wave (GW) sources from 10 to 10,000 Hz (Press & Thorne 1972; Thorne 1997) and the primary astrophysical sources detected by the Laser Interferometer Gravitational Wave Observatory (LIGO) and Virgo collaboration (LVC; LIGO Scientific Collaboration et al. 2015; Abbott et al. 2017a). Although electromagnetic (EM) follow-up observations of these events began with the first detec-

tion of a binary black hole (BBH) merger by LIGO (Abbott et al. 2016a), it was not until the discovery of the binary neutron star merger (BNS) GW170817 that EM and GW emission was observed from the same source (Abbott et al. 2017b). GW170817 was accompanied by a prompt, short gamma-ray burst viewed off-axis (sGRB; Abbott et al. 2017c; Savchenko et al. 2017)¹ and later a kilonova called AT 2017gfo² discovered at optical wavelengths (Coulter et al.

¹ Although Kasliwal et al. (2017) argue this event was much weaker than sGRBs viewed at high redshift and likely the result of a shock breakout.

² Also called SSS17a, DLT17ck, and PS17egl.

2017). Follow-up observations of this event spanned the EM spectrum, and combined with the GW data these observations enabled unique insight into the nature of its ejecta (e.g., Arcavi et al. 2017a; Cowperthwaite et al. 2017; Drout et al. 2017; Kasliwal et al. 2017; Kilpatrick et al. 2017; Smartt et al. 2017), the engines that power sGRBs (Abbott et al. 2017c; Savchenko et al. 2017; Fong et al. 2017; Murguia-Berthier et al. 2021), and the NS equation of state (Abbott et al. 2018a; Radice et al. 2018).

The precise localization of GW170817 required coordination between the LVC and optical search teams (Abbott et al. 2017d; Coulter et al. 2017). Critically, all three LVC detectors contributed to the localization of GW170817 and the distance to this event was only ~ 40 Mpc from the initial LVC analysis (Abbott et al. 2017d). This enabled a search of a relatively small volume of space that targeted galaxies in highly complete catalogs. Indeed, the greatest limiting factors in the speed with which AT 2017gfo was identified were the timescale required to generate accurate localization maps and the positioning of telescopes across the globe (Abbott et al. 2017b).

The same strategy has been less practical for all of the high-confidence NS mergers reported during LVC Observing Run 3 (O3; including GW190425, S190426c, GW190814, S190910d, S190910h, S190923y, S190930t, S191205ah, S191213g, and S200213t in Andreoni et al. 2020, 2019a; Coughlin et al. 2019; Dobie et al. 2019a; Goldstein et al. 2019c; Gomez et al. 2019b; Hosseinzadeh et al. 2019; Lundquist et al. 2019; Ackley et al. 2020; Antier et al. 2020; Coughlin et al. 2020a; Morgan et al. 2020; Paterson et al. 2020; Pozanenko et al. 2020; Thakur et al. 2020; Vieira et al. 2020; Watson et al. 2020; Alexander et al. 2021; de Wet et al. 2021). With greatly increased detector sensitivity and a higher rate of events detected at larger distances than GW170817, all LVC O3 events classified as NS mergers were less precisely localized than GW170817 with one exception. Given the rapid decline rates expected for EM counterparts (Roberts et al. 2011; Kasen et al. 2015), it is unlikely that a counterpart would be detected. This is true even in the most optimistic counterpart models (Andreoni et al. 2020; Goldstein et al. 2019c; Hosseinzadeh et al. 2019; Morgan et al. 2020; Thakur et al. 2020; Alexander et al. 2021; de Wet et al. 2021), but especially after folding in realistic assumptions about the physical properties of NS mergers implied by GW data as in the case of GW190425 (Foley et al. 2020). Although some observations rule out AT 2017gfo-like counterparts over a large fraction of the localization regions of O3 events (e.g., Coughlin et al. 2020a; Goldstein et al. 2019c; Morgan et al. 2020), the total ejecta mass, composition, and merger properties of most NS mergers remain almost entirely unconstrained.

The need for better constraints is most pressing for GW events from neutron star–black hole (NSBH) and black hole–black hole (BBH) mergers where no viable EM counterparts have been confirmed (whereas GW170817 is widely considered to be the result of a BNS merger; Abbott et al. 2017b; Kilpatrick et al. 2017). Unlike BNS mergers where disruption of both NS components and some ejecta are guaranteed (Li & Paczyński 1998; Shibata & Taniguchi 2006; Metzger et al. 2010; Roberts et al. 2011), in a NSBH merger it is possible that the NS will eject no mass before it is entirely accreted by the BH. This is because the NS must be tidally shredded before it reaches the innermost stable circular orbit to produce ejecta, and whether this happens depends on the total mass of the system, the mass ratio, spins, and the radius (and thus the equation of state) of the NS (Faber et al. 2006; Lee & Ramirez-Ruiz 2007; Ferrari et al. 2010). Thus, for each new NSBH, the LVC infers the probability that mass remains outside the merger based on numerical-relativity simulations (i.e., `HasRemnant` in LIGO Scientific Collaboration & Virgo Collaboration 2019a,b). Values reported by the LVC use an optimistic (stiff) equation of state, which maximizes the value of `HasRemnant` given constraints on the masses and spins of the merger components (Abbott et al. 2009). `HasRemnant` is often interpreted as the likelihood of seeing an EM counterpart similar to a kilonova or sGRB (Kasen et al. 2017; Troja et al. 2017). Beyond comparisons to relatively simple systems such as the GW170817 merger where ejecta are guaranteed, the validity of this estimate and the nature of EM emission from NSBH mergers have yet to be verified, and thus all `HasRemnant` estimates are subject to significant systematic uncertainties.

In the middle of O3 and roughly 2 yr after reporting GW170817, the LVC detected GW signal GW190814 on 14 Aug. 2019 at 21:11:16 UT (LIGO Scientific Collaboration & Virgo Collaboration 2019a,b; Abbott et al. 2020a). Detailed analysis indicated that this signal had high significance, implying a relatively close event with a low probability of a “false alarm” (with a rate of one per 10^{11} Hubble times that a spurious signal from correlated noise or detector “glitches” could produce GW190814; Singer & Price 2016). GW190814 was classified as a NSBH with high significance ($>99\%$; Abbott et al. 2020a). In the final analysis of the GW190814 strain, the best-fitting template to the GW strain signal being the merger of $2.59 \pm 0.08 M_{\odot}$ and $23.2_{-0.9}^{+1.0} M_{\odot}$ components at 235_{-45}^{+40} Mpc (Abbott et al. 2020a).

In addition to being the best-localized and one of the closest GW events to date, GW190814 had one of the most extreme mass ratios of all GW events detected during the LVC’s first three observing runs. However, this analysis assumes that $2.59 M_{\odot}$ NSs exist in nature, which may not be the case if the maximum-mass NS is below this threshold (Fattouev et al. 2020; Tan et al. 2020; Kanakis-Pegios et al. 2021;

Godzieba et al. 2021; Wu et al. 2021). The search for EM counterparts therefore provides unique insight into the nature of this threshold; detection of an EM counterpart from an NSBH merger with a massive secondary would imply that the maximum NS mass is at least as massive. Although analyses that classify GW190814 as a NSBH merger imply that the secondary is the most massive known NS, with significant implications for the compact binary population and their formation channels (Abbott et al. 2020b), it remains possible that GW190814 was a BBH system, incidentally making the secondary the least massive known BH.

The localization for GW190814 was rapidly refined to a localization region with size $\sim 38 \text{ deg}^2$ (90th percentile) on 14 Aug. 2019 and centered approximately at $\alpha = 24.6^\circ$, $\delta = -24.8^\circ$ (J2000), although the final localization map presented by Abbott et al. (2020a) had a 90th percentile area of 19 deg^2 (Figure 1). Initial estimates of the HasRemnant statistic by the LVC was $< 1\%$ (LIGO Scientific Collaboration & Virgo Collaboration 2019a), which is consistent with expectations that a $23.2 M_\odot + 2.59 M_\odot$ system would produce no ejecta even if the BH was maximally rotating. Significant EM follow-up observations of this event were triggered by several groups (Andreoni et al. 2020; Dobie et al. 2019a; Gomez et al. 2019b; Ackley et al. 2020; Vieira et al. 2020; Watson et al. 2020; Alexander et al. 2021; de Wet et al. 2021), which spanned gamma-ray through radio wavelengths and continued for > 250 days after merger. No prompt gamma-ray signature was detected despite coverage of the localization region by INTEGRAL, *Fermi*, and *Swift* (Molkov et al. 2019; Kocevski et al. 2019; Palmer et al. 2019), and observations at X-ray through radio wavelengths did not reveal any likely counterparts.

Here we present a joint analysis of the optical observations of the GW190814 localization region performed by the Gravity Collective, a collaboration consisting of follow-up efforts by the One-Meter Two-Hemisphere (1M2H) collaboration, the Las Cumbres Observatory network, and the Katzman Automatic Imaging Telescope (KAIT) and representing imaging obtained on fourteen 0.7–1 m telescopes across the globe. We describe our optical searches and follow-up observations of candidates, including optical photometry and spectroscopy, in Section 2. In Section 3, we discuss our criteria for classifying candidates and conclude that no optical transients discovered from any source are likely counterparts to GW190814. None of our searches found a viable EM counterpart to GW190814, and so in Section 4 we place limits on the physical nature of any EM counterpart to GW190814. We compare our limits to models of kilonova, sGRB, or rapidly fading optical emission, from which we determine that we can rule out red kilonovae with ejecta mass and velocity similar to those of AT 2017gfo at $4 \times 10^{-7}\%$ significance and blue kilonovae with ejecta mass $> 0.5 M_\odot$ (30% confidence). We

also rule out sGRB afterglows with viewing angles $< 17^\circ$ (assuming a jet opening angle of 5.2° as with GW170817 in Wu & MacFadyen 2018, 2019) and explosion energies and circumburst densities spanning the range presented by Fong et al. (2015). We conclude by discussing our overall search and follow-up strategy in Section 5 and the implications for discovering EM counterparts to GW events in future LVC Observing runs.

All magnitudes presented in this paper are given in the AB system (Oke & Gunn 1983). Milky Way extinction is derived along the corresponding lines of sight from Schlafly & Finkbeiner (2011).

2. OBSERVATIONS

1M2H coordinated follow-up observations between three 0.7–1 m telescopes in order to search for optical counterparts to GW190814. The goal of this search and those involving the Las Cumbres Network and KAIT was to localize an optical counterpart to the gravitational-wave event, which was known to resemble an NSBH merger (LIGO Scientific Collaboration & Virgo Collaboration 2019b). Based on NSBH merger models and their total ejecta masses (Faber et al. 2006; Ferrari et al. 2010; Rosswog et al. 2013), we inferred that likely counterparts would resemble a kilonova (likely redder than AT 2017gfo; e.g., see Metzger & Fernández 2014) or the afterglow from a sGRB. Based on the localization and luminosity distance to the event provided by the LVC and ultimately representing a volume of $\sim 39,000 \text{ Mpc}^3$ (Abbott et al. 2020a), our goal was therefore to localize a counterpart resembling one of these transients within the volume constrained by the event.

We prioritized 1M2H observations using the open-source code `teglon`³, which examines the LVC localization map and the GLADE galaxy catalog (Dálya et al. 2018) in order to optimally weight the priority of observing specific parts of the localization region over time. These observations were prioritized to maximize the likelihood of finding an EM counterpart under the assumption that it occurred in a galaxy in the LVC localization volume. We also prioritized follow-up observations of viable candidate counterparts with our imaging and spectroscopic resources as described below.

In addition, we coordinated observations with KAIT and 1 m telescopes in the Las Cumbres Network, all of which targeted galaxies (as in Arcavi et al. 2017b) in the localization region of GW190814. Finally, we observed eight galaxies and two counterparts in the localization region of GW190814 with Keck/MOSFIRE, although we were unable to obtain later follow-up imaging using the same instrument and filters. All observations are described below, and our follow-up

³ <https://github.com/davecouler/teglon>

images and candidate counterparts are shown relative to the final GW190814 localization region in [Figure 1](#).

2.1. Imaging Search and Follow-Up Observations

2.1.1. KAIT

The 0.76 m Katzman Automatic Imaging Telescope (KAIT; [Richmond et al. 1993](#); [Filippenko et al. 2001](#)) at Lick Observatory targeted galaxies in the localization region of GW190814 on 15 and 18 Aug. 2019, as described by [Vasylyev et al. \(2019a,b\)](#). Galaxies were selected from GLADE ([Dalya et al. 2018](#)) according to their *B*-band luminosity, with target priority reweighted by elevation at the time of observation. All observations were performed in a “Clear” filter. 161 galaxies were targeted on 15 Aug. 2019 with an additional 52 galaxies on 18 Aug. 2019. All 213 fields were reimaged from 24–25 Aug. 2019 to provide templates of the same fields for detailed analysis.

Following standard imaging and photometry procedures (e.g., [Ganeshalingam et al. 2010](#); [Zheng et al. 2017](#)), the images were calibrated and point-spread-function (PSF) photometry was performed using DAOPHOT ([Stetson 1987](#)) in IDL. The throughput of the KAIT “Clear” filter is known to be close to the *R* band ([Li et al. 2003](#)), so local AAVSO Photometric All-Sky Survey (APASS) standards ([Henden et al. 2015](#))⁴ were transformed to the Landolt *R* band ([Landolt 1992](#)) following [Jester et al. \(2005\)](#). Template images were then subtracted from the 15 and 18 Aug. epochs using a custom IDL-based image-subtraction pipeline for PSF convolution. Finally, the limiting magnitude was estimated in each subtracted image by examining the 3σ root-mean-square (RMS) noise within an aperture fixed to the size of the convolved PSF. These limits are provided in [Table 4](#).

2.1.2. Keck/MOSFIRE

We targeted 10 fields in a single epoch of target-of-opportunity imaging with the Multi-Object Spectrometer for Infra-Red Exploration (MOSFIRE; [McLean et al. 2012](#)) on the Keck-I 10 m telescope on 15 Aug. 2019 as shown in [Table 4](#) and described by [Brown et al. \(2019\)](#). Two of these fields targeted candidates within the highest probability regions of GW190814; we observed AT 2019nmd and AT 2019nme (discovered by DESGW; [Soares-Santos et al. 2019a](#); [Morgan et al. 2020](#)), both of which were undetected and later ruled out as likely minor planets (see [Table 5](#)). The remaining eight fields targeted galaxies within the inner 50th percentile localization region of GW190814. The final image mosaics consist of $6.1' \times 6.1'$ frames centered on the coordinates reported in [Table 4](#). All observations consisted of an eight-point dither pattern with 30 s of cumulative exposure time in the *J* band.

We reduced these data following standard procedures in the MOSFIRE data-reduction pipeline⁵ (e.g., [Barro et al. 2014](#)). The images were corrected for dark current and flat-fielded using calibration exposures obtained in the same instrumental configuration. We then obtained photometry of sources in each image using DoPHOT and compared these sources to their *J*-band magnitudes in the 2MASS catalog ([Cutri et al. 2003](#)) to calibrate our images. Comparing to pre-merger 2MASS images of the same fields, we did not detect any transient sources in any of the Keck/MOSFIRE images (as reported by [Brown et al. 2019](#)).

The limiting magnitudes reported in [Table 4](#) represent the average RMS sky background inside a single PSF aperture, so they should not be interpreted as the limiting magnitude for any transient sources in our images. As we were unable to obtain template exposures for these fields, we do not include the Keck/MOSFIRE limits in the analysis of our constraints on EM counterparts to GW190814.

2.1.3. Las Cumbres

We also observed the localization region of GW190814 with the Las Cumbres Observatory global network ([Brown et al. 2013](#)), specifically with its 1 m telescopes at the McDonald Observatory in Texas, the Cerro Tololo Interamerican Observatory in Chile, the Siding Spring Observatory in Australia, and the South African Astronomical Observatory. Our pointings were selected based on the galaxy-targeted search and prioritization strategy outlined by [Arcavi et al. \(2017b\)](#). We obtained 300 s exposures in the *g* and *i* bands using the Sinistro cameras mounted on these telescopes, which have a $26' \times 26'$ field of view. Our initial results were reported by [Hiramatsu et al. \(2019b\)](#). Image processing was performed by the Las Cumbres Observatory BANZAI pipeline ([McCully et al. 2018](#)) and limiting magnitudes were extracted using LCOGTSNpipe ([Valenti et al. 2016](#)). We used SDSS, PS1, or DECam reference images in the appropriate bands to perform image subtraction using PyZOGY ([Zackay et al. 2016](#); [Guevel & Hosseinzadeh 2017](#)). The limiting magnitudes were calculated by first estimating the Poisson noise due to the sky using the median absolute deviation of the entire image. Combining the Poisson and read noise, we estimate the $3\text{-}\sigma$ limiting magnitude by inverting the standard signal-to-noise equation. The observations are summarized in [Table 4](#).

2.1.4. Nickel

We used the Nickel 1 m telescope at Lick Observatory, Mt. Hamilton, California in conjunction with the Direct 2k \times 2k camera ($6.8' \times 6.8'$) to observe galaxies in the localization region of GW190814 on 14–19, 22, 27, and 30 Aug. 2019,

⁴ <https://www.aavso.org/apass>

⁵ <https://keck-datareductionpipelines.github.io/MosfireDRP/>

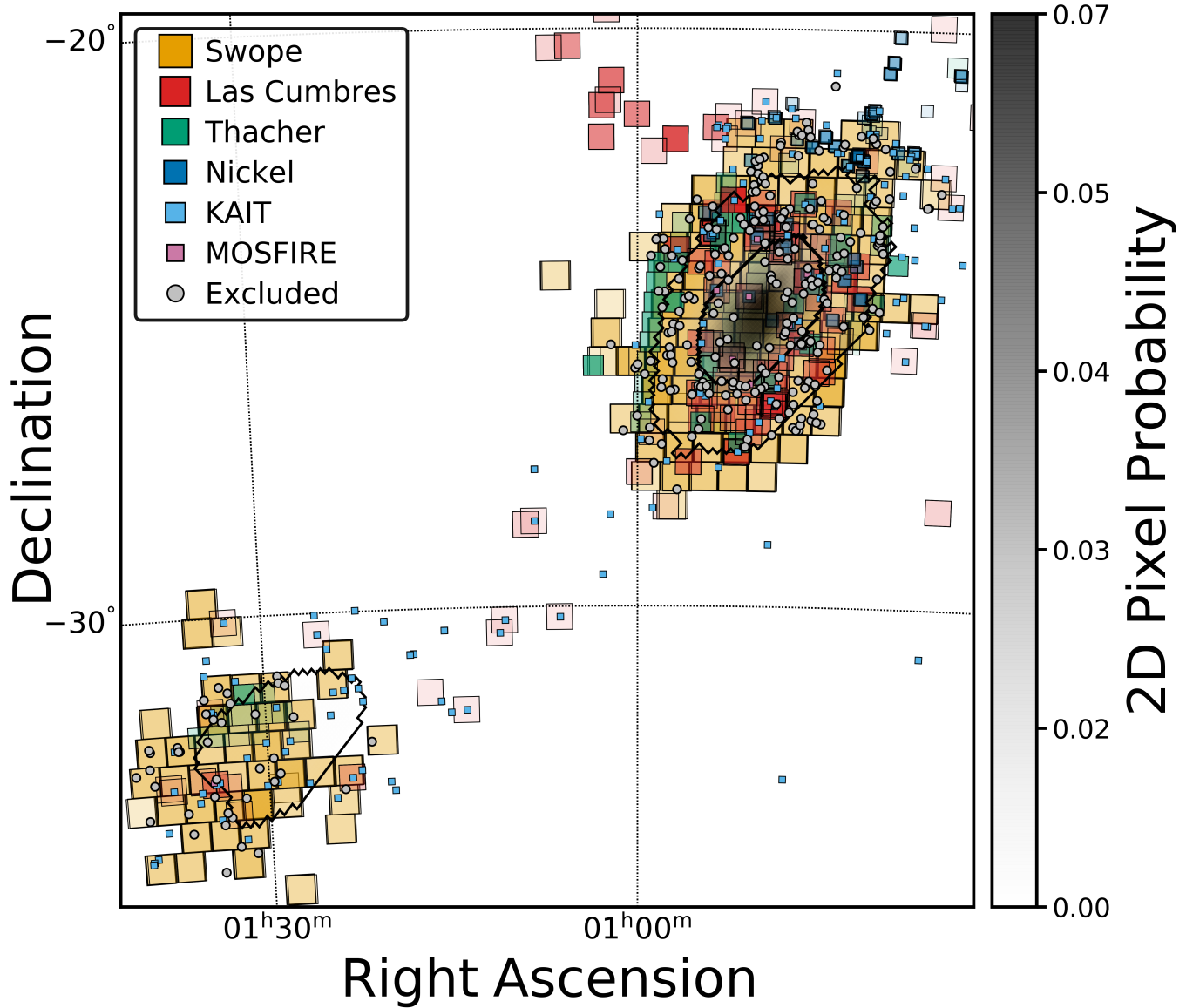


Figure 1. The LVC localization region of GW190814 with our follow-up observations from KAIT (light blue), Las Cumbres (red), Nickel (dark blue), Swope (orange), and Thacher (green) overplotted. We also show candidate counterparts imaged near the GW190814 localization region and excluded candidates (gray).

as well as on 3 and 11 Sep. 2019 (Table 4). These images were all obtained in the r band with 180 s exposures. Bias-subtraction and flat-fielding were done in `photpipe` (Rest et al. 2005) using calibration frames obtained on the same night and in the same instrumental configuration. We aligned our images using 2MASS astrometric standards in the image frame and calibrated the images with r -band standards obtained from the PS1 DR1 object catalog (Flewelling et al. 2020). Initial difference imaging was performed using `hotpants` with template images generated from the Dark Energy Camera (primarily DES DR1; Abbott et al. 2018b) and processed using the same pipeline, but our final difference-imaging analysis uses the exposures from Sep. 3

and 11. In addition, we used a custom version of `DoPhot` (Schechter et al. 1993) to detect and perform forced photometry on all candidate transient sources.

2.1.5. Swope

We observed the localization region of GW190814 with the Swope 1 m telescope at Las Campanas Observatory, Chile from 14 Aug. to 10 Sep. 2019 (Kilpatrick et al. 2019). Each observation is summarized in Table 4. The Swope/Direct 4k \times 4k camera on the Swope telescope covers $29.8' \times 29.7'$. We performed all observations in the r band with 120 s exposures. Bias-subtraction, flat-fielding, amplifier stitching, image registration, and calibration were

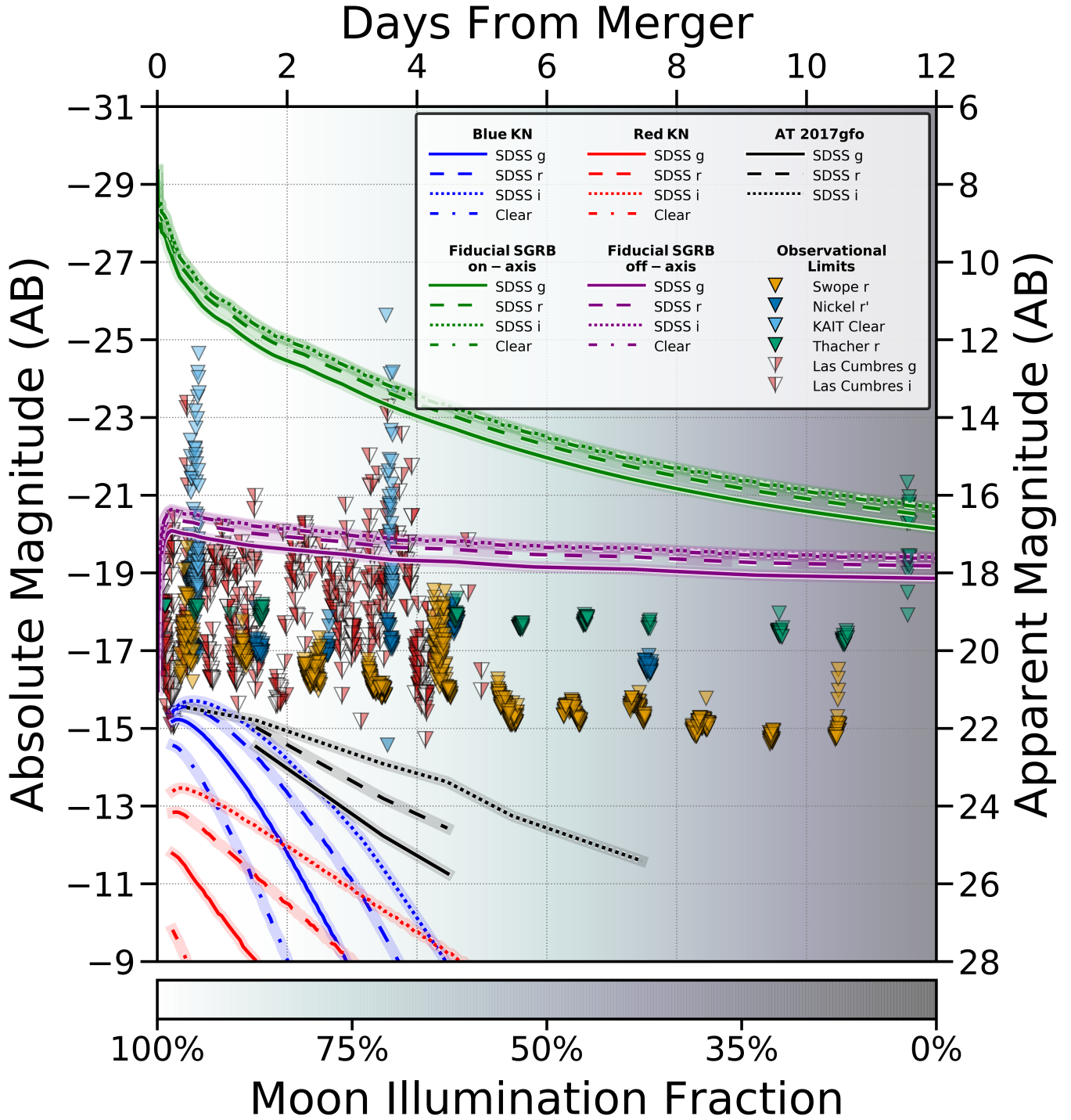


Figure 2. The limiting magnitudes from all of our follow-up observations of GW190814 with respect to the time from merger. We show the absolute magnitudes on the left-hand axis, based on the preferred distance to GW190814 of 241 Mpc, and apparent magnitudes on the right-hand axis. Each observation is colored by telescope and band as shown in the legend. We also overplot model light curves for the *gri* bands based on a blue kilonova with $M_{\text{ej}} = 0.025 M_{\odot}$, $v_{\text{ej}} = 0.26c$, $Y_e = 0.45$, and also a red kilonova with $M_{\text{ej}} = 0.059 M_{\odot}$, $v_{\text{ej}} = 0.19c$, $Y_e = 0.1$, which approximately represent the red and blue components of AT 2017gfo (see Section 4.3 and Drout et al. 2017; Kilpatrick et al. 2017). Similarly, we show GRB170817A viewed on-axis and off-axis at an angle of $\theta_{\text{obs}} = 17^{\circ}$ (Section 4.4 and Wu & MacFadyen 2018). Finally, we show smoothed *gri* light curves of AT 2017gfo derived from observations reported by Drout et al. (2017), Coulter et al. (2017), Arcavi et al. (2017a), Cowperthwaite et al. (2017), Troja et al. (2017), and Tanvir et al. (2017).

all done in `photpipe` following methods described by Kilpatrick et al. (2018). We calibrated each image using r -band photometry of stars in the PS1 DR1 object catalog transformed to the Swope natural system using the Supercal method (Scolnic et al. 2015). We performed the difference-imaging procedure described in Section 2.1.4, and our final analysis uses template exposures obtained from 2–8 Sep. 2019 and listed in Table 4.

2.1.6. Thacher

The Thacher 0.7 m telescope is a robotic telescope located at the Thacher School Observatory in Ojai, California (Swift & Vyhna1 2018). It uses an Andor iKON-L 936 2k \times 2k imager with a V -band optimized back-illuminated chip which translates to a 20.8' \times 20.8' field. We observed the localization region of GW190814 from 15 Aug. to 2 Sep. 2019 with 180 s r -band exposures (Swift et al. 2019). We followed the same calibration and reduction procedure in `photpipe` as described in Section 2.1.4. Each frame was calibrated using PS1 DR1 r -band standard stars, and we performed initial difference imaging using DECam frames and final analysis with Thacher imaging templates of each field and described in Table 4.

2.2. Spectroscopy of Candidates and Hosts

We obtained spectra of candidate EM counterparts to GW190814 and potential host galaxies with Keck, the Shane 3 m telescope at Lick Observatory, and the SOAR 4 m telescope on Cerro Pachón, Chile. Obtaining optical spectra of candidate EM counterparts to GW events can validate whether these sources resemble expectations for kilonovae and sGRB afterglows, as in the case of the initial spectrum of AT 2017gfo obtained \approx 12 hr after the GW event (Drout et al. 2017; Shappee et al. 2017). Similarly, optical spectra of transients unlikely to be associated with a GW event, such as supernovae, can be used to rule out a candidate counterpart. Finally, spectra provide a redshift to the event, enabling us to rule out candidate counterparts based on a volumetric cut in the context of the LVC localization region and luminosity distance. All of our spectroscopic observations are summarized in Table 1. Below we detail our observation and reduction procedure for each telescope.

2.3. Keck/DEIMOS

We obtained a spectrum of the GW190814 counterpart candidate AT 2019osy on 28 Aug. 2019 using the DEep Imaging Multi-Object Spectrograph (DEIMOS) (Faber et al. 2003) on the Keck-II 10 m telescope. Two 900 second exposures were taken with a 1'' long slit, 600ZD grating, and the GG455 long-pass order blocking filter.

The spectra were reduced with the `PyPeIt` version 1.3.3 (Prochaska et al. 2020a,b) with the standard reduction.

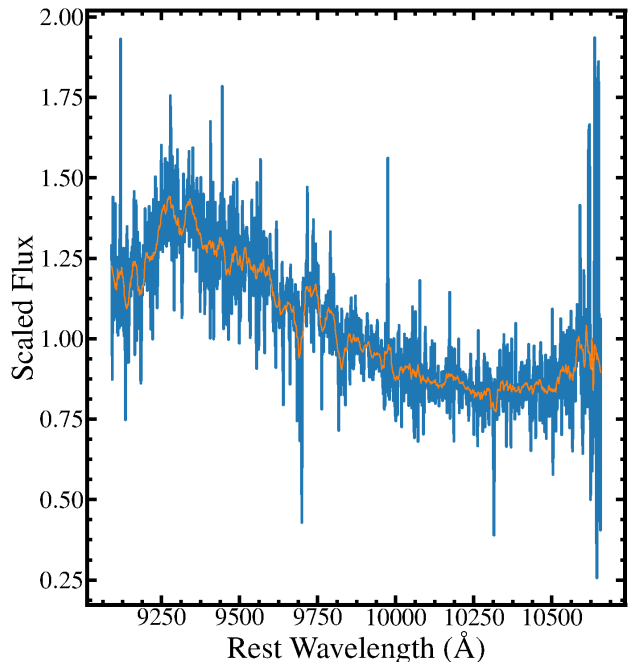


Figure 3. Keck/MOSIFRE spectrum of the GW190814 candidate counterpart AT 2019nra ($z = 0.269 \pm 0.029$) obtained on 18 Aug. 2019 as reported by Dimitriadis et al. (2019). The spectrum is largely featureless apart from a single intermediate-width feature at a rest wavelength of 9300 Å, although this wavelength does not correspond to any known features.

`PyPeIt` was also used to flux calibrate the spectra with a standard star observed on the same night and to coadd the observations into a single spectrum.

2.3.1. Keck/MOSFIRE

We used Keck/MOSFIRE to observe the candidate counterpart to GW190814 AT 2019nrm on 18 Aug. 2019 as reported by Dimitriadis et al. (2019). We obtained 4 \times 120 s (ABBA nod pattern) J -band (\sim 11,500–13,500 Å) spectroscopic observations, using the 0.7'' slit. The spectra were reduced with the MOSPY Data Reduction Pipeline⁶ and calibrated with standard-star observations, taken on the same night and in the same instrumental configuration. The final spectrum is shown in Figure 3.

2.3.2. Lick Shane/Kast

We observed candidate EM counterparts and host galaxies with the Kast double spectrograph (Miller & Stone 1993) on the Shane 3 m telescope on 26 and 31 Aug., 2, 5, and 21 Sep., and 8 Oct. 2019 as shown in Table 1. All observations were taken with the 452/3306 grism (blue arm) and

⁶ <https://keck-datareductionpipelines.github.io/MosfireDRP/>

the 300/7500 grating (red arm), using the $2''$ wide slit, covering approximately 3200–10,500 Å in the combined blue-side and red-side spectra. The spectra were reduced with standard IRAF⁷ CCD-processing and spectrum-extraction procedures, and our own IDL routines for flux calibration and telluric-line removal, using the well-exposed continua of spectrophotometric standard stars. Details on the spectroscopic reduction procedure are outlined by Silverman et al. (2012).

2.3.3. SOAR/Goodman

We used the Goodman spectrograph on the Southern Astrophysical Research (SOAR) 4 m telescope to observe candidate EM counterparts and host galaxies of GW190814 on 17 Aug. and 1 Sep. 2019. All observations were performed using the 400 line mm^{-1} M1 (3000–7000 Å) grating in conjunction with the $1.07''$ wide slit. We reduced all spectra following the same procedures as for the Shane/Kast data. These spectra are shown in Figure 4 and discussed in Section 3.

2.4. Identification of Transients

Follow-up imaging from 1M2H, KAIT, and Las Cumbres was used to identify transients that we consider candidate counterparts to GW190814 after we performed difference imaging. Here we summarize the methods used for elevating transient sources to candidate counterparts within each set of imaging. All photometry of transient sources used in this analysis, including photometry from outside sources (e.g., Andreoni et al. 2020; Ackley et al. 2020; Morgan et al. 2020), is summarized in Table 6.

2.4.1. 1M2H

As described above, all Nickel, Swope, and Thacher difference imaging was analyzed through the photpipe difference imaging and analysis pipeline. After difference imaging through hotpants and identification of transient sources using a custom version of dophot, photpipe cuts transient sources based on pixel-level statistics including the relative fraction of positive, negative, and masked (i.e., saturated) pixels within the PSF aperture and the extendedness of the source PSF relative to the PSF passed to dophot. In general, these criteria are relaxed in order to avoid cutting a significant fraction of the transient source catalog for each image, but these cuts naturally result in a loss in detection efficiency for each image (typically $\approx 3\%$ of sources on average). We perform the same cuts during fake star injection,

and so we account for this detection efficiency in our limiting magnitude for each image. On average, we detect 2 sources in each Nickel image, 12 sources in each Swope image, and 10 sources in each Thacher image.

After we construct a transient catalog for each image, sources are crossmatched across all catalogs using a search radius of 2 pixels, that is, transient sources within 2 pixels of the average coordinate of a previously identified “cluster” of detections are considered to be the same source. Sources are elevated as candidates if they are 1) detected in at least two images with $S/N > 3$, or 2) in a single image with $S/N > 10$. We obtain final photometry for every cluster of sources by taking the signal-to-noise weighted average position of each cluster and running forced photometry on this position with dophot. Finally, we visually inspect all candidate transients to validate that they are not due to poor image quality or other non-astrophysical contaminants. All 1M2H candidates are crossmatched against known minor planets before we consider them as viable candidate counterparts to GW190814.

2.4.2. KAIT

KAIT images were analyzed through part of our custom-developed LOSSPhotPipeline⁸ (Stahl et al. 2019), which adopts the ISIS package⁹ (Alard & Lupton 1998) for image subtraction. After difference imaging, identification of transient sources was based on several parameters (e.g., PSF, FWHM, mag, S/N) extracted from the original image, the template image, and the residual image using SExtractor¹⁰ (Bertin & Arnouts 1996).

Candidates passing the customized criteria were logged on a web-based list, and then further visually checked by multiple people to eliminate any non-astrophysical contaminants. Similar to 1M2H, all of our candidates were crossmatched against known minor planets before we considered them as viable candidate counterparts. If no valid candidate was found, the limiting magnitude was estimated by examining the 3σ RMS noise averaged through several locations across the entire image.

3. CLASSIFICATION OF CANDIDATES

Although no optical candidate counterparts to GW190814 were definitively identified as being similar to kilonovae or sGRBs in the extensive follow-up observations and analysis of the event (e.g., in the optical or radio; Andreoni et al. 2020; Dobie et al. 2019a; Gomez et al. 2019b; Thakur et al. 2020; Morgan et al. 2020), limits on the physical nature to any counterpart rely on the assumption that all transient sources

⁷ IRAF is distributed by the National Optical Astronomy Observatory, which is operated by the Association of Universities for Research in Astronomy (AURA), Inc., under a cooperative agreement with the National Science Foundation.

⁸ <https://github.com/benstahl92/LOSSPhotPipeline>

⁹ <http://www2.iap.fr/users/alard/package.html>

¹⁰ <https://github.com/astromatic/sextractor>

Table 1. Spectra of Candidates and Host Galaxies

Name	Observation Date	Source	Type	z	Ref.
2019noq	2019-08-21	Goodman	II	0.0591 ± 0.0003	1,4
2019npf	2019-10-03	Kast	–	0.1630 ± 0.0001	2
2019nph	2019-10-31	Kast	–	0.2689 ± 0.0003^a	2
2019npv ^b	2019-08-26	Magellan	Ibc	0.0560 ± 0.0001	1,3,4,11
2019npw	2019-08-27	Goodman	II	0.1494 ± 0.0001	3,5,6
2019nqc ^b	2019-08-23	SALT	II	0.0780 ± 0.0001	1,4,5,7,11
2019nqg	2019-08-31	Kast	–	0.1706 ± 0.0001	5
2019nqq	2019-08-17	Goodman	II	0.0711 ± 0.0001	1,4,8,11
2019nqr	2019-08-17	Goodman, FLOYDS	II	0.0832 ± 0.0001	1,4,9,10,11
2019nqx	2019-10-08	Kast	–	0.2792 ± 0.0003^a	12
2019nrd	2019-08-31	Kast	–	0.2472 ± 0.0003	12
2019nra	2019-09-21	Kast	–	0.2971 ± 0.0002^a	12,13
2019nra	2019-08-18	MOSFIRE	?		12,13
2019nrb	2019-10-09	Kast	–	1.7953 ± 0.0011^a	12
2019nrp	2019-11-06	Kast	–	0.0107 ± 0.0002^a	12
2019nrv	2019-10-09	Kast	–	0.0531 ± 0.0003^a	12
2019nte	2019-08-22	Goodman	–	0.0706 ± 0.0001	4,11,14,15
2019nte	2019-10-08	Kast	–	0.0700 ± 0.0004^a	4,11,14,15
2019ntn	2019-08-21	Goodman	Ia-CSM	0.1001 ± 0.0002	1,4,16
2019ntp	2019-09-01	Goodman	Ia	0.1141 ± 0.0001	1,4,15,16,17
2019ntr	2019-08-29	Goodman	II	0.2185 ± 0.0001	1,4,11,15,16,18
2019nts	2019-08-31	Kast	–	0.1931 ± 0.0003^a	1,16
2019nul	2019-08-31	Kast	–	0.0985 ± 0.0002	1,4,16,19
2019num	2019-08-27	Goodman	IIb	0.1274 ± 0.0001	1,4,15,16
2019nuo	2019-10-03	Kast	–	0.1151 ± 0.0001	15,19
2019nun	2019-09-05	Kast	–	0.1319 ± 0.0002	1,16,19
2019nur	2019-08-26	Kast	–	0.1394 ± 0.0002	16
2019nuu	2019-08-26	Kast	–	0.2106 ± 0.0002	16
2019nwt	2019-08-31	Kast	–	0.2458 ± 0.0003	20
2019nyv	2019-09-05	Kast	–	0.0410 ± 0.0004^a	1,21
2019nyz	2019-08-26	Kast	–	0.4146 ± 0.0002	21
2019nzg	2019-08-26	Kast	–	0.2132 ± 0.0002	21
2019nzm	2019-09-21	Kast	–	0.2143 ± 0.0002	21
2019nzn	2019-09-03	Kast	–	0.1716 ± 0.0001	19,21
2019nZR	2019-09-02	Kast	–	0.2549 ± 0.0002	1,11,15,22
2019nzs	2019-10-03	Kast	–	0.2261 ± 0.0002	22
2019oat	2019-09-21	Kast	–	0.1978 ± 0.0003^a	21
2019oaz	2019-09-03	Kast	–	0.1987 ± 0.0003	21
2019obb	2019-09-05	Kast	–	0.3157 ± 0.0002	22
2019obc ^b	2019-08-23	GTC	Ia	0.216 ± 0.005	1,4,11,15,22,23
2019odc	2019-08-26	Kast	–	0.0551 ± 0.0002	1,4,11,15,24
2019ofb	2019-08-31	Kast	–	0.1185 ± 0.0001	1,25
2019omx	2019-08-29	Goodman	–	0.1645 ± 0.0001	1,4,11,15,18,26
2019onj	2019-09-03	Kast	–	0.0665 ± 0.0001	1,11,15,27,28
2019osy	2019-08-28	DEIMOS	–	0.0738 ± 0.0003	1,29,30,31

NOTE—Our Keck/DEIMOS, Keck/MOSFIRE, Shane/Kast, and SOAR/Goodman spectra are described in Section 2.2. All dates are UTC. The spectral types for transient spectra are noted along with spectroscopic redshifts. Where we have only measured the host-galaxy redshift, we note the spectral type of the spectrum as “–.” We provide references relevant to discovery and classification of each candidate as follows: (1) Ackley et al. (2020), (2) Andreoni & Goldstein (2019a), (3) Gomez et al. (2019a), (4) Andreoni et al. (2020), (5) Andreoni & Goldstein (2019b), (6) Tucker et al. (2019a), (7) Buckley et al. (2019), (8) Herner (2019a), (9) Al (2019a), (10) Hiramatsu et al. (2019a), (11) Morgan et al. (2020), (12) Andreoni & Goldstein (2019c), (13) Dimitriadis et al. (2019), (14) Herner & Team (2019), (15) Soares-Santos et al. (2019b), (16) Andreoni & Goldstein (2019d), (17) Wiesner et al. (2019a), (18) Wiesner et al. (2019b), (19) Dobie et al. (2019b), (20) Al (2019b), (21) Andreoni & Goldstein (2019e), (22) Al (2019c), (23) Castro-Tirado et al. (2019), (24) Herner (2019b), (25) Chambers et al. (2019), (26) Al (2019d), (27) Al (2019e), (28) Japelj et al. (2019), (29) Jaodand et al. (2019), (30) Bauer et al. (2019), (31) Stewart et al. (2019b).

^a Spectra did not meet our cross-correlation height-to-noise ratio (r) threshold $r > 4$. See discussion in Section 3.4.

^b Spectra of these objects are not presented in this publication, but their classifications and redshifts are used in our analysis and can be found in the references given.

identified in the aftermath of GW190814 have been ruled out as being associated with the GW detection. In the following analysis, we discuss all known candidate optical transients that we consider potentially associated with GW190814. We assess the likelihood that one of these transient sources was the EM counterpart to the merger using the localization region and time of merger, candidate spectroscopy, premerger variability, host-galaxy associations, and candidate photometry. The following criteria describe our classification procedure and rationale.

1. **Localization:** We consider publicly-reported candidates and those discovered by our own surveys that are within the 99th percentile credible region provided by the LVC, a total area of 48.7 deg^2 and 189 viable candidates (Figure 1). This can theoretically result in missing the actual counterpart, but we expect it to occur in only 1% of cases. Furthermore, we find that for the inner 95th percentile credible region (26.8 deg^2) there are 214 viable candidates while for the 99.5th percentile (58.2 deg^2) there are 290 candidates. The fact that the number of candidates does not scale as the total search area reflects the shallower search depth of the lower-probability areas in the GW190814 localization region. Therefore, we are confident that we do not rule out any known, high-probability transients on the basis of localization.
2. **Time from Merger:** We restrict our analysis to candidates discovered within 14 days after the LVC detected the GW190814 merger signal. This will only result in false negatives if the optical counterpart to GW190814 has a rise time significantly longer than known kilonovae and sGRBs such as AT 2017gfo (implying, for example, a kilonova with an extremely large ejecta mass and optical opacity or a highly off-axis GRB; Rossi et al. 2002; Yamazaki et al. 2003; Ryan et al. 2015; Kasen et al. 2015; Metzger 2017; Kasen et al. 2017). The lack of a prompt gamma-ray counterpart implies that if there was a GRB170817A-like GRB (Troja et al. 2017; Mooley et al. 2018), it was likely off-axis and thus not detectable by INTEGRAL, *Fermi*, or *Swift* (despite coverage of the region as described by Molkov et al. 2019; Kocevski et al. 2019; Palmer et al. 2019). However, while the rise time for a GRB afterglow scales relative to the viewing angle θ_{obs} and jet opening angle θ_0 as $\theta_{\text{obs}}/\theta_0$, optical follow-up observations would likely be insensitive to a counterpart observed >14 days after merger (see models by Lazzati et al. 2017; Murguia-Berthier et al. 2017). A delayed rise in optical luminosity could also occur if the merger occurred in an evacuated circumburst medium (proposed by Ramirez-Ruiz et al. 2019, for GW170817), simi-

lar to the Galactic pulsar J1913+1102 (Lazarus et al. 2016). However, for plausibly detectable EM counterpart models, the rise time is significantly shorter than 14 days, and so we are confident that this restriction is conservative. Furthermore, we find that if we restrict our analysis to candidates discovered only within the first 10 days post-merger while keeping our localization cut the same, there are 270 viable candidates, whereas if we cut at 21 days there are 293. Similar to localization, this reflects the fact that follow-up observations decreased significantly in depth and cadence at >10 days post-trigger. Criteria #1 and #2 define our initial sample of 189 candidate counterparts, including 7 candidates identified in our own follow-up program (Table 5).

3. **Coincidence with minor planets:** Candidates that are coincident ($< 20''$) with minor planets at the time of observation and as reported by the Minor Planet Center¹¹, and are not detected in multiple epochs of imaging separated by > 30 min, are ruled out. For candidates discovered by 1M2H, KAIT, and Las Cumbres, we perform this check before considering a transient as a viable EM counterpart to GW190814, and so minor planets are not reported in Table 5. For all other publicly-reported transients, this check is typically performed before a candidate is reported, but some reported candidates were reclassified as minor planets, for example, in Andreoni et al. (2020) and Morgan et al. (2020). Overall, we rule out 11 objects based on coincidence with minor planets.
4. **Coincidence with known stars:** We checked each candidate for coincidence ($< 1''$) with nearby stars in the *Gaia* DR2 catalog (i.e., those that have parallax or proper motion measured at $> 3\sigma$; Gaia Collaboration et al. 2018). Transient detections can potentially arise from stellar variability, and so are not expected to be associated with GW190814. However, 0 objects are ruled out based solely on coincidence with *Gaia* DR2 stars.
5. **Spectroscopic classification:** Candidates with spectra that resemble known classes of transients (i.e., those with template spectra in SNID; Blondin & Tonry 2007) are ruled out as counterparts to GW190814. To perform this analysis, we consider spectra presented in publications on GW190814 (e.g., Dobie et al. 2019a; Andreoni et al. 2019a; Gomez et al. 2019b; Ackley et al. 2020; Watson et al. 2020, and references therein).

¹¹ <https://minorplanetcenter.net>

We only consider spectra that we can definitively classify as supernovae or other well-known classes of transients that are not thought to be associated with NS mergers. For example, spectra that resemble “blue continuum” or galaxy emission are not ruled out, as AT 2017gfo was initially very blue (Drout et al. 2017; Shappee et al. 2017; Kilpatrick et al. 2017) and spectra dominated by galaxy emission imply non-detection of the transient. Thus, the likelihood of false negatives is negligible. We rule out 12 candidates based solely on spectroscopic classification, which includes all sources with classifications in Table 1.

6. **Pre-merger variability:** Candidates with detections in transient surveys from before the merger are ruled out, which we derive from crossmatching ($< 1''$) to the Pan-STARRS DR2 Detection Catalog (see the description by Flewelling et al. 2020), an available light curve in the ASAS-SN Photometry Database¹² (Shappee 2014; Jayasinghe et al. 2019), or the Asteroid Terrestrial-impact Last Alert System forced photometry server (Shingles et al. 2021). Models for merging NSBH systems do not typically predict any significant premerger optical emission, for example due to accretion from a circumbinary disk (Joss & Rappaport 1984; Schröder et al. 2018); however, we further consider active galactic nucleus (AGN) variability (as in Graham et al. 2020) as a possible counterpart to GW190814 in Section 5.3. We define variability as multiple premerger detections in a single band with a significant ($>3\sigma$) change in brightness. We rule out 2 objects based solely on premerger variability, each of which is discussed below. We consider candidates ruled out by this criterion or any of the preceding steps to be “strongly ruled out” (as described in Table 5), comprising 114/189 (41%) of our sample.
7. **Spectroscopic redshifts:** The LVC constrain the distance to GW events using signal amplitude (Abadie et al. 2011). For GW190814, this resulted in a luminosity distance of 241^{+41}_{-45} Mpc ($z = 0.056 \pm 0.010$ assuming $H_0 = 70 \text{ km s}^{-1} \text{ Mpc}^{-1}$; Abbott et al. 2020a). Candidates found in host galaxies that are outside the 99th percentile credible volume (roughly $D_{\text{mean}} \pm 2.58 D_{\text{std}}$) as determined from spectroscopic redshifts are ruled out. This criterion can result in false negatives when there is a chance coincidence between a candidate and assumed host galaxy. However, the mean number density of galaxies with luminosity $> L_*$ in the local Universe is approximately

$6 \times 10^{-3} \text{ Mpc}^{-3}$ (Schechter 1976; Bell et al. 2003), implying roughly one galaxy per 85 arcmin². Where host identification is made, the median candidate-host separation is $\sim 2''$, and so the chance coincidence with a random host galaxy in the GW190814 volume is 0.004% (1 per 25,000 candidates), or a $<1\%$ chance of occurring at most once for all 189 of our candidates. To further reduce the likelihood of chance coincidence, we require that for a galaxy with a spectroscopic or photometric redshift, the projected separation between the host galaxy and transient is <300 kpc (assuming Planck 2016 cosmology; Planck Collaboration et al. 2016). We derive spectroscopic redshifts from public databases, our own observations as described below, and observations in the literature. Therefore, we do not think that false negatives from candidates ruled out this way are significant. We rule out 31 candidates based solely on spectroscopic redshifts outside the 99% credible volume.

8. **Photometric redshifts:** We repeat the previous step using photometric redshifts from the 2MASS Photometric Redshift (2MPZ; Bilicki et al. 2014), Pan-STARRS1 Source Types and Redshifts with Machine learning (PS1-STRM) catalogs (Beck et al. 2021), and the Photometric Redshifts for the Legacy Surveys (Zhou et al. 2021). We choose the “best” host-galaxy association and photometric redshift by crossmatching galaxies between each catalog and picking the host galaxy with the smallest projected separation (in kpc), and then choosing the photometric redshift with the smallest relative uncertainty σ_z/z . All of these catalogs are trained using machine-learning approaches, and on 2MASS, WISE, and SuperCOSMOS photometric data for the former and PS1 data for the latter. These result in median redshifts $z < 0.1$ for both catalogs, making them ideal for low-redshift analysis of transients in the LVC volume. We rule out 104 candidates based on photometric redshift, representing 55% candidates overall.
9. **Photometric evolution:** It is now known that NS mergers result in kilonovae and sGRBs (Abbott et al. 2017c; Kasen et al. 2017), the optical properties of which have been constrained by sGRB follow-up observations at higher redshifts and the discovery of AT 2017gfo (Arcavi et al. 2017a; Drout et al. 2017; Kilpatrick et al. 2017). Apart from the most extreme physical scenarios and geometries, theoretical models and observations imply that EM counterparts to NS mergers are quite faint, fade rapidly, and typically have colors $g - r > -1.0$ mag (all “red” kilonova models considered by Kilpatrick et al. 2017 peak at

¹² <https://asas-sn.osu.edu/>

> -18 mag, fade more rapidly than 0.1 mag day^{-1} in optical bands, and have $g-r > 1.0$ mag at all epochs). Therefore, we can rule out candidates that would be luminous at the distance to GW190814, have rising or slowly fading light curves, or are bluer than expected for sGRB afterglows. By using these limits and considering candidates with arbitrarily faint, rapidly evolving, or red light curves, we avoid false negatives due to host extinction. We rule out 28 candidates by photometric cuts, which represents all candidates not ruled out by previous cuts. Candidates ruled out only by these criteria are “weakly ruled out.”

To systematically assess the viability of each candidate counterpart, we determine the extent to which all candidates match each of these criteria in Table 5. We start from our base sample of 189 candidates derived from publicly reported transients and candidates discovered in our follow-up imaging, all of which satisfy the localization criterion and were discovered in imaging taken within 2 weeks of the GW190814 merger. We conclude that there are no viable candidate counterparts, although 28 (14%) of all candidate counterparts are “weakly ruled out” by the photometric evolution criteria. In the remainder of this section, we discuss individual candidates and whether they are likely counterparts to GW190814 in the context of our overall classification scheme. We summarize the steps we use to rule out candidates in Table 2, including the number of candidates that can be ruled out at each step ignoring all previous steps.

3.1. Coincidence with Minor Planets

The primary interloping transients in our own follow-up imaging are minor planets, which result from asteroids with proper motion that is high enough to appear in only a single epoch of imaging but low enough not to appear intrinsically extended in a 2–5 min exposure or show up in multiple exposures separated by <10 min. Andreoni et al. (2020) attempt to rule out these transients by taking multiple, non-consecutive exposures when possible, but several objects in the Minor Planet Center database were reported when transients were detected only in a single epoch or the follow-up image occurred soon after discovery. In particular, we note the following transients in the Transient Name Server that were reported with 2 detections but a short period of time between the two epochs (given here in parentheses next to each candidate): AT 2019nmd (1.4 min), AT 2019nme (1.4 min), AT 2019nqh (single epoch), AT 2019nri (8.6 min), AT 2019nrq (2.9 min), AT 2019nrt (2.9 min), AT 2019nsd (2.9 min), AT 2019nsl (2.9 min), and AT 2019nsn (2.9 min) (Andreoni et al. 2019a; Morgan et al. 2020). In both Andreoni et al. (2019a) and Morgan et al. (2020), these candidates were subsequently revised to indicate that they are in fact minor planets as we note here.

Given the coincidence ($<20''$) between these transients and minor planets reported in Table 5 as well as the correlation with transients detected in a single epoch or at most two epochs separated by <30 min, we rule out all of these sources as likely minor planets and thus unassociated with GW190814. As described in Section 2.4, this cut was performed a priori for our own data, and so no internal candidates from 1M2H, KAIT, or Las Cumbres are considered likely minor planets.

3.2. Spectroscopy of Candidate Counterparts

Our Keck, Shane, and SOAR spectra of GW190814 candidate counterparts were obtained from 17 Aug. to 1 Sep. 2019 and definitively rule out some counterparts as being likely kilonovae or sGRB afterglows. Below we examine spectroscopic classifications of individual candidates inferred from spectra discussed in Section 2 and in other publications. Our classifications are performed using SNID (Blondin & Tonry 2007), from which we derive redshift and spectral type. All of our candidate spectra are shown in Figure 4.

AT 2019noq: We obtained a SOAR/Goodman spectrum of the candidate AT 2019noq (also PS19epf, discovered on 15 Aug. 2019 by Huber et al. 2019) on 21 Aug. 2019 as reported by Rodríguez et al. (2019). The spectrum is consistent with a Type II SN at $z = 0.07$, and so we do not consider AT 2019noq to be a likely counterpart to GW190814.

AT 2019ntn: AT 2019ntn was discovered on 18 Aug. 2019 as part of DECam-GROWTH follow-up observations (Goldstein et al. 2019b,a; Andreoni et al. 2020). We obtained a spectrum with SOAR/Goodman on 21 Aug. 2019. This spectrum was reported as similar to that of a Type Ia-CSM or Ia/IIn at $z = 0.1$ by Rodríguez et al. (2019). We find similar results, and so we rule out any association between AT 2019ntn and GW190814.

AT 2019npw: AT 2019npw was initially reported by Andreoni et al. (2019b) at $i = 20.5$ mag and characterized as offset from its likely host galaxy. Tucker et al. (2019a) later obtained SOAR/Goodman spectroscopy of this source and found that it was consistent with a Type IIB SN at $z = 0.126$, which we confirm based on the same data. Therefore, we rule out any association between GW190814 and AT 2019npw.

AT 2019nqq: AT 2019nqq (also DESGW-190814c; Herner et al. 2019a) was discovered by the DESGW collaboration on 15 Aug. 2019. We obtained a spectrum of this source on 17 Aug. 2019 (Tucker et al. 2019b) that is dominated by a continuum with a broad emission line near 7000 \AA . We infer this line to be $H\alpha$, implying that AT 2019nqq is consistent with a Type II SN at $z \approx 0.07$, similar to the results reported by Lopez-Cruz et al. (2019). Therefore, we rule out any association between AT 2019nqq and GW190814.

AT 2019nte: AT 2019nte was detected by Herner et al. (2019b) in DECam imaging at $i = 20.95$ mag on 17

Table 2. Analysis of Public and Internal Candidate Counterparts to GW190814

Step	Criterion	Candidates	Candidates Cut	All Candidates Flagged ^a
0	Within Spatial (99th percentile area) and Temporal Cut (<2 weeks from merger)	189	–	–
1	Not <20'' from minor planet and not in multiple epochs separated by >30 min	178	11	11
2	Not <1'' from star with parallax in Gaia DR2	178	0	0
3	Not spectroscopically classified as an unassociated transient	166	12	12
4	No evidence for pre-merger variability	164	2	2
5	Spectroscopic redshift not outside the 99th percentile credible volume	133	31	39
6	Photometric redshift not outside the 99th percentile credible volume	28	104	127
7	Not photometrically classified as an unassociated transient	0	28	126

^aThis column indicates the number of candidates that would be cut at this stage if we disregard all previous stages.

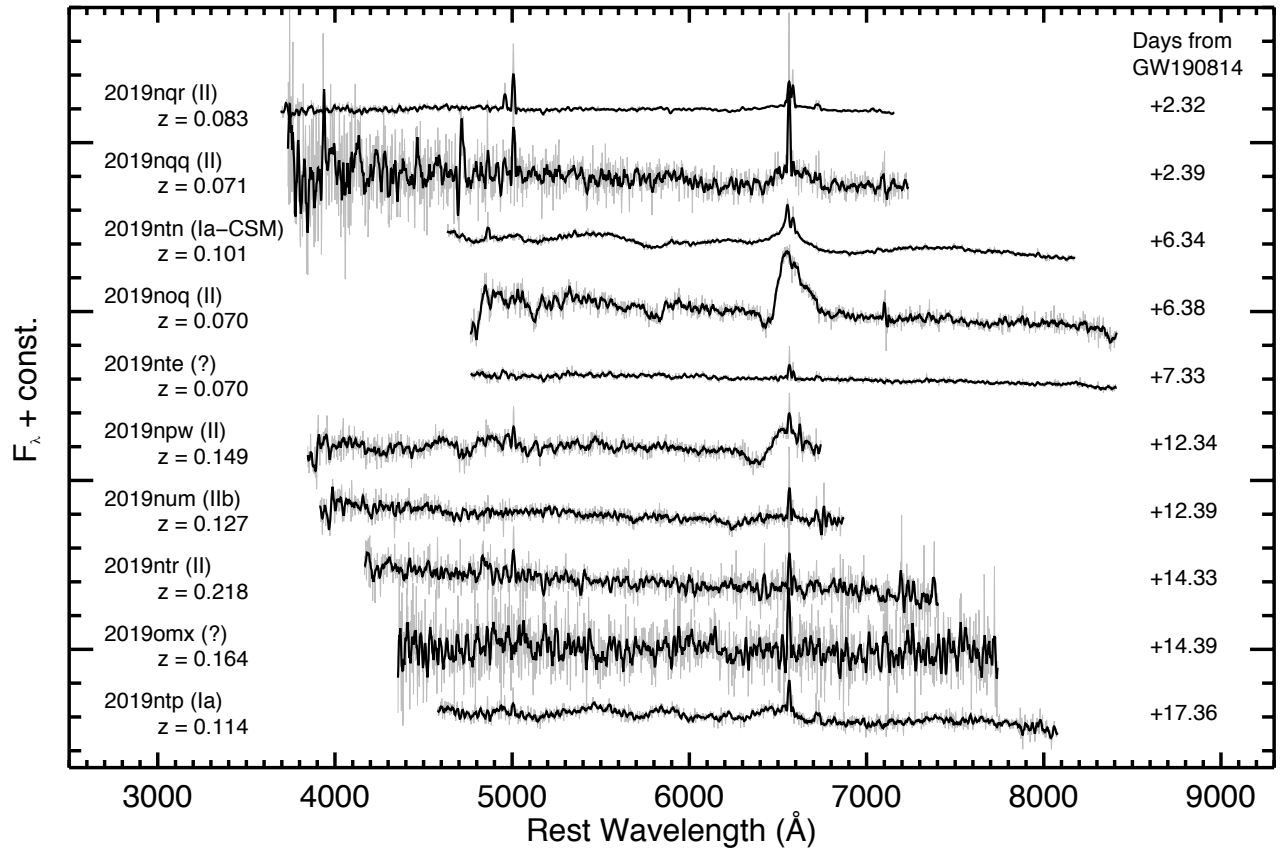


Figure 4. Spectra of candidate optical counterparts to GW190814 obtained with SOAR/Goodman. No spectra are classified as likely kilonovae or sGRBs, and thus we determine based on spectroscopic classification that most objects in this sample are unassociated with GW190814.

Aug. 2019. We obtained a spectrum of this source with SOAR/Goodman as reported by [Cartier et al. \(2019\)](#). It had too little signal to obtain a robust spectroscopic classification, but we obtained a redshift of the underlying host galaxy from the Balmer features. From this emission, we infer that AT 2019nte is at $z = 0.0701 \pm 0.0006$. At the location of AT 2019nte, this redshift is not ruled out by our volumetric cut, and so we consider AT 2019nte to be a viable candidate

counterpart to GW190814 on the basis of its spectrum and redshift.

AT 2019ntp: The candidate AT 2019ntp was discovered by DECam/GROWTH (also DG19gcwjc; [Goldstein et al. 2019b](#)) on 18 Aug. 2019 at $i = 21.0$ mag. We obtained a spectrum with SOAR/Goodman on 1 Sep. 2019 as reported by [Wiesner et al. \(2019a\)](#); AT 2019ntp is a Type Ia SN at $z = 0.114$, and so we do not consider it to be associated with GW190814.

AT 2019ntr: Candidate transient AT 2019ntr was detected by DECam/GROWTH (also DG19sbzkc; Goldstein et al. 2019b) on 18 Aug. 2019 at $z = 21.2$ mag. We obtained a SOAR/Goodman spectrum on 29 Aug. 2019 (Wiesner et al. 2019b) from which we determine that AT 2019ntr is a Type II SN at $z = 0.218$. Therefore, we do not consider AT 2019ntr to be associated with GW190814.

AT 2019num: The candidate AT 2019num was discovered by DECam/GROWTH on 18 Aug. 2019 at $i = 21.3$ mag (Goldstein et al. 2019b). We obtained a spectrum with SOAR/Goodman on 27 Aug. 2019 (Tucker et al. 2019a) from which we determine that AT 2019num is a Type II SN at $z = 0.127$, and so it is not considered to be associated with GW190814.

AT 2019omx: The candidate AT 2019omx was discovered by the DESGW on 21 Aug. 2019 at $z = 22.1$ mag (Soares-Santos et al. 2019b). We obtained a spectrum on 29 Aug. 2019 with SOAR/Goodman (Wiesner et al. 2019b). The spectral classification is inconclusive, although we are able to constrain the redshift from Balmer emission in the likely host galaxy as $z = 0.164$. Therefore, we rule out this candidate as being associated with GW190814 owing to its implied luminosity distance.

AT 2019osy: The GW190814 candidate EM counterpart AT 2019osy was discovered by the Australian Square Kilometre Array Pathfinder telescope (ASKAP) telescope (Johnston et al. 2008, 2007; McConnell et al. 2016) as a rising radio source possibly in host galaxy 2dFGRS TGS211Z177 ($z = 0.0738$) on 23 Aug. 2019 and reported to the community on 27 Aug. 2019 (Stewart et al. 2019a). We obtained a long slit Keck/DEIMOS spectrum of AT 2019osy and were unable to identify a transient. The extract spectrum is best matched by a galaxy template in SNID and we therefore determine that the transient is not detected.

3.3. Premerger Variability toward Candidate Counterparts

We analyzed the Pan-STARRS DR2 Detection catalog, ASAS-SN Photometry database, and Catalina Sky Survey DR2 catalog for coincidence with each of our candidates as described above. The PS1 DR2 Detection catalog separates multi-epoch observations into separate observations. We found two g -band detections coincident with AT 2019nto on 8 Sep. 2010 with an aperture flux of $g = 20.08 \pm 0.02$ mag and on 9 Oct. 2010 at $g = 21.56 \pm 0.05$ mag, indicating that the source is variable. It corresponds to the likely host galaxy WISEA J004203.40-244820.4 (Chung et al. 2011), with a nominal offset of $0.28''$ between AT 2019nto and the host galaxy. Therefore, we consider AT 2019nto to be unassociated with GW190814.

As described by Jayasinghe et al. (2019), the ASAS-SN photometry catalog was initially constructed from the >50 million point sources with $V < 17$ mag in the APASS

catalog (Henden et al. 2015). Thus, sources with counterparts in the ASAS-SN catalog are not necessarily variable, but we can use the catalog to crossmatch to candidate variables and check for multiple premerger detections. We identified a single candidate AT 2019nup that had a counterpart in the ASAS-SN photometry database¹³. This source is coincident with the center of a $z = 0.03665 \pm 0.00014$ galaxy in the Southern Abell Redshift Survey called SARS 013.16023-27.04103 (Way et al. 2005), with a $0.71''$ between AT 2019nup and its host. The AT 2019nup premerger counterpart exhibited a previous outburst on 15 May 2016 at $V = 15.85$ mag, and so we rule out any association with GW190814.

Despite these findings, it is possible that AT 2019nto or AT 2019nup are associated with AGN activity as a result of a compact object merger (similar to Graham et al. 2020). We revisit these objects in Section 5.3.

3.4. Redshifts of Candidate Host Galaxies

We associate candidates with their likely host galaxies on the basis of projected separation from galaxies with spectroscopic redshifts in the NASA/IPAC Extragalactic Database (NED)¹⁴. We require that the host-transient separation is at most $20'$ to be considered a candidate host galaxy and 300 kpc assuming the source is located at the host redshift and calculating an angular diameter distance using Planck Collaboration et al. (2016) cosmology. These criteria ensure that nearby extragalactic transients are selected in galaxies at large projected separations — notably AT 2019npd and AT 2019nvb, low-luminosity transients in the outer arms of the Sculptor Galaxy and separated by $9.8'$ (10.0 kpc) and $12.6'$ (12.7 kpc), respectively (Andreoni et al. 2019b; Srivastav et al. 2019). If there are multiple candidate host galaxies, we choose the galaxy with the smallest transient-host separation (in kpc). All of our host-galaxy redshifts are noted in Table 5.

In addition, we measured redshifts to host galaxies of candidates without spectroscopic redshifts in NED with Shane/Kast and SOAR/Goodman (Table 1; note that 2 objects, AT 2019nra and AT 2019nte, in our table were observed twice and 8 other objects has spectra that were too low quality to measure redshifts). From these spectra we infer the spectroscopic redshift to the candidate host galaxies. Spectroscopic redshifts were measured by cross-correlating spectra with galaxy templates using the RVSAO package (Kurtz & Mink 1998). In addition to visual inspection, the Tonry & Davis (1979) cross-correlation height-to-noise ratio (r) was used to determine the quality of the redshift match for each template, with $r > 4$ as our threshold for a reliable redshift.

¹³ This source is called AP16326416 in the ASAS-SN Photometry Database.

¹⁴ <http://ned.ipac.caltech.edu/>

The plurality of candidates we rule out are due to host-galaxy associations outside the 99th percentile volume provided by the LVC, totaling 31 with spectroscopic redshifts and 104 with photometric redshifts. Given the selection criteria and chance coincidence calculation described above, we infer that these associations are robust and it is unlikely that we have associated these transients with foreground or background galaxies outside the LVC volume by chance.

However, given the large overall fraction of galaxies with photometric redshifts and the statistical and systematic uncertainties associated with photometric redshift catalogs (see Bilicki et al. 2014; Beck et al. 2021; Zhou et al. 2021), it is possible that some host galaxies are indeed in the LVC volume. We avoid this possibility by requiring that, in order to be considered “outside the LVC volume,” the photometric redshift z_{phot} and uncertainty $\sigma_{z_{\text{phot}}}$ must satisfy $z_{\text{phot}} + \sigma_{z_{\text{phot}}} < z_{\text{LVC}} - \sigma_{z_{\text{LVC}}}$ or $z_{\text{phot}} - \sigma_{z_{\text{phot}}} > z_{\text{LVC}} + \sigma_{z_{\text{LVC}}}$ (where z_{LVC} and $\sigma_{z_{\text{LVC}}}$ are the redshift and uncertainty implied by the luminosity distance the LVC HEALPix map and assuming Planck Collaboration et al. (2016) cosmology). For analyses using GW190814 to measure the Hubble constant statistically (as by Soares-Santos et al. 2019c; The LIGO Scientific Collaboration et al. 2020; Palmese et al. 2020), additional spectroscopic observations of galaxies in the GW190814 volume will be essential to reduce the uncertainties in host-galaxy associations and the Hubble constant.

Some apparently “hostless” sGRB afterglows have been localized to regions of the sky with no apparent host galaxy to deep limits of $V \approx 26$ mag (Fong & Berger 2013; Behroozi et al. 2014). This finding suggests that some BNS and NSBH binaries experience natal kicks of $> 150 \text{ km s}^{-1}$ and potentially travel hundreds of kpc before merging and producing GW signals detectable by the LVC. This scenario is more likely in the local Universe where merging NS systems are more heavily weighted toward long delay times and thus systems that have travelled further from their birth environments (Anand et al. 2018; Safarzadeh et al. 2019). We do not consider apparently hostless transients to be ruled out as candidate counterparts to GW190814, and so the primary effect of a large projected separation between a transient and host on our analysis is the increased probability of a chance coincidence. A more detailed analysis would marginalize over the likelihoods of all candidate host galaxies for all candidate counterparts (as in, e.g., Aggarwal et al. 2021) and only cut candidates if they are associated with a galaxy outside the localization volume with high probability.

3.5. Photometric Evolution of Candidates

To constrain the optical properties of each candidate, we assign them luminosity distances on the basis of redshift (where available in Table 5) or the luminosity distance at the transient location in the LVC GW190814 HEALPix map.

Thus, we infer the absolute magnitude of every candidate that is not a minor planet in our analysis. Many of these sources are inferred to have extremely luminous absolute magnitudes (< -21 mag), likely reflecting interloping AGNs found in galaxy-targeted searches (e.g., Véron-Cetty & Véron 2010; Smith et al. 2020), and so most of these sources were ruled out on the basis of host-galaxy associations and our volume cut.

Guided by theoretical models for kilonovae, we note that there are no plausible models more luminous than -18.0 mag (e.g., in Metzger 2017; Kasen et al. 2017; Metzger 2019; Morgan et al. 2020), and thus use this limit to exclude any particularly luminous sources comprising 14 candidates. In addition, where available we analyzed any variability in all photometric bands and rule out sources that decline more slowly than 0.1 mag day^{-1} over a baseline of at least 3 days. We rule out 6 candidates (AT 2019omw, AT 2019qbz, AT 2019zza, 2019aako, 2019aakp, 2019aakq) as candidates that were either rising or slowly declining at the time of observation. In addition, we do not detect some candidates in our follow-up program after they were reported by previous groups. Thus, we can place a lower limit on their decline rate assuming the source was fainter than the limit at the time of observation (in particular, for limits reported by Andreoni et al. 2019a; Morgan et al. 2020). We rule out 8 candidates based on this criterion. The light curves and limits for all candidates ruled out by photometric cuts are shown in Figure 5.

We acknowledge that these cuts are model-dependent, and so the 28 candidates rejected at this stage remain viable if there is a potential NSBH EM counterpart model that matches any of the criteria on which we cut. In particular, we directly compare our empirical limits on the minimum absolute magnitude and decline rate (Section 4.5) to these candidates in order to highlight that our limits are consistent with sources discovered by our surveys and in the literature. However, our photometric constraints are the weakest criteria for ruling out candidate counterparts and only pertain to candidates that cannot be ruled out in any other context.

4. LIMITS ON ELECTROMAGNETIC COUNTERPARTS

Having ruled out all known candidate optical transients as viable counterparts to GW190814, we estimate the depth of all of our imaging and show our results for every individual image in Table 4. In the remainder of this section, we then analyze these limits in the context of model optical counterparts to GW190814 and place constraints on the properties of any hypothetical counterpart.

4.1. Estimates of the Limiting Magnitude

4.1.1. 1M2H

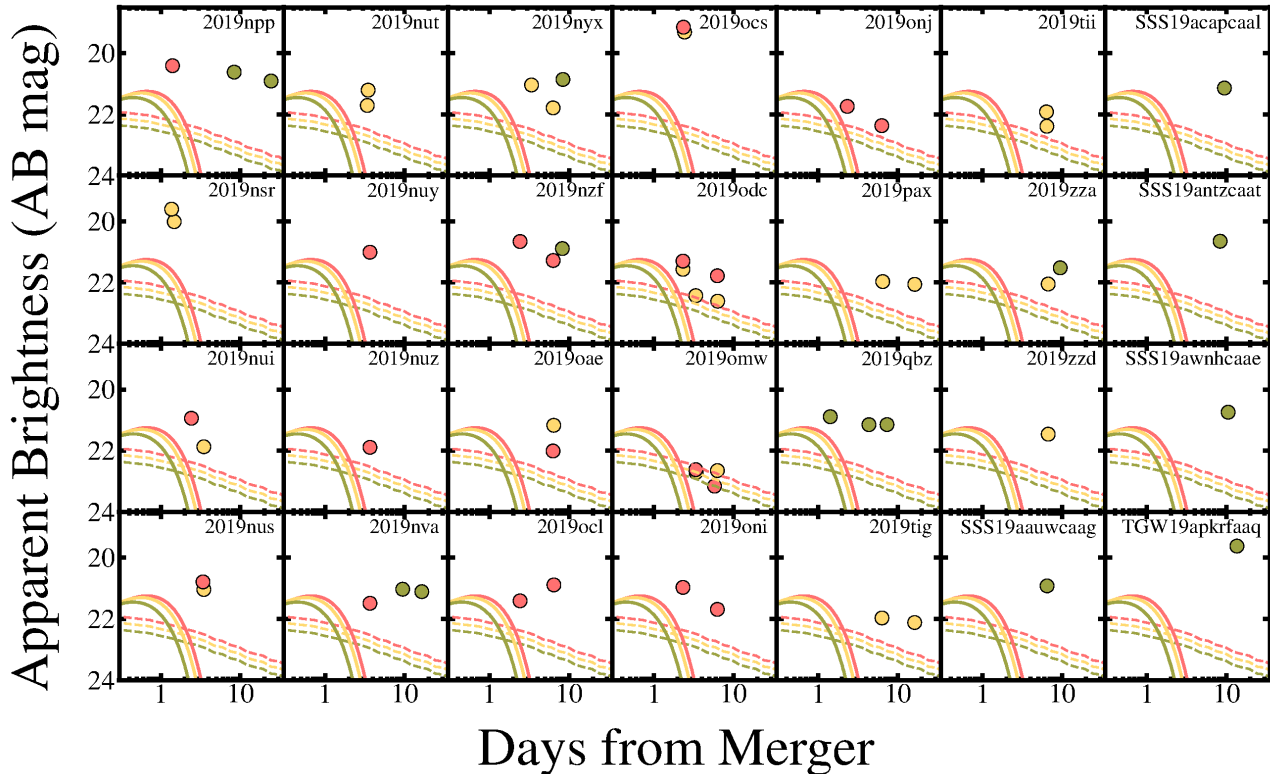


Figure 5. *riz* (green, yellow, and red, respectively) light curves of candidate counterparts to GW190814 that we ruled out on the basis of photometric cuts as described in Section 3.5. We show photometry from our own follow up (Table 6), DECam (Andreoni et al. 2019a; Morgan et al. 2020), and VLT-GRAWITA (Ackley et al. 2020) for each source that we rule out on the basis of light curve parameters. For comparison, we show blue kilonova light curves (solid lines) and γ -ray burst afterglow light curves corresponding to the off-axis GRB 170817A analog (dashed lines) corresponding to the models shown in Figure 2. We place each model light curve at the distance of each candidate using redshift information where available or the luminosity distance at its location in the GW190814 localization map (from Abbott et al. 2020a). In general, the detected candidates are significantly more luminous than the models we consider and at the observed epochs, which enable us to rule out these candidates as too luminous to be a counterpart to GW190814 in Table 2.

We estimate limiting magnitudes for Nickel, Swope, and Thacher difference images by planting artificial sources in each individual survey image, allowing us to determine the probability of finding a source as a function of magnitude. This procedure requires the following steps.

1. *Building the PSF model:* The PSF parameters for each image are determined by DoPhot (Schechter et al. 1993). We then rescale the PSF model such that the magnitude determined from the sum of the pixels in the model (given the predetermined zeropoint of the image) is equal to the magnitude we wish to simulate.
2. *Planting the artificial sources:* For each image, we plant 1500 artificial sources in the regular, unsubtracted survey image. These sources are randomly placed across the image, with magnitudes randomly chosen from a flat distribution between 18 and 25 mag.
3. *Running the reduction pipeline:* Once the sources have been planted, we run the difference-imaging and source-detection pipeline with the exact same

pipeline stages used for transient discovery, beginning at the difference-image stage to incorporate correlated pixel noise and subtraction artifacts into the detection-efficiency calculation. We have verified that using 1500 sources does not adversely affect the quality of the difference images.

4. *Measuring the detection efficiency:* For bins of 0.2 mag, we compute the detection efficiency by dividing the fraction of sources detected in the difference image by the total number of simulated sources within that magnitude bin. This gives us the full detection efficiency as a function of magnitude, as well as the magnitude at which 50% of artificial sources are recovered. We define the 3σ limiting magnitude by interpolating our efficiency curves to the magnitude at which 99.7% of the average maximum fraction of recovered sources at any magnitude are at least as bright as that magnitude threshold. This fraction can be less than 100% if sources land on cosmic rays or on top of very bright stars, and we reweight our detection efficiency for that

image by the maximum recovered fraction. These values correspond to the limiting magnitudes given for Nickel, Swope, and Thacher images in Table 4.

These steps allow an “end-to-end” measurement of image-detection efficiency that includes correlated noise from the difference image convolution procedure and the ability of our automated software to recover point sources in our images. Correlated difference image noise in particular would not be measurable from a simple sky-background-based computation. These limits are also consistent with our cuts in transient identification, which are based on the same pipeline and identification process.

As discussed above, the limiting magnitude in KAIT and Las Cumbres images was estimated using the 3σ scatter in the background measured across each image.

4.2. Constraints on EM Counterparts to GW190814

We have demonstrated that there is no candidate counterpart to GW190814 in Section 3. In the following analysis, we determine the joint limits on the presence of an EM counterpart to GW190814 using all difference imaging (neglecting our template images and Keck/MOSFIRE images for which we do not have templates). In practice, this involves comparison between the expected in-band light curves for various transient sources and the 3σ limiting magnitudes as a function of sky position and time relative to merger reported in Table 4. In order to provide a physically meaningful limit, we emphasize that our uniform sample of difference images is reduced self-consistently with (1) template exposures of each targeted field obtained in the same filter and instrumental configuration, (2) true PSF-convolved difference imaging between all science exposures and the template exposures as described in Section 2, and (3) limiting magnitudes derived in the difference images themselves and consistent with the signal-to-noise ratio of any detected transient sources. In this way, we are confident that our limiting magnitudes rule out any EM counterparts across our imaging to the magnitude level quoted in Table 4. We emphasize that while our limiting magnitudes account for Milky Way extinction in the direction of each image, we assume there is no additional source of extinction, for example in the host galaxy or local environment of the GW190814 progenitor system.

We obtained the latest GW190814 HEALPix¹⁵ (Górski et al. 2005) sky-localization map from the Gravitational-Wave Candidate Event Database¹⁶ and presented by Abbott et al. (2020a). All observations and limiting magnitudes reported in Table 4 were then ingested into our GW planning and analysis code `teglon` (see Sec-

tion 2) and crossmatched to the corresponding HEALPix pixel elements. At each pixel, we estimated the mean and standard deviation of the best-fitting LVC distance using the `moments_to_parameters` from the `ligo.skymap.distance` Python package (Singer et al. 2016a,b). Each resulting Gaussian is then truncated at zero distance and renormalized such that the total three-dimensional probability (i.e., integrated over all sky pixels and luminosity distances) is unity.

We then consider the likelihood that an optical counterpart to GW190814 would be detected for a given counterpart model, which we generically classify as kilonovae (Section 4.3), sGRBs (Section 4.4), and linearly-evolving optical counterparts (Section 4.5). Each model provides an estimate of the brightness of the counterpart as a function of time, wavelength, and distance, which we transform to in-band light curves using `pysynphot`.

Over the GW190814 localization region, most areas were observed with multiple images and in multiple filters. Therefore, to compute the net detection efficiency given all sky map pixels and all observations, we determine the detection efficiency in a given model for each sky map pixel across each epoch and filter, and then combine the result into a cumulative detection efficiency. To do this, we retrieve the absolute magnitude for a given model at the time and in the band of each observation. Our inferred detection efficiency is also dependent on specific image- and line-of-sight dependent quantities, for example the Milky Way extinction and limiting magnitude as described in Section 4.1.

We then reparameterize our limiting magnitude in terms of the distance $D_{\text{model},j,f}$ at which we would expect to detect a source in image j with a filter f and a limiting magnitude $m_{j,f}$, where the source has an absolute magnitude $M_{\text{model},j,f}$ and line-of-sight extinction A_f , as

$$\mu_{\text{model},j,f} = m_{j,f} - M_{\text{model},j,f} - A_f \quad (1)$$

$$D_{\text{model},j,f} [\text{Mpc}] = 10^{0.2 \times (\mu_{\text{model},j,f} - 25)}. \quad (2)$$

For each pixel i in the LVC localization map that overlaps with image j , we then calculate the relative efficiency of detecting this model by integrating the pixel distance distribution from zero distance to $D_{\text{model},j,f}$,

$$P_{\text{model},i,j} = \frac{1}{\sqrt{2\pi}\sigma_{D_i}} \int_0^{D_{\text{model},j,f}} e^{-\frac{1}{2}\left(\frac{\bar{D}_i - D}{\sigma_{D_i}}\right)^2} dD, \quad (3)$$

where \bar{D}_i is the mean distance and σ_{D_i} is its standard deviation corresponding to the pixel i in the localization map.

To combine independent observations that overlap with each pixel, we take the complement of the joint probability that we do not see the source in any epoch. That is, for each

¹⁵ <http://healpix.sourceforge.net>

¹⁶ <https://gracedb.ligo.org/>

pixel, we weight the relative likelihood that we would detect a specific model in image j by the LVC 2D pixel probability in each pixel P_i and sum over all pixels to obtain a cumulative probability of detecting a specific model,

$$P_{\text{model}} = \sum_i P_i \left[1 - \prod_j (1 - P_{\text{model},i,j}) \right]. \quad (4)$$

This final probability, which we interpret as the likelihood that we would have seen a source with properties described by a model for the EM counterpart to GW190814, is calculated for a wide range of models described below.

4.3. Limits on Kilonovae

The counterpart to GW170817 was initially localized by targeting optical emission from a kilonova (Abbott et al. 2017d; Coulter et al. 2017; Kasen et al. 2017), or a transient powered by the decay of r -process species synthesized in ejecta from a NS merger. As in Kilpatrick et al. (2017), we parameterize this source for a given ejecta mass m_{ej} and velocity v_{ej} . Following the numerical model presented by Metzger (2017) and used by Coughlin et al. (2019, 2020a), we allow for a varying electron fraction Y_e in the ejecta, which affects the neutronization and thus the composition of the ejecta. Broadly speaking, low electron fractions will lead to a high level of neutronization and thus heavier r -process species, which tend to be more optically thick at the optical and near-infrared wavelengths of our search. The electron fraction and distribution of r -process species have a secondary effect on the radioactive heating rate (e.g., see Lipunov & Roberts 2015), which is incorporated into our light curves, but the ejecta opacity is the dominant effect of varying Y_e .

In order to accurately estimate the ejecta opacity as a function of electron fraction, we adopt the mean opacity for kilonovae with varying compositions presented by Tanaka et al. (2020, see their Table 1) but with a floor of $\kappa = 1.0 \text{ cm}^2 \text{ g}^{-1}$ for $Y_e > 0.40$. This results in relatively high opacities of $\kappa > 30.0 \text{ cm}^2 \text{ g}^{-1}$ for $Y_e \lesssim 0.15$, and so this model is somewhat pessimistic compared with similar treatments by Andreoni et al. (2020) and Coughlin et al. (2020a). However, we are confident that our models accurately reflect a broad range of ejecta composition for varying masses and velocities.

We estimated the in-band light curves for ejecta masses $0.001\text{--}0.5 M_\odot$ and velocities $(0.001\text{--}0.5)c$. We show our estimated probability of detection for our fiducial models, a “red” kilonova ($Y_e = 0.10$) and a “blue” kilonova ($Y_e = 0.45$), in Figure 6.

4.4. Limits on sGRBs

We adopted the models of Duffell & MacFadyen (2013) and Wu & MacFadyen (2018) to model potential sGRB opti-

cal counterparts to GW190814. We parameterize these models by the isotropic kinetic energy $E_{K,\text{iso}}$ and the circumburst density n as well as the viewing angle of the sGRB jet θ_{obs} (assuming a jet opening angle identical to GRB170817A of $\theta_0 = 5.2^\circ$). In addition to these variables, we assume that the specific internal energy $\eta_0 = 7.9$, boost Lorentz factor $\gamma_B = 9.4$, spectral index $p = 2.15$, electron energy fraction $\epsilon = 0.1$, and magnetic energy fraction $\epsilon_B = 2.5 \times 10^{-4}$ from the updated GRB170817A analysis by Wu & MacFadyen (2019).

We model a range of isotropic kinetic energies (10^{48} to 10^{52} erg) and circumburst densities (10^{-6} to 1 cm^{-3}), roughly spanning the range of sGRB jet parameters presented by Fong et al. (2015). In addition, we model two jet viewing angles — an on-axis model with $\theta_{\text{obs}} = 0^\circ$ and an off-axis model with $\theta_{\text{obs}} = 17^\circ$ (see characteristic light curves in Figure 2). In the latter case, the afterglow light curve is still rising after our latest observations of the GW190814 field, and so our limits are primarily sensitive to the luminosity of the afterglow during our last observation epoch, corresponding to Swope and Nickel observations obtained on 10–11 Sep. 2019 with 3σ limiting magnitudes around $r = 20.0\text{--}21.5$ mag. Our limits are mostly insensitive to sGRB afterglow light curves with jet viewing angles greater than 17° assuming a jet opening angle of $\theta_0 = 5.2^\circ$ as in Wu & MacFadyen (2018).

4.5. Generic Limits on EM Counterparts

The final set of models we consider is defined empirically using a peak absolute magnitude and linear decline rate in units of mag day^{-1} . As kilonovae and sGRBs are rapidly evolving with extremely short rise times (i.e., for kilonovae with physical parameters similar to those of AT 2017gfo and sGRBs viewed on-axis; Arcavi et al. 2017a; Drout et al. 2017; Kilpatrick et al. 2017), we model these generic EM counterparts with a peak brightness at the time of merger as defined by the GW signal. In order to combine our limits across all wavelengths used to follow up GW190814, we further assume that the model counterpart has a flat spectral energy distribution such that the source has the same magnitude in all bands.

Following the procedure outlined above, we combine all of our limits into a likelihood of detection assuming a uniform range of peak absolute magnitudes (from -15 to -20 mag) and decline rates (from 3×10^{-3} to 1 mag day^{-1} in log space) as shown in Figure 8. For comparison, we show our joint limits along with the peak magnitudes and decline rates of various astrophysical transient sources (taken from Siebert et al. 2017).

Although our limiting magnitudes are relatively strong compared with SNe and other luminous transient sources, our empirical limits only extend to -16 mag (≈ 21 mag at

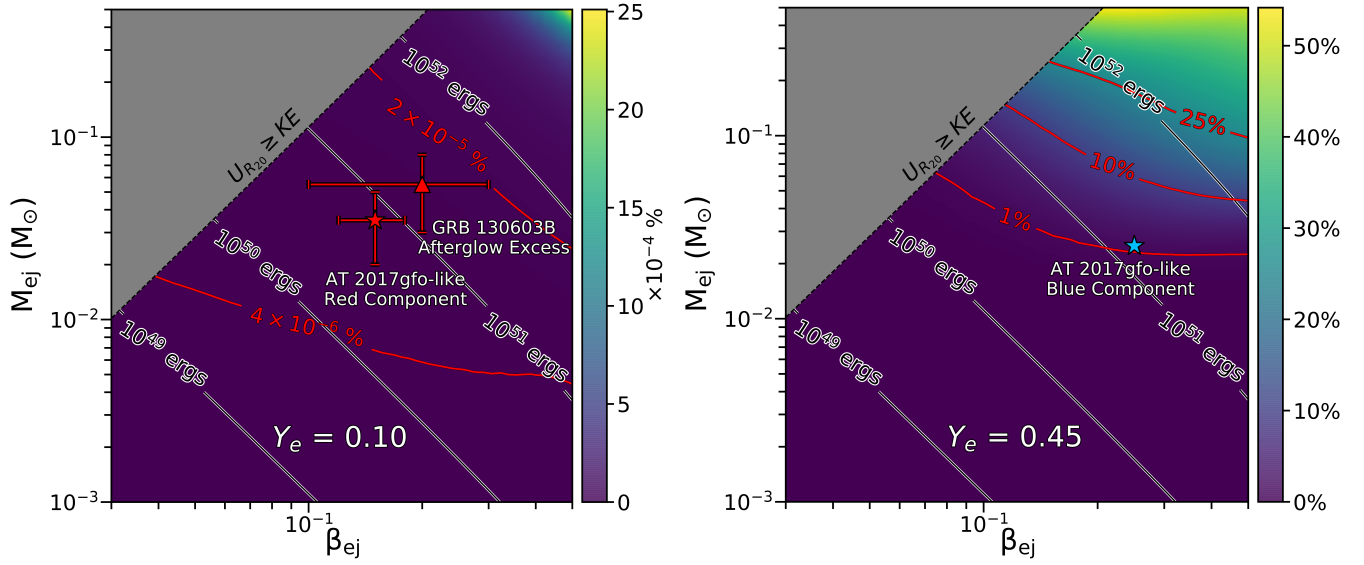


Figure 6. Constraints on the presence of a kilonova assuming an electron fraction corresponding to a “red” kilonova ($Y_e = 0.10$, *left*) and a “blue” kilonova ($Y_e = 0.45$, *right*). For both sets of models, we show the estimated likelihood that we would have detected a source for a given ejecta mass (m_{ej} in M_\odot) and velocity (β_{ej} in natural units) following the procedure in Section 4.2. We have grayed out the region where the binding energy of the ejecta (assuming an extremely stiff neutron star radius of 20 km) exceeds its kinetic energy. For context, we show contours of equal probability in red and lines of equivalent ejecta kinetic energy in black. Finally, in each panel we show the location of the corresponding kilonova ejecta component AT 2017gfo as derived by Kilpatrick et al. (2017) (specifically $\beta_{\text{ej}} = 0.15$, $M_{\text{ej}} = 0.035 M_\odot$ for the red kilonova and $\beta_{\text{ej}} = 0.25$, $M_{\text{ej}} = 0.025 M_\odot$ for the blue kilonova) as well as the putative kilonova counterpart to GRB130603B as described by Tanvir et al. (2013).

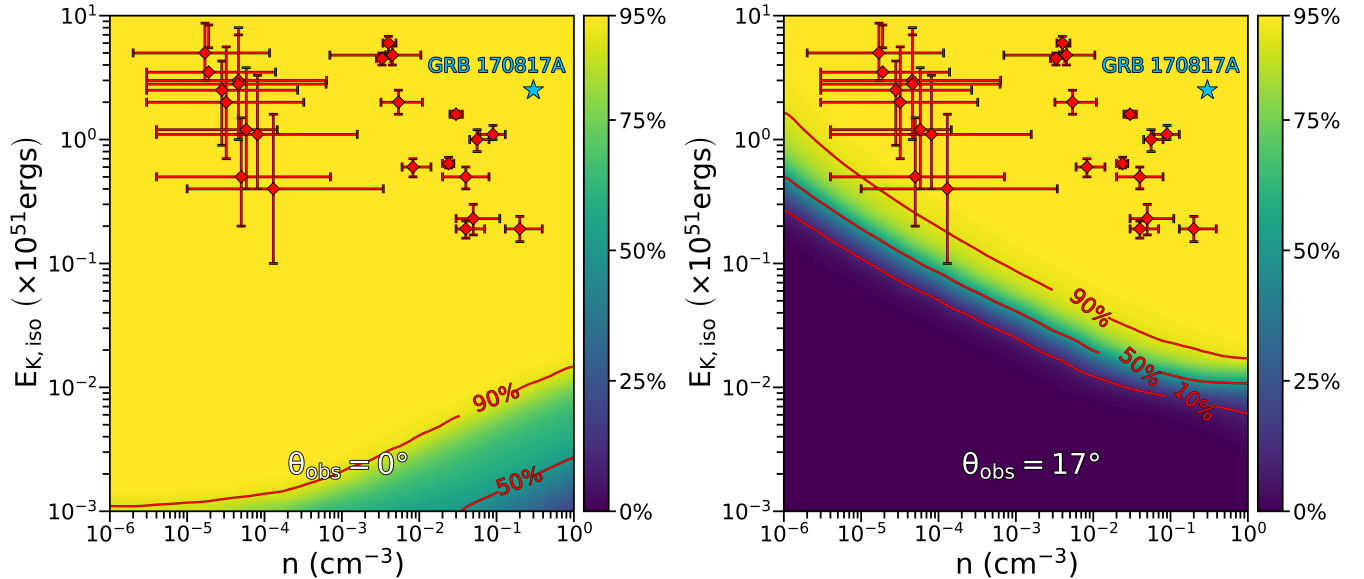


Figure 7. Constraints on the presence of an sGRB viewed on-axis (*left*, $\theta_{\text{obs}} = 0^\circ$) and off-axis (*right*, $\theta_{\text{obs}} = 17^\circ$). In both cases, we show the total observed two-dimensional LVC probability weighted by the likelihood that we would observe a counterpart with a specific explosion energy (E in units of $10^{51} \text{ ergs}^{-1}$) and circumburst density (n in units of cm^{-3}).

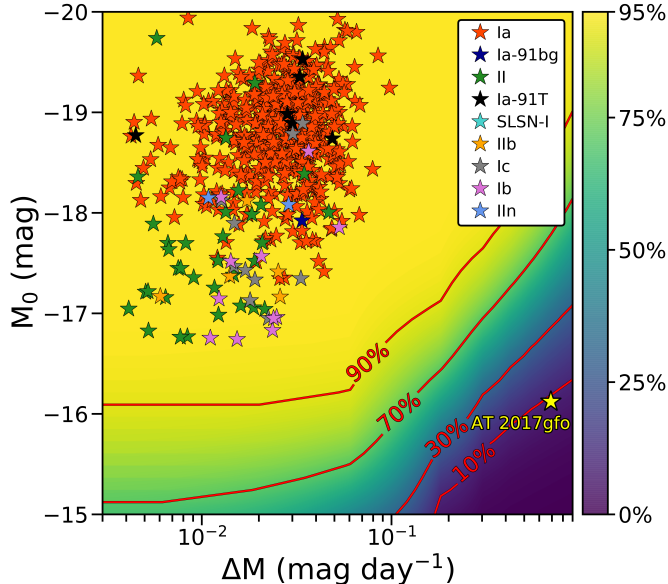


Figure 8. Constraints on the presence of a generic optical counterpart assuming peak magnitude M_0 occurs approximately at the time of merger (t_0) and the source declines at a linear rate ΔM in mag day^{-1} . We further assume that the counterpart has a flat spectral shape at all times such that its magnitude is $M_0 + (t - t_0) \Delta M$ in all bands for all times t . We show the properties of AT 2017gfo with a yellow star with r -band peak -16.5 mag and decline rate 0.3 mag day^{-1} (based on Siebert et al. 2017; Drout et al. 2017). For comparison, we show the peak magnitudes and decline rates of a range of other optical transients derived from Siebert et al. (2017). We rule out a AT 2017gfo-like counterpart (yellow star) with 6.0% confidence.

240 Mpc) for slowly-evolving (declining at $<0.1 \text{ mag day}^{-1}$) events given that we observed the GW190814 localization over 3–4 days. This places AT 2017gfo-like transients outside of what we can detect, as it began to decline at $>0.3 \text{ mag day}^{-1}$ in blueward of i -band at less than 1 day from merger (Drout et al. 2017).

5. DISCUSSION

In this section, we describe the physical implications of our limits in the context of candidate EM counterpart models described in Section 4. As the total area covered by our observations comprises $\sim 95\%$ of the total two-dimensional probability in the latest GW190814 map, the strongest constraints on EM counterparts are at this significance level. We then discuss further implications of these limits in the context of likely merger models, incorporating the gravitational-wave data from Abbott et al. (2020a). Finally, in Section 5.3 we consider the scenario where GW190814 occurred in an AGN disk.

5.1. Joint Limits on Electromagnetic Counterparts

For an AT 2017gfo-like blue kilonova as described in Section 4.2, we estimate a 50% chance of detecting the counter-

part at distances <95 Mpc. However, the overall probability of detection given the best-fitting LVC distances for this source is around 1%. As shown in Figure 2, these limits are dominated by our early-time observations, as the kilonova models decline rapidly overall. Similarly, the probability of detecting an AT 2017gfo-like red kilonova is extremely low at $\sim 4 \times 10^{-7}\%$, which is also mainly constrained by our early-time Swope r -band and Las Cumbres i -band observations. We are only sensitive to red kilonovae under the assumption that the true distance to GW190814 is much closer (<80 Mpc) than the reported LVC best-fitting distance. Finally, if the counterpart had colors between the blue and red model but the same overall luminosity as AT 2017gfo, the recovery fraction would likely be between the red-only and blue-only numbers.

Inverting these constraints, we are sensitive to the blue kilonova models with $\beta_{\text{ej}} = 0.25$ and $M_{\text{ej}} > 0.5 M_{\odot}$ at 30% significance or $M_{\text{ej}} > 0.3 M_{\odot}$ at 25% significance. These limits are extreme for GW190814, especially considering that even the most optimistic merger models for a $2.59 \pm 0.08 M_{\odot}$ and $23.2^{+1.0}_{-0.9} M_{\odot}$ NSBH merger predict effectively no ejecta mass.

Our limits for GRB models are significantly more constraining given plausible counterparts and small viewing angles. In particular, we find that all on-axis models are ruled out at our maximum 95% likelihood except for the most extreme low-energy ($\sim 10^{48}$ erg) bursts. In particular, we would have seen the on-axis optical afterglow of a burst similar to any of the bursts described by Fong et al. (2015) or a GRB170817A-like on-axis optical afterglow (following $n = 0.3 \text{ cm}^{-3}$ and $E_k = 2.5 \times 10^{51}$ erg in Murguia-Berthier et al. 2017). Varying the physical parameters of these on-axis, GRB170817-like bursts in Figure 7, we can rule out bursts with circumburst density $n = 0.3 \text{ cm}^{-3}$ and isotropic equivalent energy $E_k = 2.5 \times 10^{51}$ erg at 95% significance, $n = 0.3$ and $E_k = 2.5 \times 10^{48}$ erg at 50% significance, and $n = 10^{-6} \text{ cm}^{-3}$ and $E_k = 2.5 \times 10^{51}$ erg at 95% significance. These limits are consistent with the non-detection of GRBs by INTEGRAL, which observed the localization region of GW190814 117° off axis and constrained the isotropic equivalent energy of the burst to be $< 2.1 \times 10^{48}$ erg for a short GRB spectrum with spectral index $\alpha = -0.5$ (assuming $D_L = 239$ Mpc; Molkov et al. 2019). Similar measurements from just a few sources can lead to statistical constraints on jet geometries (Farah et al. 2020).

For larger jet viewing angles (θ_{obs}), but a fixed jet opening angle of $\theta_0 = 5.2^\circ$, we are increasingly less sensitive to optical afterglows, primarily because the optical luminosity is significantly lower at early times where the majority of our limits are. Beyond $\theta_{\text{obs}} > 17^\circ$, we are no longer able to rule out optical afterglows from GRBs similar to those of

Fong et al. (2015). In physical terms, we can rule out off-axis optical afterglows from bursts with $n = 0.3 \text{ cm}^{-3}$ and $E_k = 2.5 \times 10^{51} \text{ erg}$ at 95% significance, $n = 0.3$ and $E_k = 2.5 \times 10^{49} \text{ erg}$ at 50% significance, and $n = 10^{-6} \text{ cm}^{-3}$ and $E_k = 2.5 \times 10^{51} \text{ erg}$ at 62% significance. GW190814 had an inclination angle constrained from its gravitational wave signal of $40\text{--}70^\circ$ (Abbott et al. 2020a) implying that any associated afterglow was likely to be even further off axis and thus undetectable by our follow up.

Finally, our limits are comparable to the luminosities of most SNe and optical transients similar to those discussed as interlopers to potential GW counterparts by Siebert et al. (2017). As shown in Figure 8, while we would be able to detect or rule out the presence of virtually all SN subtypes at 241 Mpc, we would likely not be able to detect an AT 2017gfo-like transient (ruled out at 6.0% significance), which is consistent with kilonova model limits.

Assuming a faint counterpart with $\Delta M = 0.68 \text{ mag day}^{-1}$ (similar to the initial r -band decline rate for AT 2017gfo; Drout et al. 2017; Siebert et al. 2017), we rule out sources with $M_{\text{peak}} < -17.8 \text{ mag}$ at 50% significance. Similarly, if we assume that the initial magnitude of the source at the time of merger is similar to that of AT 2017gfo with $M_r = -16.1 \text{ mag}$, we can rule out sources that decline with $\Delta M = 0.06 \text{ mag day}^{-1}$ at 50% significance.

5.2. Combining GW and EM Data for GW190814

With the release of detailed fits to the GW data for GW190814, including component masses, spin constraints, and inclination (Abbott et al. 2020a), we can place more meaningful limits on likely merger scenarios and possible electromagnetic counterparts than with the initial NSBH classification. In particular, the LVC constrained the individual component masses as $2.59 \pm 0.08 M_\odot$ and $23.2^{+1.0}_{-0.9} M_\odot$ (Abbott et al. 2020a). While these final component masses are consistent with the initial NSBH classification, they imply that there is likely very little ejecta mass under most realistic merger models (Faber et al. 2006; Lee & Ramirez-Ruiz 2007; Ferrari et al. 2010; Roberts et al. 2011; Rosswog et al. 2013), consistent with the `HasRemnant=0` statistic.

However, several studies have suggested that the secondary component in this system is likely a NS (Huang et al. 2020; Zhang & Li 2020; Zevin et al. 2020; Tews et al. 2021), although see counterarguments that this component may exceed the maximum NS mass (Akmal et al. 1998; Heger & Woosley 2002; Lattimer & Prakash 2007; Foley et al. 2020). Assuming GW190814 resulted from a NSBH system, our limits place constraints both on parameters that are also constrained by the LVC such as the effective inspiral spin parameter (i.e., the total spin with respect to the orbital plane of the binary, χ_{eff}) and unconstrained parameters such as the NS equation of state. We consider the effect of varying both

of these parameters in the context of our limits on kilonova ejecta mass and velocity.

Using our constraints on ejecta mass and velocity from above for a “blue” kilonova, we consider the extent to which we can rule out different values of χ_{eff} . For the former, we consider a range of $\chi_{\text{eff}} = 0.01, 0.5, \text{ and } 0.995$ (where the first value is consistent with the effective-one-body approach waveform parameters, which imply $\chi_{\text{eff}} = 0.001^{+0.059}_{-0.056}$, in Abbott et al. 2020a). The last value implies a near-maximally spinning BH, which is inconsistent with the general population of BH binaries observed by the LVC (e.g., Abbott et al. 2016b,c, 2017a), but might be obtained in binary populations that evolve from high-mass X-ray binaries (which can have near-maximal spins; McClintock et al. 2006) or evolve through a common-envelope phase (Livio & Soker 1988; Belczynski et al. 2016).

Assuming an ejecta mass and velocity as a function of the binary component masses m_1 and m_2 and fixed χ_{eff} , we predict the total ejecta mass and velocity using equations in Kawaguchi et al. (2016). We then use our blue kilonova models to predict the extent to which we could rule out such a model (Figure 9, where the color corresponds to P_{model} as in Section 4.2). We assume a phenomenological NS equation of state that predicts $R_{\text{NS}} = 13.6 \text{ km}$ for a Chandrasekhar-mass NS (H4 in Read et al. 2009), whereas a $2.6 M_\odot$ NS would have a radius of $\approx 12 \text{ km}$ assuming this equation of state and the formalism in Kawaguchi et al. (2016). However, given the extreme mass ratio of GW190814, ejecta masses in the range of our blue kilonova limits would require a near maximally spinning BH and an unrealistic equation of state to produce any ejecta mass.

From the group of models, we only rule out the GW190814 system with significance $P_{\text{model}} > 20\%$ (see definition of P_{model} in Section 4.2) when $\chi_{\text{eff}} > 0.995$ (Figure 9). As we decrease the value of χ_{eff} , the value of P_{model} decreases significantly below 0.1%.

The availability of robust component masses and spin parameters beyond what can be inferred with low-latency LVC parameters (i.e., NSBH classification and `HasRemnant`) has an enormous impact on the predicted observability of EM counterparts. Furthermore, this problem is unique to NSBH follow-up programs where no plausible counterparts have been found. Specific component masses and spins may or may not yield significant ejecta depending on the assumptions we make above about the specific merger model and equation of state.

5.3. Constraints on AGN Counterparts to GW190814

AGNs have been discussed as potential optical counterparts to BBH mergers (Bartos et al. 2017; Antoni et al. 2019; Gröbner et al. 2020), and the discovery of an optical flare timed 34 days after and in the localization region of the BBH

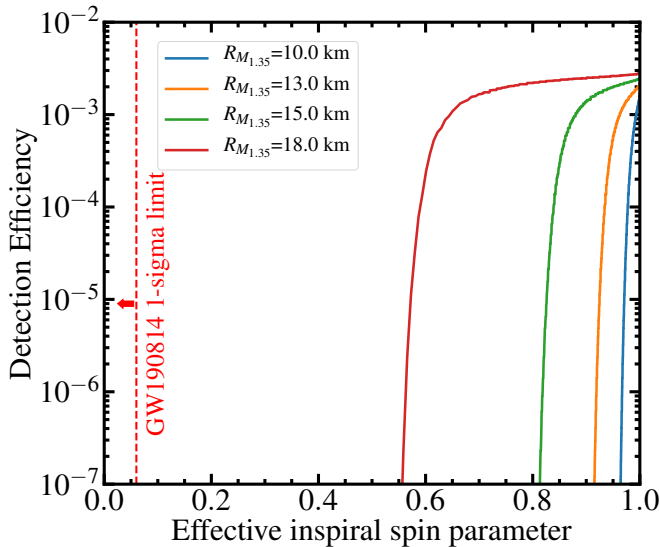


Figure 9. Detection efficiency for kilonovae (described in Section 4.3) as a function of the effective inspiral parameter (χ_{eff} , which is constrained to be < 0.06 for GW190814 by Abbott et al. 2020a). We marginalize over the best-fitting component masses for GW190814, which are $23.2^{+0.9}_{-1.0} M_{\odot}$ and $2.59 \pm 0.08 M_{\odot}$ based on the effective-one-body approach described by Abbott et al. (2020a). We use these parameters to infer kilonova ejecta mass and velocity following methods in Kawaguchi et al. (2016) and assuming various equations of state parameterized by radii of a $1.35 M_{\odot}$ NS from 10–18 km. Based on these constraints, it is not expected that there would be significant ejecta mass with parameters inferred for GW190814 even if the secondary is an NS.

merger S190521g/GW190521 (Graham et al. 2020; Abbott et al. 2020c) provides a credible candidate optical counterpart to this phenomenon (although Ashton et al. 2020, suggest there is insufficient evidence to confidently associate the AGN with GW190521). AGN activity is a result of massive gas inflows to a supermassive BH, and as a result of that cause compact object mergers have been explored in the literature (e.g., Stone et al. 2017), and so the compact object merger rate is thought to be significantly enhanced in the disks of these systems. If these systems can form in the disk environment, it is plausible that a significant fraction of LVC counterparts could originate from galaxies with AGNs.

Critically, when a compact object merger occurs in the AGN disk, it can induce an instability in the inflow of gas to the accreting BH, leading to a luminous transient (as is hypothesized to be the case for the S190521g candidate counterpart; McKernan et al. 2012; Antoni et al. 2019; Graham et al. 2020). Thus, the AGN model provides some predictive power for candidate optical counterparts, even in cases where no significant mass of baryonic ejecta is expected from the merger itself.

Here we examine what constraints can be placed on the distance to and localization of GW190814 under the assump-

tion that the event occurred in a known AGN inside the GW190814 localization region. We analyzed the AGN catalog of Secrest et al. (2015), which is selected from Mid-infrared *WISE* constraints and contains 1.4 million AGNs down to as faint as $g = 26$ mag. The catalog is estimated to be complete for known AGNs to $> 84\%$ and for all AGNs with $R < 19$ mag. Therefore, for AGNs with $z < 0.1$, the catalog is expected to be close to $> 90\%$ complete.

For this analysis, we only consider AGNs that (1) are within the 99th percentile localization region of GW190814, and (2) have a redshift that places it within the 99th percentile volume as described in Section 3. Based on these criteria, we do not identify any AGNs with redshifts listed in the Secrest et al. (2015) catalog or NED.

However, a major caveat to this analysis is that the majority of AGNs do not have measured redshifts, and so most objects would be ruled out for lying outside the volume we consider here. For example, we find 1886 AGNs that match only criterion #1 above. If we consider what fraction of those objects without spectroscopic redshifts lie within $2''$ of a source in the PS1-STRM catalog with a photometric redshift that places them in the 99th percentile volume, we are left with only 4 candidates without redshifts in Secrest et al. (2015). We list these sources along with their photometric redshifts in Table 3.

We note that none of these systems is coincident with any of our candidate counterparts to GW190814 (Table 5) or any transients listed in the Transient Name Server to within $5''$. Thus, while we consider the AGNs as candidate hosts to GW190814, any hypothetical EM counterparts induced by the merger would have to be low luminosity.

The AGN flare luminosity would scale as the total mass of the merging binary M_{NSBH}^2 as in Bartos et al. (2017) and Antoni et al. (2019). Following Equation (5) of Graham et al. (2020) for the total luminosity of such an EM counterpart with radiative efficiency $\eta = 0.1$, kick velocity for the binary in an AGN disk $v_k = 200 \text{ km s}^{-1}$, disk gas density $\rho = 10^{-10} \text{ g cm}^{-3}$, and using the total mass M_{tot} of the GW190814 merger $25.8 M_{\odot}$ (Abbott et al. 2020a), we find that the luminosity would be $L = 1.6 \times 10^{44} \text{ erg s}^{-1}$, or $M_{\text{bol}} = -21.8$ mag, which corresponds to 15.1 mag at $D_L = 241 \text{ Mpc}$. A source with this brightness is easily ruled out near our maximal efficiency ($\sim 95\%$) assuming it occurred within the 2-week time frame of our observations. On the other hand, the luminosity is easily scaled down for a lower density in the AGN disk, a higher kick velocity, or a lower radiative efficiency in the AGN.

Based on the associated AGN model of Graham et al. (2020), we would expect to see flaring activity of GW190814 if one of these objects had been associated with the merger. Therefore, we examined the ASAS-SN Sky Pa-

Table 3. Candidate AGN Hosts for GW190814

Name ^a	α (J2000)	δ (J2000)	Relative Prob. ^b	Redshift ^c
J012323.69-310826.4	01:23:23.70	-31:08:26.43	0.476	0.021±0.002
J005203.80-272348.9	00:52:03.80	-27:23:48.92	0.210	0.079±0.004
J004801.90-215442.2	00:48:01.90	-21:54:42.22	0.082	0.058±0.001
J004002.26-235053.0	00:40:02.27	-23:50:53.03	0.232	0.071±0.004

^a Name of the AGN in the GW190814 localization region in the WISEA catalog from [Secrest et al. \(2015\)](#).

^b Relative probability of each AGN given the latest GW190814 map provided by [Abbott et al. \(2020a\)](#) such that the sum of all probabilities is unity.

^c Redshift of matching counterpart given in the PS1-STRM catalog, as all candidate AGNs detected in the GW190814 localization region are matched to sources with photometric redshifts in [Beck et al. \(2021\)](#) apart from WISEA J005720.19-222256.5, whose spectroscopic redshift is derived from [Jones et al. \(2009\)](#).

tro¹⁷ ([Shappee et al. 2014](#); [Kochanek et al. 2017](#)) to determine whether there is any flaring activity potentially associated with the GW event. Although variability is detected for WISEA J005203.80-272348.9, J004801.90-215442.2, and J004002.26-235053.0 after the GW190814 merger, none of them exhibits a $> 10^{44}$ erg s⁻¹ increase in flux on a timescale of < 8 weeks from the GW event. We conclude that these candidates are unlikely to be associated with GW190814.

We also revisit the sources AT 2019nto or AT 2019nup discussed in [Section 3.3](#), which we had previously ruled out as being associated with GW190814 owing to significant pre-merger variability. This type of variability could occur in the scenario where GW190814 triggered activity in an already active accreting supermassive BH. In both cases, there is a credible optical counterpart, although both are significantly fainter (~ 20.8 mag) than we predict for an AGN counterpart at the distance to GW190814. Both events have nearly continuous coverage from the ASAS-SN Sky Patrol up to ~ 170 days from the time of merger. A source is detected at the site of AT 2019nto twice during that interval > 100 days from the time of merger, and AT 2019nup is detected almost continuously during that time but with no > 1 mag increases in brightness. If either of these objects is associated with an AGN from GW190814, that event would need to occur with an extremely low radiative efficiency ($\eta < 0.01$) or from a disk with a much lower gas density ($\rho < 10^{-12}$ g cm⁻³) compared with the model presented above.

One of the primary difficulties in detecting an AGN counterpart to a GW source is the dynamical timescale for perturbations in the disk to induce enhanced accretion in the AGN and trigger a flare. This dynamical timescale t_{dyn} (Equation 6 of [Graham et al. 2020](#)) is only ~ 5 days assuming that the

kick velocity $v_k = 200$ km s⁻¹. On the other hand, t_{dyn} scales as v_k^{-3} , and so for a marginally lower kick velocity it could easily be outside of the window of our observations (and the flare of significantly lower luminosity, as above). While this velocity needs to remain small enough that the system remains bound to the disk of the AGN to trigger a flare, scaling the kick velocity in a fixed-mass AGN and at a fixed orbital semimajor axis suggests that $v_k \propto M_{\text{tot}}^{-1/2}$, or ~ 400 km s⁻¹ compared with 200 km s⁻¹ for the BBH system of [Graham et al. \(2020\)](#).

Regardless of the presence of an EM counterpart to validate the AGN counterpart hypothesis, if we assume that the event occurred in such an environment we can obtain separate constraints on the distance to this event. There is a single AGN (WISEA J004506.98-250147.0) that represents $> 50\%$ of the normalized two-dimensional probability for GW190814 after renormalizing under the assumption that one of these candidates is the host. Accounting for the individual uncertainties and weighting by this local two-dimensional probability, we find that the best-fitting redshift is $z = 0.052 \pm 0.017$ or $D_L = 233 \pm 80$ Mpc. Compared with the GW190814 distance marginalized over the entire localization region, this inferred distance is more uncertain.

6. CONCLUSIONS

We have presented results from the joint follow-up observations of the LVC NSBH merger GW190814. Our combined constraints from optical imaging and spectroscopy demonstrate the following.

1. There are no plausible optical counterparts detected by our programs or those of any other optical or radio follow-up groups ([Gomez et al. 2019b](#); [Dobie et al. 2019a](#); [Andreoni et al. 2020](#); [Morgan et al. 2020](#); [Thakur et al. 2020](#); [Watson et al. 2020](#); [Vieira et al. 2020](#); [Ackley et al. 2020](#); [Alexander et al. 2021](#); [de](#)

¹⁷ <https://asas-sn.osu.edu/>

Wet et al. 2021). Given criteria that we describe in Section 3, we are able to rule out all known transient sources detected within the 99th percentile localization of GW190814 and discovered within 2 weeks of the merger time given by the LVC.

2. Given that there are no plausible counterparts, we are able to rule out kilonovae, GRBs, and SN-like optical counterparts to deep limits using the joint limits from all follow-up observations performed in this study. While our limits are not constraining in the context of red (low Y_e) kilonovae, we rule out blue kilonovae ($Y_e > 0.4$) with $v_{ej} = 0.25c$ and $M_{ej} > 0.3 M_\odot$ to 25% significance. We also rule out sGRBs similar to those of Fong et al. (2015) at $\sim 95\%$ significance for on-axis events and at $>50\%$ significance for viewing angles $\theta_{obs} < 17^\circ$. Finally, while our limits can probe luminosities as deep as -16 mag (21 mag at 240 Mpc) across most of the localization region, we cannot rule out events this faint with decline rates comparable to AT 2017gfo at >0.3 mag day $^{-1}$.
3. Using our joint limits on optical counterparts, we combine our EM follow-up data with the GW data of Abbott et al. (2020a) to consider scenarios in which NSBH systems would be detectable. We find that only for near-maximally spinning BHs (where the NSBH system has $\chi_{eff} > 0.995$) can we rule out merger scenarios similar to GW190814 with appreciable ($>20\%$) significance. While these parameters are inconsistent with those observed from GW190814 (with $\chi_{eff} < 0.06$ for all waveform models), these limits provide a baseline for plausible constraints on future NSBH counterparts.
4. We consider the possibility that GW190814 occurred in the disk of an AGN similar to the potential counterpart to the BBH merger S190521g proposed by Graham et al. (2020). Analyzing AGN catalogs, we find only 7 galaxies with AGNs and localized within the volume of GW190814. This is more than 3 orders of magnitude smaller than the total number of galaxies in the localization region and may provide an efficient search strategy for targeting electromagnetic emission for future compact object mergers.

This analysis was conducted on data collected by three GW follow-up efforts: 1M2H, KAIT, and Las Cumbres, each with independent observational strategies. Each collaboration used a different set of filters, targeting selection, and timescales that offer a unique constraints on EM counterparts to GW190814. Our combined data sets enable a more comprehensive and uniform analysis than was immediately possible after the discovery of the event. The future of GW

follow up efforts will benefit from similar analyses using data sharing and communication media such as the Treasure Map (Wyatt et al. 2020) and the Gamma-ray Coordinates Network (Barthelmy et al. 1995), open source software and analysis tools such as `teglon` and `gwemlightcurves` (Coughlin et al. 2020b), and increased collaboration within the GW/EM community.

Software: `astropy` (Astropy Collaboration et al. 2013), `DoPhot` (Schechter et al. 1993), `hotpants` (Becker 2015), `healpy` (Zonca et al. 2019), `IDL` (Landsman 1993), `LCOGTSNpipe` (Valenti et al. 2016), `ligo.skymap` (Singer et al. 2016a,b), `PyPeIt` (Prochaska et al. 2020a,b), `SExtractor` (Bertin & Arnouts 1996), `teglon`

Facilities: Las Cumbres (SINISTRO), Lick/Shane 3m (Kast), KAIT, Keck:I (MOSFIRE), Keck:II (DEIMOS), Nickel (Direct 2K), SOAR (Goodman), Swope (Direct 4K), Thacher (ACP)

ACKNOWLEDGMENTS

We thank T. M. Davis, W. Fong, and J. X. Prochaska for helpful comments on this manuscript as well as J. J. Hermes and S. Points for support with the SOAR observations. We thank the staffs at the various observatories where data were obtained for their expert assistance.

Much of this work was performed during the ‘‘Astrophysics in the LIGO/Virgo Era’’ meeting at the Aspen Center for Physics during Summer 2019 with C.D.K., D.A.C., I.A., D.O.J., C.R.-B., E.R.-R., A.R., and M.R.S. all participating. The Aspen Center for Physics is supported by National Science Foundation grant PHY-1607611.

The UCSC team is supported in part by NASA grant NNG17PX03C, NSF grant AST-1815935, the Gordon & Betty Moore Foundation, the Heising-Simons Foundation, and by fellowships from the David and Lucile Packard Foundation to R.J.F. D.A.C. acknowledges support from the National Science Foundation Graduate Research Fellowship under Grant DGE1339067. A.V.F.’s group at U.C. Berkeley is grateful for financial assistance from the Miller Institute for Basic Research in Science (in which A.V.F. is a Miller Senior Fellow), the Christopher R. Redlich Fund, Steven Nelson, and many other individual donors. D.E.H. was supported by NSF grants PHY-1708081 and PHY-2011997, and the Kavli Institute for Cosmological Physics at the University of Chicago through an endowment from the Kavli Foundation. Time domain research by D.J.S. is supported by NSF grants AST-1821987, 1813466, & 1908972, and by the Heising-Simons Foundation under grant #2020-1864. F.O.E. acknowledges support from the FONDECYT grant nr. 1201223. I.A. is a CIFAR Azrieli Global Scholar in the

Gravity and the Extreme Universe Program and acknowledges support from that program, from the European Research Council (ERC) under the European Union’s Horizon 2020 research and innovation program (grant agreement number 852097), from the Israel Science Foundation (grant number 2752/19), from the United States - Israel Binational Science Foundation (BSF), and from the Israeli Council for Higher Education Alon Fellowship. J.B. is supported by NSF grants AST-1313484 and AST-1911225, as well as by NASA grant 80NSSC19kf1639. J.C. acknowledges support from the Australian Research Council Centre of Excellence for Gravitational Wave Discovery (OzGrav) project number CE170100004. J.G.B. is supported by MINECO project PGC2018-094773-B-C32. L.S.S. acknowledges the financial support from FAPESP through the grant #2020/03301-5. M.M. is supported by CONICET, CNPq and FAPERJ. M.R.S. is supported by the National Science Foundation Graduate Research Fellowship Program under grant No. 184240. The UM team is supported by NSF grant AST-1910719 and fellowships from the Alfred P. Sloan Foundation and the Cottrell Scholar Award to M.S.-S. N.H. acknowledges support for this work by Israel Science Foundation grant No. 541/17. R.R.d.C. acknowledges the financial support from FAPESP through the grant #2014/11156-4. R.R.M. acknowledges partial support from project BASAL AFB-170002 as well as FONDECYT project N°1170364. S.B.R. acknowledges support from Conselho Nacional de Desenvolvimento Científico e Tecnológico – CNPq. T.D. is supported by ARC grant FL180100168. T.L.P. acknowledges financial support from CAPES.

This work includes data obtained with the Swope Telescope at Las Campanas Observatory, Chile, as part of the

Swope Time Domain Key Project (PI Piro, Co-Is Burns, Cowperthwaite, Dimitriadis, Drout, Foley, French, Holoien, Hsiao, Kilpatrick, Madore, Phillips, and Rojas-Bravo). This work makes use of observations from the LCO Network. The LCO Group is supported by NSF grant AST-1911151.

Some of the data presented herein were obtained at the W. M. Keck Observatory, which is operated as a scientific partnership among the California Institute of Technology, the University of California, and NASA. The Observatory was made possible by the generous financial support of the W. M. Keck Foundation. The authors wish to recognize and acknowledge the very significant cultural role and reverence that the summit of Maunakea has always had within the indigenous Hawaiian community. We are most fortunate to have the opportunity to conduct observations from this mountain.

Based in part on observations obtained at the Southern Astrophysical Research (SOAR) telescope, which is a joint project of the Ministério da Ciência, Tecnologia, Inovações e Comunicações (MCTIC) do Brasil, the U.S. National Optical Astronomy Observatory (NOAO), the University of North Carolina at Chapel Hill (UNC), and Michigan State University (MSU).

Research at Lick Observatory is partially supported by a generous gift from Google. KAIT and its ongoing operation were made possible by donations from Sun Microsystems, Inc., the Hewlett-Packard Company, AutoScope Corporation, Lick Observatory, the NSF, the University of California, the Sylvia and Jim Katzman Foundation, and the TABASGO Foundation.

REFERENCES

- Abadie, J., Abbott, B. P., Abbott, R., et al. 2011, *PhRvL*, 107, 271102, doi: [10.1103/PhysRevLett.107.271102](https://doi.org/10.1103/PhysRevLett.107.271102)
- Abbott, B. P., Abbott, R., Adhikari, R., et al. 2009, *Reports on Progress in Physics*, 72, 076901, doi: [10.1088/0034-4885/72/7/076901](https://doi.org/10.1088/0034-4885/72/7/076901)
- Abbott, B. P., Abbott, R., Abbott, T. D., et al. 2016a, *Physical Review Letters*, 116, 061102, doi: [10.1103/PhysRevLett.116.061102](https://doi.org/10.1103/PhysRevLett.116.061102)
- , 2016b, *PhRvL*, 116, 241102, doi: [10.1103/PhysRevLett.116.241102](https://doi.org/10.1103/PhysRevLett.116.241102)
- , 2016c, *Physical Review Letters*, 116, 241103, doi: [10.1103/PhysRevLett.116.241103](https://doi.org/10.1103/PhysRevLett.116.241103)
- , 2017a, *PhRvL*, 119, 141101, doi: [10.1103/PhysRevLett.119.141101](https://doi.org/10.1103/PhysRevLett.119.141101)
- , 2017b, *Physical Review Letters*, 118, 221101, doi: [10.1103/PhysRevLett.118.221101](https://doi.org/10.1103/PhysRevLett.118.221101)
- , 2017c, *ApJL*, 848, L13, doi: [10.3847/2041-8213/aa920c](https://doi.org/10.3847/2041-8213/aa920c)
- , 2017d, *Physical Review X*. <https://arxiv.org/abs/1606.04856>
- , 2018a, *PhRvL*, 121, 161101, doi: [10.1103/PhysRevLett.121.161101](https://doi.org/10.1103/PhysRevLett.121.161101)
- Abbott, R., Abbott, T. D., Abraham, S., et al. 2020a, *ApJL*, 896, L44, doi: [10.3847/2041-8213/ab960f](https://doi.org/10.3847/2041-8213/ab960f)
- , 2020b, *arXiv e-prints*, arXiv:2010.14527. <https://arxiv.org/abs/2010.14527>
- , 2020c, *PhRvL*, 125, 101102, doi: [10.1103/PhysRevLett.125.101102](https://doi.org/10.1103/PhysRevLett.125.101102)
- Abbott, T. M. C., Abdalla, F. B., Allam, S., et al. 2018b, *ApJS*, 239, 18, doi: [10.3847/1538-4365/aae9f0](https://doi.org/10.3847/1538-4365/aae9f0)
- Ackley, K., Amati, L., Barbieri, C., et al. 2020, *A&A*, 643, A113, doi: [10.1051/0004-6361/202037669](https://doi.org/10.1051/0004-6361/202037669)
- Aggarwal, K., Budavári, T., Deller, A. T., et al. 2021, *arXiv e-prints*, arXiv:2102.10627. <https://arxiv.org/abs/2102.10627>

- Akmal, A., Pandharipande, V. R., & Ravenhall, D. G. 1998, *PhRvC*, 58, 1804, doi: [10.1103/PhysRevC.58.1804](https://doi.org/10.1103/PhysRevC.58.1804)
- Al, M. S. E. 2019a, Transient Name Server Discovery Report, 2019-1509, 1
- . 2019b, Transient Name Server Discovery Report, 2019-1536, 1
- . 2019c, Transient Name Server Discovery Report, 2019-1563, 1
- . 2019d, Transient Name Server Discovery Report, 2019-1604, 1
- . 2019e, Transient Name Server Discovery Report, 2019-1615, 1
- Alard, C., & Lupton, R. H. 1998, *ApJ*, 503, 325, doi: [10.1086/305984](https://doi.org/10.1086/305984)
- Alexander, K. D., Schroeder, G., Paterson, K., et al. 2021, arXiv e-prints, arXiv:2102.08957. <https://arxiv.org/abs/2102.08957>
- Anand, N., Shahid, M., & Resmi, L. 2018, *MNRAS*, 481, 4332, doi: [10.1093/mnras/sty2530](https://doi.org/10.1093/mnras/sty2530)
- Andreoni, I., & Goldstein, D. 2019a, Transient Name Server Discovery Report, 2019-1496, 1
- . 2019b, Transient Name Server Discovery Report, 2019-1507, 1
- . 2019c, Transient Name Server Discovery Report, 2019-1516, 1
- . 2019d, Transient Name Server Discovery Report, 2019-1525, 1
- . 2019e, Transient Name Server Discovery Report, 2019-1562, 1
- Andreoni, I., Goldstein, D. A., Anand, S., et al. 2019a, *ApJL*, 881, L16, doi: [10.3847/2041-8213/ab3399](https://doi.org/10.3847/2041-8213/ab3399)
- Andreoni, I., Goldstein, D. A., Ahumada, T., et al. 2019b, GRB Coordinates Network, 25362, 1
- Andreoni, I., Goldstein, D. A., Kasliwal, M. M., et al. 2020, *ApJ*, 890, 131, doi: [10.3847/1538-4357/ab6a1b](https://doi.org/10.3847/1538-4357/ab6a1b)
- Antier, S., Agayeva, S., Aivazyan, V., et al. 2020, *MNRAS*, 492, 3904, doi: [10.1093/mnras/stz3142](https://doi.org/10.1093/mnras/stz3142)
- Antoni, A., MacLeod, M., & Ramirez-Ruiz, E. 2019, *ApJ*, 884, 22, doi: [10.3847/1538-4357/ab3466](https://doi.org/10.3847/1538-4357/ab3466)
- Arcavi, I., Hosseinzadeh, G., Howell, D. A., et al. 2017a, *Nature*, 551, 64, doi: [10.1038/nature24291](https://doi.org/10.1038/nature24291)
- Arcavi, I., McCully, C., Hosseinzadeh, G., et al. 2017b, *ApJL*, 848, L33, doi: [10.3847/2041-8213/aa910f](https://doi.org/10.3847/2041-8213/aa910f)
- Ashton, G., Ackley, K., Magaña Hernandez, I., & Piotrkowski, B. 2020, arXiv e-prints, arXiv:2009.12346. <https://arxiv.org/abs/2009.12346>
- Astropy Collaboration, Robitaille, T. P., Tollerud, E. J., et al. 2013, *A&A*, 558, A33, doi: [10.1051/0004-6361/201322068](https://doi.org/10.1051/0004-6361/201322068)
- Barro, G., Trump, J. R., Koo, D. C., et al. 2014, *ApJ*, 795, 145, doi: [10.1088/0004-637X/795/2/145](https://doi.org/10.1088/0004-637X/795/2/145)
- Barthelmy, S. D., Butterworth, P., Cline, T. L., et al. 1995, *Ap&SS*, 231, 235, doi: [10.1007/BF00658623](https://doi.org/10.1007/BF00658623)
- Bartos, I., Kocsis, B., Haiman, Z., & Márka, S. 2017, *ApJ*, 835, 165, doi: [10.3847/1538-4357/835/2/165](https://doi.org/10.3847/1538-4357/835/2/165)
- Bauer, F. E., Fruchter, A. S., Gonzalez Lopez, J., et al. 2019, GRB Coordinates Network, 25801, 1
- Beck, R., Szapudi, I., Flewelling, H., et al. 2021, *MNRAS*, 500, 1633, doi: [10.1093/mnras/staa2587](https://doi.org/10.1093/mnras/staa2587)
- Becker, A. 2015, HOTPANTS: High Order Transform of PSF AND Template Subtraction, Astrophysics Source Code Library. <http://ascl.net/1504.004>
- Behroozi, P. S., Ramirez-Ruiz, E., & Fryer, C. L. 2014, *ApJ*, 792, 123, doi: [10.1088/0004-637X/792/2/123](https://doi.org/10.1088/0004-637X/792/2/123)
- Belczynski, K., Holz, D. E., Bulik, T., & O’Shaughnessy, R. 2016, *Nature*, 534, 512, doi: [10.1038/nature18322](https://doi.org/10.1038/nature18322)
- Bell, E. F., McIntosh, D. H., Katz, N., & Weinberg, M. D. 2003, *ApJS*, 149, 289, doi: [10.1086/378847](https://doi.org/10.1086/378847)
- Bertin, E., & Arnouts, S. 1996, *A&AS*, 117, 393, doi: [10.1051/aas:1996164](https://doi.org/10.1051/aas:1996164)
- Bilicki, M., Jarrett, T. H., Peacock, J. A., Cluver, M. E., & Steward, L. 2014, *ApJS*, 210, 9, doi: [10.1088/0067-0049/210/1/9](https://doi.org/10.1088/0067-0049/210/1/9)
- Blondin, S., & Tonry, J. L. 2007, *ApJ*, 666, 1024, doi: [10.1086/520494](https://doi.org/10.1086/520494)
- Brown, J. S., Foley, R. J., Coulter, D. A., et al. 2019, GRB Coordinates Network, 25344, 1
- Brown, T. M., Baliber, N., Bianco, F. B., et al. 2013, *PASP*, 125, 1031, doi: [10.1086/673168](https://doi.org/10.1086/673168)
- Buckley, D., Ciroi, S., Gromadzki, M., et al. 2019, Transient Name Server Classification Report, 2019-1652, 1
- Cartier, R., Briceño, C., Olivares, F., et al. 2019, GRB Coordinates Network, 25784, 1
- Castro-Tirado, A. J., Valeev, A. F., Hu, Y. D., et al. 2019, GRB Coordinates Network, 25543, 1
- Chambers, K. C., Boer, T. D., Bulger, J., et al. 2019, Transient Name Server Discovery Report, 2019-1584, 1
- Chung, S. M., Eisenhardt, P. R., Gonzalez, A. H., et al. 2011, *ApJ*, 743, 34, doi: [10.1088/0004-637X/743/1/34](https://doi.org/10.1088/0004-637X/743/1/34)
- Coughlin, M. W., Ahumada, T., Anand, S., et al. 2019, *ApJL*, 885, L19, doi: [10.3847/2041-8213/ab4ad8](https://doi.org/10.3847/2041-8213/ab4ad8)
- Coughlin, M. W., Dietrich, T., Antier, S., et al. 2020a, *MNRAS*, 492, 863, doi: [10.1093/mnras/stz3457](https://doi.org/10.1093/mnras/stz3457)
- Coughlin, M. W., Antier, S., Dietrich, T., et al. 2020b, *Nature Communications*, 11, 4129, doi: [10.1038/s41467-020-17998-5](https://doi.org/10.1038/s41467-020-17998-5)
- Coulter, D. A., Foley, R. J., Kilpatrick, C. D., et al. 2017, *Science*, 358, 1556, doi: [10.1126/science.aap9811](https://doi.org/10.1126/science.aap9811)
- Cowperthwaite, P. S., Berger, E., Villar, V. A., et al. 2017, *ApJL*, 848, L17, doi: [10.3847/2041-8213/aa8fc7](https://doi.org/10.3847/2041-8213/aa8fc7)
- Cutri, R. M., Skrutskie, M. F., van Dyk, S., et al. 2003, 2MASS All Sky Catalog of point sources. (NASA/IPAC Infrared Science Archive)
- Dálya, G., Galgóczi, G., Dobos, L., et al. 2018, *MNRAS*, 479, 2374, doi: [10.1093/mnras/sty1703](https://doi.org/10.1093/mnras/sty1703)
- de Wet, S., Groot, P. J., Bloemen, S., et al. 2021, arXiv e-prints, arXiv:2103.02399. <https://arxiv.org/abs/2103.02399>
- Dimitriadis, G., Brown, J. S., Seibert, M. R., et al. 2019, GRB Coordinates Network, 25395, 1
- Dobie, D., Stewart, A., Murphy, T., et al. 2019a, *ApJL*, 887, L13, doi: [10.3847/2041-8213/ab59db](https://doi.org/10.3847/2041-8213/ab59db)

- Dobie, D., Stewart, A., Wang, Z., et al. 2019b, GRB Coordinates Network, 25445, 1
- Drout, M. R., Piro, A. L., Shappee, B. J., et al. 2017, *Science*, 358, 1570, doi: [10.1126/science.aaq0049](https://doi.org/10.1126/science.aaq0049)
- Drout et al. 2017, GRB Coordinates Network, 21547
- Duffell, P. C., & MacFadyen, A. I. 2013, *ApJL*, 776, L9, doi: [10.1088/2041-8205/776/1/L9](https://doi.org/10.1088/2041-8205/776/1/L9)
- Faber, J. A., Baumgarte, T. W., Shapiro, S. L., & Taniguchi, K. 2006, *ApJL*, 641, L93, doi: [10.1086/504111](https://doi.org/10.1086/504111)
- Faber, S. M., Phillips, A. C., Kibrick, R. I., et al. 2003, in *Society of Photo-Optical Instrumentation Engineers (SPIE) Conference Series*, Vol. 4841, Instrument Design and Performance for Optical/Infrared Ground-based Telescopes, ed. M. Iye & A. F. M. Moorwood, 1657–1669, doi: [10.1117/12.460346](https://doi.org/10.1117/12.460346)
- Farah, A., Essick, R., Doctor, Z., Fishbach, M., & Holz, D. E. 2020, *ApJ*, 895, 108, doi: [10.3847/1538-4357/ab8d26](https://doi.org/10.3847/1538-4357/ab8d26)
- Fattoyev, F. J., Horowitz, C. J., Piekarewicz, J., & Reed, B. 2020, *PhRvC*, 102, 065805, doi: [10.1103/PhysRevC.102.065805](https://doi.org/10.1103/PhysRevC.102.065805)
- Ferrari, V., Gualtieri, L., & Panarale, F. 2010, *PhRvD*, 81, 064026, doi: [10.1103/PhysRevD.81.064026](https://doi.org/10.1103/PhysRevD.81.064026)
- Filippenko, A. V., Li, W. D., Treffers, R. R., & Modjaz, M. 2001, in *Astronomical Society of the Pacific Conference Series*, Vol. 246, IAU Colloq. 183: Small Telescope Astronomy on Global Scales, ed. B. Paczynski, W.-P. Chen, & C. Lemme, 121
- Flewelling, H. A., Magnier, E. A., Chambers, K. C., et al. 2020, *ApJS*, 251, 7, doi: [10.3847/1538-4365/abb82d](https://doi.org/10.3847/1538-4365/abb82d)
- Foley, R. J., Coulter, D. A., Kilpatrick, C. D., et al. 2020, *MNRAS*, 494, 190, doi: [10.1093/mnras/staa725](https://doi.org/10.1093/mnras/staa725)
- Fong, W., & Berger, E. 2013, *ApJ*, 776, 18, doi: [10.1088/0004-637X/776/1/18](https://doi.org/10.1088/0004-637X/776/1/18)
- Fong, W., Berger, E., Margutti, R., & Zauderer, B. A. 2015, *ApJ*, 815, 102, doi: [10.1088/0004-637X/815/2/102](https://doi.org/10.1088/0004-637X/815/2/102)
- Fong, W., Berger, E., Blanchard, P. K., et al. 2017, *ApJL*, 848, L23, doi: [10.3847/2041-8213/aa9018](https://doi.org/10.3847/2041-8213/aa9018)
- Gaia Collaboration, Brown, A. G. A., Vallenari, A., et al. 2018, *A&A*, 616, A1, doi: [10.1051/0004-6361/201833051](https://doi.org/10.1051/0004-6361/201833051)
- Ganeshalingam, M., Li, W., Filippenko, A. V., et al. 2010, *ApJS*, 190, 418, doi: [10.1088/0067-0049/190/2/418](https://doi.org/10.1088/0067-0049/190/2/418)
- Godzieba, D. A., Radice, D., & Bernuzzi, S. 2021, *ApJ*, 908, 122, doi: [10.3847/1538-4357/abd4dd](https://doi.org/10.3847/1538-4357/abd4dd)
- Goldstein, D., Anand, S., & Growth Collaboration. 2019a, GRB Coordinates Network, 25394, 1
- Goldstein, D., Andreoni, I., Hankins, M., et al. 2019b, GRB Coordinates Network, 25393, 1
- Goldstein, D. A., Andreoni, I., Nugent, P. E., et al. 2019c, *ApJL*, 881, L7, doi: [10.3847/2041-8213/ab3046](https://doi.org/10.3847/2041-8213/ab3046)
- Gomez, S., Hosseinzadeh, G., Blanchard, P., et al. 2019a, Transient Name Server Classification Report, 2019-1643, 1
- Gomez, S., Hosseinzadeh, G., Cowperthwaite, P. S., et al. 2019b, *ApJL*, 884, L55, doi: [10.3847/2041-8213/ab4ad5](https://doi.org/10.3847/2041-8213/ab4ad5)
- Górski, K. M., Hivon, E., Banday, A. J., et al. 2005, *ApJ*, 622, 759, doi: [10.1086/427976](https://doi.org/10.1086/427976)
- Graham, M. J., Ford, K. E. S., McKernan, B., et al. 2020, *PhRvL*, 124, 251102, doi: [10.1103/PhysRevLett.124.251102](https://doi.org/10.1103/PhysRevLett.124.251102)
- Gröbner, M., Ishibashi, W., Tiwari, S., Haney, M., & Jetzer, P. 2020, *A&A*, 638, A119, doi: [10.1051/0004-6361/202037681](https://doi.org/10.1051/0004-6361/202037681)
- Guevel, D., & Hosseinzadeh, G. 2017, Dguevel/Pyzogy: Initial Release, v0.0.1, Zenodo, doi: [10.5281/zenodo.1043973](https://doi.org/10.5281/zenodo.1043973)
- Heger, A., & Woosley, S. E. 2002, *ApJ*, 567, 532, doi: [10.1086/338487](https://doi.org/10.1086/338487)
- Henden, A. A., Levine, S., Terrell, D., & Welch, D. L. 2015, in *American Astronomical Society Meeting Abstracts*, Vol. 225, American Astronomical Society Meeting Abstracts #225, 336.16
- Herner, K. 2019a, Transient Name Server Discovery Report, 2019-1508, 1
- . 2019b, Transient Name Server Discovery Report, 2019-1579, 1
- Herner, K., & Team, B. O. T. D. 2019, Transient Name Server Discovery Report, 2019-1526, 1
- Herner, K., Palmese, A., Soares-Santos, M., et al. 2019a, GRB Coordinates Network, 25373, 1
- . 2019b, GRB Coordinates Network, 25398, 1
- Hiramatsu, D., Arcavi, I., Howell, D. A., et al. 2019a, Transient Name Server Classification Report, 2019-1522, 1
- Hiramatsu, D., Howell, D. A., Arcavi, I., et al. 2019b, GRB Coordinates Network, 25422, 1
- Hosseinzadeh, G., Cowperthwaite, P. S., Gomez, S., et al. 2019, *ApJL*, 880, L4, doi: [10.3847/2041-8213/ab271c](https://doi.org/10.3847/2041-8213/ab271c)
- Huang, K., Hu, J., Zhang, Y., & Shen, H. 2020, *ApJ*, 904, 39, doi: [10.3847/1538-4357/abb37](https://doi.org/10.3847/1538-4357/abb37)
- Huber, M., Smith, K. W., Chambers, K., et al. 2019, GRB Coordinates Network, 25356, 1
- Jaodand, A., Campana, S., Brightman, M., et al. 2019, GRB Coordinates Network, 25822, 1
- Japelj, J., Kankare, E., Kool, E., et al. 2019, GRB Coordinates Network, 25526, 1
- Jayasinghe, T., Stanek, K. Z., Kochanek, C. S., et al. 2019, *MNRAS*, 485, 961, doi: [10.1093/mnras/stz444](https://doi.org/10.1093/mnras/stz444)
- Jester, S., Schneider, D. P., Richards, G. T., et al. 2005, *AJ*, 130, 873, doi: [10.1086/432466](https://doi.org/10.1086/432466)
- Johnston, S., Bailes, M., Bartel, N., et al. 2007, *PASA*, 24, 174, doi: [10.1071/AS07033](https://doi.org/10.1071/AS07033)
- Johnston, S., Taylor, R., Bailes, M., et al. 2008, *Experimental Astronomy*, 22, 151, doi: [10.1007/s10686-008-9124-7](https://doi.org/10.1007/s10686-008-9124-7)
- Jones, D. H., Read, M. A., Saunders, W., et al. 2009, *MNRAS*, 399, 683, doi: [10.1111/j.1365-2966.2009.15338.x](https://doi.org/10.1111/j.1365-2966.2009.15338.x)
- Joss, P. C., & Rappaport, S. A. 1984, *ARA&A*, 22, 537, doi: [10.1146/annurev.aa.22.090184.002541](https://doi.org/10.1146/annurev.aa.22.090184.002541)
- Kanakis-Pegios, A., Koliogiannis, P. S., & Moustakidis, C. C. 2021, *Symmetry*, 13, 183, doi: [10.3390/sym13020183](https://doi.org/10.3390/sym13020183)

- Kasen, D., Fernández, R., & Metzger, B. D. 2015, *MNRAS*, 450, 1777, doi: [10.1093/mnras/stv721](https://doi.org/10.1093/mnras/stv721)
- Kasen, D., Metzger, B., Barnes, J., Quataert, E., & Ramirez-Ruiz, E. 2017, *Nature*, 551, 80, doi: [10.1038/nature24453](https://doi.org/10.1038/nature24453)
- Kasliwal, M. M., Nakar, E., Singer, L. P., et al. 2017, *Science*, 358, 1559, doi: [10.1126/science.aap9455](https://doi.org/10.1126/science.aap9455)
- Kawaguchi, K., Kyutoku, K., Shibata, M., & Tanaka, M. 2016, *ApJ*, 825, 52, doi: [10.3847/0004-637X/825/1/52](https://doi.org/10.3847/0004-637X/825/1/52)
- Kilpatrick, C. D., Foley, R. J., Kasen, D., et al. 2017, *Science*, 358, 1583, doi: [10.1126/science.aaq0073](https://doi.org/10.1126/science.aaq0073)
- Kilpatrick, C. D., Foley, R. J., Drout, M. R., et al. 2018, *MNRAS*, 473, 4805, doi: [10.1093/mnras/stx2675](https://doi.org/10.1093/mnras/stx2675)
- Kilpatrick, C. D., Coulter, D. A., Brown, J. S., et al. 2019, *GRB Coordinates Network*, 25350, 1
- Kocevski, D., Fermi-GBM Team, & GBM-LIGO/Virgo Group. 2019, *GRB Coordinates Network*, 25326, 1
- Kochanek, C. S., Shappee, B. J., Stanek, K. Z., et al. 2017, *PASP*, 129, 104502, doi: [10.1088/1538-3873/aa80d9](https://doi.org/10.1088/1538-3873/aa80d9)
- Kurtz, M. J., & Mink, D. J. 1998, *PASP*, 110, 934, doi: [10.1086/316207](https://doi.org/10.1086/316207)
- Landolt, A. U. 1992, *AJ*, 104, 340, doi: [10.1086/116242](https://doi.org/10.1086/116242)
- Landsman, W. B. 1993, in *Astronomical Society of the Pacific Conference Series*, Vol. 52, *Astronomical Data Analysis Software and Systems II*, ed. R. J. Hanisch, R. J. V. Brissenden, & J. Barnes, 246
- Lattimer, J. M., & Prakash, M. 2007, *PhR*, 442, 109, doi: [10.1016/j.physrep.2007.02.003](https://doi.org/10.1016/j.physrep.2007.02.003)
- Lazarus, P., Freire, P. C. C., Allen, B., et al. 2016, *ApJ*, 831, 150, doi: [10.3847/0004-637X/831/2/150](https://doi.org/10.3847/0004-637X/831/2/150)
- Lazzati, D., Deich, A., Morsony, B. J., & Workman, J. C. 2017, *MNRAS*, 471, 1652, doi: [10.1093/mnras/stx1683](https://doi.org/10.1093/mnras/stx1683)
- Lee, W. H., & Ramirez-Ruiz, E. 2007, *New Journal of Physics*, 9, 17, doi: [10.1088/1367-2630/9/1/017](https://doi.org/10.1088/1367-2630/9/1/017)
- Li, L.-X., & Paczyński, B. 1998, *ApJL*, 507, L59, doi: [10.1086/311680](https://doi.org/10.1086/311680)
- Li, W., Filippenko, A. V., Chornock, R., & Jha, S. 2003, *PASP*, 115, 844, doi: [10.1086/376432](https://doi.org/10.1086/376432)
- LIGO Scientific Collaboration, & Virgo Collaboration. 2019a, *GRB Coordinates Network*, 25324, 1
- . 2019b, *GRB Coordinates Network*, 25333, 1
- LIGO Scientific Collaboration, Aasi, J., Abbott, B. P., et al. 2015, *Classical and Quantum Gravity*, 32, 074001, doi: [10.1088/0264-9381/32/7/074001](https://doi.org/10.1088/0264-9381/32/7/074001)
- Lippuner, J., & Roberts, L. F. 2015, *ApJ*, 815, 82, doi: [10.1088/0004-637X/815/2/82](https://doi.org/10.1088/0004-637X/815/2/82)
- Livio, M., & Soker, N. 1988, *ApJ*, 329, 764, doi: [10.1086/166419](https://doi.org/10.1086/166419)
- Lopez-Cruz, O., Castro-Tirado, A. J., Macri, L., et al. 2019, *GRB Coordinates Network*, 25419, 1
- Lundquist, M. J., Paterson, K., Fong, W., et al. 2019, *ApJL*, 881, L26, doi: [10.3847/2041-8213/ab32f2](https://doi.org/10.3847/2041-8213/ab32f2)
- McClintock, J. E., Shafee, R., Narayan, R., et al. 2006, *ApJ*, 652, 518, doi: [10.1086/508457](https://doi.org/10.1086/508457)
- McConnell, D., Allison, J. R., Bannister, K., et al. 2016, *PASA*, 33, e042, doi: [10.1017/pasa.2016.37](https://doi.org/10.1017/pasa.2016.37)
- McCully, C., Volgenau, N. H., Harbeck, D.-R., et al. 2018, in *Society of Photo-Optical Instrumentation Engineers (SPIE) Conference Series*, Vol. 10707, *Proc. SPIE*, 107070K, doi: [10.1117/12.2314340](https://doi.org/10.1117/12.2314340)
- McKernan, B., Ford, K. E. S., Lyra, W., & Perets, H. B. 2012, *MNRAS*, 425, 460, doi: [10.1111/j.1365-2966.2012.21486.x](https://doi.org/10.1111/j.1365-2966.2012.21486.x)
- McLean, I. S., Steidel, C. C., Epps, H. W., et al. 2012, *Proc. SPIE*, 8446, 84460J, doi: [10.1117/12.924794](https://doi.org/10.1117/12.924794)
- Metzger, B. D. 2017, *Living Reviews in Relativity*, 20, 3, doi: [10.1007/s41114-017-0006-z](https://doi.org/10.1007/s41114-017-0006-z)
- . 2019, *Living Reviews in Relativity*, 23, 1, doi: [10.1007/s41114-019-0024-0](https://doi.org/10.1007/s41114-019-0024-0)
- Metzger, B. D., & Fernández, R. 2014, *MNRAS*, 441, 3444, doi: [10.1093/mnras/stu802](https://doi.org/10.1093/mnras/stu802)
- Metzger, B. D., Martínez-Pinedo, G., Darbha, S., et al. 2010, *MNRAS*, 406, 2650, doi: [10.1111/j.1365-2966.2010.16864.x](https://doi.org/10.1111/j.1365-2966.2010.16864.x)
- Miller, J., & Stone, R. 1993, *Lick Obs. Tech. Rep.*, 66
- Molkov, S., Mereghetti, S., Savchenko, V., et al. 2019, *GRB Coordinates Network*, 25323, 1
- Mooley, K. P., Nakar, E., Hotokezaka, K., et al. 2018, *Nature*, 554, 207, doi: [10.1038/nature25452](https://doi.org/10.1038/nature25452)
- Morgan, R., Soares-Santos, M., Annis, J., et al. 2020, *ApJ*, 901, 83, doi: [10.3847/1538-4357/abafaa](https://doi.org/10.3847/1538-4357/abafaa)
- Murguía-Berthier, A., Ramirez-Ruiz, E., De Colle, F., et al. 2021, *ApJ*, 908, 152, doi: [10.3847/1538-4357/abd08e](https://doi.org/10.3847/1538-4357/abd08e)
- Murguía-Berthier, A., Ramirez-Ruiz, E., Kilpatrick, C. D., et al. 2017, *ApJL*, 848, L34, doi: [10.3847/2041-8213/aa91b3](https://doi.org/10.3847/2041-8213/aa91b3)
- Oke, J. B., & Gunn, J. E. 1983, *ApJ*, 266, 713, doi: [10.1086/160817](https://doi.org/10.1086/160817)
- Palmer, D. M., Barthelmy, S. D., Lien, A. Y., et al. 2019, *GRB Coordinates Network*, 25341, 1
- Palmese, A., deVicente, J., Pereira, M. E. S., et al. 2020, *ApJL*, 900, L33, doi: [10.3847/2041-8213/abaeff](https://doi.org/10.3847/2041-8213/abaeff)
- Paterson, K., Lundquist, M. J., Rastinejad, J. C., et al. 2020, *arXiv e-prints*, arXiv:2012.11700. <https://arxiv.org/abs/2012.11700>
- Planck Collaboration, Ade, P. A. R., Aghanim, N., et al. 2016, *A&A*, 594, A13, doi: [10.1051/0004-6361/201525830](https://doi.org/10.1051/0004-6361/201525830)
- Pozanenko, A. S., Minaev, P. Y., Grebenev, S. A., & Chelovekov, I. V. 2020, *Astronomy Letters*, 45, 710, doi: [10.1134/S1063773719110057](https://doi.org/10.1134/S1063773719110057)
- Press, W. H., & Thorne, K. S. 1972, *ARA&A*, 10, 335, doi: [10.1146/annurev.aa.10.090172.002003](https://doi.org/10.1146/annurev.aa.10.090172.002003)
- Prochaska, J., Hennawi, J., Westfall, K., et al. 2020a, *The Journal of Open Source Software*, 5, 2308, doi: [10.21105/joss.02308](https://doi.org/10.21105/joss.02308)
- Prochaska, J. X., Hennawi, J., Cooke, R., et al. 2020b, *pypeit/PypeIt: Release 1.0.0, v1.0.0*, Zenodo, doi: [10.5281/zenodo.3743493](https://doi.org/10.5281/zenodo.3743493)

- Radice, D., Perego, A., Zappa, F., & Bernuzzi, S. 2018, *ApJL*, 852, L29, doi: [10.3847/2041-8213/aaa402](https://doi.org/10.3847/2041-8213/aaa402)
- Ramirez-Ruiz, E., Andrews, J. J., & Schröder, S. L. 2019, *ApJL*, 883, L6, doi: [10.3847/2041-8213/ab3f2c](https://doi.org/10.3847/2041-8213/ab3f2c)
- Read, J. S., Lackey, B. D., Owen, B. J., & Friedman, J. L. 2009, *PhRvD*, 79, 124032, doi: [10.1103/PhysRevD.79.124032](https://doi.org/10.1103/PhysRevD.79.124032)
- Rest, A., Stubbs, C., Becker, A. C., et al. 2005, *ApJ*, 634, 1103, doi: [10.1086/497060](https://doi.org/10.1086/497060)
- Richmond, M., Treffers, R. R., & Filippenko, A. V. 1993, *PASP*, 105, 1164, doi: [10.1086/133294](https://doi.org/10.1086/133294)
- Roberts, L. F., Kasen, D., Lee, W. H., & Ramirez-Ruiz, E. 2011, *ApJL*, 736, L21, doi: [10.1088/2041-8205/736/1/L21](https://doi.org/10.1088/2041-8205/736/1/L21)
- Rodríguez, Ó., Meza-Retamal, N., Quirola, J., et al. 2019, *GRB Coordinates Network*, 25423, 1
- Rossi, E., Lazzati, D., & Rees, M. J. 2002, *MNRAS*, 332, 945, doi: [10.1046/j.1365-8711.2002.05363.x](https://doi.org/10.1046/j.1365-8711.2002.05363.x)
- Rosswog, S., Piran, T., & Nakar, E. 2013, *MNRAS*, 430, 2585, doi: [10.1093/mnras/sts708](https://doi.org/10.1093/mnras/sts708)
- Ryan, G., van Eerten, H., MacFadyen, A., & Zhang, B.-B. 2015, *ApJ*, 799, 3, doi: [10.1088/0004-637X/799/1/3](https://doi.org/10.1088/0004-637X/799/1/3)
- Safarzadeh, M., Berger, E., Leja, J., & Speagle, J. S. 2019, *ApJL*, 878, L14, doi: [10.3847/2041-8213/ab24e3](https://doi.org/10.3847/2041-8213/ab24e3)
- Savchenko, V., Ferrigno, C., Kuulkers, E., et al. 2017, *ApJL*, 848, L15, doi: [10.3847/2041-8213/aa8f94](https://doi.org/10.3847/2041-8213/aa8f94)
- Schechter, P. 1976, *ApJ*, 203, 297, doi: [10.1086/154079](https://doi.org/10.1086/154079)
- Schechter, P. L., Mateo, M., & Saha, A. 1993, *PASP*, 105, 1342, doi: [10.1086/133316](https://doi.org/10.1086/133316)
- Schlafly, E. F., & Finkbeiner, D. P. 2011, *ApJ*, 737, 103, doi: [10.1088/0004-637X/737/2/103](https://doi.org/10.1088/0004-637X/737/2/103)
- Schröder, S. L., Batta, A., & Ramirez-Ruiz, E. 2018, *ApJL*, 862, L3, doi: [10.3847/2041-8213/aacf8d](https://doi.org/10.3847/2041-8213/aacf8d)
- Scolnic, D., Casertano, S., Riess, A., et al. 2015, *ApJ*, 815, 117, doi: [10.1088/0004-637X/815/2/117](https://doi.org/10.1088/0004-637X/815/2/117)
- Secrest, N. J., Dudik, R. P., Dorland, B. N., et al. 2015, *ApJS*, 221, 12, doi: [10.1088/0067-0049/221/1/12](https://doi.org/10.1088/0067-0049/221/1/12)
- Shappee, B. J. 2014, PhD thesis, The Ohio State University
- Shappee, B. J., Prieto, J. L., Grupe, D., et al. 2014, *ApJ*, 788, 48, doi: [10.1088/0004-637X/788/1/48](https://doi.org/10.1088/0004-637X/788/1/48)
- Shappee, B. J., Simon, J. D., Drout, M. R., et al. 2017, *Science*, 358, 1574, doi: [10.1126/science.aag0186](https://doi.org/10.1126/science.aag0186)
- Shibata, M., & Taniguchi, K. 2006, *PhRvD*, 73, 064027, doi: [10.1103/PhysRevD.73.064027](https://doi.org/10.1103/PhysRevD.73.064027)
- Shingles, L., Smith, K. W., Young, D. R., et al. 2021, *Transient Name Server AstroNote*, 7, 1
- Siebert, M. R., Foley, R. J., Drout, M. R., et al. 2017, *ApJL*, 848, L26, doi: [10.3847/2041-8213/aa905e](https://doi.org/10.3847/2041-8213/aa905e)
- Silverman, J. M., Kong, J. J., & Filippenko, A. V. 2012, *MNRAS*, 425, 1819, doi: [10.1111/j.1365-2966.2012.21269.x](https://doi.org/10.1111/j.1365-2966.2012.21269.x)
- Singer, L. P., & Price, L. R. 2016, *PhRvD*, 93, 024013, doi: [10.1103/PhysRevD.93.024013](https://doi.org/10.1103/PhysRevD.93.024013)
- Singer, L. P., Chen, H.-Y., Holz, D. E., et al. 2016a, *ApJL*, 829, L15, doi: [10.3847/2041-8205/829/1/L15](https://doi.org/10.3847/2041-8205/829/1/L15)
- . 2016b, *ApJS*, 226, 10, doi: [10.3847/0067-0049/226/1/10](https://doi.org/10.3847/0067-0049/226/1/10)
- Smartt, S. J., Chen, T. W., Jerkstrand, A., et al. 2017, *Nature*, 551, 75, doi: [10.1038/nature24303](https://doi.org/10.1038/nature24303)
- Smith, K. W., Smartt, S. J., Young, D. R., et al. 2020, *PASP*, 132, 085002, doi: [10.1088/1538-3873/ab936e](https://doi.org/10.1088/1538-3873/ab936e)
- Soares-Santos, M., Tucker, D., Allam, S., et al. 2019a, *GRB Coordinates Network*, 25336, 1
- Soares-Santos, M., Annis, J., Herner, K., et al. 2019b, *GRB Coordinates Network*, 25486, 1
- Soares-Santos, M., Palmese, A., Hartley, W., et al. 2019c, *ApJL*, 876, L7, doi: [10.3847/2041-8213/ab14f1](https://doi.org/10.3847/2041-8213/ab14f1)
- Srivastav, S., Huber, M., Smartt, S. J., et al. 2019, *GRB Coordinates Network*, 25417, 1
- Stahl, B. E., Zheng, W., de Jaeger, T., et al. 2019, *MNRAS*, 490, 3882, doi: [10.1093/mnras/stz2742](https://doi.org/10.1093/mnras/stz2742)
- Stetson, P. B. 1987, *PASP*, 99, 191, doi: [10.1086/131977](https://doi.org/10.1086/131977)
- Stewart, A., Dobie, D., Murphy, T., et al. 2019a, *Transient Name Server Discovery Report*, 2019-1637, 1
- . 2019b, *GRB Coordinates Network*, 25487, 1
- Stone, N. C., Metzger, B. D., & Haiman, Z. 2017, *MNRAS*, 464, 946, doi: [10.1093/mnras/stw2260](https://doi.org/10.1093/mnras/stw2260)
- Swift, J., & Vyhnał, C. 2018, *Robotic Telescope, Student Research and Education Proceedings*, 1, 281
- Swift, J., Yin, Y., Kilpatrick, C. D., et al. 2019, *GRB Coordinates Network*, 25351, 1
- Tan, H., Noronha-Hostler, J., & Yunes, N. 2020, *PhRvL*, 125, 261104, doi: [10.1103/PhysRevLett.125.261104](https://doi.org/10.1103/PhysRevLett.125.261104)
- Tanaka, M., Kato, D., Gaigalas, G., & Kawaguchi, K. 2020, *MNRAS*, 496, 1369, doi: [10.1093/mnras/staa1576](https://doi.org/10.1093/mnras/staa1576)
- Tanvir, N. R., Levan, A. J., Fruchter, A. S., et al. 2013, *Nature*, 500, 547, doi: [10.1038/nature12505](https://doi.org/10.1038/nature12505)
- Tanvir, N. R., Levan, A. J., González-Fernández, C., et al. 2017, *ApJL*, 848, L27, doi: [10.3847/2041-8213/aa90b6](https://doi.org/10.3847/2041-8213/aa90b6)
- Tews, I., Pang, P. T. H., Dietrich, T., et al. 2021, *ApJL*, 908, L1, doi: [10.3847/2041-8213/abdaae](https://doi.org/10.3847/2041-8213/abdaae)
- Thakur, A. L., Dichiara, S., Troja, E., et al. 2020, *MNRAS*, 499, 3868, doi: [10.1093/mnras/staa2798](https://doi.org/10.1093/mnras/staa2798)
- The LIGO Scientific Collaboration, the Virgo Collaboration, Abbott, B. P., et al. 2020, *arXiv e-prints*, arXiv:2006.14961. <https://arxiv.org/abs/2006.14961>
- Thorne, K. S. 1997, *arXiv e-prints*, gr. <https://arxiv.org/abs/gr-qc/9704042>
- Tonry, J., & Davis, M. 1979, *AJ*, 84, 1511, doi: [10.1086/112569](https://doi.org/10.1086/112569)
- Troja, E., Piro, L., van Eerten, H., et al. 2017, *Nature*, 551, 71, doi: [10.1038/nature24290](https://doi.org/10.1038/nature24290)
- Tucker, D., Butner, M., Wiesner, M., et al. 2019a, *GRB Coordinates Network*, 25484, 1

- Tucker, D., Allam, S., Wiesner, M., et al. 2019b, GRB Coordinates Network, 25379, 1
- Valenti, S., Howell, D. A., Stritzinger, M. D., et al. 2016, MNRAS, 459, 3939, doi: [10.1093/mnras/stw870](https://doi.org/10.1093/mnras/stw870)
- Vasylyev, S., Stahl, B., Zhang, K. D., et al. 2019a, GRB Coordinates Network, 25353, 1
- Vasylyev, S., Stahl, B. E., Zhang, K. D., et al. 2019b, GRB Coordinates Network, 25437, 1
- Véron-Cetty, M. P., & Véron, P. 2010, A&A, 518, A10, doi: [10.1051/0004-6361/201014188](https://doi.org/10.1051/0004-6361/201014188)
- Vieira, N., Ruan, J. J., Haggard, D., et al. 2020, ApJ, 895, 96, doi: [10.3847/1538-4357/ab917d](https://doi.org/10.3847/1538-4357/ab917d)
- Watson, A. M., Butler, N. R., Lee, W. H., et al. 2020, MNRAS, 492, 5916, doi: [10.1093/mnras/staa161](https://doi.org/10.1093/mnras/staa161)
- Way, M. J., Quintana, H., Infante, L., Lambas, D. G., & Muriel, H. 2005, AJ, 130, 2012, doi: [10.1086/462418](https://doi.org/10.1086/462418)
- Wiesner, M., Butner, M., Allam, S., et al. 2019a, GRB Coordinates Network, 25596, 1
- Wiesner, M., Butner, M., Tucker, D., et al. 2019b, GRB Coordinates Network, 25540, 1
- Wu, X., Bao, S., Shen, H., & Xu, R. 2021, arXiv e-prints, arXiv:2101.05476. <https://arxiv.org/abs/2101.05476>
- Wu, Y., & MacFadyen, A. 2018, ApJ, 869, 55, doi: [10.3847/1538-4357/aae9de](https://doi.org/10.3847/1538-4357/aae9de)
- . 2019, ApJL, 880, L23, doi: [10.3847/2041-8213/ab2fd4](https://doi.org/10.3847/2041-8213/ab2fd4)
- Wyatt, S. D., Tohuvavohu, A., Arcavi, I., et al. 2020, ApJ, 894, 127, doi: [10.3847/1538-4357/ab855e](https://doi.org/10.3847/1538-4357/ab855e)
- Yamazaki, R., Yonetoku, D., & Nakamura, T. 2003, ApJL, 594, L79, doi: [10.1086/378736](https://doi.org/10.1086/378736)
- Zackay, B., Ofek, E. O., & Gal-Yam, A. 2016, ApJ, 830, 27, doi: [10.3847/0004-637X/830/1/27](https://doi.org/10.3847/0004-637X/830/1/27)
- Zevin, M., Spera, M., Berry, C. P. L., & Kalogera, V. 2020, ApJL, 899, L1, doi: [10.3847/2041-8213/aba74e](https://doi.org/10.3847/2041-8213/aba74e)
- Zhang, N.-B., & Li, B.-A. 2020, ApJ, 902, 38, doi: [10.3847/1538-4357/abb470](https://doi.org/10.3847/1538-4357/abb470)
- Zheng, W., Filippenko, A. V., Mauerhan, J., et al. 2017, ApJ, 841, 64, doi: [10.3847/1538-4357/aa6dfa](https://doi.org/10.3847/1538-4357/aa6dfa)
- Zhou, R., Newman, J. A., Mao, Y.-Y., et al. 2021, MNRAS, 501, 3309, doi: [10.1093/mnras/staa3764](https://doi.org/10.1093/mnras/staa3764)
- Zonca, A., Singer, L., Lenz, D., et al. 2019, The Journal of Open Source Software, 4, 1298, doi: [10.21105/joss.01298](https://doi.org/10.21105/joss.01298)

APPENDIX

Table 4. Optical/IR Imaging of the GW190814 Localization Region

Source ^a	α (J2000)	δ (J2000)	Date (MJD)	Filter	Magnitude Limit ^b (3σ)
S	01:27:55.560	-34:41:50.280	58715.2170	<i>r</i>	20.64
S	01:27:56.496	-34:42:01.800	58716.3976	<i>r</i>	21.04
S	01:27:58.248	-34:42:09.360	58718.3350	<i>r</i>	21.12
S	01:27:46.752	-34:42:55.080	58736.1369	<i>r</i>	20.69
S	01:32:06.792	-34:12:16.560	58713.2037	<i>r</i>	20.37
S	01:32:07.752	-34:13:05.520	58714.2115	<i>r</i>	19.58
S	01:32:09.456	-34:11:59.640	58715.3197	<i>r</i>	21.03
S	01:32:12.288	-34:12:12.240	58716.2327	<i>r</i>	20.73
S	01:32:08.400	-34:12:25.200	58718.3299	<i>r</i>	21.04
S	01:32:06.096	-34:12:53.280	58733.3072	<i>r</i>	20.84
S	01:31:58.488	-34:12:58.680	58736.1481	<i>r</i>	20.75
S	01:37:00.744	-34:12:27.360	58711.1746	<i>r</i>	19.76
S	01:36:55.152	-34:12:28.800	58714.2161	<i>r</i>	19.94
S	01:36:54.528	-34:12:01.800	58715.3443	<i>r</i>	20.98
S	01:36:56.904	-34:12:09.720	58717.3657	<i>r</i>	20.96
S	01:36:49.776	-34:12:15.120	58734.3786	<i>r</i>	21.49
S	01:39:23.520	-34:12:49.320	58711.1639	<i>r</i>	19.73
S	01:39:18.072	-34:12:34.200	58714.2183	<i>r</i>	19.48
S	01:39:20.376	-34:12:00.360	58715.3419	<i>r</i>	21.04
S	01:39:19.728	-34:12:11.520	58717.3682	<i>r</i>	20.93
S	01:39:10.536	-34:12:13.680	58734.3640	<i>r</i>	21.44
S	01:24:24.192	-33:42:43.200	58717.1619	<i>r</i>	20.66
S	01:24:24.408	-33:42:24.120	58718.3374	<i>r</i>	20.52
S	01:24:24.912	-33:42:34.200	58719.3679	<i>r</i>	21.15
S	01:24:18.720	-33:42:25.560	58734.2767	<i>r</i>	21.18
S	01:31:37.176	-33:42:38.520	58711.1941	<i>r</i>	19.64
S	01:31:29.232	-33:42:43.920	58714.2212	<i>r</i>	20.12
S	01:31:32.280	-33:42:07.200	58715.3558	<i>r</i>	20.62
S	01:31:32.232	-33:42:15.120	58715.3629	<i>r</i>	20.93
S	01:31:32.664	-33:42:17.280	58717.3632	<i>r</i>	20.84
S	01:31:23.064	-33:43:10.560	58736.1774	<i>r</i>	20.81
S	01:33:49.800	-33:42:25.560	58712.3427	<i>r</i>	20.03
S	01:33:52.008	-33:42:29.160	58713.3958	<i>r</i>	20.45
S	01:33:51.144	-33:43:06.240	58714.4027	<i>r</i>	20.45
S	01:33:53.400	-33:42:17.280	58715.3490	<i>r</i>	20.98
S	01:33:56.616	-33:42:12.960	58718.3263	<i>r</i>	21.06
S	01:33:45.048	-33:43:09.120	58736.1701	<i>r</i>	20.81
S	01:36:12.240	-33:42:12.600	58712.3480	<i>r</i>	20.00
S	01:36:16.560	-33:42:29.520	58713.3931	<i>r</i>	20.49
S	01:36:15.336	-33:42:38.520	58714.4002	<i>r</i>	20.45
S	01:36:18.792	-33:42:14.760	58715.3269	<i>r</i>	21.02
S	01:36:16.224	-33:42:49.320	58717.3709	<i>r</i>	20.94
S	01:36:10.344	-33:43:01.560	58734.3823	<i>r</i>	21.56
S	01:23:59.832	-33:13:02.640	58717.1676	<i>r</i>	20.58
S	01:24:02.088	-33:12:58.680	58718.2688	<i>r</i>	21.10
S	01:23:59.952	-33:12:51.480	58719.3726	<i>r</i>	21.42
S	01:23:52.320	-33:13:03.000	58734.2804	<i>r</i>	21.38

Table 4 continued

Table 4 (*continued*)

Source ^a	α (J2000)	δ (J2000)	Date (MJD)	Filter	Magnitude Limit ^b (3σ)
S	01:28:48.480	-32:57:37.080	58711.1663	<i>r</i>	19.69
S	01:28:39.936	-33:12:56.160	58714.2239	<i>r</i>	19.76
S	01:28:44.232	-33:12:27.000	58715.3150	<i>r</i>	20.94
S	01:28:42.144	-33:12:38.520	58717.3605	<i>r</i>	20.94
S	01:28:32.664	-33:13:19.560	58736.1846	<i>r</i>	20.84
S	01:31:03.312	-33:13:26.400	58710.2745	<i>r</i>	19.25
S	01:31:09.048	-33:13:25.320	58711.1530	<i>r</i>	19.76
S	01:31:01.632	-33:12:41.760	58712.3376	<i>r</i>	20.02
S	01:31:02.352	-33:12:44.280	58713.3905	<i>r</i>	20.43
S	01:31:01.224	-33:12:00.360	58714.3971	<i>r</i>	20.51
S	01:31:03.696	-33:12:27.720	58715.3535	<i>r</i>	20.94
S	01:31:06.480	-33:12:43.200	58716.3915	<i>r</i>	20.96
S	01:31:05.832	-33:13:11.640	58717.3581	<i>r</i>	20.95
S	01:31:07.776	-33:12:54.360	58718.2883	<i>r</i>	21.09
S	01:31:04.848	-33:12:50.760	58719.3142	<i>r</i>	21.37
S	01:31:05.184	-33:12:56.880	58725.2536	<i>r</i>	21.35
S	01:31:02.232	-33:13:18.120	58733.3110	<i>r</i>	20.87
S	01:30:54.840	-33:13:42.600	58736.1809	<i>r</i>	20.69
S	01:33:26.712	-33:13:12.720	58710.3842	<i>r</i>	19.81
S	01:33:31.368	-33:12:58.680	58711.1827	<i>r</i>	19.47
S	01:33:23.448	-33:12:31.320	58712.3570	<i>r</i>	19.85
S	01:33:26.952	-33:12:44.640	58713.3329	<i>r</i>	20.44
S	01:33:27.408	-33:12:57.960	58714.3234	<i>r</i>	19.88
S	01:33:26.352	-33:12:32.400	58715.3513	<i>r</i>	20.95
S	01:33:26.232	-33:13:23.880	58733.3286	<i>r</i>	20.88
S	01:33:17.184	-33:13:27.480	58736.1664	<i>r</i>	20.75
S	01:35:45.816	-33:13:21.720	58710.4065	<i>r</i>	19.23
S	01:35:53.280	-33:12:23.040	58711.2645	<i>r</i>	19.83
S	01:35:44.328	-33:13:06.600	58712.3503	<i>r</i>	20.16
S	01:35:47.040	-33:12:49.320	58713.3880	<i>r</i>	20.42
S	01:35:45.192	-33:12:57.600	58714.3931	<i>r</i>	20.46
S	01:35:47.448	-33:12:16.200	58715.3466	<i>r</i>	21.03
S	01:35:42.432	-33:12:40.320	58734.3750	<i>r</i>	21.46
S	01:38:15.360	-33:13:12.360	58711.1885	<i>r</i>	19.52
S	01:38:06.936	-33:13:03.720	58712.3453	<i>r</i>	20.17
S	01:38:10.056	-33:12:41.400	58713.3982	<i>r</i>	20.39
S	01:38:08.496	-33:13:22.440	58714.4052	<i>r</i>	20.39
S	01:38:09.624	-33:12:29.880	58715.3396	<i>r</i>	21.01
S	01:38:01.968	-33:12:52.200	58734.3675	<i>r</i>	21.43
S	01:40:32.616	-33:13:14.880	58725.2589	<i>r</i>	21.26
S	01:40:25.344	-33:12:48.960	58734.3601	<i>r</i>	21.36
S	01:23:31.128	-32:43:27.840	58710.4262	<i>r</i>	19.84
S	01:23:35.664	-32:42:46.800	58715.3075	<i>r</i>	20.95
S	01:23:34.584	-32:43:28.920	58716.3750	<i>r</i>	21.05
S	01:23:36.336	-32:43:34.320	58718.2712	<i>r</i>	21.10
S	01:23:27.384	-32:42:54.000	58734.2842	<i>r</i>	21.31
S	01:25:53.352	-32:43:38.280	58710.4230	<i>r</i>	20.18
S	01:25:54.360	-32:42:25.200	58715.3653	<i>r</i>	20.94
S	01:25:55.128	-32:42:54.000	58717.3258	<i>r</i>	20.74
S	01:25:55.656	-32:43:05.880	58718.3325	<i>r</i>	21.10
S	01:25:44.592	-32:43:43.680	58736.1406	<i>r</i>	20.68
S	01:28:15.168	-32:43:40.080	58710.3038	<i>r</i>	19.34
S	01:28:22.608	-32:43:40.800	58711.2357	<i>r</i>	19.90

Table 4 *continued*

Table 4 (*continued*)

Source ^a	α (J2000)	δ (J2000)	Date (MJD)	Filter	Magnitude Limit ^b (3σ)
S	01:28:11.832	-32:43:17.760	58712.1672	<i>r</i>	20.00
S	01:28:14.712	-32:42:56.520	58713.2062	<i>r</i>	20.29
S	01:28:14.184	-32:42:44.640	58714.2138	<i>r</i>	19.76
S	01:28:14.808	-32:42:45.720	58715.3868	<i>r</i>	20.91
S	01:28:18.216	-32:43:01.920	58716.3860	<i>r</i>	21.05
S	01:28:16.272	-32:42:55.800	58717.3232	<i>r</i>	20.64
S	01:28:19.200	-32:43:10.560	58718.2828	<i>r</i>	21.04
S	01:28:10.176	-32:42:56.520	58734.2958	<i>r</i>	21.26
S	01:30:36.480	-32:43:46.920	58710.2631	<i>r</i>	19.42
S	01:30:33.312	-32:42:53.280	58712.3547	<i>r</i>	20.10
S	01:30:38.784	-32:42:53.280	58713.3477	<i>r</i>	20.45
S	01:30:38.520	-32:43:09.480	58714.3515	<i>r</i>	20.47
S	01:30:37.536	-32:42:47.160	58715.3892	<i>r</i>	21.01
S	01:30:36.312	-32:42:51.120	58717.3736	<i>r</i>	20.99
S	01:30:27.912	-32:43:38.640	58736.1554	<i>r</i>	20.74
S	01:32:58.152	-32:43:38.280	58710.2974	<i>r</i>	19.44
S	01:32:54.360	-32:42:55.800	58712.3643	<i>r</i>	20.32
S	01:32:57.552	-32:43:00.480	58713.2159	<i>r</i>	20.35
S	01:32:57.024	-32:43:15.960	58714.1674	<i>r</i>	20.04
S	01:32:52.920	-32:42:41.400	58734.3101	<i>r</i>	21.75
S	01:35:18.384	-32:43:43.680	58710.2446	<i>r</i>	20.10
S	01:35:16.224	-32:43:17.400	58712.1717	<i>r</i>	20.03
S	01:35:19.392	-32:43:25.680	58713.1532	<i>r</i>	20.00
S	01:35:18.432	-32:43:23.880	58714.1582	<i>r</i>	18.84
S	01:35:17.592	-32:42:46.440	58715.4103	<i>r</i>	20.93
S	01:35:13.800	-32:42:45.000	58734.3220	<i>r</i>	21.75
S	01:37:38.256	-32:42:58.320	58712.3525	<i>r</i>	20.07
S	01:37:39.576	-32:43:21.720	58713.1445	<i>r</i>	19.91
S	01:37:39.240	-32:43:28.560	58714.1496	<i>r</i>	19.27
S	01:37:40.752	-32:42:47.160	58715.4056	<i>r</i>	21.03
S	01:37:43.800	-32:43:08.400	58718.3212	<i>r</i>	21.12
S	01:37:35.616	-32:42:57.960	58734.3337	<i>r</i>	21.83
S	01:40:02.472	-32:43:04.080	58713.2014	<i>r</i>	20.34
S	01:40:03.360	-32:43:09.480	58714.3372	<i>r</i>	20.31
S	01:40:03.984	-32:42:45.000	58715.3373	<i>r</i>	20.95
S	01:40:05.856	-32:42:58.680	58716.2467	<i>r</i>	20.75
S	01:40:04.800	-32:43:08.760	58718.3156	<i>r</i>	20.94
S	01:39:55.872	-32:43:01.560	58734.3562	<i>r</i>	21.58
S	01:20:40.800	-32:13:29.640	58717.1647	<i>r</i>	20.63
S	01:20:43.848	-32:13:28.200	58718.2653	<i>r</i>	21.12
S	01:20:41.016	-32:13:17.760	58719.3702	<i>r</i>	21.16
S	01:20:35.688	-32:13:06.960	58734.2729	<i>r</i>	21.38
S	01:27:41.832	-32:14:13.560	58710.2843	<i>r</i>	19.56
S	01:27:47.880	-32:13:15.600	58711.2437	<i>r</i>	19.88
S	01:27:41.688	-32:12:42.480	58715.3172	<i>r</i>	21.05
S	01:27:43.704	-32:13:15.240	58716.3832	<i>r</i>	21.07
S	01:27:45.384	-32:13:24.240	58718.2801	<i>r</i>	21.04
S	01:27:32.880	-32:13:55.920	58736.1444	<i>r</i>	20.77
S	01:30:01.968	-32:14:17.160	58710.3448	<i>r</i>	18.65
S	01:30:07.800	-32:13:39.360	58711.2070	<i>r</i>	19.72
S	01:29:59.280	-32:13:10.920	58712.3356	<i>r</i>	20.15
S	01:30:02.088	-32:13:09.840	58713.3452	<i>r</i>	20.50
S	01:30:02.016	-32:13:23.520	58714.3489	<i>r</i>	20.40

Table 4 (*continued*)

Table 4 (continued)

Source ^a	α (J2000)	δ (J2000)	Date (MJD)	Filter	Magnitude Limit ^b (3σ)
S	01:30:00.192	-32:13:03.000	58715.4149	r	20.98
S	01:30:04.008	-32:13:45.480	58716.3890	r	21.02
S	01:30:01.776	-32:13:38.280	58733.3248	r	20.95
S	01:29:52.080	-32:13:55.920	58736.1738	r	20.80
S	01:32:18.120	-32:12:55.080	58712.3594	r	20.19
S	01:32:22.752	-32:13:36.840	58713.2086	r	20.35
S	01:32:20.616	-32:13:55.200	58714.1604	r	19.57
S	01:32:22.248	-32:13:00.120	58715.3985	r	20.99
S	01:32:23.040	-32:13:26.040	58718.3239	r	21.08
S	01:32:13.032	-32:13:50.520	58736.1627	r	20.76
S	01:34:39.888	-32:13:12.720	58712.3617	r	20.21
S	01:34:43.272	-32:13:38.640	58713.2137	r	20.36
S	01:34:42.192	-32:13:55.200	58714.1652	r	19.54
S	01:34:42.288	-32:13:04.800	58715.4009	r	21.06
S	01:34:36.504	-32:13:00.120	58734.3180	r	21.74
S	01:37:00.240	-32:12:51.480	58712.3401	r	20.09
S	01:37:04.368	-32:12:55.440	58713.3356	r	20.50
S	01:37:02.736	-32:13:48.720	58714.3396	r	20.30
S	01:37:02.688	-32:13:01.560	58715.4032	r	20.94
S	01:37:04.152	-32:13:45.120	58718.3187	r	20.98
S	01:37:02.688	-32:13:29.640	58720.3864	r	21.21
S	01:36:55.944	-32:13:10.920	58734.3374	r	21.63
S	01:39:19.392	-32:13:25.680	58712.1988	r	20.10
S	01:39:24.312	-32:13:18.840	58713.1992	r	20.35
S	01:39:24.408	-32:13:23.520	58714.3350	r	20.32
S	01:39:23.544	-32:13:06.600	58715.4080	r	21.02
S	01:39:25.920	-32:13:23.520	58718.3128	r	20.96
S	01:39:16.704	-32:13:14.520	58734.3523	r	21.45
S	01:27:17.352	-31:43:34.320	58713.1898	r	20.32
S	01:27:16.056	-31:43:19.560	58714.3259	r	20.08
S	01:27:15.624	-31:42:45.720	58715.3603	r	21.00
S	01:27:19.416	-31:43:47.280	58716.2295	r	20.77
S	01:27:17.664	-31:43:16.320	58718.2856	r	21.11
S	01:27:08.808	-31:43:45.480	58734.3002	r	21.48
S	01:29:35.640	-31:44:06.720	58710.3487	r	19.12
S	01:29:41.640	-31:43:35.040	58711.2098	r	19.72
S	01:29:31.824	-31:43:27.120	58712.3333	r	20.28
S	01:29:34.392	-31:43:43.680	58713.1468	r	20.00
S	01:29:33.792	-31:43:41.880	58714.1517	r	19.59
S	01:29:33.744	-31:42:53.280	58715.3917	r	20.91
S	01:29:41.160	-31:43:09.840	58733.3205	r	20.90
S	01:29:24.648	-31:44:09.240	58736.1519	r	20.75
S	01:31:52.584	-31:43:25.320	58712.3308	r	20.16
S	01:31:57.096	-31:43:08.400	58713.3502	r	20.49
S	01:31:56.304	-31:43:23.520	58714.3538	r	20.42
S	01:31:53.184	-31:43:12.000	58715.3962	r	20.97
S	01:31:56.256	-31:42:59.400	58717.3761	r	21.02
S	01:31:49.968	-31:43:23.520	58734.3044	r	21.66
S	01:34:14.544	-31:44:16.440	58710.3195	r	19.66
S	01:34:21.384	-31:43:51.600	58711.2466	r	19.97
S	01:34:11.352	-31:43:24.240	58712.1695	r	20.07
S	01:34:15.456	-31:43:28.560	58713.1967	r	20.35
S	01:34:16.104	-31:43:28.920	58714.3326	r	20.33

Table 4 continued

Table 4 (continued)

Source ^a	α (J2000)	δ (J2000)	Date (MJD)	Filter	Magnitude Limit ^b (3σ)
S	01:34:13.008	-31:42:58.680	58715.4126	r	20.91
S	01:34:15.744	-31:43:27.840	58717.3789	r	20.91
S	01:34:17.784	-31:43:38.640	58718.2993	r	20.92
S	01:34:14.712	-31:43:47.640	58720.3841	r	21.17
S	01:34:07.488	-31:43:35.760	58734.3258	r	21.68
S	01:38:56.448	-31:43:24.960	58713.3403	r	20.47
S	01:38:55.200	-31:43:33.600	58714.3442	r	20.42
S	01:38:56.040	-31:43:07.680	58716.2499	r	20.76
S	01:38:56.976	-31:43:36.840	58718.3096	r	21.01
S	01:38:47.448	-31:43:30.360	58734.3490	r	21.41
S	01:24:31.440	-31:13:48.720	58710.3875	r	19.89
S	01:24:34.752	-31:13:28.560	58715.3102	r	20.91
S	01:24:33.720	-31:13:47.640	58716.3803	r	21.00
S	01:24:35.400	-31:13:53.040	58718.2774	r	20.98
S	01:24:26.256	-31:13:25.320	58734.2918	r	21.21
S	01:29:10.488	-31:14:11.760	58713.1920	r	20.30
S	01:29:11.160	-31:14:19.680	58714.3283	r	20.17
S	01:29:09.816	-31:13:28.200	58715.3220	r	20.97
S	01:29:12.360	-31:13:22.800	58716.2359	r	20.69
S	01:29:11.184	-31:13:36.480	58718.2909	r	21.04
S	01:28:58.776	-31:14:23.280	58736.1590	r	20.87
S	01:31:26.304	-31:14:22.920	58710.4400	r	19.71
S	01:31:31.320	-31:13:30.720	58715.3245	r	20.95
S	01:31:29.088	-31:13:39.000	58717.3207	r	20.73
S	01:31:32.472	-31:13:58.080	58718.2935	r	21.03
S	01:31:21.264	-31:13:41.880	58734.3140	r	21.82
S	01:33:48.192	-31:13:49.440	58713.1945	r	20.34
S	01:33:48.864	-31:13:53.760	58714.3305	r	20.32
S	01:33:47.664	-31:13:09.480	58715.3299	r	20.96
S	01:33:51.264	-31:13:47.280	58716.2387	r	20.65
S	01:33:51.024	-31:13:54.480	58718.2969	r	20.93
S	01:33:46.392	-31:14:00.960	58720.3820	r	21.16
S	01:33:39.768	-31:13:43.320	58734.3713	r	21.47
S	01:23:59.136	-30:44:52.440	58710.3811	r	19.24
S	01:24:00.936	-30:43:36.840	58715.3126	r	20.92
S	01:24:00.864	-30:43:35.400	58716.3780	r	20.99
S	01:24:02.328	-30:44:13.200	58718.2748	r	21.00
S	01:23:53.832	-30:43:58.440	58734.2879	r	21.34
S	01:32:46.608	-30:14:06.720	58715.2146	r	20.64
S	01:32:46.656	-30:13:54.480	58716.3945	r	20.96
S	01:32:46.392	-30:14:01.680	58718.3020	r	20.92
S	01:32:37.512	-30:14:01.680	58734.3297	r	21.60
S	01:35:02.256	-30:13:55.200	58713.3379	r	20.50
S	01:35:01.872	-30:12:59.760	58714.3418	r	20.35
S	01:35:03.744	-30:13:57.000	58715.3348	r	20.97
S	01:35:05.832	-30:14:11.040	58716.2444	r	20.72
S	01:35:05.328	-30:14:20.040	58718.3067	r	21.02
S	01:34:55.752	-30:14:08.520	58734.3451	r	21.55
S	01:34:35.352	-29:44:06.000	58713.3427	r	20.41
S	01:34:35.328	-29:44:17.160	58714.3465	r	20.40
S	01:34:36.552	-29:43:55.560	58715.3325	r	20.87
S	01:34:38.472	-29:44:31.200	58716.2415	r	20.65
S	01:34:38.448	-29:45:02.160	58718.3043	r	20.96

Table 4 continued

Table 4 (continued)

Source ^a	α (J2000)	δ (J2000)	Date (MJD)	Filter	Magnitude Limit ^b (3σ)
S	01:34:27.672	-29:44:22.560	58734.3414	r	21.58
S	00:57:21.000	-28:15:27.360	58717.1707	r	20.74
S	00:57:20.496	-28:15:33.480	58718.3569	r	21.06
S	00:57:11.016	-28:15:06.120	58736.1249	r	20.70
S	00:50:22.080	-27:45:24.480	58713.3089	r	20.34
S	00:50:22.608	-27:45:23.760	58715.1730	r	20.65
S	00:50:21.504	-27:46:15.240	58716.1342	r	20.85
S	00:50:13.512	-27:45:33.120	58734.1515	r	21.01
S	00:52:30.744	-27:45:28.440	58712.3258	r	19.91
S	00:52:35.760	-27:45:45.720	58713.1401	r	20.13
S	00:52:35.160	-27:45:54.720	58714.1454	r	20.00
S	00:52:36.696	-27:45:20.880	58715.1971	r	20.64
S	00:52:36.840	-27:45:48.240	58718.3719	r	21.04
S	00:52:33.984	-27:45:57.240	58727.1635	r	21.51
S	00:54:55.296	-27:45:07.920	58711.2126	r	19.81
S	00:54:46.680	-27:45:29.520	58712.3135	r	20.02
S	00:54:47.736	-27:45:42.840	58713.1511	r	20.10
S	00:54:47.304	-27:45:57.240	58714.1562	r	19.91
S	00:54:50.568	-27:45:16.200	58715.2349	r	20.58
S	00:54:53.328	-27:45:34.920	58726.2576	r	21.93
S	00:57:09.768	-27:45:32.040	58711.2253	r	19.74
S	00:57:00.624	-27:45:28.080	58712.3287	r	20.11
S	00:57:03.432	-27:45:23.760	58713.1490	r	20.16
S	00:57:03.168	-27:45:30.960	58714.1540	r	18.71
S	00:57:02.088	-27:45:25.920	58715.4199	r	20.86
S	00:57:05.520	-27:45:35.640	58716.4008	r	20.97
S	00:56:53.976	-27:46:23.520	58736.1286	r	20.71
S	00:59:17.976	-27:45:46.080	58717.1783	r	20.62
S	00:59:19.392	-27:45:45.360	58718.3479	r	21.06
S	00:59:21.624	-27:45:39.240	58726.2919	r	22.02
S	00:47:51.072	-27:15:43.920	58712.3184	r	19.98
S	00:47:51.840	-27:16:15.240	58713.1424	r	20.17
S	00:47:51.552	-27:16:29.280	58714.1475	r	19.45
S	00:47:54.648	-27:15:36.720	58715.1706	r	20.70
S	00:47:56.280	-27:15:22.680	58716.2785	r	20.60
S	00:47:57.360	-27:15:42.840	58726.2538	r	21.93
S	00:50:13.368	-27:15:52.920	58711.1802	r	19.57
S	00:50:03.240	-27:15:44.280	58712.2922	r	20.24
S	00:50:05.712	-27:15:43.200	58713.2255	r	20.31
S	00:50:05.016	-27:16:01.560	58714.1760	r	19.84
S	00:50:08.328	-27:15:22.680	58715.1897	r	20.50
S	00:50:00.168	-27:15:43.920	58734.1677	r	21.04
S	00:52:25.392	-27:15:47.520	58711.2224	r	19.70
S	00:52:17.952	-27:15:42.480	58712.2827	r	20.16
S	00:52:19.512	-27:15:37.440	58713.2376	r	20.35
S	00:52:18.072	-27:15:55.800	58714.1871	r	19.78
S	00:52:21.288	-27:15:11.880	58715.2196	r	20.58
S	00:52:21.552	-27:15:38.160	58717.3175	r	20.66
S	00:52:21.000	-27:16:41.160	58718.3740	r	20.99
S	00:52:21.120	-27:15:47.520	58719.3092	r	21.33
S	00:52:19.344	-27:15:58.320	58720.3294	r	21.36
S	00:52:22.440	-27:15:49.320	58725.2510	r	21.28
S	00:52:19.488	-27:16:15.960	58727.1599	r	21.40

Table 4 continued

Table 4 (*continued*)

Source ^a	α (J2000)	δ (J2000)	Date (MJD)	Filter	Magnitude Limit ^b (3σ)
S	00:54:28.392	-27:15:51.120	58712.3743	r	19.48
S	00:54:34.992	-27:15:44.280	58713.2502	r	20.38
S	00:54:33.720	-27:15:52.560	58714.2337	r	20.32
S	00:54:35.448	-27:15:33.120	58715.2326	r	20.65
S	00:54:33.576	-27:15:39.960	58718.3594	r	21.10
S	00:54:25.896	-27:16:28.920	58736.1213	r	20.67
S	00:56:53.256	-27:15:38.880	58711.1692	r	19.74
S	00:56:45.144	-27:15:43.920	58712.2899	r	20.18
S	00:56:47.832	-27:15:44.280	58713.2285	r	20.32
S	00:56:47.232	-27:16:11.640	58714.1783	r	19.95
S	00:56:45.288	-27:16:09.840	58715.4221	r	20.79
S	00:56:48.912	-27:15:43.560	58716.3328	r	20.85
S	00:56:49.800	-27:15:59.040	58725.2445	r	21.31
S	00:56:51.408	-27:15:52.560	58726.2726	r	21.89
S	00:58:57.024	-27:15:52.560	58712.1966	r	20.17
S	00:59:01.176	-27:15:48.600	58713.1804	r	20.26
S	00:59:02.208	-27:15:45.000	58714.3161	r	20.33
S	00:59:00.264	-27:15:30.960	58715.3744	r	20.91
S	00:59:01.320	-27:15:47.880	58716.3530	r	20.92
S	00:58:52.608	-27:16:22.080	58736.1325	r	20.69
S	00:45:26.280	-26:46:14.520	58713.1286	r	19.99
S	00:45:26.544	-26:46:08.040	58714.1306	r	19.09
S	00:45:29.040	-26:45:56.520	58715.1513	r	20.51
S	00:45:29.160	-26:46:58.440	58718.1278	r	21.06
S	00:45:19.512	-26:46:15.240	58734.1014	r	20.77
S	00:47:36.480	-26:46:03.360	58712.2758	r	20.18
S	00:47:40.632	-26:46:05.160	58713.1647	r	20.12
S	00:47:41.784	-26:45:54.360	58715.1683	r	20.62
S	00:47:43.416	-26:45:57.600	58716.2760	r	20.66
S	00:47:39.744	-26:45:55.440	58717.3151	r	20.67
S	00:47:42.240	-26:46:36.480	58718.1380	r	21.10
S	00:49:53.808	-26:46:48.360	58710.3139	r	19.66
S	00:49:50.736	-26:45:59.040	58712.2691	r	20.16
S	00:49:52.656	-26:45:54.360	58713.2570	r	20.35
S	00:49:55.008	-26:45:48.240	58715.1873	r	20.46
S	00:49:44.952	-26:46:45.480	58736.1174	r	20.67
S	00:52:05.208	-26:46:41.520	58710.4160	r	19.90
S	00:51:59.664	-26:46:04.800	58712.3893	r	19.93
S	00:52:05.544	-26:46:03.720	58713.3786	r	20.31
S	00:52:03.792	-26:46:18.120	58714.3826	r	20.30
S	00:52:06.936	-26:45:41.760	58715.2268	r	20.57
S	00:52:08.760	-26:45:55.080	58716.3077	r	20.74
S	00:52:04.992	-26:45:57.240	58727.2125	r	21.81
S	00:54:12.504	-26:46:03.000	58712.3843	r	20.29
S	00:54:17.904	-26:46:04.440	58713.3857	r	20.32
S	00:54:16.368	-26:46:17.040	58714.3900	r	20.41
S	00:54:15.696	-26:46:13.440	58715.4243	r	20.79
S	00:54:18.360	-26:45:49.680	58716.4033	r	20.97
S	00:54:20.688	-26:45:40.680	58717.3124	r	20.55
S	00:54:19.320	-26:46:39.720	58718.3617	r	21.12
S	00:54:20.208	-26:46:21.360	58719.3117	r	21.23
S	00:54:18.216	-26:46:31.080	58720.3468	r	21.21
S	00:54:19.488	-26:46:40.800	58725.2467	r	21.32

Table 4 *continued*

Table 4 (*continued*)

Source ^a	α (J2000)	δ (J2000)	Date (MJD)	Filter	Magnitude Limit ^b (3σ)
S	00:54:16.248	-26:46:09.840	58727.4277	r	19.82
S	00:54:12.096	-26:45:55.800	58734.2121	r	21.18
S	00:56:38.640	-26:46:04.080	58711.2174	r	19.69
S	00:56:25.968	-26:46:02.640	58712.3697	r	20.17
S	00:56:32.688	-26:45:58.680	58713.2451	r	20.40
S	00:56:31.896	-26:46:07.680	58714.2291	r	20.12
S	00:56:29.832	-26:45:29.160	58715.4176	r	20.84
S	00:56:33.576	-26:34:37.560	58716.3303	r	20.85
S	00:56:35.808	-26:46:07.320	58726.2882	r	21.97
S	00:58:50.616	-26:46:16.680	58711.1582	r	19.84
S	00:58:42.120	-26:45:55.800	58712.3017	r	19.96
S	00:58:45.336	-26:45:59.760	58713.2209	r	20.37
S	00:58:44.784	-26:46:20.280	58714.1720	r	19.91
S	00:58:44.160	-26:45:44.640	58715.3718	r	20.92
S	00:58:46.416	-26:45:57.240	58716.3469	r	20.85
S	00:58:45.264	-26:46:10.920	58727.2533	r	21.99
S	01:00:59.904	-26:45:47.880	58715.2097	r	20.63
S	01:00:58.848	-26:46:01.200	58716.3658	r	20.94
S	01:01:00.528	-26:46:11.640	58718.2346	r	20.89
S	01:00:57.912	-26:46:19.560	58727.2648	r	21.97
S	00:45:12.432	-26:16:06.240	58712.3087	r	19.96
S	00:45:13.176	-26:16:33.960	58713.1668	r	20.14
S	00:45:12.480	-26:16:28.200	58714.1978	r	19.35
S	00:45:15.912	-26:16:05.880	58715.1606	r	20.54
S	00:45:18.168	-26:16:09.480	58716.2625	r	20.55
S	00:45:14.448	-26:16:05.520	58717.3093	r	20.63
S	00:45:15.864	-26:17:09.600	58718.1304	r	21.11
S	00:45:13.008	-26:16:36.120	58720.3939	r	21.07
S	00:45:15.264	-26:16:35.760	58725.1960	r	21.38
S	00:45:06.744	-26:15:32.400	58734.1092	r	20.89
S	00:47:25.872	-26:16:54.120	58710.4125	r	19.11
S	00:47:32.160	-26:16:16.320	58711.2412	r	19.86
S	00:47:23.784	-26:16:10.560	58712.2575	r	20.13
S	00:47:28.104	-26:16:03.000	58713.2619	r	20.29
S	00:47:27.000	-26:16:18.840	58714.2453	r	19.72
S	00:47:29.472	-26:16:06.240	58715.1777	r	20.67
S	00:47:19.560	-26:16:15.240	58734.1442	r	20.90
S	00:49:38.616	-26:16:33.960	58710.2495	r	19.99
S	00:49:35.424	-26:16:13.440	58712.2464	r	20.29
S	00:49:37.680	-26:16:16.320	58713.3714	r	20.36
S	00:49:36.264	-26:16:30.000	58714.3747	r	20.43
S	00:49:41.040	-26:16:01.200	58715.1944	r	20.60
S	00:49:42.456	-26:16:09.840	58716.2942	r	20.67
S	00:49:39.024	-26:16:04.080	58717.3063	r	20.62
S	00:49:40.248	-26:16:33.600	58718.3791	r	21.00
S	00:49:40.656	-26:16:28.200	58726.3571	r	21.51
S	00:49:32.304	-26:16:09.120	58734.1795	r	21.15
S	00:51:50.904	-26:16:30.360	58710.2691	r	19.32
S	00:51:47.880	-26:16:11.640	58712.2391	r	20.19
S	00:51:52.704	-26:16:09.120	58713.2786	r	20.21
S	00:51:52.824	-26:16:21.720	58714.2607	r	18.93
S	00:51:52.848	-26:16:00.120	58715.2246	r	20.58
S	00:51:51.360	-26:16:06.960	58717.3036	r	20.38

Table 4 (*continued*)

Table 4 (*continued*)

Source ^a	α (J2000)	δ (J2000)	Date (MJD)	Filter	Magnitude Limit ^b (3σ)
S	00:51:50.928	-26:16:28.920	58718.3641	r	21.03
S	00:51:50.448	-26:16:24.960	58719.3611	r	21.32
S	00:51:50.688	-26:16:33.240	58720.3395	r	21.28
S	00:51:51.840	-26:16:23.520	58725.2489	r	21.30
S	00:51:49.848	-26:16:15.240	58727.2090	r	21.75
S	00:54:03.504	-26:17:03.480	58710.3276	r	19.64
S	00:53:56.856	-26:16:20.280	58712.3967	r	20.24
S	00:54:03.456	-26:16:27.840	58713.3738	r	20.37
S	00:54:01.896	-26:16:36.840	58714.3772	r	20.46
S	00:54:05.712	-26:15:59.760	58715.2400	r	20.67
S	00:54:05.496	-26:16:10.920	58716.3244	r	20.83
S	00:54:05.328	-26:16:38.280	58717.3008	r	20.52
S	00:54:04.752	-26:16:31.800	58718.3546	r	21.09
S	00:54:03.576	-26:16:24.960	58719.3588	r	21.42
S	00:54:01.128	-26:16:35.400	58720.3794	r	21.08
S	00:54:05.760	-26:16:24.960	58725.2183	r	21.44
S	00:53:57.360	-26:16:04.080	58734.2199	r	21.16
S	00:56:22.656	-26:16:13.800	58711.2546	r	19.87
S	00:56:11.040	-26:16:26.040	58712.3821	r	20.20
S	00:56:18.312	-26:16:04.800	58713.3221	r	20.31
S	00:56:16.848	-26:15:56.160	58714.3000	r	19.51
S	00:56:17.568	-26:15:59.400	58715.2548	r	20.63
S	00:56:17.688	-26:16:10.200	58716.3387	r	20.96
S	00:56:14.616	-26:16:35.400	58720.3771	r	21.03
S	00:56:19.296	-26:16:23.160	58726.3549	r	21.60
S	00:56:09.864	-26:15:58.680	58734.2290	r	21.14
S	00:58:25.848	-26:16:35.040	58710.4437	r	19.50
S	00:58:33.936	-26:15:46.080	58711.2387	r	19.84
S	00:58:26.016	-26:16:12.720	58712.2997	r	20.16
S	00:58:30.792	-26:16:08.040	58713.3246	r	20.31
S	00:58:29.400	-26:16:25.680	58714.3021	r	19.53
S	00:58:27.432	-26:16:00.480	58715.3792	r	20.83
S	00:58:29.712	-26:16:14.160	58716.3582	r	20.86
S	00:58:30.672	-26:16:10.920	58717.2537	r	20.63
S	00:58:29.640	-26:16:23.880	58718.3404	r	21.06
S	00:58:28.392	-26:16:21.720	58719.3563	r	21.43
S	00:58:27.792	-26:16:39.360	58720.3585	r	21.12
S	00:58:29.352	-26:16:25.320	58725.2395	r	21.37
S	00:58:28.152	-26:16:54.120	58727.2570	r	21.88
S	00:45:06.000	-25:47:08.880	58710.2915	r	18.05
S	00:45:06.912	-25:47:25.440	58710.2946	r	19.87
S	00:45:12.408	-25:46:01.200	58711.2676	r	19.81
S	00:45:04.368	-25:46:25.320	58712.2801	r	20.19
S	00:45:05.664	-25:46:02.640	58713.2400	r	20.31
S	00:45:03.984	-25:46:15.600	58714.1890	r	19.79
S	00:45:07.968	-25:46:18.840	58715.1584	r	20.37
S	00:45:09.144	-25:46:25.320	58716.2734	r	20.55
S	00:45:06.288	-25:46:26.400	58717.2512	r	20.70
S	00:44:55.032	-25:17:00.960	58718.1329	r	21.23
S	00:45:07.848	-25:47:06.720	58718.1356	r	21.14
S	00:45:07.224	-25:46:39.360	58719.3543	r	21.43
S	00:45:03.624	-25:46:57.720	58720.3915	r	21.05
S	00:45:06.864	-25:46:40.440	58725.1983	r	21.34

Table 4 *continued*

Table 4 (continued)

Source ^a	α (J2000)	δ (J2000)	Date (MJD)	Filter	Magnitude Limit ^b (3σ)
S	00:44:58.272	-25:46:32.520	58734.1327	r	20.90
S	00:47:17.160	-25:47:08.520	58710.4002	r	19.11
S	00:47:12.720	-25:46:26.400	58712.2485	r	20.26
S	00:47:18.096	-25:46:24.240	58713.2718	r	20.31
S	00:47:16.656	-25:46:35.400	58714.2540	r	19.78
S	00:47:19.416	-25:46:19.560	58715.1850	r	20.64
S	00:47:20.928	-25:46:24.960	58716.2890	r	20.69
S	00:47:11.400	-25:46:29.640	58734.1635	r	21.04
S	00:49:28.128	-25:46:43.680	58710.2298	r	19.74
S	00:49:24.360	-25:46:26.040	58712.2091	r	20.19
S	00:49:31.416	-25:46:15.600	58713.2840	r	20.38
S	00:49:30.912	-25:46:35.400	58714.2655	r	20.10
S	00:49:31.488	-25:46:13.800	58715.2045	r	20.45
S	00:49:32.472	-25:46:18.120	58716.2971	r	20.69
S	00:49:30.096	-25:46:28.560	58717.2484	r	20.62
S	00:49:29.592	-25:46:46.200	58718.3765	r	21.00
S	00:49:28.704	-25:46:58.440	58727.1562	r	21.51
S	00:51:40.992	-25:47:16.800	58710.2363	r	20.07
S	00:51:37.728	-25:46:29.640	58712.1942	r	20.17
S	00:51:42.840	-25:46:30.000	58713.3622	r	20.28
S	00:51:40.872	-25:46:45.120	58714.3659	r	20.37
S	00:51:42.864	-25:46:18.840	58715.2293	r	20.62
S	00:51:44.160	-25:46:00.840	58716.3124	r	20.71
S	00:51:41.808	-25:46:27.840	58717.2458	r	20.54
S	00:51:42.432	-25:46:45.120	58718.3664	r	21.05
S	00:51:41.784	-25:46:48.360	58727.2305	r	21.80
S	00:53:49.992	-25:46:35.400	58712.2342	r	20.32
S	00:53:53.688	-25:46:28.200	58713.3670	r	20.36
S	00:53:52.392	-25:46:44.040	58714.3701	r	20.43
S	00:53:54.864	-25:46:36.120	58715.2423	r	20.66
S	00:53:56.160	-25:46:18.120	58716.3217	r	20.82
S	00:53:54.072	-25:46:21.000	58718.3503	r	21.06
S	00:53:54.144	-25:46:37.560	58727.2458	r	21.80
S	00:56:11.280	-25:46:49.800	58711.2571	r	19.88
S	00:56:01.392	-25:46:53.400	58712.1556	r	19.94
S	00:56:06.696	-25:46:31.800	58713.1781	r	20.21
S	00:56:05.880	-25:46:41.520	58714.2069	r	19.38
S	00:56:07.848	-25:46:15.600	58715.2524	r	20.64
S	00:56:07.008	-25:46:27.840	58716.3444	r	20.83
S	00:56:07.656	-25:46:28.560	58717.2434	r	20.55
S	00:56:05.496	-25:47:25.440	58718.3428	r	21.03
S	00:56:07.200	-25:46:34.320	58719.3520	r	21.41
S	00:56:02.976	-25:46:49.440	58720.3729	r	20.03
S	00:56:03.528	-25:47:03.120	58720.3748	r	20.36
S	00:56:07.824	-25:46:39.720	58725.2257	r	21.45
S	00:55:58.824	-25:46:17.400	58734.2329	r	21.12
S	00:58:23.256	-25:46:24.240	58711.1558	r	19.74
S	00:58:15.696	-25:46:06.600	58712.2948	r	20.18
S	00:58:16.872	-25:46:22.440	58713.2232	r	20.30
S	00:58:16.464	-25:46:27.840	58714.1740	r	20.13
S	00:58:15.816	-25:45:52.920	58715.3768	r	20.86
S	00:58:18.576	-25:46:29.640	58716.3632	r	20.87
S	00:58:16.416	-25:45:57.600	58717.3822	r	20.90

Table 4 continued

Table 4 (*continued*)

Source ^a	α (J2000)	δ (J2000)	Date (MJD)	Filter	Magnitude Limit ^b (3σ)
S	00:58:20.856	-25:46:40.080	58718.2318	r	20.95
S	00:58:18.360	-25:46:06.240	58719.3170	r	21.45
S	00:58:15.792	-25:46:49.800	58720.3698	r	20.14
S	00:58:19.728	-25:46:41.160	58725.2302	r	21.36
S	00:58:11.232	-25:46:11.640	58734.2408	r	21.10
S	01:00:27.384	-25:45:56.520	58712.3234	r	19.80
S	01:00:29.952	-25:46:42.600	58713.1335	r	19.92
S	01:00:29.184	-25:46:52.680	58714.1382	r	19.61
S	01:00:28.752	-25:46:15.960	58715.3840	r	20.87
S	01:00:29.784	-25:46:06.600	58716.3688	r	20.95
S	01:00:32.904	-25:46:37.560	58718.2508	r	20.94
S	01:00:29.400	-25:46:49.080	58720.3654	r	20.56
S	01:00:33.312	-25:46:35.040	58726.3430	r	21.88
S	01:02:42.696	-25:46:33.240	58717.1810	r	20.62
S	01:01:44.832	-25:46:36.840	58718.2566	r	21.01
S	01:02:35.280	-25:46:11.280	58734.2573	r	21.20
S	00:42:41.184	-25:17:03.480	58710.4194	r	19.47
S	00:42:49.272	-25:16:26.400	58711.2150	r	19.66
S	00:42:39.696	-25:16:42.240	58712.3158	r	19.75
S	00:42:42.456	-25:16:34.320	58713.1557	r	20.14
S	00:42:40.536	-25:17:17.880	58714.1912	r	19.73
S	00:42:44.040	-25:16:37.200	58715.1561	r	20.46
S	00:42:45.864	-25:16:42.240	58716.2567	r	20.66
S	00:42:42.720	-25:16:41.160	58717.2410	r	20.60
S	00:42:33.480	-25:16:49.080	58734.1053	r	20.86
S	00:44:53.880	-25:17:20.040	58710.3553	r	18.69
S	00:44:50.616	-25:16:41.520	58712.2667	r	20.15
S	00:44:53.808	-25:16:18.480	58713.2592	r	20.28
S	00:44:52.128	-25:16:47.280	58714.2430	r	19.44
S	00:44:55.704	-25:16:39.360	58715.1660	r	20.49
S	00:44:57.528	-25:16:39.360	58716.2710	r	20.55
S	00:44:46.680	-25:16:50.520	58734.1289	r	20.88
S	00:47:02.640	-25:17:41.640	58710.2406	r	20.04
S	00:46:59.736	-25:16:40.440	58712.2438	r	20.20
S	00:47:05.520	-25:17:03.480	58713.2739	r	20.34
S	00:47:04.920	-25:17:18.240	58714.2561	r	19.84
S	00:47:06.840	-25:16:35.040	58715.1828	r	20.63
S	00:47:08.352	-25:16:38.280	58716.2864	r	20.57
S	00:47:04.560	-25:16:42.600	58717.2382	r	20.54
S	00:47:06.984	-25:17:17.520	58718.1518	r	21.11
S	00:47:04.272	-25:16:53.400	58719.3499	r	21.34
S	00:47:03.336	-25:16:40.440	58720.3892	r	21.00
S	00:47:06.336	-25:16:58.440	58725.2049	r	21.36
S	00:47:02.808	-25:16:57.360	58727.4175	r	20.84
S	00:46:57.696	-25:16:29.640	58734.1757	r	21.07
S	00:49:10.800	-25:16:48.360	58712.1897	r	20.11
S	00:49:17.904	-25:16:35.760	58713.2883	r	20.32
S	00:49:15.984	-25:16:54.480	58714.2699	r	20.11
S	00:49:18.216	-25:16:27.840	58715.2022	r	20.60
S	00:49:19.200	-25:16:40.440	58716.3051	r	20.75
S	00:49:18.672	-25:16:43.680	58717.2357	r	20.63
S	00:49:15.696	-25:17:17.880	58718.3688	r	20.93
S	00:49:17.712	-25:16:55.560	58719.3477	r	21.39

Table 4 *continued*

Table 4 (continued)

Source ^a	α (J2000)	δ (J2000)	Date (MJD)	Filter	Magnitude Limit ^b (3σ)
S	00:49:15.648	-25:17:02.040	58720.3270	r	21.36
S	00:49:18.120	-25:16:37.920	58725.2115	r	21.54
S	00:49:15.552	-25:17:16.440	58727.1522	r	21.51
S	00:49:20.592	-25:16:46.920	58737.3559	r	20.77
S	00:51:24.168	-25:16:51.600	58712.1830	r	20.02
S	00:51:27.312	-25:16:46.560	58713.3551	r	20.19
S	00:51:25.392	-25:16:56.280	58714.3588	r	20.36
S	00:51:27.936	-25:16:08.040	58715.2373	r	20.61
S	00:51:29.952	-25:16:39.360	58716.3180	r	20.78
S	00:51:25.632	-25:16:44.040	58717.3846	r	20.83
S	00:51:31.440	-25:17:02.040	58718.1888	r	21.30
S	00:51:27.816	-25:17:04.200	58727.2269	r	21.68
S	00:53:34.848	-25:16:48.720	58712.2038	r	20.13
S	00:53:39.360	-25:16:36.480	58713.3170	r	20.31
S	00:53:38.280	-25:16:52.320	58714.2953	r	18.83
S	00:53:40.776	-25:16:30.360	58715.2501	r	20.62
S	00:53:40.416	-25:16:43.320	58716.3271	r	20.84
S	00:53:39.288	-25:16:45.120	58717.3875	r	20.84
S	00:53:39.768	-25:17:26.880	58718.3524	r	21.19
S	00:53:43.944	-25:16:48.360	58726.2689	r	21.97
S	00:55:50.472	-25:17:21.840	58710.3766	r	18.75
S	00:55:47.016	-25:16:53.400	58712.1761	r	19.95
S	00:55:50.616	-25:16:35.760	58713.3300	r	20.33
S	00:55:49.536	-25:16:51.960	58714.3071	r	19.06
S	00:55:49.416	-25:15:58.680	58715.3681	r	20.92
S	00:55:51.312	-25:16:46.920	58716.3415	r	20.82
S	00:55:49.800	-25:16:42.600	58717.3900	r	20.83
S	00:55:55.032	-25:16:51.960	58726.3109	r	21.93
S	00:58:08.520	-25:16:51.600	58711.1994	r	19.62
S	00:57:57.504	-25:16:21.720	58712.3718	r	19.73
S	00:58:01.920	-25:16:46.560	58713.1873	r	20.22
S	00:58:03.528	-25:16:53.400	58714.3208	r	19.49
S	00:58:00.288	-25:16:35.040	58715.3814	r	20.86
S	00:58:02.040	-25:16:22.080	58716.3607	r	20.85
S	00:58:01.296	-25:16:28.920	58727.2607	r	21.86
S	01:02:25.632	-25:16:12.360	58713.3272	r	20.30
S	01:02:25.272	-25:16:36.120	58714.3046	r	19.17
S	01:02:26.496	-25:16:28.200	58715.3049	r	20.72
S	01:02:27.360	-25:17:09.600	58716.1895	r	20.66
S	01:02:27.432	-25:16:48.360	58718.2625	r	20.92
S	01:02:17.544	-25:16:28.560	58734.2610	r	21.28
S	00:38:10.728	-24:46:57.720	58717.1735	r	20.62
S	00:38:10.248	-24:47:47.400	58718.1167	r	21.19
S	00:38:08.472	-24:46:45.480	58719.3753	r	21.20
S	00:38:12.840	-24:47:00.960	58726.2495	r	22.02
S	00:40:17.184	-24:47:48.480	58710.4345	r	19.42
S	00:40:22.008	-24:46:58.440	58715.1488	r	20.52
S	00:40:22.896	-24:46:31.080	58716.2535	r	20.66
S	00:40:22.872	-24:47:52.440	58718.1197	r	21.18
S	00:40:16.080	-24:47:41.640	58736.1092	r	20.61
S	00:42:30.312	-24:46:55.200	58710.3975	r	19.23
S	00:42:35.496	-24:46:54.120	58711.2520	r	19.72
S	00:42:27.936	-24:46:39.000	58712.3039	r	19.99

Table 4 continued

Table 4 (*continued*)

Source ^a	α (J2000)	δ (J2000)	Date (MJD)	Filter	Magnitude Limit ^b (3σ)
S	00:42:30.240	-24:46:35.040	58713.2185	r	20.32
S	00:42:30.120	-24:47:20.760	58714.1698	r	19.54
S	00:42:31.200	-24:46:31.080	58715.1538	r	20.41
S	00:42:33.432	-24:47:19.680	58716.2599	r	20.64
S	00:42:30.960	-24:46:57.720	58717.2330	r	20.61
S	00:42:21.792	-24:47:06.360	58734.1131	r	20.96
S	00:44:36.840	-24:46:46.560	58712.2554	r	20.15
S	00:44:41.472	-24:46:47.280	58713.2641	r	20.32
S	00:44:40.512	-24:46:48.000	58714.2476	r	19.32
S	00:44:41.880	-24:46:27.120	58715.1754	r	20.62
S	00:44:43.440	-24:46:17.760	58716.2810	r	20.57
S	00:44:35.184	-24:47:02.400	58734.1404	r	20.76
S	00:46:46.512	-24:46:52.680	58712.2366	r	20.22
S	00:46:52.440	-24:46:37.560	58713.2812	r	20.26
S	00:46:51.456	-24:46:51.960	58714.2631	r	19.42
S	00:46:52.440	-24:46:26.400	58715.1921	r	20.54
S	00:46:54.792	-24:46:52.680	58716.2918	r	20.62
S	00:46:52.176	-24:47:00.240	58717.2306	r	20.60
S	00:46:55.056	-24:47:39.840	58718.1496	r	21.24
S	00:46:52.944	-24:47:08.160	58719.3456	r	21.39
S	00:46:50.856	-24:47:10.680	58720.3248	r	21.36
S	00:46:53.952	-24:47:17.160	58725.2027	r	21.36
S	00:46:49.200	-24:47:13.200	58727.4197	r	20.65
S	00:46:43.752	-24:47:00.600	58734.1718	r	21.09
S	00:48:58.272	-24:47:22.200	58712.1919	r	20.15
S	00:49:01.680	-24:46:58.440	58713.3596	r	20.31
S	00:49:00.408	-24:47:09.240	58714.3634	r	20.40
S	00:49:02.640	-24:46:42.960	58715.2220	r	20.62
S	00:49:06.216	-24:46:54.480	58716.3028	r	20.72
S	00:49:04.896	-24:47:01.320	58717.2280	r	20.60
S	00:49:05.352	-24:47:33.000	58718.1621	r	21.18
S	00:49:03.984	-24:46:47.640	58719.3191	r	21.53
S	00:49:02.160	-24:47:16.440	58720.3366	r	21.21
S	00:49:02.664	-24:47:22.200	58727.1715	r	21.66
S	00:51:13.896	-24:47:36.240	58710.3168	r	19.71
S	00:51:09.360	-24:47:02.760	58712.1875	r	20.07
S	00:51:16.128	-24:46:55.560	58713.2913	r	20.42
S	00:51:14.736	-24:47:06.720	58714.2724	r	19.79
S	00:51:10.752	-24:46:30.720	58715.4269	r	20.60
S	00:51:15.456	-24:46:41.520	58716.3156	r	20.81
S	00:51:16.296	-24:47:14.280	58718.1980	r	21.15
S	00:51:14.328	-24:47:18.600	58727.2380	r	21.72
S	00:53:24.768	-24:47:38.400	58710.3078	r	18.78
S	00:53:20.064	-24:47:16.800	58712.1648	r	19.99
S	00:53:23.136	-24:46:57.720	58713.1848	r	20.28
S	00:53:23.304	-24:47:04.200	58714.3184	r	19.95
S	00:53:26.568	-24:46:44.760	58715.2478	r	20.59
S	00:53:25.536	-24:46:59.160	58716.3360	r	20.85
S	00:53:23.952	-24:46:42.600	58718.3455	r	20.95
S	00:53:28.320	-24:47:05.640	58726.2840	r	21.89
S	00:55:29.928	-24:47:04.560	58712.3942	r	19.87
S	00:55:37.080	-24:47:15.720	58713.3198	r	20.24
S	00:55:36.120	-24:47:30.840	58714.2974	r	19.07

Table 4 *continued*

Table 4 (continued)

Source ^a	α (J2000)	δ (J2000)	Date (MJD)	Filter	Magnitude Limit ^b (3σ)
S	00:55:36.648	-24:47:06.000	58715.1345	r	20.40
S	00:55:34.848	-24:46:34.680	58716.3555	r	20.93
S	00:55:38.136	-24:47:13.920	58718.2231	r	21.05
S	00:55:36.624	-24:47:06.000	58719.3213	r	21.47
S	00:55:34.560	-24:47:19.680	58720.3541	r	21.16
S	00:55:36.144	-24:46:53.760	58725.2421	r	21.39
S	00:55:39.024	-24:47:10.680	58726.3191	r	21.99
S	00:57:51.552	-24:47:20.400	58711.1719	r	19.78
S	00:57:40.992	-24:47:00.600	58712.3674	r	19.67
S	00:57:46.104	-24:46:56.280	58713.2351	r	20.38
S	00:57:45.384	-24:47:15.360	58714.1850	r	19.54
S	00:57:47.040	-24:47:00.240	58715.1437	r	20.39
S	00:57:46.008	-24:46:59.880	58717.3952	r	20.87
S	00:57:49.656	-24:47:09.960	58718.2409	r	20.88
S	00:57:47.376	-24:47:03.840	58719.3236	r	21.38
S	00:57:44.184	-24:46:51.600	58720.3607	r	20.89
S	00:57:47.424	-24:47:18.960	58725.2324	r	21.36
S	00:57:51.792	-24:47:18.960	58737.3516	r	20.91
S	01:02:09.648	-24:47:08.880	58725.2371	r	21.33
S	01:02:00.672	-24:46:45.120	58734.2649	r	21.28
S	00:42:18.744	-24:17:07.800	58712.2779	r	20.18
S	00:42:22.368	-24:16:47.640	58713.2426	r	20.34
S	00:42:22.848	-24:16:55.920	58714.2267	r	20.07
S	00:42:23.088	-24:17:15.000	58717.2251	r	20.61
S	00:42:15.144	-24:17:21.480	58734.1249	r	20.88
S	00:44:33.600	-24:18:19.800	58710.3106	r	18.62
S	00:44:39.552	-24:16:42.240	58711.2494	r	19.83
S	00:44:28.560	-24:16:42.960	58712.2506	r	20.28
S	00:44:33.888	-24:17:25.800	58713.2663	r	20.30
S	00:44:33.072	-24:17:18.960	58714.2497	r	20.22
S	00:44:33.288	-24:17:13.560	58717.2225	r	20.59
S	00:44:35.880	-24:17:47.760	58718.1440	r	21.22
S	00:44:30.984	-24:17:25.080	58720.3183	r	21.26
S	00:44:35.424	-24:17:08.880	58725.2563	r	21.27
S	00:44:26.088	-24:17:11.040	58734.1597	r	21.01
S	00:46:43.920	-24:17:26.880	58710.3005	r	19.54
S	00:46:40.176	-24:17:25.800	58712.1620	r	19.99
S	00:46:44.232	-24:17:12.480	58713.1690	r	20.14
S	00:46:44.136	-24:17:24.360	58714.2001	r	19.54
S	00:46:45.720	-24:17:20.040	58715.1251	r	20.34
S	00:46:46.776	-24:16:51.240	58716.2654	r	20.55
S	00:46:45.120	-24:17:14.280	58717.2201	r	20.59
S	00:46:45.192	-24:17:28.680	58718.1546	r	21.27
S	00:46:43.272	-24:17:15.360	58719.3437	r	21.31
S	00:46:42.984	-24:17:12.840	58720.3227	r	21.22
S	00:46:44.712	-24:17:31.560	58725.2072	r	21.51
S	00:46:37.296	-24:17:00.600	58734.2000	r	21.19
S	00:48:49.488	-24:17:00.600	58712.2012	r	20.16
S	00:48:54.192	-24:16:49.080	58713.2859	r	20.38
S	00:48:52.944	-24:16:53.400	58714.2676	r	20.21
S	00:48:55.368	-24:18:11.880	58718.1645	r	21.31
S	00:48:53.832	-24:17:33.000	58727.2233	r	21.53
S	00:50:59.256	-24:17:02.400	58712.1851	r	19.98

Table 4 continued

Table 4 (*continued*)

Source ^a	α (J2000)	δ (J2000)	Date (MJD)	Filter	Magnitude Limit ^b (3σ)
S	00:51:03.312	-24:17:07.800	58713.3576	r	20.32
S	00:51:02.544	-24:17:10.680	58714.3611	r	20.36
S	00:51:06.336	-24:17:27.240	58715.1277	r	20.13
S	00:51:07.272	-24:17:25.800	58718.1948	r	21.22
S	00:51:03.840	-24:18:35.640	58727.2418	r	21.81
S	00:53:10.632	-24:17:04.200	58712.1739	r	19.94
S	00:53:13.656	-24:17:08.160	58713.3691	r	20.36
S	00:53:12.600	-24:17:33.720	58714.3722	r	20.36
S	00:53:17.112	-24:17:42.360	58716.1564	r	20.71
S	00:53:17.592	-24:17:22.920	58718.2120	r	20.90
S	00:53:18.840	-24:17:23.280	58726.2804	r	21.87
S	00:55:20.040	-24:16:54.120	58712.3870	r	20.15
S	00:55:24.792	-24:17:14.640	58713.3809	r	20.33
S	00:55:23.280	-24:17:24.720	58714.3850	r	20.36
S	00:55:26.808	-24:17:23.280	58715.1323	r	20.33
S	00:55:27.504	-24:17:42.000	58716.1740	r	20.71
S	00:55:28.032	-24:17:27.240	58718.2293	r	20.90
S	00:55:24.888	-24:17:41.640	58719.3258	r	21.40
S	00:55:23.712	-24:17:29.040	58720.3562	r	21.13
S	00:55:26.184	-24:17:05.280	58725.2279	r	21.34
S	00:55:17.136	-24:17:05.640	58734.2371	r	21.10
S	00:57:41.496	-24:17:02.040	58711.2331	r	19.86
S	00:57:33.312	-24:17:07.080	58712.2852	r	20.12
S	00:57:36.072	-24:17:09.960	58713.2332	r	20.35
S	00:57:35.112	-24:17:32.280	58714.1828	r	20.02
S	00:57:37.032	-24:17:15.720	58715.1414	r	20.40
S	00:57:38.232	-24:17:24.720	58718.2482	r	20.87
S	00:57:39.168	-24:17:25.440	58726.3390	r	21.89
S	01:06:18.456	-24:17:07.080	58719.3326	r	21.42
S	01:06:16.056	-24:17:09.600	58720.3677	r	21.02
S	01:06:10.440	-24:17:06.000	58734.2690	r	21.32
S	00:42:15.432	-23:47:46.320	58711.1502	r	19.76
S	00:42:06.048	-23:47:29.760	58712.1807	r	19.94
S	00:42:12.024	-23:46:52.680	58713.2936	r	20.21
S	00:42:10.728	-23:47:10.680	58714.2747	r	20.01
S	00:42:12.312	-23:47:36.600	58715.1228	r	20.42
S	00:42:04.584	-23:47:34.800	58734.1208	r	20.95
S	00:44:19.536	-23:47:54.960	58710.4370	r	19.34
S	00:44:17.064	-23:47:25.440	58712.2646	r	20.18
S	00:44:20.256	-23:47:33.360	58713.1602	r	20.05
S	00:44:20.616	-23:47:32.640	58714.3092	r	18.57
S	00:44:21.264	-23:47:27.960	58717.2176	r	20.67
S	00:44:22.224	-23:47:25.800	58718.3816	r	21.00
S	00:44:19.824	-23:47:38.040	58720.3205	r	21.35
S	00:44:22.176	-23:47:14.280	58725.2006	r	21.40
S	00:44:14.856	-23:47:28.680	58734.1922	r	21.14
S	00:46:37.296	-23:47:16.080	58711.1913	r	19.18
S	00:46:36.936	-23:47:40.560	58711.1970	r	19.56
S	00:46:27.936	-23:47:47.400	58712.2529	r	20.12
S	00:46:29.256	-23:47:28.680	58713.3761	r	20.33
S	00:46:27.528	-23:47:22.920	58714.3802	r	20.33
S	00:46:30.744	-23:48:01.440	58727.1483	r	21.60
S	00:48:39.936	-23:48:07.200	58710.3739	r	19.41

Table 4 (*continued*)

Table 4 (continued)

Source ^a	α (J2000)	δ (J2000)	Date (MJD)	Filter	Magnitude Limit ^b (3σ)
S	00:48:35.448	-23:47:22.560	58712.2415	r	20.19
S	00:48:42.504	-23:47:15.720	58713.2761	r	20.27
S	00:48:41.592	-23:47:10.320	58714.2583	r	19.21
S	00:48:40.704	-23:47:33.360	58717.2153	r	20.60
S	00:48:43.392	-23:47:37.320	58718.1860	r	21.23
S	00:48:42.048	-23:47:29.760	58719.3415	r	21.31
S	00:48:39.456	-23:47:47.760	58720.3422	r	21.37
S	00:48:41.976	-23:47:27.600	58725.2138	r	21.46
S	00:48:40.968	-23:47:32.640	58727.2198	r	21.72
S	00:50:51.600	-23:48:09.000	58710.3381	r	17.41
S	00:50:51.528	-23:48:11.160	58710.3393	r	18.65
S	00:50:45.312	-23:47:16.080	58712.2067	r	20.09
S	00:50:50.280	-23:47:33.360	58713.3645	r	20.29
S	00:50:48.528	-23:47:22.200	58714.3679	r	20.34
S	00:50:52.392	-23:47:56.760	58716.1508	r	20.69
S	00:50:52.152	-23:47:34.800	58717.2124	r	20.57
S	00:50:52.848	-23:47:43.800	58718.2008	r	21.12
S	00:50:54.672	-23:47:34.080	58726.2652	r	21.93
S	00:52:56.064	-23:47:57.120	58712.1534	r	19.89
S	00:53:01.080	-23:47:32.640	58713.1758	r	20.17
S	00:53:00.072	-23:47:41.280	58714.2045	r	19.61
S	00:53:02.328	-23:47:42.000	58715.1300	r	20.20
S	00:53:02.736	-23:48:08.280	58716.1630	r	20.71
S	00:53:03.168	-23:47:43.080	58718.2181	r	20.93
S	00:52:59.664	-23:47:31.560	58719.3280	r	21.20
S	00:53:00.168	-23:47:49.200	58720.3519	r	21.16
S	00:53:02.664	-23:47:41.640	58725.2235	r	21.37
S	00:53:03.984	-23:47:38.040	58726.3072	r	21.95
S	00:55:09.216	-23:47:24.000	58710.3522	r	18.73
S	00:55:05.592	-23:47:32.640	58712.3795	r	19.84
S	00:55:11.112	-23:47:22.920	58713.2545	r	20.26
S	00:55:09.912	-23:47:34.800	58714.2384	r	19.36
S	00:55:11.088	-23:47:17.880	58715.1367	r	20.40
S	00:55:14.040	-23:47:39.120	58726.3309	r	21.84
S	00:57:16.224	-23:47:38.040	58712.1576	r	19.99
S	00:57:18.600	-23:47:13.560	58713.1825	r	20.21
S	00:57:20.136	-23:47:38.040	58714.2091	r	19.84
S	00:57:20.784	-23:47:39.120	58715.1462	r	20.34
S	00:57:22.776	-23:47:52.800	58716.1864	r	20.62
S	00:57:22.296	-23:47:40.200	58718.2435	r	20.89
S	00:57:21.048	-23:47:34.440	58719.3302	r	21.25
S	00:57:18.192	-23:47:29.400	58720.3631	r	21.11
S	00:57:21.480	-23:47:25.800	58725.2347	r	21.31
S	00:57:12.696	-23:47:36.600	58734.2526	r	21.00
S	00:59:30.288	-23:47:34.800	58717.1759	r	20.62
S	00:59:31.464	-23:47:17.520	58718.2593	r	21.01
S	00:59:28.680	-23:47:24.720	58727.2684	r	21.86
S	00:41:59.928	-23:18:21.960	58710.3620	r	19.32
S	00:42:06.624	-23:17:36.960	58711.1611	r	19.73
S	00:41:55.608	-23:18:08.640	58712.1511	r	19.95
S	00:41:58.944	-23:17:53.520	58713.1377	r	20.02
S	00:41:58.728	-23:18:08.640	58714.1431	r	18.56
S	00:41:51.912	-23:17:48.120	58734.1367	r	20.90

Table 4 continued

Table 4 (*continued*)

Source ^a	α (J2000)	δ (J2000)	Date (MJD)	Filter	Magnitude Limit ^b (3σ)
S	00:44:15.432	-23:17:57.120	58711.1774	r	19.73
S	00:44:04.848	-23:17:54.960	58712.1599	r	19.98
S	00:44:08.208	-23:17:25.080	58713.1712	r	20.16
S	00:44:07.704	-23:17:36.240	58714.2023	r	19.73
S	00:44:10.368	-23:17:14.280	58716.3496	r	20.90
S	00:44:09.144	-23:17:47.400	58717.2100	r	20.67
S	00:44:11.280	-23:18:26.280	58718.1467	r	21.10
S	00:44:02.304	-23:18:27.720	58736.1134	r	20.64
S	00:46:14.712	-23:17:43.800	58712.2624	r	20.14
S	00:46:18.624	-23:17:25.800	58713.3118	r	20.30
S	00:46:18.144	-23:17:21.480	58714.2909	r	18.95
S	00:46:19.704	-23:17:52.800	58716.1391	r	20.88
S	00:46:18.648	-23:17:48.480	58717.2075	r	20.63
S	00:46:20.952	-23:18:03.960	58718.1594	r	21.14
S	00:46:18.384	-23:17:50.280	58719.3394	r	21.40
S	00:46:17.064	-23:18:01.800	58720.3342	r	21.21
S	00:46:15.168	-23:17:33.360	58727.4216	r	20.38
S	00:46:11.208	-23:17:45.600	58734.2037	r	21.11
S	00:48:25.368	-23:18:02.880	58710.4320	r	19.70
S	00:48:21.216	-23:17:21.480	58712.3920	r	19.61
S	00:48:29.496	-23:17:03.120	58713.2693	r	20.28
S	00:48:27.960	-23:17:25.800	58714.2520	r	19.66
S	00:48:30.144	-23:17:49.560	58717.2052	r	20.56
S	00:48:29.544	-23:18:21.600	58718.1830	r	21.33
S	00:48:27.480	-23:17:56.040	58719.3372	r	21.33
S	00:48:26.352	-23:18:33.480	58720.3443	r	21.35
S	00:48:29.088	-23:18:16.200	58725.2159	r	21.51
S	00:48:25.056	-23:17:59.280	58727.4256	r	20.02
S	00:48:20.088	-23:17:43.080	58734.2159	r	21.12
S	00:50:37.248	-23:17:54.960	58710.2881	r	19.20
S	00:50:34.104	-23:17:21.120	58712.2599	r	20.15
S	00:50:35.112	-23:17:28.320	58713.3832	r	20.34
S	00:50:33.456	-23:17:37.680	58714.3874	r	20.34
S	00:50:39.216	-23:18:14.040	58716.1482	r	20.75
S	00:50:39.360	-23:18:26.280	58718.2093	r	20.96
S	00:50:38.832	-23:17:44.880	58719.3351	r	21.27
S	00:50:35.664	-23:18:06.840	58720.3495	r	21.33
S	00:50:37.680	-23:17:36.240	58725.2210	r	21.46
S	00:50:32.520	-23:17:57.120	58727.4301	r	19.53
S	00:50:29.136	-23:17:40.200	58734.2245	r	21.17
S	00:52:51.384	-23:17:21.480	58711.2281	r	19.80
S	00:52:40.272	-23:17:17.880	58712.3769	r	19.86
S	00:52:45.936	-23:17:12.480	58713.2524	r	20.32
S	00:52:44.688	-23:17:27.600	58714.2361	r	19.85
S	00:52:47.904	-23:18:07.200	58716.1717	r	20.65
S	00:52:50.160	-23:17:51.000	58726.3035	r	22.00
S	00:54:53.544	-23:18:23.760	58710.4032	r	19.87
S	00:55:00.264	-23:17:02.760	58711.2595	r	19.89
S	00:54:51.792	-23:17:17.880	58712.2973	r	20.18
S	00:54:57.480	-23:17:39.120	58713.3146	r	20.31
S	00:54:56.352	-23:17:52.800	58714.2931	r	18.91
S	00:54:57.480	-23:18:06.480	58716.1835	r	20.67
S	00:54:58.872	-23:17:57.840	58726.3526	r	21.50

Table 4 (*continued*)

Table 4 (continued)

Source ^a	α (J2000)	δ (J2000)	Date (MJD)	Filter	Magnitude Limit ^b (3σ)
S	00:54:47.496	-23:17:36.600	58734.2450	r	21.17
S	00:57:04.896	-23:17:09.240	58715.2122	r	20.64
S	00:57:04.368	-23:17:44.520	58716.3716	r	20.92
S	00:57:06.384	-23:17:31.920	58718.2535	r	20.88
S	00:57:06.144	-23:17:52.440	58726.3467	r	21.97
S	00:37:37.632	-22:48:03.240	58717.1841	r	20.61
S	00:37:35.856	-22:48:20.880	58718.1233	r	21.08
S	00:37:27.792	-22:47:49.920	58734.0967	r	20.78
S	00:41:51.816	-22:48:10.440	58710.3586	r	19.26
S	00:41:54.048	-22:47:53.520	58713.2960	r	20.32
S	00:41:52.800	-22:47:47.760	58714.2770	r	19.71
S	00:41:54.000	-22:48:14.040	58718.1416	r	21.20
S	00:41:44.280	-22:48:06.840	58734.1557	r	20.94
S	00:43:59.640	-22:47:32.280	58712.3062	r	19.86
S	00:44:03.600	-22:47:49.200	58713.2985	r	20.38
S	00:44:02.400	-22:48:08.640	58714.2790	r	19.75
S	00:44:01.584	-22:48:02.880	58717.2028	r	20.53
S	00:43:53.784	-22:48:11.160	58734.1961	r	21.18
S	00:46:16.704	-22:47:51.000	58711.2019	r	19.54
S	00:46:05.832	-22:47:52.800	58712.2712	r	20.18
S	00:46:11.400	-22:48:00.720	58713.1626	r	20.09
S	00:46:11.664	-22:48:01.800	58714.3113	r	19.41
S	00:46:12.504	-22:48:03.600	58717.2003	r	20.53
S	00:46:12.720	-22:48:54.360	58726.3503	r	21.52
S	00:46:06.936	-22:48:32.760	58727.4235	r	20.24
S	00:46:03.504	-22:47:56.760	58734.2076	r	21.17
S	00:48:16.392	-22:48:00.720	58712.2733	r	20.16
S	00:48:18.576	-22:47:32.640	58713.2475	r	20.31
S	00:48:17.688	-22:47:40.560	58714.2313	r	20.14
S	00:48:21.288	-22:48:15.840	58718.1919	r	21.23
S	00:48:17.664	-22:47:57.840	58727.2342	r	21.75
S	00:50:24.000	-22:47:36.240	58712.2876	r	20.07
S	00:50:26.952	-22:47:28.320	58713.2308	r	20.34
S	00:50:26.880	-22:48:20.520	58714.1806	r	18.94
S	00:50:29.208	-22:48:15.840	58716.1537	r	20.73
S	00:50:30.840	-22:48:13.320	58718.2065	r	20.98
S	00:50:30.840	-22:47:44.880	58726.2766	r	21.89
S	00:52:36.216	-22:48:37.800	58710.3946	r	19.45
S	00:52:42.168	-22:48:24.480	58711.2304	r	19.73
S	00:52:34.608	-22:47:29.760	58712.3112	r	19.96
S	00:52:35.976	-22:47:30.840	58713.2113	r	20.29
S	00:52:35.808	-22:48:18.720	58714.1629	r	19.26
S	00:52:39.168	-22:48:26.640	58716.1686	r	20.65
S	00:52:39.024	-22:47:49.560	58726.3151	r	22.02
S	00:54:51.360	-22:47:44.520	58711.1856	r	19.50
S	00:54:40.992	-22:48:20.880	58712.1455	r	19.84
S	00:54:45.456	-22:48:01.800	58713.1309	r	19.85
S	00:54:45.360	-22:48:10.080	58714.1331	r	19.43
S	00:54:46.296	-22:48:02.160	58715.1389	r	20.40
S	00:54:48.000	-22:48:25.560	58716.1802	r	20.65
S	00:54:48.216	-22:47:48.840	58726.3350	r	21.92
S	00:39:36.720	-22:18:52.920	58710.3320	r	19.21
S	00:39:37.584	-22:17:44.160	58715.1632	r	20.50

Table 4 continued

Table 4 (*continued*)

Source ^a	α (J2000)	δ (J2000)	Date (MJD)	Filter	Magnitude Limit ^b (3σ)
S	00:39:39.336	-22:17:51.360	58716.2681	r	20.58
S	00:39:36.912	-22:18:17.280	58717.1978	r	20.59
S	00:39:28.176	-22:18:17.280	58734.1171	r	20.93
S	00:41:44.544	-22:18:59.040	58710.3654	r	19.86
S	00:41:46.008	-22:17:45.960	58715.1802	r	20.59
S	00:41:47.184	-22:17:53.520	58716.2835	r	20.63
S	00:41:46.104	-22:18:14.760	58717.1953	r	20.51
S	00:41:38.280	-22:17:58.200	58734.1879	r	21.14
S	00:43:53.160	-22:18:36.360	58710.2801	r	19.23
S	00:43:58.632	-22:18:46.080	58711.2044	r	19.59
S	00:43:54.216	-22:17:41.280	58715.1997	r	20.47
S	00:43:55.920	-22:18:20.160	58717.1918	r	20.53
S	00:43:51.816	-22:18:48.600	58727.1446	r	21.45
S	00:46:00.480	-22:18:24.120	58710.3917	r	19.33
S	00:46:07.440	-22:18:34.560	58711.1473	r	19.67
S	00:45:57.264	-22:17:57.840	58712.1784	r	19.90
S	00:46:02.496	-22:18:01.800	58713.1734	r	20.17
S	00:46:02.304	-22:18:51.840	58714.3134	r	19.60
S	00:46:01.344	-22:18:39.600	58727.2162	r	21.74
S	00:48:05.784	-22:18:33.120	58712.1488	r	19.91
S	00:48:09.768	-22:18:05.400	58713.1355	r	19.98
S	00:48:09.816	-22:18:21.600	58714.1406	r	19.21
S	00:48:12.192	-22:18:43.920	58716.1455	r	20.90
S	00:48:13.248	-22:17:57.840	58726.2616	r	21.88
S	00:50:19.848	-22:18:20.160	58713.1580	r	20.04
S	00:50:19.248	-22:18:24.120	58714.1935	r	19.86
S	00:50:20.376	-22:17:47.400	58715.2964	r	20.63
S	00:50:19.152	-22:17:46.320	58715.3019	r	20.73
S	00:50:19.440	-22:18:23.760	58716.1594	r	20.67
S	00:50:19.872	-22:18:21.960	58718.2151	r	21.01
S	00:50:22.392	-22:18:20.880	58726.2996	r	21.91
S	00:52:27.120	-22:18:21.240	58717.1589	r	20.66
S	00:52:28.728	-22:17:56.760	58718.2259	r	21.03
S	00:52:27.792	-22:18:03.240	58719.3641	r	21.17
S	00:52:29.640	-22:18:03.240	58726.3231	r	21.84
S	00:41:34.440	-21:48:35.640	58710.3241	r	19.45
S	00:41:34.488	-21:48:09.360	58713.3011	r	20.24
S	00:41:33.120	-21:48:30.240	58714.2813	r	19.50
S	00:41:34.368	-21:48:34.560	58717.1895	r	20.52
S	00:41:26.232	-21:48:28.800	58734.1840	r	20.95
S	00:43:40.080	-21:49:19.560	58710.4096	r	19.19
S	00:43:42.672	-21:47:58.560	58715.2071	r	20.55
S	00:43:44.328	-21:48:30.600	58716.3000	r	20.64
S	00:43:43.944	-21:48:27.000	58717.1870	r	20.48
S	00:43:41.016	-21:49:03.360	58727.1676	r	21.50
S	00:47:59.616	-21:48:30.240	58713.3037	r	20.35
S	00:47:58.584	-21:48:38.160	58714.2840	r	19.71
S	00:47:58.776	-21:48:15.480	58715.2450	r	20.46
S	00:48:00.048	-21:48:41.760	58716.1418	r	20.83
S	00:47:59.064	-21:48:17.280	58718.2037	r	21.07
S	00:47:57.384	-21:48:51.480	58727.2495	r	21.84
S	00:50:07.488	-21:48:19.800	58713.3062	r	20.30
S	00:50:06.408	-21:48:33.840	58714.2861	r	19.56

Table 4 (*continued*)

Table 4 (continued)

Source ^a	α (J2000)	δ (J2000)	Date (MJD)	Filter	Magnitude Limit ^b (3σ)
S	00:50:07.392	-21:48:41.040	58715.2940	r	20.75
S	00:50:06.312	-21:48:29.520	58716.1657	r	20.68
S	00:50:06.840	-21:48:17.280	58718.2205	r	20.93
S	00:50:08.448	-21:48:12.600	58726.2960	r	21.89
S	00:52:12.840	-21:48:04.680	58713.3529	r	20.27
S	00:52:11.856	-21:47:57.840	58714.3565	r	20.36
S	00:52:15.360	-21:48:34.920	58715.2989	r	20.77
S	00:52:14.232	-21:48:36.360	58716.1766	r	20.63
S	00:52:15.720	-21:48:13.680	58718.2380	r	20.92
S	00:52:16.440	-21:48:37.440	58726.3271	r	21.77
K	00:02:48.256	-26:55:24.772	58710.3670	C	18.07
K	00:02:50.376	-26:57:57.784	58710.3678	C	18.29
K	00:02:53.811	-27:08:39.775	58710.3686	C	18.18
K	00:04:01.524	-28:49:48.542	58710.3694	C	18.03
K	00:04:32.655	-27:22:21.035	58710.3702	C	18.09
K	00:07:01.627	-25:50:43.142	58710.3710	C	18.25
K	00:07:06.313	-26:45:43.349	58710.3718	C	18.18
K	00:08:41.386	-25:45:24.485	58710.3726	C	18.24
K	00:10:27.998	-25:20:36.705	58710.3734	C	18.24
K	00:10:35.590	-25:06:14.715	58710.3742	C	18.35
K	00:10:45.970	-25:17:42.966	58710.3750	C	18.27
K	00:11:17.310	-24:58:52.178	58710.3758	C	18.21
K	00:11:42.828	-25:19:12.814	58710.3766	C	18.03
K	00:34:06.560	-21:27:16.152	58710.3807	C	17.15
K	00:35:44.145	-23:01:20.192	58710.3815	C	18.39
K	00:36:16.257	-23:01:57.684	58710.3823	C	18.43
K	00:36:51.446	-24:37:15.278	58710.3831	C	18.20
K	00:36:52.281	-22:31:47.070	58710.3839	C	18.28
K	00:37:50.706	-25:05:20.608	58710.3847	C	18.20
K	00:38:00.275	-25:04:58.874	58710.3855	C	18.22
K	00:38:14.423	-22:21:33.487	58710.3863	C	18.48
K	00:38:57.242	-23:56:55.427	58710.3887	C	18.00
K	00:39:00.356	-22:19:35.192	58710.3895	C	18.16
K	00:39:00.996	-22:20:52.367	58710.3903	C	18.39
K	00:39:05.073	-23:23:20.069	58710.3911	C	18.36
K	00:39:06.770	-22:06:57.712	58710.3919	C	14.72
K	00:39:24.117	-25:42:39.172	58710.3927	C	18.18
K	00:39:28.289	-22:09:16.553	58710.3935	C	18.27
K	00:39:33.909	-22:12:33.560	58710.3943	C	18.30
K	00:39:42.355	-24:36:53.903	58710.3951	C	15.14
K	00:39:51.544	-22:30:14.015	58710.3959	C	15.54
K	00:39:56.518	-23:53:52.735	58710.3967	C	18.18
K	00:39:59.346	-22:50:18.849	58710.3975	C	18.45
K	00:40:14.842	-24:40:56.063	58710.3984	C	18.02
K	00:40:40.198	-21:56:18.658	58710.3992	C	18.53
K	00:40:51.661	-22:05:44.899	58710.4000	C	18.38
K	00:40:55.961	-25:13:49.662	58710.4008	C	16.05
K	00:41:25.554	-22:39:23.565	58710.4016	C	18.22
K	00:41:57.441	-21:23:01.127	58710.4024	C	15.70
K	00:42:04.188	-23:36:14.902	58710.4032	C	18.11
K	00:42:10.086	-21:47:10.317	58710.4040	C	18.13
K	00:42:10.817	-21:50:18.852	58710.4083	C	18.20
K	00:42:27.448	-22:52:45.066	58710.4091	C	18.16

Table 4 continued

Table 4 (*continued*)

Source ^a	α (J2000)	δ (J2000)	Date (MJD)	Filter	Magnitude Limit ^b (3σ)
K	00:42:33.951	-21:48:46.609	58710.4099	C	18.10
K	00:42:36.439	-21:47:12.496	58710.4107	C	18.19
K	00:42:48.711	-22:15:55.189	58710.4116	C	17.98
K	00:43:21.019	-22:12:06.457	58710.4123	C	18.39
K	00:44:04.768	-22:21:31.810	58710.4131	C	18.36
K	00:44:08.508	-25:07:18.460	58710.4140	C	18.22
K	00:44:23.404	-23:18:34.816	58710.4148	C	15.71
K	00:44:42.337	-22:07:42.667	58710.4155	C	17.97
K	00:44:44.715	-23:10:15.363	58710.4163	C	18.09
K	00:45:00.322	-22:07:53.900	58710.4171	C	18.36
K	00:45:09.498	-20:44:28.651	58710.4179	C	18.20
K	00:45:47.555	-23:47:02.922	58710.4188	C	18.34
K	00:45:52.779	-21:38:59.307	58710.4196	C	18.30
K	00:45:53.633	-26:31:02.503	58710.4204	C	18.25
K	00:46:04.432	-24:39:44.282	58710.4212	C	18.17
K	00:46:10.844	-24:17:28.165	58710.4220	C	18.14
K	00:46:59.478	-24:14:59.001	58710.4236	C	18.24
K	00:47:01.768	-24:22:53.118	58710.4244	C	17.67
K	00:47:22.261	-23:02:01.761	58710.4252	C	18.46
K	00:47:23.160	-25:27:04.509	58710.4261	C	18.25
K	00:47:40.828	-25:03:27.342	58710.4269	C	18.34
K	00:48:10.875	-21:32:32.937	58710.4277	C	17.73
K	00:48:16.345	-25:08:13.349	58710.4284	C	18.46
K	00:48:23.398	-22:09:27.776	58710.4293	C	18.55
K	00:48:24.274	-21:22:15.053	58710.4301	C	18.53
K	00:48:30.267	-21:22:33.121	58710.4309	C	18.59
K	00:48:37.930	-23:34:19.301	58710.4317	C	18.39
K	00:00:27.244	-28:29:44.436	58710.4330	C	18.32
K	00:01:13.790	-27:25:51.253	58710.4338	C	17.93
K	00:01:33.392	-27:34:24.524	58710.4347	C	18.04
K	00:02:07.170	-28:55:23.530	58710.4355	C	17.87
K	00:03:54.155	-28:37:25.473	58710.4362	C	18.40
K	00:06:55.299	-26:56:42.357	58710.4370	C	18.19
K	00:08:49.750	-30:03:21.864	58710.4378	C	18.29
K	00:12:58.380	-24:13:19.683	58710.4387	C	18.59
K	00:14:28.971	-24:42:35.773	58710.4395	C	18.52
K	00:15:01.251	-24:41:56.283	58710.4403	C	16.50
K	00:15:06.366	-23:53:22.184	58710.4411	C	18.50
K	00:17:18.451	-23:35:26.134	58710.4419	C	18.72
K	00:17:27.034	-24:13:50.792	58710.4427	C	17.50
K	00:24:06.532	-23:56:58.876	58710.4435	C	18.52
K	00:29:57.105	-20:33:59.336	58710.4443	C	18.66
K	00:31:03.293	-22:37:37.182	58710.4451	C	18.27
K	00:31:15.525	-26:16:10.853	58710.4459	C	18.31
K	00:34:03.528	-21:26:39.558	58710.4467	C	17.72
K	00:34:08.948	-21:26:49.372	58710.4476	C	18.02
K	00:35:19.188	-24:00:36.474	58710.4484	C	17.50
K	00:36:08.766	-19:08:17.643	58710.4492	C	18.92
K	00:37:29.744	-30:50:24.602	58710.4500	C	18.46
K	00:38:17.361	-18:52:18.443	58710.4509	C	18.87
K	00:46:44.115	-16:04:25.529	58710.4517	C	18.94
K	00:46:52.115	-17:38:44.477	58710.4525	C	18.86
K	00:48:10.507	-32:57:39.164	58710.4533	C	17.91

Table 4 *continued*

Table 4 (*continued*)

Source ^a	α (J2000)	δ (J2000)	Date (MJD)	Filter	Magnitude Limit ^b (3σ)
K	00:49:44.184	-28:55:45.774	58710.4541	C	18.59
K	00:50:17.115	-19:17:16.275	58710.4550	C	18.41
K	00:54:57.628	-19:00:46.534	58710.4558	C	18.20
K	00:56:00.418	+26:17:41.845	58710.4567	C	19.40
K	00:48:53.897	-25:41:54.993	58710.4609	C	18.61
K	00:49:10.151	-23:51:46.452	58710.4618	C	14.92
K	00:49:12.595	-26:13:24.097	58710.4626	C	18.32
K	00:49:15.475	-26:28:50.127	58710.4634	C	18.62
K	00:49:18.868	-26:30:43.322	58710.4642	C	18.55
K	00:49:23.282	-26:32:34.830	58710.4650	C	18.74
K	00:49:37.756	-21:32:19.732	58710.4658	C	18.87
K	00:49:41.727	-26:26:48.890	58710.4667	C	18.60
K	00:50:25.735	-21:15:37.436	58710.4675	C	18.99
K	00:50:35.667	-26:49:01.098	58710.4683	C	14.95
K	00:50:42.386	-21:35:23.729	58710.4691	C	13.97
K	00:50:49.482	-21:54:07.903	58710.4699	C	18.91
K	00:51:16.985	-26:59:35.455	58710.4707	C	15.18
K	00:52:02.417	-22:40:59.805	58710.4716	C	18.58
K	00:52:10.795	-27:19:53.456	58710.4724	C	18.04
K	00:52:42.073	-22:58:39.156	58710.4732	C	18.78
K	00:52:49.466	-22:26:22.447	58710.4740	C	18.71
K	00:53:14.342	-21:41:50.049	58710.4748	C	14.41
K	00:53:21.625	-21:44:17.744	58710.4756	C	18.32
K	00:53:24.883	-21:54:45.349	58710.4764	C	18.91
K	00:53:40.680	-27:36:27.153	58710.4772	C	18.65
K	00:53:43.546	-23:19:56.965	58710.4780	C	15.09
K	00:53:50.718	-24:04:41.827	58710.4789	C	16.62
K	00:53:56.014	-21:40:41.869	58710.4797	C	18.73
K	00:54:03.822	-21:42:54.428	58710.4805	C	18.56
K	00:54:16.912	-23:33:12.256	58710.4813	C	18.39
K	00:54:29.349	-23:29:43.654	58710.4821	C	15.79
K	00:54:45.562	-26:22:16.602	58710.4829	C	18.41
K	00:54:58.456	-25:07:06.784	58710.4837	C	18.56
K	00:55:01.094	-23:31:27.149	58710.4845	C	15.33
K	00:55:05.348	-25:27:31.615	58710.4977	C	14.16
K	00:55:09.830	-26:19:25.830	58710.4985	C	17.83
K	00:56:57.266	-23:50:22.449	58710.4994	C	18.22
K	00:57:13.584	-24:00:07.639	58710.5002	C	17.57
K	00:57:43.000	-27:30:15.198	58710.5009	C	16.68
K	00:58:20.174	-23:13:36.248	58710.5018	C	18.72
K	00:58:48.332	-28:18:20.634	58710.5026	C	18.51
K	00:59:08.176	-26:28:39.901	58710.5034	C	18.62
K	00:59:43.751	-27:07:21.658	58710.5042	C	13.60
K	01:00:08.700	-25:29:46.275	58710.5050	C	18.03
K	01:02:06.973	-28:25:08.405	58710.5058	C	18.50
K	01:02:43.388	-29:27:12.074	58710.5066	C	12.97
K	01:06:08.313	-30:10:55.403	58710.5074	C	17.97
K	01:08:02.178	-27:37:52.273	58710.5082	C	18.56
K	01:08:05.098	-28:31:35.165	58710.5091	C	18.46
K	01:10:31.588	-30:13:31.064	58710.5099	C	18.02
K	01:10:57.174	-30:26:33.739	58710.5107	C	16.96
K	01:13:43.319	-31:45:05.410	58710.5115	C	17.52
K	01:14:59.933	-31:47:18.092	58710.5123	C	17.42

Table 4 *continued*

Table 4 (*continued*)

Source ^a	α (J2000)	δ (J2000)	Date (MJD)	Filter	Magnitude Limit ^b (3σ)
K	01:15:24.129	-30:22:43.899	58710.5131	C	17.82
K	01:15:47.382	-31:35:38.787	58710.5139	C	17.84
K	01:17:55.059	-30:46:01.428	58710.5147	C	17.26
K	01:18:11.206	-30:46:44.325	58710.5155	C	18.01
K	01:19:43.547	-33:05:17.892	58710.5163	C	13.11
K	01:20:11.667	-30:11:22.132	58710.5171	C	16.86
K	01:22:07.216	-31:32:51.470	58710.5179	C	15.50
K	01:22:24.794	-32:43:18.905	58710.5187	C	12.48
K	01:22:28.580	-29:59:10.231	58710.5195	C	17.65
K	01:22:57.262	-31:08:30.149	58710.5203	C	17.54
K	01:23:10.595	-32:50:45.940	58710.5211	C	15.89
K	01:23:37.029	-31:20:51.060	58710.5253	C	13.50
K	00:44:09.284	-25:06:53.530	58713.4050	C	11.50
K	00:49:19.566	-26:30:44.266	58713.4280	C	15.62
K	00:53:41.355	-27:36:38.085	58713.4421	C	15.51
K	00:58:49.066	-28:18:27.795	58713.4534	C	16.16
K	00:59:08.728	-26:28:46.355	58713.4542	C	16.39
K	01:00:09.391	-25:29:51.282	58713.4558	C	15.21
K	01:08:02.971	-27:38:00.458	58713.4566	C	16.66
K	01:15:24.913	-30:22:53.316	58713.4583	C	17.09
K	01:17:55.808	-30:46:11.271	58713.4591	C	17.06
K	01:18:11.879	-30:46:54.001	58713.4598	C	17.26
K	01:20:04.227	-32:56:19.897	58713.4607	C	17.17
K	01:20:12.121	-30:11:32.278	58713.4615	C	16.34
K	01:22:07.348	-31:32:53.370	58713.4716	C	16.50
K	01:22:24.907	-32:43:21.240	58713.4724	C	13.01
K	01:22:27.091	-31:19:19.110	58713.4732	C	18.43
K	01:22:57.458	-31:08:32.148	58713.4740	C	18.19
K	01:23:10.876	-32:50:45.983	58713.4748	C	16.40
K	01:23:37.069	-31:20:49.677	58713.4757	C	18.35
K	01:24:29.243	-31:22:14.167	58713.4765	C	18.32
K	01:24:30.548	-33:10:40.930	58713.4773	C	17.45
K	01:24:46.347	-31:45:37.975	58713.4781	C	18.20
K	01:24:51.388	-30:37:28.380	58713.4789	C	17.47
K	01:25:33.403	-30:22:07.397	58713.4797	C	18.17
K	01:25:43.649	-30:02:15.119	58713.4805	C	18.61
K	01:26:42.000	-32:54:00.669	58713.4813	C	14.46
K	01:28:08.371	-32:10:06.200	58713.4821	C	18.25
K	01:28:34.030	-32:20:45.675	58713.4829	C	18.34
K	01:29:06.535	-31:34:55.220	58713.4837	C	18.48
K	01:29:18.497	-32:51:11.003	58713.4845	C	18.04
K	01:30:04.543	-32:10:17.874	58713.4853	C	18.59
K	01:30:08.338	-32:54:26.363	58713.4861	C	18.47
K	01:31:41.459	-32:25:08.994	58713.4869	C	18.64
K	01:32:00.451	-33:48:22.656	58713.4877	C	15.85
K	01:32:17.688	-31:05:42.991	58713.4885	C	18.50
K	01:32:54.654	-30:05:06.100	58713.4901	C	16.86
K	01:33:58.523	-33:26:48.936	58713.4909	C	18.38
K	01:34:00.794	-32:48:43.111	58713.4918	C	18.33
K	01:34:11.022	-31:39:05.985	58713.4926	C	15.26
K	01:34:14.215	-32:44:38.752	58713.4934	C	18.21
K	01:34:19.214	-32:50:16.168	58713.4942	C	18.36
K	01:34:20.886	-31:36:28.469	58713.4950	C	18.41

Table 4 *continued*

Table 4 (continued)

Source ^a	α (J2000)	δ (J2000)	Date (MJD)	Filter	Magnitude Limit ^b (3σ)
K	01:34:30.126	-30:42:39.326	58713.5035	C	18.42
K	01:34:45.811	-30:58:52.960	58713.5043	C	14.58
K	01:35:28.188	-32:58:18.395	58713.5051	C	18.60
K	01:35:40.208	-33:08:14.789	58713.5059	C	18.51
K	01:37:31.451	-32:13:49.522	58713.5067	C	16.11
K	01:37:46.592	-32:54:41.840	58713.5075	C	18.14
K	01:38:25.839	-33:36:34.893	58713.5083	C	18.35
K	01:39:27.662	-34:02:31.941	58713.5092	C	18.49
K	01:39:49.239	-34:05:41.057	58713.5100	C	13.51
K	01:39:52.893	-34:07:30.289	58713.5108	C	12.97
K	01:47:41.896	-33:36:11.211	58713.5116	C	17.98
N	00:43:08.424	-22:30:25.920	58710.4455	r	19.64
N	00:43:05.784	-22:31:32.880	58717.4079	r	19.92
N	00:43:03.264	-22:31:27.480	58722.5062	r	20.47
N	00:49:42.912	-25:03:32.760	58714.4616	r	19.28
N	00:49:44.448	-25:03:02.520	58717.4349	r	19.93
N	00:49:40.776	-25:03:12.960	58725.3952	r	20.70
N	00:49:39.960	-25:03:09.720	58725.5088	r	20.39
N	00:49:41.472	-25:03:28.080	58729.3932	r	20.52
N	00:49:40.992	-25:03:08.640	58729.4822	r	20.48
N	00:51:28.104	-22:16:45.480	58711.4899	r	19.68
N	00:51:29.160	-22:17:01.320	58712.5134	r	19.66
N	00:51:30.480	-22:17:12.120	58714.5169	r	19.18
N	00:51:31.392	-22:16:37.560	58717.4821	r	20.04
N	00:51:29.424	-22:17:08.160	58729.4467	r	20.50
N	00:51:30.264	-22:16:53.040	58737.4022	r	20.04
N	00:44:16.416	-22:19:39.720	58710.4369	r	19.62
N	00:44:09.936	-22:20:48.480	58711.4858	r	19.68
N	00:44:10.776	-22:21:03.960	58712.5091	r	19.76
N	00:44:11.688	-22:21:14.760	58714.5126	r	19.14
N	00:44:12.552	-22:20:41.280	58717.4779	r	20.00
N	00:44:09.528	-22:20:54.960	58725.4317	r	20.64
N	00:44:10.560	-22:21:12.960	58729.4422	r	20.51
N	00:44:11.496	-22:20:57.840	58737.4061	r	20.02
N	00:44:14.064	-24:19:49.440	58711.4259	r	19.72
N	00:44:14.928	-24:19:59.880	58712.4341	r	19.68
N	00:44:12.432	-24:20:31.920	58713.4850	r	19.49
N	00:44:16.032	-24:20:09.960	58714.4481	r	19.34
N	00:44:17.784	-24:19:40.080	58717.4207	r	19.92
N	00:44:16.056	-24:19:24.960	58722.5262	r	19.79
N	00:44:15.456	-24:19:43.680	58737.4103	r	19.99
N	00:40:30.072	-22:05:42.000	58710.4190	r	19.63
N	00:40:24.768	-22:06:55.800	58711.4056	r	19.64
N	00:40:25.608	-22:07:05.160	58712.4157	r	19.74
N	00:40:29.040	-22:06:44.640	58717.4037	r	19.98
N	00:40:26.352	-22:06:47.520	58722.4982	r	20.41
N	00:40:25.488	-22:06:52.920	58737.4143	r	20.02
N	00:47:29.016	-25:26:26.880	58711.4612	r	19.50
N	00:47:29.304	-25:26:42.720	58712.4774	r	19.56
N	00:47:30.024	-25:26:53.160	58714.4825	r	19.07
N	00:47:31.200	-25:26:17.880	58717.4544	r	19.75
N	00:47:30.144	-25:26:55.320	58722.4075	r	20.54
N	00:47:29.088	-25:26:31.920	58737.4181	r	19.82

Table 4 continued

Table 4 (continued)

Source ^a	α (J2000)	δ (J2000)	Date (MJD)	Filter	Magnitude Limit ^b (3σ)
N	00:48:21.960	-25:07:34.320	58711.4564	r	19.65
N	00:48:21.960	-25:07:53.400	58712.4705	r	19.71
N	00:48:22.992	-25:08:02.400	58714.4780	r	19.29
N	00:48:24.240	-25:07:28.920	58717.4498	r	19.98
N	00:48:23.184	-25:08:04.920	58722.4031	r	20.66
N	00:48:22.296	-25:07:42.960	58737.4220	r	20.01
N	00:54:05.880	-23:11:58.200	58712.4943	r	19.74
N	00:54:04.560	-23:11:48.120	58725.4210	r	20.62
N	00:54:05.112	-23:12:04.680	58729.4282	r	20.61
N	00:54:05.136	-23:11:44.520	58729.5155	r	20.28
N	00:50:09.816	-23:16:50.880	58711.4681	r	19.74
N	00:50:09.984	-23:17:03.840	58712.4898	r	19.70
N	00:50:11.016	-23:17:14.640	58714.4897	r	19.19
N	00:50:11.880	-23:16:40.080	58717.4609	r	19.97
N	00:50:08.808	-23:16:57.000	58725.4176	r	20.67
N	00:50:09.552	-23:17:14.280	58729.4228	r	20.61
N	00:50:09.096	-23:16:53.040	58729.5111	r	20.20
N	00:43:20.880	-24:05:07.440	58711.4330	r	19.71
N	00:43:21.528	-24:05:16.800	58712.4400	r	19.72
N	00:43:18.720	-24:05:49.200	58713.4943	r	19.52
N	00:43:22.512	-24:05:27.960	58714.4547	r	19.37
N	00:43:24.384	-24:04:54.480	58717.4278	r	19.98
N	00:43:21.816	-24:05:24.000	58722.3773	r	20.57
N	00:43:21.744	-24:05:09.240	58737.4259	r	20.06
N	00:48:41.472	-23:22:18.480	58711.4351	r	19.76
N	00:48:42.096	-23:22:27.840	58712.4420	r	19.70
N	00:48:39.360	-23:22:58.440	58713.4967	r	19.60
N	00:48:43.104	-23:22:37.920	58714.4569	r	19.30
N	00:48:45.096	-23:22:06.600	58717.4300	r	19.94
N	00:48:40.488	-23:22:19.560	58725.3901	r	20.74
N	00:48:39.864	-23:22:14.880	58725.5048	r	20.43
N	00:48:40.752	-23:22:33.240	58729.3887	r	20.78
N	00:48:42.648	-23:16:53.040	58729.3985	r	20.68
N	00:48:41.208	-23:22:14.880	58729.4773	r	20.58
N	00:45:03.864	-25:01:10.200	58711.4429	r	19.70
N	00:45:03.816	-25:01:30.720	58712.4577	r	19.72
N	00:45:00.960	-25:02:02.760	58713.5058	r	19.66
N	00:45:04.800	-25:01:39.360	58714.4642	r	19.34
N	00:45:06.672	-25:01:08.760	58717.4372	r	20.00
N	00:45:04.920	-25:01:40.440	58722.3870	r	20.61
N	00:45:04.560	-25:01:18.840	58737.4332	r	20.03
N	00:44:13.200	-24:19:37.200	58711.4473	r	19.68
N	00:44:13.464	-24:19:59.520	58712.4618	r	19.69
N	00:44:10.800	-24:20:31.200	58713.5123	r	19.58
N	00:44:14.544	-24:20:07.800	58714.4687	r	19.29
N	00:44:15.960	-24:19:36.120	58717.4414	r	19.97
N	00:44:13.992	-24:20:07.080	58722.3921	r	20.64
N	00:44:13.680	-24:19:49.080	58737.4370	r	20.04
N	00:49:01.608	-23:48:43.200	58711.4703	r	19.76
N	00:49:01.944	-23:48:56.160	58712.4921	r	19.66
N	00:49:02.640	-23:49:06.960	58714.4967	r	19.17
N	00:49:03.768	-23:48:33.840	58717.4632	r	19.97
N	00:49:03.000	-23:49:10.200	58722.4186	r	20.72

Table 4 continued

Table 4 (continued)

Source ^a	α (J2000)	δ (J2000)	Date (MJD)	Filter	Magnitude Limit ^b (3σ)
N	00:49:01.488	-23:48:50.760	58737.4411	r	20.03
N	00:36:02.328	-20:43:20.280	58710.3950	r	19.71
N	00:35:55.968	-20:44:29.400	58711.3908	r	19.50
N	00:35:56.952	-20:44:30.480	58712.3981	r	19.71
N	00:35:54.192	-20:44:58.200	58713.4256	r	19.16
N	00:35:58.464	-20:44:39.120	58714.3976	r	19.35
N	00:36:00.456	-20:44:09.960	58717.3855	r	19.96
N	00:35:59.040	-20:44:34.800	58722.3350	r	20.14
N	00:35:57.552	-20:44:20.400	58737.4504	r	20.17
N	00:54:15.792	-23:32:12.480	58711.4748	r	19.72
N	00:54:16.224	-23:32:24.720	58712.4965	r	19.69
N	00:54:16.944	-23:32:35.160	58714.5013	r	19.12
N	00:54:17.928	-23:32:01.680	58717.4674	r	19.93
N	00:54:17.400	-23:32:36.600	58722.4252	r	20.61
N	00:54:16.488	-23:32:17.880	58737.4544	r	20.10
N	00:39:19.776	-22:05:06.720	58710.4271	r	19.59
N	00:39:13.920	-22:06:29.880	58711.3990	r	19.68
N	00:39:12.192	-22:06:03.960	58711.4968	r	19.72
N	00:39:14.088	-22:06:25.920	58712.4086	r	19.72
N	00:39:13.728	-22:06:21.240	58712.5180	r	19.65
N	00:39:17.712	-22:06:05.760	58717.3972	r	19.81
N	00:39:15.864	-22:06:55.440	58722.3455	r	20.37
N	00:43:01.416	-24:39:10.440	58711.4307	r	19.73
N	00:43:02.088	-24:39:19.440	58712.4381	r	19.71
N	00:42:59.256	-24:39:51.120	58713.4914	r	19.46
N	00:43:03.000	-24:39:28.800	58714.4526	r	19.29
N	00:43:04.872	-24:38:58.560	58717.4258	r	20.05
N	00:43:02.088	-24:39:09.000	58737.4623	r	20.20
N	00:51:29.592	-24:38:34.800	58711.4589	r	19.62
N	00:51:29.976	-24:38:49.560	58712.4749	r	19.70
N	00:51:32.160	-24:38:26.160	58717.4523	r	19.99
N	00:51:28.872	-24:38:41.640	58725.4104	r	20.67
N	00:51:27.552	-24:38:42.720	58725.5233	r	20.11
N	00:51:29.424	-24:38:57.480	58729.4129	r	20.53
N	00:51:28.968	-24:38:37.320	58729.5018	r	20.32
N	00:53:57.696	-24:32:38.760	58711.4636	r	19.67
N	00:53:56.208	-24:32:35.880	58711.5079	r	19.56
N	00:53:57.864	-24:32:53.160	58712.4798	r	19.62
N	00:53:57.504	-24:32:51.000	58712.5266	r	19.10
N	00:53:58.800	-24:33:02.160	58714.4848	r	19.25
N	00:54:00.024	-24:32:26.520	58717.4568	r	19.96
N	00:53:56.808	-24:32:41.640	58725.4140	r	20.70
N	00:53:57.360	-24:32:57.840	58729.4181	r	20.64
N	00:53:57.096	-24:32:37.320	58729.5061	r	20.45
N	00:47:05.424	-24:14:35.520	58712.4638	r	19.68
N	00:47:02.736	-24:15:06.840	58713.5149	r	19.54
N	00:47:06.504	-24:14:45.600	58714.4711	r	19.19
N	00:47:07.872	-24:14:14.280	58717.4435	r	20.07
N	00:47:04.128	-24:14:30.120	58725.4027	r	20.67
N	00:47:02.904	-24:14:28.320	58725.5163	r	20.30
N	00:47:04.488	-24:14:43.440	58729.4037	r	20.54
N	00:47:04.032	-24:14:25.440	58729.4923	r	20.56
N	00:43:32.928	-23:57:19.800	58711.4286	r	19.74

Table 4 continued

Table 4 (continued)

Source ^a	α (J2000)	δ (J2000)	Date (MJD)	Filter	Magnitude Limit ^b (3σ)
N	00:43:32.280	-23:57:06.840	58711.5044	r	19.71
N	00:43:33.696	-23:57:28.440	58712.4361	r	19.75
N	00:43:33.072	-23:57:24.480	58712.5244	r	19.27
N	00:43:31.128	-23:57:59.400	58713.4879	r	19.60
N	00:43:34.656	-23:57:38.520	58714.4503	r	19.40
N	00:43:36.552	-23:57:08.280	58717.4238	r	20.06
N	00:43:33.912	-23:57:43.560	58722.3730	r	20.44
N	00:48:42.912	-23:46:25.320	58711.4449	r	19.71
N	00:48:42.864	-23:46:43.320	58712.4598	r	19.68
N	00:48:40.104	-23:47:15.360	58713.5094	r	19.60
N	00:48:43.944	-23:46:52.680	58714.4665	r	19.22
N	00:48:45.696	-23:46:21.000	58717.4394	r	20.00
N	00:48:41.976	-23:46:35.760	58725.3989	r	20.69
N	00:48:41.040	-23:46:33.600	58725.5125	r	20.35
N	00:48:42.096	-23:46:31.080	58729.4877	r	20.50
N	00:48:43.128	-23:46:28.920	58737.4702	r	20.22
N	00:50:54.528	-23:37:58.800	58711.4658	r	19.76
N	00:50:54.720	-23:38:12.480	58712.4821	r	19.74
N	00:50:54.192	-23:38:11.760	58712.4874	r	19.71
N	00:50:56.664	-23:37:46.920	58717.4589	r	20.03
N	00:50:55.896	-23:38:22.200	58722.4126	r	20.67
N	00:50:53.976	-23:38:01.680	58737.4742	r	20.30
N	00:54:29.472	-23:35:30.840	58711.4792	r	19.70
N	00:54:29.952	-23:35:45.240	58712.5021	r	19.71
N	00:54:30.936	-23:35:56.040	58714.5058	r	19.13
N	00:54:31.680	-23:35:21.480	58717.4717	r	20.05
N	00:54:30.072	-23:35:34.440	58737.4777	r	20.29
N	00:51:14.376	-23:17:30.840	58711.4814	r	19.67
N	00:51:14.856	-23:17:44.880	58712.5043	r	19.72
N	00:51:15.696	-23:17:51.720	58714.5081	r	19.19
N	00:51:16.368	-23:17:21.840	58717.4738	r	19.97
N	00:51:13.464	-23:17:37.320	58725.4280	r	20.70
N	00:51:14.664	-23:17:53.160	58729.4372	r	20.71
N	00:51:15.120	-23:17:35.880	58737.4814	r	20.33
N	00:54:53.952	-23:11:13.920	58711.4835	r	19.62
N	00:54:54.672	-23:11:29.400	58712.5067	r	19.68
N	00:54:55.488	-23:11:39.840	58714.5102	r	19.11
N	00:54:56.280	-23:11:06.000	58717.4758	r	20.05
N	00:54:56.808	-23:11:43.080	58722.4405	r	20.70
N	00:54:54.048	-23:11:21.480	58737.4851	r	20.17
N	00:46:52.368	-23:02:11.400	58711.4236	r	19.72
N	00:46:53.256	-23:02:17.520	58712.4321	r	19.81
N	00:46:50.640	-23:02:51.000	58713.4822	r	19.68
N	00:46:54.552	-23:02:29.040	58714.4459	r	19.30
N	00:46:56.064	-23:01:58.800	58717.4186	r	20.01
N	00:46:53.904	-23:02:34.080	58722.3684	r	20.43
N	00:46:53.088	-23:02:06.360	58737.4892	r	20.21
N	00:43:06.408	-22:14:40.560	58710.4317	r	19.64
N	00:42:59.352	-22:15:58.320	58711.4075	r	19.71
N	00:43:00.264	-22:16:07.680	58712.4182	r	19.71
N	00:42:57.768	-22:16:39.360	58713.4597	r	19.24
N	00:43:03.504	-22:15:47.160	58717.4058	r	20.02
N	00:43:01.848	-22:16:14.160	58722.3549	r	20.47

Table 4 continued

Table 4 (continued)

Source ^a	α (J2000)	δ (J2000)	Date (MJD)	Filter	Magnitude Limit ^b (3σ)
N	00:43:00.192	-22:15:52.920	58737.4931	r	20.08
N	00:43:42.600	-22:12:33.480	58710.4537	r	19.66
N	00:43:35.208	-22:13:45.120	58711.4878	r	19.82
N	00:43:36.024	-22:14:02.400	58712.5112	r	19.77
N	00:43:37.800	-22:13:37.560	58717.4801	r	20.02
N	00:43:37.560	-22:14:15.720	58722.4464	r	20.70
N	00:43:36.096	-22:13:57.360	58737.4974	r	20.14
N	00:43:33.288	-22:10:14.160	58710.4428	r	19.69
N	00:43:26.424	-22:11:34.080	58711.4181	r	19.76
N	00:43:27.264	-22:11:40.920	58712.4277	r	19.72
N	00:43:24.816	-22:12:15.120	58713.4746	r	19.59
N	00:43:28.584	-22:11:54.600	58714.4291	r	19.05
N	00:43:28.440	-22:11:54.600	58714.4402	r	18.91
N	00:43:30.120	-22:11:21.840	58717.4142	r	20.01
N	00:43:28.032	-22:11:56.760	58722.3640	r	20.53
N	00:43:27.144	-22:11:30.480	58737.5015	r	20.13
N	00:43:23.016	-22:09:11.520	58710.4480	r	19.68
N	00:43:33.600	-22:09:12.960	58710.4216	r	19.66
N	00:43:28.968	-22:10:23.880	58711.4161	r	19.74
N	00:43:29.808	-22:10:31.080	58712.4257	r	19.77
N	00:43:27.336	-22:11:05.280	58713.4703	r	19.30
N	00:43:30.936	-22:10:46.200	58714.4379	r	18.86
N	00:43:32.736	-22:10:13.080	58717.4122	r	19.94
N	00:43:31.200	-22:10:02.640	58722.5130	r	20.41
N	00:43:30.144	-22:10:21.720	58737.5054	r	20.18
N	00:46:59.400	-22:00:56.880	58710.4563	r	19.65
N	00:46:51.696	-22:02:25.440	58711.4032	r	19.57
N	00:46:51.288	-22:02:08.880	58711.5017	r	19.70
N	00:46:52.848	-22:02:31.200	58712.4135	r	19.77
N	00:46:52.536	-22:02:26.160	58712.5223	r	19.51
N	00:46:50.208	-22:03:03.960	58713.4533	r	19.24
N	00:46:53.544	-22:02:45.600	58714.4136	r	18.96
N	00:46:56.328	-22:02:12.120	58717.4014	r	19.96
N	00:46:54.672	-22:02:38.040	58722.3503	r	20.40
N	00:46:53.160	-22:02:19.320	58737.5092	r	20.14
N	00:45:16.560	-21:59:40.920	58710.4615	r	19.68
N	00:45:09.816	-22:01:08.760	58711.4010	r	18.92
N	00:45:09.072	-22:00:49.680	58711.4996	r	19.61
N	00:45:10.536	-22:01:12.000	58712.4111	r	19.69
N	00:45:10.224	-22:01:06.960	58712.5201	r	19.62
N	00:45:07.848	-22:01:44.760	58713.4484	r	19.26
N	00:45:14.064	-22:00:52.200	58717.3993	r	19.87
N	00:45:11.448	-22:00:57.240	58722.4928	r	20.35
N	00:48:08.328	-21:53:30.480	58710.4664	r	19.67
N	00:48:03.432	-21:54:33.840	58717.4863	r	19.95
N	00:48:00.384	-21:54:50.760	58725.4387	r	20.67
N	00:48:01.608	-21:55:04.440	58729.4513	r	20.64
N	00:42:26.784	-21:50:27.240	58710.4160	r	19.67
N	00:45:59.400	-21:50:06.720	58710.4589	r	19.68
N	00:45:52.008	-21:51:34.560	58711.4214	r	19.73
N	00:45:52.824	-21:51:41.040	58712.4297	r	19.78
N	00:45:50.256	-21:52:12.000	58713.4780	r	19.58
N	00:45:54.144	-21:51:53.640	58714.4314	r	18.86

Table 4 continued

Table 4 (*continued*)

Source ^a	α (J2000)	δ (J2000)	Date (MJD)	Filter	Magnitude Limit ^b (3σ)
N	00:45:54.024	-21:51:52.560	58714.4434	r	18.88
N	00:45:55.680	-21:51:23.040	58717.4164	r	20.00
N	00:45:54.144	-21:51:10.800	58722.5201	r	20.16
N	00:41:44.808	-21:46:16.320	58710.4134	r	19.61
N	00:42:38.304	-21:44:54.240	58710.4106	r	19.69
N	00:51:51.000	-21:37:09.120	58710.4720	r	19.77
N	00:51:45.576	-21:38:07.080	58717.4907	r	20.05
N	00:51:42.288	-21:38:24.360	58725.4422	r	20.64
N	00:51:43.512	-21:38:37.320	58729.4556	r	20.65
N	00:49:49.080	-21:30:53.280	58710.4750	r	19.71
N	00:49:41.496	-21:32:19.680	58711.4134	r	19.68
N	00:49:42.336	-21:32:26.880	58712.4234	r	19.73
N	00:49:39.768	-21:32:57.840	58713.4664	r	19.47
N	00:49:43.536	-21:32:40.560	58714.4237	r	18.78
N	00:49:45.408	-21:32:07.080	58717.4101	r	20.00
N	00:49:43.560	-21:32:37.320	58722.3593	r	20.46
N	00:43:06.000	-21:30:16.920	58717.4887	r	19.93
N	00:43:05.664	-21:30:44.640	58722.4613	r	20.57
N	00:42:35.928	-21:24:57.960	58710.4082	r	19.63
N	00:42:22.944	-21:28:29.640	58710.4342	r	19.64
N	00:42:31.416	-21:26:13.920	58711.3970	r	19.66
N	00:42:28.968	-21:26:42.360	58713.4331	r	19.16
N	00:42:35.232	-21:25:51.960	58717.3939	r	19.85
N	00:42:32.616	-21:25:53.760	58722.4814	r	20.39
N	00:42:20.184	-21:22:19.920	58710.4639	r	19.71
N	00:42:15.312	-21:23:22.920	58717.4842	r	20.01
N	00:42:15.552	-21:23:54.240	58722.4532	r	20.60
N	00:38:23.640	-21:21:54.360	58710.4034	r	19.65
N	00:48:30.048	-21:16:42.600	58710.4778	r	19.70
N	00:48:24.648	-21:17:45.600	58717.4927	r	19.89
N	00:35:54.696	-20:53:53.520	58710.3983	r	19.71
N	00:41:16.704	-20:43:28.920	58710.4006	r	19.65
N	00:41:11.088	-20:44:37.680	58711.3929	r	19.57
N	00:41:10.344	-20:44:15.720	58711.4941	r	19.76
N	00:41:11.568	-20:44:39.120	58712.4012	r	19.66
N	00:41:11.736	-20:44:31.560	58712.5155	r	19.66
N	00:41:10.536	-20:44:47.400	58713.4284	r	21.51
N	00:41:15.168	-20:44:18.960	58717.3877	r	19.86
N	00:41:13.560	-20:44:24.000	58722.4750	r	20.54
N	00:40:59.472	-20:31:41.160	58710.4057	r	19.65
N	00:40:54.384	-20:32:52.080	58711.3950	r	19.66
N	00:40:54.576	-20:32:49.200	58712.4037	r	19.66
N	00:40:52.032	-20:33:20.520	58713.4311	r	19.23
N	00:40:58.128	-20:32:29.400	58717.3899	r	19.94
N	00:40:55.896	-20:32:56.400	58722.3398	r	20.17
N	00:40:34.248	-20:05:32.640	58710.4999	r	19.76
N	00:40:29.304	-20:06:35.280	58717.4947	r	19.90
N	00:40:26.328	-20:06:56.160	58725.4458	r	20.76
N	00:40:27.552	-20:07:06.600	58729.4602	r	20.58
N	00:42:57.288	-24:39:01.080	58711.4374	r	19.74
N	00:42:57.768	-24:39:10.440	58712.4460	r	19.69
N	00:42:54.984	-24:39:45.360	58713.5004	r	19.55
N	00:42:58.608	-24:39:21.240	58714.4593	r	19.29

Table 4 (*continued*)

Table 4 (continued)

Source ^a	α (J2000)	δ (J2000)	Date (MJD)	Filter	Magnitude Limit ^b (3σ)
N	00:43:00.456	-24:38:53.160	58717.4321	<i>r</i>	19.89
N	00:42:57.936	-24:39:17.640	58722.3821	<i>r</i>	20.65
N	00:50:57.144	-23:33:32.400	58711.4770	<i>r</i>	19.72
N	00:50:57.504	-23:33:46.800	58712.4999	<i>r</i>	19.76
N	00:50:59.712	-23:33:23.040	58717.4697	<i>r</i>	20.02
N	00:50:56.376	-23:33:38.520	58725.4246	<i>r</i>	20.71
N	00:50:57.432	-23:33:54.720	58729.4329	<i>r</i>	20.70
N	00:50:56.544	-23:33:32.040	58729.5205	<i>r</i>	20.23
L	01:02:40.002	-21:20:09.758	58710.0492	<i>i</i>	20.52
L	01:02:40.002	-21:20:09.758	58710.0542	<i>i</i>	20.50
L	01:02:40.002	-21:20:09.758	58711.3752	<i>g</i>	17.79
L	01:02:40.002	-21:20:09.758	58711.3791	<i>i</i>	16.49
L	01:02:40.002	-21:20:09.758	58713.1356	<i>g</i>	19.75
L	01:02:40.002	-21:20:09.758	58713.1395	<i>i</i>	18.25
L	01:02:40.002	-21:20:09.758	58714.1590	<i>g</i>	20.53
L	01:02:40.002	-21:20:09.758	58714.1630	<i>i</i>	19.23
L	01:22:27.355	-12:57:09.191	58710.0088	<i>i</i>	20.22
L	01:22:27.355	-12:57:09.191	58710.1499	<i>i</i>	21.11
L	01:11:14.308	-16:15:54.788	58710.0088	<i>i</i>	20.47
L	01:11:14.308	-16:15:54.788	58710.1088	<i>i</i>	19.61
L	01:11:14.308	-16:15:54.788	58710.1094	<i>i</i>	21.12
L	01:11:14.308	-16:15:54.788	58712.1530	<i>g</i>	18.38
L	01:11:14.308	-16:15:54.788	58712.1569	<i>i</i>	17.33
L	01:11:14.308	-16:15:54.788	58713.1792	<i>g</i>	18.36
L	01:11:14.308	-16:15:54.788	58713.1832	<i>i</i>	17.60
L	00:20:36.036	-31:22:16.925	58710.0391	<i>i</i>	20.79
L	00:20:36.036	-31:22:16.925	58710.1223	<i>i</i>	17.38
L	01:00:02.053	-21:29:18.499	58710.0770	<i>i</i>	21.21
L	01:00:02.053	-21:29:18.499	58710.0852	<i>i</i>	20.71
L	01:00:02.053	-21:29:18.499	58710.0886	<i>i</i>	21.04
L	01:00:02.053	-21:29:18.499	58712.2235	<i>g</i>	18.31
L	01:00:02.053	-21:29:18.499	58712.2275	<i>i</i>	17.40
L	01:00:02.053	-21:29:18.499	58714.0109	<i>g</i>	22.41
L	01:00:02.053	-21:29:18.499	58714.0149	<i>i</i>	20.41
L	00:47:07.527	-24:22:14.329	58709.9464	<i>g</i>	19.30
L	00:47:07.527	-24:22:14.329	58709.9504	<i>i</i>	18.50
L	00:47:07.527	-24:22:14.329	58710.9759	<i>i</i>	18.52
L	00:47:07.527	-24:22:14.329	58712.0045	<i>i</i>	17.75
L	00:47:07.527	-24:22:14.329	58712.8789	<i>g</i>	19.69
L	00:47:07.527	-24:22:14.329	58712.8829	<i>i</i>	19.54
L	00:47:07.527	-24:22:14.329	58713.3495	<i>i</i>	18.39
L	00:47:07.527	-24:22:14.329	58713.3629	<i>i</i>	18.32
L	00:47:07.527	-24:22:14.329	58714.0200	<i>g</i>	21.29
L	00:47:07.527	-24:22:14.329	58714.0239	<i>i</i>	20.69
L	01:17:23.818	-16:03:44.600	58709.9936	<i>i</i>	19.31
L	01:17:23.818	-16:03:44.600	58710.0592	<i>i</i>	20.36
L	01:27:33.415	-04:40:58.537	58710.0937	<i>i</i>	21.75
L	01:27:33.415	-04:40:58.537	58710.0986	<i>i</i>	21.77
L	01:25:16.213	-11:54:50.170	58709.9784	<i>g</i>	19.49
L	01:25:16.213	-11:54:50.170	58709.9823	<i>i</i>	18.94
L	01:25:16.213	-11:54:50.170	58710.1173	<i>i</i>	21.33
L	01:25:16.213	-11:54:50.170	58710.1397	<i>i</i>	20.85
L	01:25:16.213	-11:54:50.170	58711.7224	<i>g</i>	21.35

Table 4 continued

Table 4 (*continued*)

Source ^a	α (J2000)	δ (J2000)	Date (MJD)	Filter	Magnitude Limit ^b (3σ)
L	01:25:16.213	-11:54:50.170	58711.7264	<i>i</i>	20.82
L	01:25:16.213	-11:54:50.170	58713.7983	<i>g</i>	16.68
L	01:25:16.213	-11:54:50.170	58713.7983	<i>g</i>	16.68
L	01:25:16.213	-11:54:50.170	58713.8023	<i>i</i>	15.39
L	00:47:28.948	-25:26:26.358	58709.9886	<i>i</i>	19.35
L	00:47:28.948	-25:26:26.358	58710.0987	<i>i</i>	20.69
L	00:47:28.948	-25:26:26.358	58711.0731	<i>i</i>	20.48
L	00:47:28.948	-25:26:26.358	58712.4249	<i>i</i>	17.92
L	00:47:28.948	-25:26:26.358	58713.3278	<i>i</i>	18.15
L	00:47:28.948	-25:26:26.358	58713.7535	<i>i</i>	17.36
L	00:47:28.948	-25:26:26.358	58713.8162	<i>i</i>	17.96
L	01:19:37.246	-12:32:17.794	58710.0708	<i>i</i>	20.93
L	01:19:37.246	-12:32:17.794	58710.1440	<i>i</i>	20.94
L	23:54:57.854	-34:36:05.213	58709.9555	<i>g</i>	19.34
L	23:54:57.854	-34:36:05.213	58709.9594	<i>i</i>	18.66
L	23:54:57.854	-34:36:05.213	58712.8695	<i>g</i>	20.33
L	23:54:57.854	-34:36:05.213	58712.8735	<i>i</i>	20.06
L	23:54:57.854	-34:36:05.213	58714.0074	<i>g</i>	21.23
L	23:54:57.854	-34:36:05.213	58714.0113	<i>i</i>	20.15
L	23:51:30.381	-34:27:08.230	58709.9782	<i>g</i>	20.99
L	23:51:30.381	-34:27:08.230	58709.9822	<i>i</i>	19.50
L	23:51:30.381	-34:27:08.230	58710.0772	<i>i</i>	17.77
L	23:51:30.381	-34:27:08.230	58710.1024	<i>i</i>	17.37
L	23:51:30.381	-34:27:08.230	58711.8442	<i>g</i>	20.43
L	23:51:30.381	-34:27:08.230	58711.8482	<i>i</i>	19.43
L	23:51:30.381	-34:27:08.230	58711.8618	<i>g</i>	21.28
L	23:51:30.381	-34:27:08.230	58711.8657	<i>i</i>	19.53
L	23:51:30.381	-34:27:08.230	58713.8523	<i>g</i>	21.23
L	23:51:30.381	-34:27:08.230	58713.8563	<i>i</i>	20.02
L	23:51:30.381	-34:27:08.230	58714.8710	<i>g</i>	21.16
L	23:51:30.381	-34:27:08.230	58714.8749	<i>i</i>	20.64
L	01:08:49.703	-15:56:54.798	58709.9986	<i>i</i>	20.26
L	01:08:49.703	-15:56:54.798	58710.0442	<i>i</i>	20.91
L	00:36:26.277	-28:17:59.449	58709.9936	<i>i</i>	20.72
L	00:36:26.277	-28:17:59.449	58710.1335	<i>i</i>	17.83
L	01:05:15.119	-19:16:57.821	58710.0290	<i>i</i>	21.57
L	01:05:15.119	-19:16:57.821	58710.0543	<i>i</i>	20.88
L	01:29:06.703	-07:38:30.048	58710.0341	<i>i</i>	20.75
L	01:29:06.703	-07:38:30.048	58710.0771	<i>i</i>	21.21
L	01:29:06.703	-07:38:30.048	58710.0886	<i>i</i>	21.29
L	01:29:06.703	-07:38:30.048	58712.9276	<i>g</i>	20.19
L	01:29:06.703	-07:38:30.048	58712.9315	<i>i</i>	17.69
L	01:36:39.837	-01:23:44.729	58710.1293	<i>i</i>	22.07
L	01:36:39.837	-01:23:44.729	58710.1386	<i>i</i>	21.26
L	01:36:39.837	-01:23:44.729	58710.1475	<i>i</i>	22.02
L	01:02:03.780	-19:27:02.804	58709.9556	<i>g</i>	18.88
L	01:02:03.780	-19:27:02.804	58709.9595	<i>i</i>	17.93
L	01:02:03.780	-19:27:02.804	58712.8127	<i>g</i>	18.52
L	01:02:03.780	-19:27:02.804	58712.8167	<i>i</i>	17.33
L	01:06:35.094	-20:19:55.999	58710.0648	<i>i</i>	20.89
L	01:06:35.094	-20:19:55.999	58710.0708	<i>i</i>	20.97
L	01:14:23.885	-15:22:17.368	58710.0037	<i>i</i>	20.32
L	01:14:23.885	-15:22:17.368	58710.1523	<i>i</i>	21.01

Table 4 *continued*

Table 4 (continued)

Source ^a	α (J2000)	δ (J2000)	Date (MJD)	Filter	Magnitude Limit ^b (3σ)
L	01:13:50.066	-14:50:44.124	58709.9646	<i>g</i>	18.91
L	01:13:50.066	-14:50:44.124	58709.9685	<i>i</i>	18.08
L	01:13:50.066	-14:50:44.124	58710.1141	<i>i</i>	21.22
L	01:13:50.066	-14:50:44.124	58710.1344	<i>i</i>	18.96
L	01:13:50.066	-14:50:44.124	58710.1349	<i>i</i>	20.81
L	01:13:50.066	-14:50:44.124	58711.7419	<i>g</i>	21.40
L	01:13:50.066	-14:50:44.124	58711.7459	<i>i</i>	20.93
L	01:13:50.066	-14:50:44.124	58713.3718	<i>g</i>	20.34
L	01:13:50.066	-14:50:44.124	58713.3757	<i>i</i>	18.90
L	00:20:33.685	-31:18:14.940	58710.1038	<i>i</i>	18.19
L	00:20:33.685	-31:18:14.940	58710.1185	<i>i</i>	17.59
L	01:13:28.527	-16:14:30.102	58710.0391	<i>i</i>	21.09
L	01:13:28.527	-16:14:30.102	58710.0592	<i>i</i>	20.78
L	01:13:28.527	-16:14:30.102	58710.0696	<i>i</i>	20.08
L	01:12:58.920	-19:00:29.556	58710.0644	<i>i</i>	20.54
L	01:12:58.920	-19:00:29.556	58710.1396	<i>i</i>	20.56
L	00:49:27.554	-26:32:17.884	58710.0883	<i>i</i>	20.71
L	00:49:27.554	-26:32:17.884	58710.0932	<i>i</i>	20.59
L	00:49:27.554	-26:32:17.884	58711.0265	<i>i</i>	19.20
L	00:49:27.554	-26:32:17.884	58712.5832	<i>i</i>	18.49
L	00:49:27.554	-26:32:17.884	58713.9076	<i>i</i>	21.02
L	00:49:27.554	-26:32:17.884	58713.9377	<i>i</i>	20.38
L	01:19:24.945	-15:42:00.778	58709.9863	<i>g</i>	19.93
L	01:19:24.945	-15:42:00.778	58710.0442	<i>i</i>	20.92
L	01:19:24.945	-15:42:00.778	58710.1192	<i>i</i>	20.87
L	01:19:24.945	-15:42:00.778	58711.7833	<i>g</i>	21.44
L	01:19:24.945	-15:42:00.778	58711.7872	<i>i</i>	21.16
L	01:19:24.945	-15:42:00.778	58712.7979	<i>g</i>	18.07
L	01:19:24.945	-15:42:00.778	58712.8019	<i>i</i>	16.99
L	01:08:51.135	-15:24:22.799	58709.9864	<i>g</i>	19.89
L	01:08:51.135	-15:24:22.799	58710.0240	<i>i</i>	20.20
L	01:08:51.135	-15:24:22.799	58710.0340	<i>i</i>	19.54
L	01:08:51.135	-15:24:22.799	58712.8960	<i>g</i>	19.60
L	01:08:51.135	-15:24:22.799	58712.9000	<i>i</i>	19.48
L	01:30:41.164	-03:56:42.688	58709.9374	<i>g</i>	19.22
L	01:30:41.164	-03:56:42.688	58709.9414	<i>i</i>	18.62
L	01:30:41.164	-03:56:42.688	58711.7100	<i>g</i>	21.52
L	01:30:41.164	-03:56:42.688	58711.7140	<i>i</i>	21.03
L	01:30:41.164	-03:56:42.688	58712.7253	<i>g</i>	21.28
L	01:30:41.164	-03:56:42.688	58712.7293	<i>i</i>	20.63
L	01:16:12.201	-15:54:34.528	58709.9374	<i>g</i>	19.17
L	01:16:12.201	-15:54:34.528	58709.9414	<i>i</i>	18.19
L	01:16:12.201	-15:54:34.528	58711.3901	<i>g</i>	21.14
L	01:16:12.201	-15:54:34.528	58711.3941	<i>i</i>	20.82
L	01:16:12.201	-15:54:34.528	58713.1460	<i>g</i>	20.02
L	01:16:12.201	-15:54:34.528	58713.1500	<i>i</i>	18.61
L	01:06:04.405	-19:00:14.778	58710.0542	<i>i</i>	20.34
L	01:06:04.405	-19:00:14.778	58710.1084	<i>i</i>	20.73
L	01:06:04.405	-19:00:14.778	58710.1141	<i>i</i>	20.95
L	01:06:04.405	-19:00:14.778	58711.3691	<i>i</i>	20.36
L	01:06:04.405	-19:00:14.778	58711.3843	<i>g</i>	18.00
L	01:06:04.405	-19:00:14.778	58711.3882	<i>i</i>	16.16
L	01:06:04.405	-19:00:14.778	58713.1254	<i>g</i>	20.17

Table 4 continued

Table 4 (*continued*)

Source ^a	α (J2000)	δ (J2000)	Date (MJD)	Filter	Magnitude Limit ^b (3σ)
L	01:06:04.405	-19:00:14.778	58713.1293	<i>i</i>	19.05
L	01:11:09.093	-13:57:39.791	58709.9886	<i>i</i>	19.46
L	01:11:09.093	-13:57:39.791	58710.0037	<i>i</i>	19.85
L	00:54:07.466	-21:42:50.555	58710.0342	<i>i</i>	20.12
L	00:54:07.466	-21:42:50.555	58710.0391	<i>i</i>	20.60
L	00:54:07.466	-21:42:50.555	58710.3497	<i>i</i>	20.58
L	00:52:46.173	-22:58:30.065	58709.9647	<i>g</i>	19.98
L	00:52:46.173	-22:58:30.065	58709.9687	<i>i</i>	18.08
L	00:52:46.173	-22:58:30.065	58709.9987	<i>i</i>	19.96
L	00:52:46.173	-22:58:30.065	58710.0138	<i>i</i>	20.35
L	00:52:46.173	-22:58:30.065	58710.9606	<i>g</i>	19.01
L	00:52:46.173	-22:58:30.065	58710.9645	<i>i</i>	17.90
L	00:52:46.173	-22:58:30.065	58710.9669	<i>i</i>	17.72
L	00:52:46.173	-22:58:30.065	58712.7394	<i>i</i>	18.75
L	00:52:46.173	-22:58:30.065	58712.8827	<i>g</i>	20.00
L	00:52:46.173	-22:58:30.065	58712.8866	<i>i</i>	19.58
L	00:52:46.173	-22:58:30.065	58713.8798	<i>i</i>	20.27
L	00:52:46.173	-22:58:30.065	58713.9273	<i>i</i>	20.52
L	00:52:46.173	-22:58:30.065	58714.0165	<i>g</i>	21.32
L	00:52:46.173	-22:58:30.065	58714.0204	<i>i</i>	20.44
L	00:03:12.980	-35:56:13.243	58709.9374	<i>g</i>	18.89
L	00:03:12.980	-35:56:13.243	58709.9413	<i>i</i>	17.84
L	00:03:12.980	-35:56:13.243	58711.3670	<i>g</i>	18.54
L	00:03:12.980	-35:56:13.243	58711.3709	<i>i</i>	17.70
L	00:03:12.980	-35:56:13.243	58713.0185	<i>g</i>	21.94
L	00:03:12.980	-35:56:13.243	58713.0225	<i>i</i>	19.99
L	00:03:12.980	-35:56:13.243	58714.0292	<i>g</i>	21.72
L	00:03:12.980	-35:56:13.243	58714.0331	<i>i</i>	21.40
L	01:24:38.972	-12:38:08.117	58709.9464	<i>g</i>	19.59
L	01:24:38.972	-12:38:08.117	58709.9504	<i>i</i>	19.99
L	01:24:38.972	-12:38:08.117	58712.1563	<i>g</i>	19.97
L	01:24:38.972	-12:38:08.117	58712.1603	<i>i</i>	19.36
L	01:24:38.972	-12:38:08.117	58713.1702	<i>g</i>	15.92
L	01:24:38.972	-12:38:08.117	58713.1742	<i>i</i>	16.68
L	23:57:00.681	-34:40:50.171	58710.0291	<i>i</i>	20.77
L	23:57:00.681	-34:40:50.171	58710.1072	<i>i</i>	17.49
L	01:19:20.805	-11:52:07.550	58710.0189	<i>i</i>	20.21
L	01:19:20.805	-11:52:07.550	58710.1425	<i>i</i>	21.17
L	01:19:20.805	-11:52:07.550	58710.1490	<i>i</i>	20.98
L	01:02:11.290	-21:14:29.774	58710.0442	<i>i</i>	20.82
L	01:02:11.290	-21:14:29.774	58710.0492	<i>i</i>	20.72
L	23:57:00.689	-34:45:33.178	58709.9988	<i>i</i>	20.23
L	23:57:00.689	-34:45:33.178	58710.1123	<i>i</i>	17.11
L	23:57:00.689	-34:45:33.178	58710.1171	<i>i</i>	17.04
L	23:57:00.689	-34:45:33.178	58712.8616	<i>g</i>	20.02
L	23:57:00.689	-34:45:33.178	58712.8655	<i>i</i>	19.72
L	23:57:00.689	-34:45:33.178	58714.0256	<i>g</i>	21.21
L	23:57:00.689	-34:45:33.178	58714.0295	<i>i</i>	21.37
L	01:07:04.937	-19:22:29.424	58710.0290	<i>i</i>	20.30
L	01:07:04.937	-19:22:29.424	58710.1223	<i>i</i>	20.76
L	01:07:04.937	-19:22:29.424	58712.9142	<i>g</i>	19.87
L	01:07:04.937	-19:22:29.424	58712.9181	<i>i</i>	19.54
L	01:26:20.577	-07:28:36.012	58710.0836	<i>i</i>	21.81

Table 4 *continued*

Table 4 (continued)

Source ^a	α (J2000)	δ (J2000)	Date (MJD)	Filter	Magnitude Limit ^b (3σ)
L	01:26:20.577	-07:28:36.012	58710.1324	<i>i</i>	21.84
L	00:57:01.119	-23:50:14.269	58710.0037	<i>i</i>	20.39
L	00:57:01.119	-23:50:14.269	58710.0492	<i>i</i>	21.00
L	00:57:01.119	-23:50:14.269	58711.3053	<i>i</i>	20.21
L	00:57:01.119	-23:50:14.269	58712.6991	<i>i</i>	20.05
L	00:57:01.119	-23:50:14.269	58713.9462	<i>i</i>	20.51
L	00:57:01.119	-23:50:14.269	58713.9895	<i>i</i>	20.19
L	01:20:54.888	-12:36:16.211	58709.9464	<i>g</i>	19.20
L	01:20:54.888	-12:36:16.211	58709.9504	<i>i</i>	18.50
L	01:20:54.888	-12:36:16.211	58709.9504	<i>i</i>	18.50
L	01:20:54.888	-12:36:16.211	58712.9067	<i>g</i>	18.54
L	01:20:54.888	-12:36:16.211	58712.9107	<i>i</i>	17.81
L	01:02:17.356	-19:40:08.774	58710.0801	<i>i</i>	20.82
L	01:02:17.356	-19:40:08.774	58710.1234	<i>i</i>	20.42
L	01:20:58.515	-13:51:00.220	58709.9838	<i>g</i>	20.14
L	01:20:58.515	-13:51:00.220	58709.9936	<i>i</i>	19.02
L	01:20:58.515	-13:51:00.220	58710.1089	<i>i</i>	18.87
L	01:20:58.515	-13:51:00.220	58710.1094	<i>i</i>	20.60
L	01:20:58.515	-13:51:00.220	58712.7798	<i>g</i>	18.16
L	01:20:58.515	-13:51:00.220	58712.7838	<i>i</i>	16.39
L	01:19:02.302	-14:31:13.490	58710.0138	<i>i</i>	20.18
L	01:19:02.302	-14:31:13.490	58710.0645	<i>i</i>	20.48
L	01:19:02.302	-14:31:13.490	58712.9051	<i>g</i>	19.53
L	01:19:02.302	-14:31:13.490	58712.9090	<i>i</i>	19.10
L	01:01:57.129	-20:54:03.809	58709.9863	<i>g</i>	20.04
L	01:01:57.129	-20:54:03.809	58710.0696	<i>i</i>	20.48
L	01:01:57.129	-20:54:03.809	58710.1511	<i>i</i>	16.72
L	01:01:57.129	-20:54:03.809	58711.4174	<i>g</i>	20.64
L	01:01:57.129	-20:54:03.809	58711.4213	<i>i</i>	19.85
L	01:01:57.129	-20:54:03.809	58713.4147	<i>g</i>	19.42
L	01:01:57.129	-20:54:03.809	58713.4186	<i>i</i>	18.37
L	01:01:57.129	-20:54:03.809	58714.6690	<i>g</i>	18.64
L	01:01:57.129	-20:54:03.809	58714.6729	<i>i</i>	17.30
L	01:02:41.771	-21:52:55.754	58710.0088	<i>i</i>	19.88
L	01:02:41.771	-21:52:55.754	58710.0138	<i>i</i>	20.02
L	01:02:41.771	-21:52:55.754	58712.8894	<i>g</i>	19.51
L	01:02:41.771	-21:52:55.754	58712.8894	<i>g</i>	19.51
L	01:02:41.771	-21:52:55.754	58712.8934	<i>i</i>	18.20
L	01:02:41.771	-21:52:55.754	58714.0383	<i>g</i>	21.23
L	01:02:41.771	-21:52:55.754	58714.0423	<i>i</i>	19.90
L	01:25:16.372	-08:52:25.064	58710.0606	<i>i</i>	20.82
L	01:25:16.372	-08:52:25.064	58710.1133	<i>i</i>	21.10
L	01:23:15.825	-09:01:41.430	58710.1335	<i>i</i>	20.61
L	01:23:15.825	-09:01:41.430	58710.1525	<i>i</i>	21.15
L	01:26:20.302	-08:05:20.011	58709.9645	<i>g</i>	19.58
L	01:26:20.302	-08:05:20.011	58709.9686	<i>i</i>	19.49
L	01:26:20.302	-08:05:20.011	58710.0937	<i>i</i>	22.04
L	01:26:20.302	-08:05:20.011	58710.1274	<i>i</i>	21.95
L	01:26:20.302	-08:05:20.011	58711.7743	<i>g</i>	21.47
L	01:26:20.302	-08:05:20.011	58711.7782	<i>i</i>	21.09
L	01:26:20.302	-08:05:20.011	58713.2954	<i>i</i>	15.58
L	00:48:43.287	-23:33:42.070	58710.0189	<i>i</i>	20.83
L	00:48:43.287	-23:33:42.070	58710.0747	<i>i</i>	20.65

Table 4 continued

Table 4 (continued)

Source ^a	α (J2000)	δ (J2000)	Date (MJD)	Filter	Magnitude Limit ^b (3σ)
L	00:48:43.287	-23:33:42.070	58710.1421	<i>i</i>	17.50
L	00:48:43.287	-23:33:42.070	58711.1091	<i>i</i>	20.76
L	00:48:43.287	-23:33:42.070	58711.9714	<i>i</i>	17.41
L	00:48:43.287	-23:33:42.070	58713.2423	<i>i</i>	19.61
L	00:48:43.287	-23:33:42.070	58713.4115	<i>i</i>	17.22
L	01:05:11.425	-20:18:01.829	58710.1284	<i>i</i>	20.34
L	01:05:11.425	-20:18:01.829	58710.1448	<i>i</i>	20.90
L	01:05:11.425	-20:18:01.829	58712.7889	<i>g</i>	18.82
L	01:05:11.425	-20:18:01.829	58712.7928	<i>i</i>	17.73
L	01:05:11.425	-20:18:01.829	58714.0109	<i>g</i>	21.61
L	01:05:11.425	-20:18:01.829	58714.0149	<i>i</i>	21.53
L	01:12:51.492	-18:07:51.233	58710.1034	<i>i</i>	20.96
L	01:12:51.492	-18:07:51.233	58710.1242	<i>i</i>	20.82
L	01:12:58.856	-19:00:15.210	58710.0189	<i>i</i>	20.58
L	01:12:58.856	-19:00:15.210	58710.0240	<i>i</i>	20.26
L	01:17:06.387	-13:59:51.619	58709.9886	<i>i</i>	19.86
L	01:17:06.387	-13:59:51.619	58710.0984	<i>i</i>	21.33
L	01:17:06.387	-13:59:51.619	58711.7328	<i>g</i>	21.51
L	01:17:06.387	-13:59:51.619	58711.7368	<i>i</i>	21.05
L	01:17:06.387	-13:59:51.619	58713.6447	<i>g</i>	15.62
L	01:17:06.387	-13:59:51.619	58713.6487	<i>i</i>	14.56
L	00:57:08.579	-21:55:11.237	58709.9555	<i>g</i>	18.97
L	00:57:08.579	-21:55:11.237	58709.9594	<i>i</i>	18.09
L	00:57:08.579	-21:55:11.237	58710.3536	<i>i</i>	19.66
L	00:57:08.579	-21:55:11.237	58712.8859	<i>g</i>	19.74
L	00:57:08.579	-21:55:11.237	58712.8898	<i>i</i>	19.66
L	00:57:08.579	-21:55:11.237	58714.0488	<i>g</i>	20.36
L	00:57:08.579	-21:55:11.237	58714.0528	<i>i</i>	19.06
L	01:12:42.201	-17:20:35.851	58710.1038	<i>i</i>	21.18
L	01:12:42.201	-17:20:35.851	58710.1374	<i>i</i>	20.99
L	01:12:42.201	-17:20:35.851	58711.4167	<i>g</i>	20.58
L	01:12:42.201	-17:20:35.851	58711.4206	<i>i</i>	19.69
L	00:58:46.371	-22:07:33.564	58710.0239	<i>i</i>	20.62
L	00:58:46.371	-22:07:33.564	58710.0837	<i>i</i>	21.32
L	01:32:35.274	-33:22:15.319	58710.3466	<i>i</i>	20.06
L	00:36:23.086	-23:01:00.721	58710.2813	<i>i</i>	20.29
L	01:37:49.334	-32:54:36.590	58710.2962	<i>i</i>	20.08
L	00:38:07.332	-25:04:03.389	58710.3013	<i>i</i>	19.90
L	00:53:28.665	-21:54:40.752	58710.3063	<i>i</i>	20.34
L	01:25:37.151	-30:21:55.742	58710.3368	<i>i</i>	19.31
L	00:36:59.589	-22:30:52.232	58710.3114	<i>i</i>	20.22
L	01:08:47.538	-28:34:56.568	58710.3516	<i>i</i>	19.82
L	01:08:47.538	-28:34:56.568	58710.3572	<i>i</i>	20.00
L	00:58:53.387	-26:59:51.464	58710.3363	<i>i</i>	19.23
L	00:49:05.009	-22:04:24.762	58710.3396	<i>i</i>	13.90
L	00:59:52.211	-27:40:59.063	58710.3437	<i>i</i>	13.76
L	00:51:44.158	-21:38:16.066	58710.3485	<i>i</i>	19.79
L	01:23:14.857	-32:50:28.601	58710.3566	<i>i</i>	15.89
L	01:23:14.857	-32:50:28.601	58710.3569	<i>i</i>	19.47
L	01:23:14.857	-32:50:28.601	58710.3618	<i>i</i>	19.75
L	01:45:57.431	-34:49:11.258	58710.3114	<i>i</i>	20.34
L	01:45:57.431	-34:49:11.258	58710.3171	<i>i</i>	20.11
L	00:39:30.866	-25:41:48.322	58710.2912	<i>i</i>	19.73

Table 4 continued

Table 4 (continued)

Source ^a	α (J2000)	δ (J2000)	Date (MJD)	Filter	Magnitude Limit ^b (3σ)
L	00:42:54.699	-22:15:09.580	58710.3374	<i>i</i>	18.28
L	00:42:54.699	-22:15:09.580	58710.3446	<i>i</i>	17.22
L	00:44:27.058	-25:23:11.274	58710.2764	<i>i</i>	19.55
L	00:47:40.290	-21:36:12.251	58710.3217	<i>i</i>	20.01
L	00:54:07.466	-21:42:50.555	58710.0342	<i>i</i>	20.12
L	00:54:07.466	-21:42:50.555	58710.0391	<i>i</i>	20.60
L	00:54:07.466	-21:42:50.555	58710.3497	<i>i</i>	20.58
L	01:06:12.223	-30:10:41.174	58710.3418	<i>i</i>	19.63
L	01:38:08.996	-32:51:16.956	58710.2813	<i>i</i>	19.53
L	00:37:57.617	-25:04:25.442	58710.2912	<i>i</i>	19.81
L	00:57:46.992	-28:17:00.848	58710.3413	<i>i</i>	19.28
L	00:59:49.426	-27:41:16.066	58710.2861	<i>i</i>	19.44
L	00:37:21.521	-19:56:03.286	58710.3386	<i>i</i>	15.37
L	01:13:47.280	-31:44:50.100	58710.2861	<i>i</i>	19.40
L	00:34:13.637	-21:26:19.043	58710.2764	<i>i</i>	20.25
L	01:34:24.358	-31:36:20.135	58710.3262	<i>i</i>	19.74
L	01:11:01.124	-30:26:18.632	58710.3317	<i>i</i>	19.32
L	01:08:09.048	-28:31:25.378	58710.3063	<i>i</i>	20.35
L	00:50:29.945	-21:15:27.176	58710.3013	<i>i</i>	19.74
L	01:10:35.613	-30:13:16.558	58710.3570	<i>i</i>	17.70
L	01:33:18.645	-32:53:35.066	58710.3165	<i>i</i>	19.63
L	01:33:18.645	-32:53:35.066	58710.3172	<i>i</i>	20.17
L	01:16:41.067	-31:26:02.216	58710.3620	<i>i</i>	18.01
L	01:35:21.551	-32:46:35.170	58710.3470	<i>i</i>	20.03
L	01:35:21.551	-32:46:35.170	58710.3521	<i>i</i>	20.21
L	00:57:08.579	-21:55:11.237	58709.9555	<i>g</i>	18.97
L	00:57:08.579	-21:55:11.237	58709.9594	<i>i</i>	18.09
L	00:57:08.579	-21:55:11.237	58710.3536	<i>i</i>	19.66
L	00:57:08.579	-21:55:11.237	58712.8859	<i>g</i>	19.74
L	00:57:08.579	-21:55:11.237	58712.8898	<i>i</i>	19.66
L	00:57:08.579	-21:55:11.237	58714.0488	<i>g</i>	20.36
L	00:57:08.579	-21:55:11.237	58714.0528	<i>i</i>	19.06
L	00:53:12.305	-21:31:17.749	58710.2962	<i>i</i>	19.64
L	01:32:58.309	-30:04:57.270	58710.3311	<i>i</i>	19.14
L	00:47:21.761	-23:35:07.858	58710.3165	<i>i</i>	19.53
L	00:47:21.761	-23:35:07.858	58710.3213	<i>i</i>	20.04
L	00:54:24.345	-25:27:50.587	58710.8953	<i>i</i>	17.81
L	00:54:24.345	-25:27:50.587	58711.2953	<i>i</i>	19.73
L	00:54:24.345	-25:27:50.587	58712.6890	<i>i</i>	19.74
L	00:54:24.345	-25:27:50.587	58713.9204	<i>i</i>	21.03
L	00:54:24.345	-25:27:50.587	58713.9740	<i>i</i>	19.92
L	00:50:06.164	-25:57:28.580	58710.8061	<i>i</i>	17.77
L	00:50:06.164	-25:57:28.580	58710.9516	<i>i</i>	17.88
L	00:50:06.164	-25:57:28.580	58712.1617	<i>i</i>	16.85
L	00:50:06.164	-25:57:28.580	58713.4266	<i>i</i>	16.68
L	00:50:06.164	-25:57:28.580	58713.6538	<i>i</i>	17.43
L	00:45:03.577	-25:01:11.158	58710.6356	<i>i</i>	17.71
L	00:45:03.577	-25:01:11.158	58711.0488	<i>i</i>	20.32
L	00:45:03.577	-25:01:11.158	58711.9613	<i>i</i>	18.45
L	00:45:03.577	-25:01:11.158	58713.2306	<i>i</i>	19.08
L	00:45:03.577	-25:01:11.158	58713.3613	<i>i</i>	18.48
L	00:55:04.329	-26:46:12.551	58710.9004	<i>i</i>	17.85
L	00:55:04.329	-26:46:12.551	58710.9060	<i>i</i>	18.12

Table 4 continued

Table 4 (continued)

Source ^a	α (J2000)	δ (J2000)	Date (MJD)	Filter	Magnitude Limit ^b (3σ)
L	00:55:04.329	-26:46:12.551	58710.9620	<i>i</i>	18.01
L	00:55:04.329	-26:46:12.551	58712.6183	<i>i</i>	18.26
L	00:55:04.329	-26:46:12.551	58713.3664	<i>i</i>	18.38
L	00:55:04.329	-26:46:12.551	58713.9134	<i>i</i>	20.69
L	00:44:50.543	-23:09:32.504	58710.5797	<i>i</i>	17.73
L	00:44:50.543	-23:09:32.504	58710.9434	<i>i</i>	17.81
L	00:44:50.543	-23:09:32.504	58712.1130	<i>i</i>	17.43
L	00:44:50.543	-23:09:32.504	58713.1519	<i>i</i>	16.94
L	00:44:50.543	-23:09:32.504	58713.3329	<i>i</i>	19.12
L	00:55:09.151	-25:27:20.534	58710.8919	<i>i</i>	17.94
L	00:55:09.151	-25:27:20.534	58710.8987	<i>i</i>	18.00
L	00:55:09.151	-25:27:20.534	58711.3679	<i>i</i>	18.89
L	00:55:09.151	-25:27:20.534	58711.3789	<i>i</i>	17.86
L	00:55:09.151	-25:27:20.534	58712.5731	<i>i</i>	18.05
L	00:55:09.151	-25:27:20.534	58713.9844	<i>i</i>	20.42
L	00:55:09.151	-25:27:20.534	58714.0002	<i>i</i>	20.37
L	00:50:09.705	-23:16:48.173	58710.6808	<i>i</i>	20.19
L	00:50:09.705	-23:16:48.173	58711.2029	<i>i</i>	17.56
L	00:50:09.705	-23:16:48.173	58712.7050	<i>i</i>	20.17
L	00:50:09.705	-23:16:48.173	58713.1775	<i>i</i>	18.38
L	00:50:09.705	-23:16:48.173	58713.3682	<i>i</i>	18.31
L	00:52:41.582	-25:44:01.867	58710.7133	<i>i</i>	20.82
L	00:52:41.582	-25:44:01.867	58711.0404	<i>i</i>	19.47
L	00:52:41.582	-25:44:01.867	58712.4264	<i>i</i>	17.41
L	00:52:41.582	-25:44:01.867	58713.9689	<i>i</i>	19.97
L	00:52:41.582	-25:44:01.867	58713.9895	<i>i</i>	20.41
L	00:52:46.690	-25:40:17.886	58710.7549	<i>i</i>	18.48
L	00:52:46.690	-25:40:17.886	58711.2865	<i>i</i>	19.48
L	00:52:46.690	-25:40:17.886	58712.6044	<i>i</i>	18.76
L	00:52:46.690	-25:40:17.886	58713.8960	<i>i</i>	20.55
L	00:45:50.556	-25:32:33.706	58710.6662	<i>i</i>	19.94
L	00:45:50.556	-25:32:33.706	58711.1134	<i>i</i>	18.26
L	00:45:50.556	-25:32:33.706	58712.0157	<i>i</i>	17.57
L	00:45:50.556	-25:32:33.706	58713.3446	<i>i</i>	18.30
L	00:49:01.481	-23:48:40.741	58710.7657	<i>i</i>	17.71
L	00:49:01.481	-23:48:40.741	58711.1041	<i>i</i>	20.96
L	00:49:01.481	-23:48:40.741	58711.1141	<i>i</i>	20.90
L	00:49:01.481	-23:48:40.741	58712.6738	<i>i</i>	18.41
L	00:49:01.481	-23:48:40.741	58713.3926	<i>i</i>	18.34
L	00:49:01.481	-23:48:40.741	58713.7434	<i>i</i>	19.03
L	00:44:14.580	-24:19:39.266	58710.5949	<i>i</i>	17.52
L	00:44:14.580	-24:19:39.266	58711.1272	<i>i</i>	18.17
L	00:44:14.580	-24:19:39.266	58711.2085	<i>i</i>	17.58
L	00:44:14.580	-24:19:39.266	58712.0384	<i>i</i>	18.33
L	00:44:14.580	-24:19:39.266	58713.1569	<i>i</i>	15.89
L	00:49:16.822	-26:13:09.044	58710.6609	<i>i</i>	19.92
L	00:49:16.822	-26:13:09.044	58711.0349	<i>i</i>	19.39
L	00:49:16.822	-26:13:09.044	58712.5391	<i>i</i>	18.66
L	00:49:16.822	-26:13:09.044	58713.3905	<i>i</i>	17.99
L	00:49:16.822	-26:13:09.044	58713.7815	<i>i</i>	18.46
L	00:49:16.822	-26:13:09.044	58713.9171	<i>i</i>	20.25
L	00:51:21.179	-26:59:22.020	58710.6255	<i>i</i>	18.39
L	00:51:21.179	-26:59:22.020	58711.2988	<i>i</i>	19.72

Table 4 continued

Table 4 (continued)

Source ^a	α (J2000)	δ (J2000)	Date (MJD)	Filter	Magnitude Limit ^b (3σ)
L	00:51:21.179	-26:59:22.020	58713.9621	<i>i</i>	20.09
L	00:51:21.179	-26:59:22.020	58713.9689	<i>i</i>	20.09
L	00:49:17.677	-26:28:34.039	58710.6559	<i>i</i>	18.92
L	00:49:17.677	-26:28:34.039	58710.9828	<i>i</i>	18.21
L	00:49:17.677	-26:28:34.039	58712.6612	<i>i</i>	19.00
L	00:49:17.677	-26:28:34.039	58713.5808	<i>i</i>	17.13
L	00:49:17.677	-26:28:34.039	58713.7376	<i>i</i>	17.52
L	00:49:17.677	-26:28:34.039	58713.7485	<i>i</i>	17.47
L	00:54:05.477	-23:11:40.686	58710.6458	<i>i</i>	18.30
L	00:54:05.477	-23:11:40.686	58711.2571	<i>i</i>	17.94
L	00:54:05.477	-23:11:40.686	58712.6839	<i>i</i>	19.33
L	00:54:05.477	-23:11:40.686	58713.8913	<i>i</i>	20.18
L	00:54:05.477	-23:11:40.686	58713.9529	<i>i</i>	20.52
L	00:45:46.307	-25:55:12.695	58710.6859	<i>i</i>	20.40
L	00:45:46.307	-25:55:12.695	58711.1075	<i>i</i>	18.10
L	00:45:46.307	-25:55:12.695	58712.1738	<i>i</i>	17.07
L	00:45:46.307	-25:55:12.695	58713.2502	<i>i</i>	19.72
L	00:45:46.307	-25:55:12.695	58713.3578	<i>i</i>	18.25
L	00:43:01.682	-24:39:00.713	58710.8815	<i>i</i>	17.04
L	00:43:01.682	-24:39:00.713	58710.8878	<i>i</i>	16.95
L	00:43:01.682	-24:39:00.713	58711.1127	<i>i</i>	18.04
L	00:43:01.682	-24:39:00.713	58711.1252	<i>i</i>	20.65
L	00:43:01.682	-24:39:00.713	58711.8168	<i>i</i>	17.08
L	00:43:01.682	-24:39:00.713	58713.8732	<i>i</i>	20.12
L	00:43:01.682	-24:39:00.713	58713.8734	<i>i</i>	20.52
L	00:54:49.133	-26:22:16.522	58710.8162	<i>i</i>	18.29
L	00:54:49.133	-26:22:16.522	58712.7202	<i>i</i>	18.40
L	00:54:49.133	-26:22:16.522	58713.9844	<i>i</i>	20.35
L	00:54:49.133	-26:22:16.522	58714.0058	<i>i</i>	21.21
L	00:51:29.863	-24:38:32.978	58710.5898	<i>i</i>	18.22
L	00:51:29.863	-24:38:32.978	58711.0488	<i>i</i>	19.44
L	00:51:29.863	-24:38:32.978	58712.2177	<i>i</i>	17.64
L	00:51:29.863	-24:38:32.978	58713.8789	<i>i</i>	20.54
L	00:51:29.863	-24:38:32.978	58713.9636	<i>i</i>	19.77
L	00:54:19.288	-23:34:06.589	58710.9012	<i>i</i>	17.84
L	00:54:19.288	-23:34:06.589	58711.1717	<i>i</i>	20.45
L	00:54:19.288	-23:34:06.589	58712.7445	<i>i</i>	19.07
L	00:54:19.288	-23:34:06.589	58713.8850	<i>i</i>	20.07
L	00:54:19.288	-23:34:06.589	58714.0002	<i>i</i>	21.10
L	00:50:54.447	-23:37:54.793	58710.6757	<i>i</i>	20.13
L	00:50:54.447	-23:37:54.793	58711.0811	<i>i</i>	20.69
L	00:50:54.447	-23:37:54.793	58712.7101	<i>i</i>	19.56
L	00:50:54.447	-23:37:54.793	58713.4115	<i>i</i>	18.21
L	00:50:54.447	-23:37:54.793	58713.4215	<i>i</i>	19.04
L	00:50:54.447	-23:37:54.793	58713.4364	<i>i</i>	16.48
L	00:50:54.447	-23:37:54.793	58713.6110	<i>i</i>	16.04
L	00:53:54.509	-24:04:37.315	58710.7448	<i>i</i>	20.85
L	00:53:54.509	-24:04:37.315	58711.3039	<i>i</i>	19.76
L	00:53:54.509	-24:04:37.315	58712.6561	<i>i</i>	19.24
L	00:53:54.509	-24:04:37.315	58713.9205	<i>i</i>	20.39
L	00:53:54.509	-24:04:37.315	58713.9585	<i>i</i>	20.39
L	00:46:10.416	-24:39:00.691	58710.7808	<i>i</i>	17.71
L	00:46:10.416	-24:39:00.691	58711.0662	<i>i</i>	20.65

Table 4 continued

Table 4 (continued)

Source ^a	α (J2000)	δ (J2000)	Date (MJD)	Filter	Magnitude Limit ^b (3σ)
L	00:46:10.416	-24:39:00.691	58711.9898	<i>i</i>	18.17
L	00:46:10.416	-24:39:00.691	58711.9986	<i>i</i>	18.17
L	00:46:10.416	-24:39:00.691	58713.4045	<i>i</i>	18.50
L	00:48:21.859	-25:07:36.530	58710.7234	<i>i</i>	20.60
L	00:48:21.859	-25:07:36.530	58710.9929	<i>i</i>	17.80
L	00:48:21.859	-25:07:36.530	58712.4199	<i>i</i>	18.04
L	00:48:21.859	-25:07:36.530	58713.6978	<i>i</i>	17.79
L	00:48:21.859	-25:07:36.530	58713.7779	<i>i</i>	18.41
L	00:48:21.859	-25:07:36.530	58713.8960	<i>i</i>	19.79
L	00:48:21.859	-25:07:36.530	58713.9076	<i>i</i>	19.97
L	00:53:26.155	-26:35:59.341	58710.7354	<i>i</i>	20.93
L	00:53:26.155	-26:35:59.341	58711.3003	<i>i</i>	20.05
L	00:53:26.155	-26:35:59.341	58712.5662	<i>i</i>	18.05
L	00:53:26.155	-26:35:59.341	58713.9414	<i>i</i>	20.48
L	00:53:26.155	-26:35:59.341	58713.9794	<i>i</i>	20.22
L	00:50:39.874	-26:48:48.222	58710.7910	<i>i</i>	18.13
L	00:50:39.874	-26:48:48.222	58711.1183	<i>i</i>	18.22
L	00:50:39.874	-26:48:48.222	58712.6284	<i>i</i>	18.63
L	00:50:39.874	-26:48:48.222	58713.4164	<i>i</i>	18.18
L	00:50:39.874	-26:48:48.222	58713.4278	<i>i</i>	14.04
L	00:50:39.874	-26:48:48.222	58713.9794	<i>i</i>	20.12
L	00:53:11.809	-26:05:38.324	58710.7707	<i>i</i>	18.19
L	00:53:11.809	-26:05:38.324	58711.3318	<i>i</i>	19.76
L	00:53:11.809	-26:05:38.324	58712.1738	<i>i</i>	17.30
L	00:53:11.809	-26:05:38.324	58713.8801	<i>i</i>	20.19
L	00:53:11.809	-26:05:38.324	58713.9323	<i>i</i>	21.11
L	00:46:13.218	-25:57:00.677	58710.6050	<i>i</i>	17.84
L	00:46:13.218	-25:57:00.677	58710.9879	<i>i</i>	18.01
L	00:46:13.218	-25:57:00.677	58712.0931	<i>i</i>	17.85
L	00:46:13.218	-25:57:00.677	58713.3127	<i>i</i>	19.89
L	00:46:13.218	-25:57:00.677	58713.3481	<i>i</i>	18.54
L	00:55:13.534	-26:19:16.511	58710.8918	<i>i</i>	17.45
L	00:55:13.534	-26:19:16.511	58710.8987	<i>i</i>	17.38
L	00:55:13.534	-26:19:16.511	58711.3629	<i>i</i>	20.36
L	00:55:13.534	-26:19:16.511	58711.3771	<i>i</i>	17.79
L	00:55:13.534	-26:19:16.511	58712.5292	<i>i</i>	17.70
L	00:55:13.534	-26:19:16.511	58713.8913	<i>i</i>	20.69
L	00:55:13.534	-26:19:16.511	58714.0058	<i>i</i>	20.54
L	00:54:17.033	-23:33:09.583	58710.6508	<i>i</i>	18.35
L	00:54:17.033	-23:33:09.583	58711.2699	<i>i</i>	18.69
L	00:54:17.033	-23:33:09.583	58712.6094	<i>i</i>	19.08
L	00:54:17.033	-23:33:09.583	58713.9428	<i>i</i>	20.97
L	00:54:17.033	-23:33:09.583	58713.9478	<i>i</i>	20.87
L	00:49:27.554	-26:32:17.884	58710.0883	<i>i</i>	20.71
L	00:49:27.554	-26:32:17.884	58710.0932	<i>i</i>	20.59
L	00:49:27.554	-26:32:17.884	58711.0265	<i>i</i>	19.20
L	00:49:27.554	-26:32:17.884	58712.5832	<i>i</i>	18.49
L	00:49:27.554	-26:32:17.884	58713.9076	<i>i</i>	21.02
L	00:49:27.554	-26:32:17.884	58713.9377	<i>i</i>	20.38
L	00:49:46.032	-26:26:34.933	58710.5747	<i>i</i>	18.25
L	00:49:46.032	-26:26:34.933	58711.0939	<i>i</i>	20.88
L	00:49:46.032	-26:26:34.933	58712.1563	<i>i</i>	16.89
L	00:49:46.032	-26:26:34.933	58712.1668	<i>i</i>	16.96

Table 4 continued

Table 4 (continued)

Source ^a	α (J2000)	δ (J2000)	Date (MJD)	Filter	Magnitude Limit ^b (3σ)
L	00:49:46.032	-26:26:34.933	58713.4364	<i>i</i>	13.86
L	00:49:46.032	-26:26:34.933	58713.7321	<i>i</i>	17.81
L	00:49:46.032	-26:26:34.933	58713.7882	<i>i</i>	18.42
L	00:49:14.671	-23:51:30.769	58710.7076	<i>i</i>	20.69
L	00:49:14.671	-23:51:30.769	58711.0434	<i>i</i>	20.18
L	00:49:14.671	-23:51:30.769	58712.2112	<i>i</i>	17.41
L	00:47:28.948	-25:26:26.358	58709.9886	<i>i</i>	19.35
L	00:47:28.948	-25:26:26.358	58710.0987	<i>i</i>	20.69
L	00:47:28.948	-25:26:26.358	58711.0731	<i>i</i>	20.48
L	00:47:28.948	-25:26:26.358	58712.4249	<i>i</i>	17.92
L	00:47:28.948	-25:26:26.358	58713.3278	<i>i</i>	18.15
L	00:47:28.948	-25:26:26.358	58713.7535	<i>i</i>	17.36
L	00:47:28.948	-25:26:26.358	58713.8162	<i>i</i>	17.96
L	00:51:14.003	-26:27:40.028	58710.6000	<i>i</i>	18.30
L	00:51:14.003	-26:27:40.028	58711.0990	<i>i</i>	20.95
L	00:51:14.003	-26:27:40.028	58712.6385	<i>i</i>	18.59
L	00:51:14.003	-26:27:40.028	58713.9585	<i>i</i>	20.26
L	00:51:14.003	-26:27:40.028	58713.9689	<i>i</i>	21.02
L	00:57:01.119	-23:50:14.269	58710.0037	<i>i</i>	20.39
L	00:57:01.119	-23:50:14.269	58710.0492	<i>i</i>	21.00
L	00:57:01.119	-23:50:14.269	58711.3053	<i>i</i>	20.21
L	00:57:01.119	-23:50:14.269	58712.6991	<i>i</i>	20.05
L	00:57:01.119	-23:50:14.269	58713.9462	<i>i</i>	20.51
L	00:57:01.119	-23:50:14.269	58713.9895	<i>i</i>	20.19
L	00:52:46.173	-22:58:30.065	58709.9647	<i>g</i>	19.98
L	00:52:46.173	-22:58:30.065	58709.9687	<i>i</i>	18.08
L	00:52:46.173	-22:58:30.065	58709.9987	<i>i</i>	19.96
L	00:52:46.173	-22:58:30.065	58710.0138	<i>i</i>	20.35
L	00:52:46.173	-22:58:30.065	58710.9606	<i>g</i>	19.01
L	00:52:46.173	-22:58:30.065	58710.9645	<i>i</i>	17.90
L	00:52:46.173	-22:58:30.065	58710.9669	<i>i</i>	17.72
L	00:52:46.173	-22:58:30.065	58712.7394	<i>i</i>	18.75
L	00:52:46.173	-22:58:30.065	58712.8827	<i>g</i>	20.00
L	00:52:46.173	-22:58:30.065	58712.8866	<i>i</i>	19.58
L	00:52:46.173	-22:58:30.065	58713.8798	<i>i</i>	20.27
L	00:52:46.173	-22:58:30.065	58713.9273	<i>i</i>	20.52
L	00:52:46.173	-22:58:30.065	58714.0165	<i>g</i>	21.32
L	00:52:46.173	-22:58:30.065	58714.0204	<i>i</i>	20.44
L	00:50:34.509	-23:37:06.769	58710.7185	<i>i</i>	20.85
L	00:50:34.509	-23:37:06.769	58711.1220	<i>i</i>	18.90
L	00:50:34.509	-23:37:06.769	58712.6334	<i>i</i>	18.83
L	00:50:34.509	-23:37:06.769	58713.4237	<i>i</i>	18.34
L	00:50:34.509	-23:37:06.769	58713.7250	<i>i</i>	19.01
L	00:49:29.035	-25:59:28.896	58710.6909	<i>i</i>	20.50
L	00:49:29.035	-25:59:28.896	58711.0974	<i>i</i>	20.08
L	00:49:29.035	-25:59:28.896	58712.6662	<i>i</i>	18.67
L	00:49:29.035	-25:59:28.896	58713.4230	<i>i</i>	18.82
L	00:49:29.035	-25:59:28.896	58713.5910	<i>i</i>	17.12
L	00:49:23.120	-26:30:26.993	58710.6101	<i>i</i>	18.18
L	00:49:23.120	-26:30:26.993	58710.9346	<i>i</i>	17.89
L	00:49:23.120	-26:30:26.993	58712.7344	<i>i</i>	18.88
L	00:49:23.120	-26:30:26.993	58712.7502	<i>i</i>	19.18
L	00:49:23.120	-26:30:26.993	58713.9219	<i>i</i>	20.41

Table 4 continued

Table 4 (continued)

Source ^a	α (J2000)	δ (J2000)	Date (MJD)	Filter	Magnitude Limit ^b (3σ)
L	00:49:23.120	-26:30:26.993	58713.9844	<i>i</i>	20.50
L	00:50:57.715	-23:33:28.782	58710.7960	<i>i</i>	17.80
L	00:50:57.715	-23:33:28.782	58711.1860	<i>i</i>	17.35
L	00:50:57.715	-23:33:28.782	58712.5782	<i>i</i>	18.99
L	00:50:57.715	-23:33:28.782	58713.6010	<i>i</i>	17.25
L	00:50:57.715	-23:33:28.782	58713.6929	<i>i</i>	18.02
L	00:47:07.527	-24:22:14.329	58709.9464	<i>g</i>	19.30
L	00:47:07.527	-24:22:14.329	58709.9504	<i>i</i>	18.50
L	00:47:07.527	-24:22:14.329	58710.9759	<i>i</i>	18.52
L	00:47:07.527	-24:22:14.329	58712.0045	<i>i</i>	17.75
L	00:47:07.527	-24:22:14.329	58712.8789	<i>g</i>	19.69
L	00:47:07.527	-24:22:14.329	58712.8829	<i>i</i>	19.54
L	00:47:07.527	-24:22:14.329	58713.3495	<i>i</i>	18.39
L	00:47:07.527	-24:22:14.329	58713.3629	<i>i</i>	18.32
L	00:47:07.527	-24:22:14.329	58714.0200	<i>g</i>	21.29
L	00:47:07.527	-24:22:14.329	58714.0239	<i>i</i>	20.69
L	00:43:21.228	-24:04:57.104	58710.6960	<i>i</i>	20.83
L	00:43:21.228	-24:04:57.104	58710.7015	<i>i</i>	20.84
L	00:43:21.228	-24:04:57.104	58711.0052	<i>i</i>	17.98
L	00:43:21.228	-24:04:57.104	58711.0160	<i>i</i>	19.07
L	00:43:21.228	-24:04:57.104	58712.0280	<i>i</i>	18.09
L	00:43:21.228	-24:04:57.104	58713.3178	<i>i</i>	19.01
L	00:43:21.228	-24:04:57.104	58713.8736	<i>i</i>	20.24
L	00:48:42.776	-23:46:23.070	58710.6306	<i>i</i>	18.14
L	00:48:42.776	-23:46:23.070	58711.0538	<i>i</i>	19.68
L	00:48:42.776	-23:46:23.070	58711.9815	<i>i</i>	17.87
L	00:48:42.776	-23:46:23.070	58713.9046	<i>i</i>	18.93
L	00:48:42.776	-23:46:23.070	58713.9740	<i>i</i>	19.81
L	00:48:58.272	-25:41:36.420	58710.8112	<i>i</i>	17.86
L	00:48:58.272	-25:41:36.420	58711.1025	<i>i</i>	19.34
L	00:48:58.272	-25:41:36.420	58712.5594	<i>i</i>	18.79
L	00:48:58.272	-25:41:36.420	58713.2258	<i>i</i>	17.67
L	00:48:58.272	-25:41:36.420	58713.2357	<i>i</i>	18.22
L	00:48:58.272	-25:41:36.420	58713.3995	<i>i</i>	18.38
L	00:55:13.061	-24:02:38.519	58710.9012	<i>i</i>	17.52
L	00:55:13.061	-24:02:38.519	58712.5883	<i>i</i>	19.02
L	00:55:13.061	-24:02:38.519	58712.5973	<i>i</i>	19.03
L	00:55:13.061	-24:02:38.519	58713.9323	<i>i</i>	20.47
L	00:55:13.061	-24:02:38.519	58713.9636	<i>i</i>	19.86
L	00:50:33.089	-23:17:43.757	58710.5628	<i>i</i>	18.16
L	00:50:33.089	-23:17:43.757	58710.9796	<i>i</i>	17.81
L	00:50:33.089	-23:17:43.757	58711.9764	<i>i</i>	18.04
L	00:50:33.089	-23:17:43.757	58713.6059	<i>i</i>	17.51
L	00:50:33.089	-23:17:43.757	58713.9794	<i>i</i>	19.57
L	01:34:22.761	-32:50:07.138	58710.9173	<i>i</i>	18.00
L	01:34:22.761	-32:50:07.138	58711.1466	<i>i</i>	18.70
L	01:34:22.761	-32:50:07.138	58712.1493	<i>i</i>	17.20
L	01:34:22.761	-32:50:07.138	58713.1651	<i>i</i>	17.66
L	01:34:22.761	-32:50:07.138	58713.1654	<i>i</i>	17.26
L	00:52:19.127	-27:20:45.431	58710.7758	<i>i</i>	18.12
L	00:52:19.127	-27:20:45.431	58711.1356	<i>i</i>	19.68
L	00:52:19.127	-27:20:45.431	58712.6511	<i>i</i>	19.09
L	00:52:19.127	-27:20:45.431	58713.9026	<i>i</i>	20.00

Table 4 continued

Table 4 (*continued*)

Source ^a	α (J2000)	δ (J2000)	Date (MJD)	Filter	Magnitude Limit ^b (3σ)
L	00:52:19.127	-27:20:45.431	58713.9377	<i>i</i>	21.18
L	00:45:53.292	-23:46:20.860	58710.8842	<i>i</i>	17.63
L	00:45:53.292	-23:46:20.860	58711.0201	<i>i</i>	19.14
L	00:45:53.292	-23:46:20.860	58712.0076	<i>i</i>	18.83
L	00:45:53.292	-23:46:20.860	58713.1205	<i>i</i>	18.30
L	00:45:53.292	-23:46:20.860	58713.3531	<i>i</i>	18.62
L	00:44:43.618	-23:51:17.539	58710.8827	<i>i</i>	17.62
L	00:44:43.618	-23:51:17.539	58710.8883	<i>i</i>	17.72
L	00:44:43.618	-23:51:17.539	58710.9525	<i>i</i>	17.89
L	00:44:43.618	-23:51:17.539	58712.1461	<i>i</i>	18.06
L	00:44:43.618	-23:51:17.539	58713.3057	<i>i</i>	19.66
L	00:49:32.547	-26:32:18.917	58710.5848	<i>i</i>	18.20
L	00:49:32.547	-26:32:18.917	58711.0589	<i>i</i>	19.67
L	00:49:32.547	-26:32:18.917	58712.6789	<i>i</i>	18.73
L	00:49:32.547	-26:32:18.917	58713.3822	<i>i</i>	18.28
L	00:49:32.547	-26:32:18.917	58713.9273	<i>i</i>	20.61
L	00:48:41.981	-23:22:07.072	58710.7498	<i>i</i>	20.19
L	00:48:41.981	-23:22:07.072	58711.0761	<i>i</i>	20.68
L	00:48:41.981	-23:22:07.072	58711.9563	<i>i</i>	18.15
L	00:48:41.981	-23:22:07.072	58713.1874	<i>i</i>	18.14
L	00:56:02.632	-27:30:28.447	58710.8903	<i>i</i>	17.42
L	00:56:02.632	-27:30:28.447	58711.3460	<i>i</i>	17.91
L	00:56:02.632	-27:30:28.447	58712.5340	<i>i</i>	18.54
L	00:56:02.632	-27:30:28.447	58713.7932	<i>i</i>	18.20
L	00:56:02.632	-27:30:28.447	58713.8074	<i>i</i>	18.12
L	00:56:02.632	-27:30:28.447	58713.9026	<i>i</i>	20.07
L	00:54:15.943	-23:32:06.583	58710.5696	<i>i</i>	18.23
L	00:54:15.943	-23:32:06.583	58711.2444	<i>i</i>	17.53
L	00:54:15.943	-23:32:06.583	58712.6460	<i>i</i>	19.18
L	00:54:15.943	-23:32:06.583	58713.8916	<i>i</i>	19.97
L	00:54:15.943	-23:32:06.583	58713.9134	<i>i</i>	20.98
L	00:52:14.999	-27:19:41.430	58710.7397	<i>i</i>	19.60
L	00:52:14.999	-27:19:41.430	58711.0832	<i>i</i>	20.83
L	00:52:14.999	-27:19:41.430	58712.6940	<i>i</i>	19.77
L	00:52:14.999	-27:19:41.430	58713.8995	<i>i</i>	20.35
L	00:52:14.999	-27:19:41.430	58713.9740	<i>i</i>	21.15
L	00:51:18.760	-26:10:05.016	58710.7010	<i>i</i>	18.68
L	00:51:18.760	-26:10:05.016	58710.8011	<i>i</i>	17.74
L	00:51:18.760	-26:10:05.016	58711.0066	<i>i</i>	17.96
L	00:51:18.760	-26:10:05.016	58713.9529	<i>i</i>	21.54
L	00:51:18.760	-26:10:05.016	58714.0002	<i>i</i>	20.58
L	00:50:33.407	-23:00:59.767	58710.6205	<i>i</i>	18.29
L	00:50:33.407	-23:00:59.767	58711.1711	<i>i</i>	18.09
L	00:50:33.407	-23:00:59.767	58711.9663	<i>i</i>	18.08
L	00:50:33.407	-23:00:59.767	58713.6595	<i>i</i>	17.51
L	00:50:33.407	-23:00:59.767	58713.8850	<i>i</i>	20.47
L	00:48:43.287	-23:33:42.070	58710.0189	<i>i</i>	20.83
L	00:48:43.287	-23:33:42.070	58710.0747	<i>i</i>	20.65
L	00:48:43.287	-23:33:42.070	58710.1421	<i>i</i>	17.50
L	00:48:43.287	-23:33:42.070	58711.1091	<i>i</i>	20.76
L	00:48:43.287	-23:33:42.070	58711.9714	<i>i</i>	17.41
L	00:48:43.287	-23:33:42.070	58713.2423	<i>i</i>	19.61
L	00:48:43.287	-23:33:42.070	58713.4115	<i>i</i>	17.22

Table 4 (*continued*)

Table 4 (continued)

Source ^a	α (J2000)	δ (J2000)	Date (MJD)	Filter	Magnitude Limit ^b (3σ)
L	00:52:35.921	-26:45:03.359	58710.6407	<i>i</i>	18.24
L	00:52:35.921	-26:45:03.359	58711.0782	<i>i</i>	20.87
L	00:52:35.921	-26:45:03.359	58712.6233	<i>i</i>	18.34
L	00:52:35.921	-26:45:03.359	58713.9478	<i>i</i>	21.20
L	00:52:35.921	-26:45:03.359	58713.9513	<i>i</i>	20.32
L	00:51:10.523	-25:57:15.019	58710.7284	<i>i</i>	20.88
L	00:51:10.523	-25:57:15.019	58711.2750	<i>i</i>	19.14
L	00:51:10.523	-25:57:15.019	58713.9323	<i>i</i>	20.72
L	00:51:10.523	-25:57:15.019	58713.9895	<i>i</i>	20.45
L	00:44:13.189	-24:19:39.266	58710.7606	<i>i</i>	17.60
L	00:44:13.189	-24:19:39.266	58711.0385	<i>i</i>	19.99
L	00:44:13.189	-24:19:39.266	58712.0315	<i>i</i>	18.35
L	00:44:13.189	-24:19:39.266	58713.1519	<i>i</i>	15.12
L	00:44:13.189	-24:19:39.266	58713.2050	<i>i</i>	15.80
L	00:47:05.254	-24:14:19.331	58710.6707	<i>i</i>	20.10
L	00:47:05.254	-24:14:19.331	58711.1302	<i>i</i>	21.51
L	00:47:05.254	-24:14:19.331	58712.0106	<i>i</i>	17.68
L	00:47:05.254	-24:14:19.331	58712.0207	<i>i</i>	18.26
L	00:47:28.192	-23:01:22.836	58710.6151	<i>i</i>	18.05
L	00:47:28.192	-23:01:22.836	58710.6162	<i>i</i>	18.05
L	00:47:28.192	-23:01:22.836	58711.1086	<i>i</i>	19.76
L	00:47:28.192	-23:01:22.836	58712.0289	<i>i</i>	19.21
L	00:47:28.192	-23:01:22.836	58712.0445	<i>i</i>	19.25
L	00:47:28.192	-23:01:22.836	58713.1823	<i>i</i>	19.15
L	00:47:28.192	-23:01:22.836	58713.2120	<i>i</i>	19.41
L	00:53:57.737	-24:32:35.311	58710.7859	<i>i</i>	18.25
L	00:53:57.737	-24:32:35.311	58711.2814	<i>i</i>	19.26
L	00:53:57.737	-24:32:35.311	58711.2917	<i>i</i>	19.43
L	00:53:57.737	-24:32:35.311	58712.7152	<i>i</i>	19.59
L	00:53:57.737	-24:32:35.311	58713.9273	<i>i</i>	20.89
L	00:53:57.737	-24:32:35.311	58713.9427	<i>i</i>	20.73
M	00:51:29.000	-22:28:16.960	58710.5526	J	–
M	00:50:32.560	-22:13:33.700	58710.5486	J	–
M	01:34:29.640	-32:48:22.460	58710.5652	J	–
M	00:48:21.860	-25:07:36.520	58710.5543	J	–
M	00:51:18.760	-26:10:05.010	58710.5635	J	–
M	00:51:29.860	-24:38:32.970	58710.5589	J	–
M	00:53:57.740	-24:32:35.300	58710.5573	J	–
M	00:47:05.250	-24:14:19.320	58710.5558	J	–
M	00:50:56.150	-23:38:53.380	58710.5620	J	–
M	00:52:41.580	-25:44:01.860	58710.5604	J	–
T	01:27:22.392	-32:00:23.760	58714.4818	<i>r</i>	19.02
T	01:27:22.392	-32:00:23.760	58714.4818	<i>r</i>	19.03
T	01:30:38.448	-32:00:28.440	58715.4820	<i>r</i>	19.26
T	01:32:16.440	-32:00:26.280	58715.4846	<i>r</i>	19.29
T	01:33:54.192	-32:00:23.400	58714.4870	<i>r</i>	19.05
T	01:33:54.192	-32:00:23.400	58714.4870	<i>r</i>	19.05
T	01:33:54.408	-32:00:25.920	58715.4872	<i>r</i>	19.32
T	01:35:32.184	-32:00:24.480	58714.4895	<i>r</i>	19.08
T	01:35:32.184	-32:00:24.480	58714.4895	<i>r</i>	19.08
T	01:35:32.424	-32:00:26.280	58715.4897	<i>r</i>	19.30
T	01:28:42.480	-31:39:40.320	58715.4794	<i>r</i>	19.38
T	01:28:42.432	-31:39:24.480	58717.4750	<i>r</i>	19.19

Table 4 continued

Table 4 (continued)

Source ^a	α (J2000)	δ (J2000)	Date (MJD)	Filter	Magnitude Limit ^b (3σ)
T	01:30:19.848	-31:39:38.160	58714.4844	r	19.10
T	01:30:19.848	-31:39:38.160	58714.4844	r	19.08
T	01:30:20.160	-31:39:38.160	58715.5000	r	19.26
T	01:31:57.504	-31:39:36.000	58714.4947	r	19.19
T	01:31:57.504	-31:39:36.000	58714.4947	r	19.17
T	01:31:57.744	-31:39:38.880	58715.4949	r	19.35
T	01:33:35.136	-31:39:36.000	58714.4921	r	19.08
T	01:33:35.136	-31:39:36.000	58714.4921	r	19.08
T	01:33:35.448	-31:39:38.520	58715.4923	r	19.36
T	01:30:01.728	-31:18:47.160	58714.4998	r	19.12
T	01:30:01.728	-31:18:47.160	58714.4998	r	19.11
T	01:30:01.920	-31:18:48.960	58715.5026	r	19.36
T	01:31:38.904	-31:18:49.320	58714.4973	r	18.66
T	01:31:38.904	-31:18:49.320	58714.4973	r	18.66
T	01:31:39.144	-31:18:52.920	58715.4975	r	19.35
T	01:31:40.944	-31:19:09.480	58720.4931	r	19.47
T	01:31:41.160	-31:19:01.920	58722.4877	r	19.45
T	01:31:41.112	-31:19:05.880	58724.4848	r	19.43
T	01:31:41.040	-31:19:01.920	58725.4802	r	19.43
T	01:31:41.136	-31:19:06.960	58726.4766	r	19.63
T	01:31:41.280	-31:18:57.600	58727.4754	r	19.60
T	00:52:12.600	-27:09:52.920	58719.4684	r	19.46
T	00:52:12.672	-27:09:55.440	58720.4655	r	19.69
T	00:52:12.816	-27:09:48.600	58721.4664	r	15.25
T	00:52:12.864	-27:09:48.240	58722.4601	r	19.71
T	00:52:12.744	-27:09:54.000	58723.4614	r	19.93
T	00:52:12.864	-27:09:50.760	58724.4577	r	19.64
T	00:52:12.912	-27:09:47.880	58725.4554	r	19.56
T	00:52:12.960	-27:09:52.560	58726.4492	r	19.72
T	00:52:13.080	-27:09:45.000	58727.4464	r	19.70
T	00:53:34.080	-26:48:53.640	58715.4561	r	19.30
T	00:55:08.712	-26:49:08.040	58719.4555	r	19.56
T	00:55:08.784	-26:49:10.560	58720.4526	r	19.60
T	00:55:08.904	-26:49:02.640	58721.4535	r	16.13
T	00:55:08.928	-26:49:03.360	58722.4472	r	19.64
T	00:55:08.784	-26:49:09.480	58723.4383	r	19.91
T	00:55:08.952	-26:49:05.880	58724.4448	r	19.76
T	00:55:08.976	-26:49:03.000	58725.4426	r	19.61
T	00:55:09.048	-26:49:07.320	58726.4363	r	19.84
T	00:55:09.144	-26:48:59.760	58727.4336	r	19.63
T	00:59:46.248	-26:48:50.760	58714.4714	r	19.20
T	00:59:46.392	-26:48:52.560	58715.4639	r	19.32
T	00:59:46.248	-26:48:50.760	58714.4714	r	19.21
T	00:59:46.464	-26:48:37.080	58717.4617	r	19.26
T	00:59:34.728	-26:28:04.080	58714.4740	r	19.19
T	00:59:34.872	-26:28:05.880	58715.4665	r	19.38
T	00:59:34.728	-26:28:04.080	58714.4740	r	19.20
T	00:59:34.920	-26:27:50.400	58717.4643	r	19.31
T	00:50:13.056	-26:07:37.200	58719.4426	r	19.48
T	00:50:13.128	-26:07:40.440	58720.4397	r	19.75
T	00:50:13.272	-26:07:32.880	58721.4406	r	19.08
T	00:50:13.272	-26:07:33.240	58722.4343	r	19.76
T	00:50:13.104	-26:07:36.840	58723.4357	r	20.00

Table 4 continued

Table 4 (continued)

Source ^a	α (J2000)	δ (J2000)	Date (MJD)	Filter	Magnitude Limit ^b (3σ)
T	00:50:13.224	-26:07:35.400	58724.4319	r	19.72
T	00:50:13.248	-26:07:32.520	58725.4297	r	19.57
T	00:50:13.416	-26:07:36.840	58726.4234	r	19.81
T	00:50:13.440	-26:07:30.360	58727.4207	r	19.61
T	00:50:13.560	-26:07:36.840	58728.4213	r	18.30
T	00:51:44.256	-26:07:19.200	58711.4909	r	19.09
T	00:51:44.424	-26:07:15.240	58716.4848	r	19.13
T	00:53:16.752	-26:07:19.560	58711.4754	r	18.95
T	00:53:16.872	-26:07:13.440	58716.4693	r	19.18
T	00:54:51.000	-26:07:35.040	58719.4581	r	19.01
T	00:54:51.072	-26:07:37.920	58720.4552	r	19.71
T	00:54:51.216	-26:07:30.720	58722.4498	r	19.72
T	00:54:51.096	-26:07:35.760	58723.4486	r	19.93
T	00:54:51.216	-26:07:33.240	58724.4474	r	19.71
T	00:54:51.240	-26:07:30.360	58725.4451	r	19.64
T	00:54:51.336	-26:07:34.320	58726.4389	r	19.88
T	00:54:51.432	-26:07:27.480	58727.4361	r	19.65
T	00:59:27.072	-26:07:18.120	58714.4766	r	19.07
T	00:59:27.240	-26:07:20.280	58715.4690	r	19.42
T	00:59:27.072	-26:07:18.120	58714.4766	r	19.07
T	00:51:34.440	-25:46:32.160	58711.4934	r	19.14
T	00:51:34.632	-25:46:29.280	58716.4874	r	19.20
T	00:53:06.576	-25:46:31.440	58711.4781	r	18.87
T	00:53:06.672	-25:46:27.120	58716.4719	r	19.29
T	00:54:40.464	-25:46:48.360	58719.4606	r	19.53
T	00:54:40.512	-25:46:51.960	58720.4577	r	19.69
T	00:54:40.704	-25:46:46.200	58721.4431	r	17.69
T	00:54:40.704	-25:46:44.400	58722.4524	r	19.71
T	00:54:40.584	-25:46:49.440	58723.4511	r	19.92
T	00:54:40.728	-25:46:46.920	58724.4500	r	19.73
T	00:54:40.680	-25:46:46.920	58725.4323	r	19.36
T	00:54:40.824	-25:46:48.360	58726.4414	r	19.88
T	00:54:40.920	-25:46:41.160	58727.4387	r	19.77
T	00:59:15.696	-25:46:31.080	58714.4792	r	19.09
T	00:59:15.888	-25:46:33.600	58715.4716	r	19.43
T	00:59:15.696	-25:46:31.080	58714.4792	r	19.08
T	01:03:25.176	-25:49:57.000	58717.4575	r	19.24
T	01:03:26.832	-25:50:29.040	58719.4529	r	19.53
T	01:03:26.904	-25:50:30.480	58720.4500	r	19.72
T	01:03:27.096	-25:50:22.200	58721.4509	r	15.45
T	01:03:27.024	-25:50:23.280	58722.4447	r	19.62
T	01:03:26.928	-25:50:27.960	58723.4460	r	19.95
T	01:03:27.024	-25:50:26.160	58724.4422	r	19.77
T	01:03:26.928	-25:50:24.000	58725.4400	r	19.63
T	01:03:27.192	-25:50:26.880	58726.4337	r	19.84
T	01:03:27.144	-25:50:19.680	58727.4310	r	19.63
T	00:43:46.128	-25:26:01.320	58725.4220	r	19.59
T	00:46:48.288	-25:25:48.360	58711.4627	r	19.04
T	00:46:48.216	-25:25:44.040	58716.4487	r	19.23
T	00:46:49.968	-25:26:00.960	58719.4761	r	19.47
T	00:46:49.944	-25:26:03.840	58720.4733	r	19.69
T	00:46:50.016	-25:26:01.680	58721.4354	r	16.23
T	00:46:50.184	-25:25:57.360	58722.4679	r	19.64

Table 4 continued

Table 4 (*continued*)

Source ^a	α (J2000)	δ (J2000)	Date (MJD)	Filter	Magnitude Limit ^b (3σ)
T	00:46:50.016	-25:26:02.760	58723.4640	<i>r</i>	19.90
T	00:46:50.160	-25:25:59.520	58724.4654	<i>r</i>	19.67
T	00:46:50.088	-25:26:01.680	58725.4245	<i>r</i>	19.53
T	00:46:50.256	-25:26:01.320	58726.4569	<i>r</i>	19.74
T	00:46:50.424	-25:25:53.400	58727.4542	<i>r</i>	19.70
T	00:46:50.400	-25:26:06.000	58728.4162	<i>r</i>	18.77
T	00:49:52.416	-25:25:49.080	58715.4535	<i>r</i>	19.37
T	00:51:24.672	-25:25:46.920	58711.4960	<i>r</i>	19.15
T	00:51:24.960	-25:25:44.040	58716.5003	<i>r</i>	19.11
T	00:52:56.496	-25:25:46.200	58711.4806	<i>r</i>	19.04
T	00:52:56.640	-25:25:41.880	58716.4745	<i>r</i>	19.29
T	00:54:28.440	-25:25:47.640	58711.4678	<i>r</i>	19.08
T	00:54:28.392	-25:25:42.600	58716.4564	<i>r</i>	19.30
T	00:59:04.800	-25:25:46.200	58714.5025	<i>r</i>	19.06
T	00:59:04.560	-25:25:47.280	58715.4742	<i>r</i>	19.41
T	00:59:04.800	-25:25:46.200	58714.5025	<i>r</i>	19.07
T	00:59:05.952	-25:26:00.240	58723.5055	<i>r</i>	20.03
T	00:59:06.312	-25:25:54.120	58724.5180	<i>r</i>	19.56
T	00:59:06.168	-25:25:57.360	58726.4983	<i>r</i>	19.59
T	00:43:37.752	-25:05:16.440	58721.4328	<i>r</i>	14.09
T	00:49:42.840	-25:04:48.360	58717.4482	<i>r</i>	19.35
T	00:51:15.024	-25:05:03.480	58711.5088	<i>r</i>	18.89
T	00:52:46.416	-25:04:59.520	58711.4832	<i>r</i>	19.04
T	00:52:46.560	-25:04:55.200	58716.4771	<i>r</i>	19.29
T	00:58:53.232	-25:05:02.040	58715.4613	<i>r</i>	19.36
T	00:58:54.768	-25:05:11.400	58719.5131	<i>r</i>	19.42
T	00:58:54.720	-25:05:13.560	58720.5123	<i>r</i>	19.54
T	00:58:54.696	-25:05:14.280	58723.5030	<i>r</i>	19.97
T	00:58:54.936	-25:05:10.680	58724.5017	<i>r</i>	19.57
T	00:58:54.912	-25:05:06.000	58725.4993	<i>r</i>	19.66
T	00:58:54.912	-25:05:11.040	58726.4958	<i>r</i>	19.69
T	00:41:58.872	-24:44:02.400	58717.4427	<i>r</i>	19.42
T	00:42:00.504	-24:44:33.360	58719.4374	<i>r</i>	19.47
T	00:42:00.576	-24:44:36.600	58720.4345	<i>r</i>	19.69
T	00:42:00.672	-24:44:29.760	58722.4292	<i>r</i>	19.78
T	00:42:00.840	-24:44:32.640	58726.4182	<i>r</i>	19.83
T	00:43:32.448	-24:44:34.080	58728.4136	<i>r</i>	18.96
T	00:48:06.600	-24:44:28.320	58719.4710	<i>r</i>	19.55
T	00:48:06.648	-24:44:31.200	58720.4681	<i>r</i>	19.82
T	00:48:06.816	-24:44:23.640	58721.4689	<i>r</i>	15.65
T	00:48:06.840	-24:44:24.720	58722.4627	<i>r</i>	19.63
T	00:48:06.552	-24:44:33.000	58723.4305	<i>r</i>	19.97
T	00:48:06.864	-24:44:27.240	58724.4603	<i>r</i>	19.74
T	00:48:06.888	-24:44:24.360	58725.4580	<i>r</i>	19.57
T	00:48:06.936	-24:44:27.960	58726.4517	<i>r</i>	19.81
T	00:48:07.032	-24:44:21.120	58727.4490	<i>r</i>	19.79
T	00:51:08.376	-24:44:13.920	58711.4986	<i>r</i>	19.09
T	00:51:08.616	-24:44:11.040	58716.4951	<i>r</i>	19.13
T	00:52:39.720	-24:44:14.640	58711.4858	<i>r</i>	19.02
T	00:52:39.864	-24:44:10.320	58716.4797	<i>r</i>	19.26
T	00:54:10.944	-24:44:11.040	58710.4723	<i>r</i>	18.86
T	00:54:11.088	-24:44:11.040	58716.4539	<i>r</i>	19.25
T	00:57:14.208	-24:44:16.800	58715.4587	<i>r</i>	19.37

Table 4 (*continued*)

Table 4 (continued)

Source ^a	α (J2000)	δ (J2000)	Date (MJD)	Filter	Magnitude Limit ^b (3σ)
T	00:57:15.744	-24:44:31.200	58719.4477	r	19.46
T	00:57:15.792	-24:44:34.440	58720.4474	r	19.77
T	00:57:15.984	-24:44:26.160	58721.4457	r	17.45
T	00:57:15.936	-24:44:27.240	58722.4395	r	19.79
T	00:57:15.840	-24:44:31.560	58723.4408	r	20.03
T	00:57:16.008	-24:44:29.400	58724.4370	r	19.79
T	00:57:15.984	-24:44:26.880	58725.4348	r	19.69
T	00:57:16.104	-24:44:30.120	58726.4311	r	19.93
T	00:57:16.104	-24:44:24.000	58727.4259	r	19.80
T	00:57:16.248	-24:44:30.840	58728.4265	r	14.24
T	00:58:46.056	-24:44:14.280	58714.5051	r	19.08
T	00:58:45.840	-24:44:14.640	58715.4768	r	19.42
T	00:58:46.056	-24:44:14.280	58714.5051	r	19.07
T	00:58:47.256	-24:44:27.960	58720.5080	r	19.63
T	00:58:47.448	-24:44:21.480	58722.5044	r	19.67
T	00:58:47.256	-24:44:28.680	58723.4987	r	19.99
T	00:58:47.400	-24:44:25.080	58724.4991	r	19.73
T	00:58:47.424	-24:44:20.400	58725.4967	r	19.65
T	00:58:47.424	-24:44:26.160	58726.4914	r	19.93
T	00:58:47.856	-24:44:20.040	58727.4781	r	19.82
T	00:46:24.480	-24:23:25.440	58710.4647	r	18.85
T	00:46:25.296	-24:23:25.800	58716.5054	r	19.15
T	00:46:26.232	-24:23:46.680	58719.4400	r	19.47
T	00:46:26.304	-24:23:49.920	58720.4371	r	19.73
T	00:46:26.472	-24:23:41.640	58721.4380	r	18.50
T	00:46:26.424	-24:23:43.080	58722.4318	r	19.76
T	00:46:26.352	-24:23:44.880	58724.4267	r	19.75
T	00:46:26.472	-24:23:41.640	58725.4271	r	19.52
T	00:46:26.592	-24:23:45.960	58726.4208	r	19.89
T	00:46:26.592	-24:23:39.840	58727.4182	r	19.70
T	00:46:26.712	-24:23:46.320	58728.4187	r	18.73
T	00:50:58.416	-24:23:29.760	58711.4652	r	19.09
T	00:50:58.920	-24:23:25.800	58716.4977	r	19.11
T	00:54:00.960	-24:23:28.680	58711.4703	r	19.21
T	00:54:00.936	-24:23:24.000	58716.4590	r	19.27
T	00:58:35.088	-24:23:30.840	58715.5053	r	19.43
T	00:58:36.192	-24:23:39.840	58719.5062	r	19.63
T	00:58:36.120	-24:23:42.000	58720.5054	r	19.65
T	00:58:36.288	-24:23:36.240	58722.5018	r	19.71
T	00:58:36.120	-24:23:43.080	58723.4961	r	19.97
T	00:58:36.288	-24:23:40.560	58724.4948	r	19.75
T	00:58:36.264	-24:23:35.520	58725.4923	r	19.71
T	00:58:36.312	-24:23:40.200	58726.4889	r	19.88
T	00:40:14.640	-24:02:45.240	58715.4458	r	19.37
T	00:40:14.448	-24:02:38.760	58716.4435	r	19.31
T	00:40:14.568	-24:02:30.840	58717.4401	r	19.39
T	00:40:16.176	-24:03:01.440	58719.4349	r	19.52
T	00:40:16.224	-24:03:04.320	58720.4320	r	19.72
T	00:40:16.344	-24:02:58.200	58722.4267	r	19.84
T	00:40:16.224	-24:02:58.920	58724.4216	r	19.80
T	00:40:16.488	-24:03:00.720	58726.4157	r	19.76
T	00:40:16.512	-24:02:53.880	58727.4131	r	19.60
T	00:44:49.344	-24:02:54.240	58719.4787	r	19.49

Table 4 continued

Table 4 (continued)

Source ^a	α (J2000)	δ (J2000)	Date (MJD)	Filter	Magnitude Limit ^b (3σ)
T	00:44:49.344	-24:02:57.480	58720.4758	r	19.75
T	00:44:49.584	-24:02:50.280	58721.4741	r	17.45
T	00:44:49.584	-24:02:50.640	58722.4705	r	19.74
T	00:44:49.392	-24:02:56.400	58723.4691	r	19.99
T	00:44:49.464	-24:02:57.480	58724.4293	r	19.75
T	00:44:49.608	-24:02:51.000	58725.4657	r	19.63
T	00:44:49.632	-24:02:54.960	58726.4595	r	19.77
T	00:44:49.824	-24:02:47.400	58727.4568	r	19.70
T	00:50:52.224	-24:02:42.720	58711.5012	r	18.99
T	00:50:52.464	-24:02:39.480	58716.4900	r	19.17
T	00:56:56.592	-24:02:45.960	58715.5130	r	19.26
T	00:56:57.720	-24:02:59.280	58719.4503	r	19.60
T	00:56:57.840	-24:03:02.160	58720.4448	r	19.79
T	00:56:57.936	-24:02:53.880	58721.4483	r	17.98
T	00:56:57.936	-24:02:54.600	58722.4421	r	19.79
T	00:56:57.864	-24:02:58.560	58723.4434	r	20.01
T	00:56:57.960	-24:02:56.760	58724.4396	r	19.83
T	00:56:57.984	-24:02:54.240	58725.4374	r	19.64
T	00:56:58.128	-24:02:58.560	58726.4285	r	19.86
T	00:56:58.272	-24:02:58.200	58728.4291	r	13.95
T	00:58:26.928	-24:02:41.280	58714.4688	r	19.24
T	00:58:26.928	-24:02:41.280	58714.4688	r	19.24
T	00:58:27.648	-24:02:45.240	58715.5079	r	19.39
T	00:58:28.776	-24:02:54.240	58719.5036	r	19.64
T	00:58:28.728	-24:02:56.400	58720.5028	r	19.60
T	00:58:28.944	-24:02:49.920	58722.4974	r	19.75
T	00:58:28.728	-24:02:57.840	58723.4919	r	20.01
T	00:58:28.944	-24:02:53.880	58724.4922	r	19.75
T	00:58:28.896	-24:02:49.560	58725.4898	r	19.66
T	00:58:28.896	-24:02:54.600	58726.4863	r	19.84
T	00:41:37.848	-23:41:57.480	58711.4575	r	19.15
T	00:41:37.704	-23:41:52.800	58716.4461	r	19.29
T	00:44:40.896	-23:42:09.360	58719.4813	r	19.53
T	00:44:40.896	-23:42:12.240	58720.4784	r	19.76
T	00:44:41.136	-23:42:05.760	58721.4767	r	16.20
T	00:44:41.184	-23:42:04.320	58722.4731	r	19.85
T	00:44:40.968	-23:42:11.160	58723.4717	r	20.05
T	00:44:41.160	-23:42:08.280	58724.4680	r	19.83
T	00:44:41.184	-23:42:05.400	58725.4631	r	19.64
T	00:44:41.256	-23:42:09.000	58726.4621	r	19.85
T	00:44:41.256	-23:42:07.920	58727.4156	r	19.47
T	00:46:10.128	-23:41:57.840	58715.4510	r	19.37
T	00:49:11.400	-23:41:53.160	58710.4672	r	18.92
T	00:49:12.168	-23:41:53.880	58716.5029	r	19.18
T	00:50:42.744	-23:41:58.200	58711.5063	r	18.88
T	00:50:42.912	-23:41:54.600	58716.4925	r	19.18
T	00:53:44.160	-23:41:53.520	58710.5042	r	18.95
T	00:53:43.968	-23:41:51.000	58716.4616	r	19.06
T	00:53:45.384	-23:42:10.080	58719.4632	r	19.58
T	00:53:45.456	-23:42:13.320	58720.4603	r	19.81
T	00:53:45.744	-23:42:05.400	58721.4586	r	15.33
T	00:53:45.648	-23:42:06.120	58722.4550	r	19.77
T	00:53:45.504	-23:42:11.160	58723.4537	r	19.96

Table 4 continued

Table 4 (*continued*)

Source ^a	α (J2000)	δ (J2000)	Date (MJD)	Filter	Magnitude Limit ^b (3σ)
T	00:53:45.528	-23:42:11.520	58724.4344	r	19.75
T	00:53:45.648	-23:42:06.480	58725.4477	r	19.76
T	00:53:45.768	-23:42:10.080	58726.4440	r	19.92
T	00:53:45.840	-23:42:03.600	58727.4413	r	19.74
T	00:53:45.840	-23:42:12.600	58728.4239	r	15.91
T	00:56:45.648	-23:41:40.560	58717.4722	r	19.43
T	00:56:47.088	-23:41:58.920	58725.5183	r	19.47
T	00:41:34.248	-23:21:25.920	58721.4303	r	17.72
T	00:41:34.056	-23:21:27.720	58723.4254	r	19.96
T	00:41:34.392	-23:21:25.920	58725.4194	r	19.63
T	00:41:34.656	-23:21:29.520	58728.4111	r	18.54
T	00:44:33.744	-23:21:10.800	58711.4601	r	19.21
T	00:44:34.224	-23:21:07.560	58716.5080	r	19.14
T	00:50:36.312	-23:21:11.520	58711.5037	r	18.81
T	00:50:35.952	-23:21:06.120	58716.4513	r	19.28
T	00:52:06.816	-23:21:06.120	58710.5093	r	18.86
T	00:52:06.720	-23:21:10.080	58711.4883	r	19.12
T	00:52:06.912	-23:21:06.480	58716.4822	r	19.31
T	00:52:08.064	-23:21:23.760	58719.4658	r	19.61
T	00:52:08.136	-23:21:27.360	58720.4629	r	19.81
T	00:52:08.256	-23:21:19.440	58721.4638	r	17.75
T	00:52:08.328	-23:21:19.800	58722.4576	r	19.76
T	00:52:08.136	-23:21:25.560	58723.4589	r	20.07
T	00:52:08.280	-23:21:23.040	58724.4551	r	19.90
T	00:52:08.352	-23:21:20.160	58725.4529	r	19.74
T	00:52:08.400	-23:21:24.120	58726.4466	r	19.92
T	00:52:08.520	-23:21:17.280	58727.4439	r	19.77
T	00:52:08.016	-23:21:15.120	58728.5104	r	17.79
T	00:53:38.664	-23:21:27.000	58719.4451	r	19.46
T	00:53:38.736	-23:21:30.600	58720.4422	r	19.76
T	00:53:38.880	-23:21:19.440	58721.4612	r	14.98
T	00:53:38.856	-23:21:24.120	58722.4369	r	19.81
T	00:53:38.760	-23:21:25.920	58723.4563	r	19.99
T	00:53:38.880	-23:21:23.400	58724.4525	r	19.85
T	00:53:38.952	-23:21:20.520	58725.4503	r	19.71
T	00:53:39.000	-23:21:27.360	58726.4259	r	19.89
T	00:53:39.024	-23:21:20.520	58727.4233	r	19.78
T	00:53:38.544	-23:21:16.920	58728.5078	r	18.07
T	00:56:38.760	-23:21:12.960	58715.5104	r	19.34
T	00:56:39.936	-23:21:14.040	58725.5155	r	19.61
T	00:42:56.712	-23:00:39.600	58724.4242	r	19.81
T	00:44:26.880	-23:00:41.760	58723.4280	r	20.00
T	00:47:27.552	-23:00:37.080	58719.4735	r	19.60
T	00:47:27.600	-23:00:39.960	58720.4707	r	19.81
T	00:47:27.792	-23:00:32.400	58721.4715	r	17.50
T	00:47:27.792	-23:00:32.760	58722.4653	r	19.71
T	00:47:27.528	-23:00:40.680	58723.4331	r	20.02
T	00:47:27.792	-23:00:36.000	58724.4628	r	19.84
T	00:47:27.888	-23:00:37.080	58726.4543	r	19.83
T	00:47:28.008	-23:00:29.880	58727.4516	r	19.79
T	00:53:26.904	-23:00:19.800	58710.4698	r	18.92
T	00:53:27.168	-23:00:18.720	58716.4642	r	19.17
T	00:42:49.704	-22:39:39.960	58715.4484	r	19.38

Table 4 *continued*

Table 4 (continued)

Source ^a	α (J2000)	δ (J2000)	Date (MJD)	Filter	Magnitude Limit ^b (3σ)
T	00:53:20.712	-22:39:33.840	58710.5068	<i>r</i>	18.84
T	00:53:20.448	-22:39:36.720	58711.4729	<i>r</i>	19.14
T	00:53:20.616	-22:39:32.400	58716.4668	<i>r</i>	19.22
T	00:39:41.832	-22:18:48.600	58710.4595	<i>r</i>	19.05
T	00:48:41.064	-22:18:37.080	58717.4549	<i>r</i>	19.39
T	00:42:30.936	-21:37:15.960	58710.4621	<i>r</i>	18.98
T	00:36:17.376	-20:34:58.440	58710.4570	<i>r</i>	18.96

^a Surveys correspond to KAIT (K), Keck/MOSFIRE (M), Las Cumbres Observatory (L), Nickel (N), Swope (S), and Thacher (T) imaging as described in Section 2.

^b In-band 3σ limit for the reported image as described in Section 2 and Section 4. The “Clear” filter is abbreviated as “C” for all KAIT observations. All magnitudes are on the AB system (Oke & Gunn 1983).

Table 5. Candidate Electromagnetic Counterparts to GW190814

Name	α (J2000)	δ (J2000)	Cumulative LVC Prob. ^a	Discovery Date (MJD)	Redshift ^b	Absolute Magnitude ^c (AB mag)	Note ^d
2019nmd	00:51:29.004	-22:28:16.96	0.9626	58710.27800	–	–	(MP) 2010 GA33
2019nme	00:50:32.558	-22:13:33.70	0.9723	58710.27800	–	–	(MP) 2005 OL33
2019noq	00:48:47.882	-25:18:23.46	0.3030	58710.58500	0.05907±0.00033 (s)	$i=-17.28\pm0.25$ (0.7 d)	(SN) II
2019nor	00:49:51.992	-24:16:17.71	0.1808	58710.58500	0.43652±0.00015 (s)	$r=-22.33\pm0.23$ (0.7 d)	(Z)
2019npd	00:46:56.705	-25:22:36.66	0.5377	58710.28000	0.00081±0.00001 (s)	$i=-8.68\pm0.30$ (0.4 d)	(Z; Sculptor Galaxy)
2019npe	00:41:33.330	-23:44:31.94	0.8787	58710.27600	0.17233±0.02355 (PS1)	$z=-19.55\pm0.30$ (0.4 d)	(Z)
2019npf	00:44:25.379	-23:11:52.08	0.7192	58710.27600	0.17953±0.02702 (PS1)	$z=-20.28\pm0.30$ (0.4 d)	(Z)
2019nph	00:58:07.613	-27:12:20.27	0.9362	58710.30899	0.23849±0.06683 (PS1)	$r=-20.88\pm0.30$ (0.4 d)	(Z)
2019nph	00:45:15.389	-20:58:23.75	0.9855	58710.30600	–	–	(MP) 2015 XV140
2019npl	00:42:07.934	-21:57:09.23	0.9515	58710.30500	–	–	(MP) 2014 VF30
2019npp	01:21:32.078	-32:14:23.62	0.9579	58711.28600	0.16168±0.10660 (LDR8)	$z=-19.14\pm0.30$ (1.4 d)	(PHOT; bright)
2019npv	00:53:32.309	-23:49:58.64	0.7397	58711.32300	0.05600±0.00010 (s)	$i=-17.37\pm0.23$ (0.6 d)	(SN) Ibc
2019npw	00:55:52.399	-25:46:59.81	0.5610	58711.31899	0.14936±0.00013 (s)	$z=-18.47\pm0.23$ (0.6 d)	(SN) II
2019npy	00:56:12.025	-25:29:24.50	0.6620	58711.24199	0.46141±0.17703 (LDR8)	$z=-21.70\pm0.30$ (1.4 d)	(Z)
2019npz	00:53:05.560	-24:21:38.71	0.5276	58711.24800	0.21228±0.03472 (LDR8)	$z=-22.97\pm0.43$ (0.6 d)	(Z)
2019nqa	00:52:39.170	-25:00:14.97	0.1744	58711.24399	0.19930±0.00030 (s)	$z=-22.82\pm0.43$ (0.6 d)	(Z)
2019nqb	01:39:29.813	-32:12:48.62	0.9894	58711.30100	0.16431±0.02454 (LDR8)	$z=-18.49\pm0.30$ (1.4 d)	(Z)
2019nqc	01:29:03.673	-32:42:18.50	0.7825	58711.34999	0.07800±0.00010 (s)	$i=-17.22\pm0.24$ (0.6 d)	(SN) II
2019nqg	00:56:35.642	-24:01:23.15	0.9268	58711.24699	0.17096±0.00018 (s)	$z=-19.55\pm0.30$ (1.4 d)	(Z)
2019nqh	00:47:13.220	-24:24:38.32	0.3500	58711.23100	–	–	(MP) 2008 SD335
2019nqp	00:56:50.424	-24:20:50.03	0.8987	58710.58699	0.40278±0.11514 (LDR8)	$z=-21.13\pm0.28$ (0.7 d)	(Z)
2019nqq	01:23:49.217	-33:02:05.00	0.9693	58710.29800	0.07108±0.00008 (s)	$i=-16.89\pm0.22$ (0.4 d)	(SN) II
2019nqr	01:34:17.649	-32:44:30.41	0.8920	58711.27199	0.08319±0.00007 (s)	$z=-19.65\pm0.22$ (1.4 d)	(SN) II
2019nqs	01:33:35.164	-31:46:48.48	0.8857	58711.29699	0.12630±0.00100 (s)	$z=-19.26\pm0.22$ (1.4 d)	(Z)
2019nqt	00:57:15.826	-25:07:46.16	0.8278	58711.24399	0.38773±0.11565 (LDR8)	$z=-21.62\pm0.30$ (1.4 d)	(Z)
2019nqv	00:46:50.738	-22:40:03.32	0.8328	58711.31199	0.46462±0.03153 (LDR8)	$z=-21.28\pm0.30$ (1.4 d)	(Z)
2019nqw	00:56:46.712	-25:09:33.27	0.7343	58711.34600	0.45393±0.20120 (PS1)	$z=-22.06\pm0.30$ (1.5 d)	(Z)
2019nqx	00:47:29.061	-26:56:58.36	0.9653	58711.31500	0.26467±0.02604 (PS1)	$r=-19.77\pm0.30$ (1.4 d)	(Z)
2019nqy	00:56:23.197	-24:41:11.29	0.7849	58711.32000	0.16852±0.08018 (PS1)	$z=-18.83\pm0.30$ (1.4 d)	(Z)
2019nqz	00:46:46.416	-24:20:12.06	0.4014	58711.30699	0.12769±0.05122 (PS1)	$z=-21.71\pm0.43$ (0.6 d)	(Z)
2019nra	00:55:10.705	-25:56:57.12	0.5861	58711.25100	0.26867±0.02940 (PS1)	$r=-20.30\pm0.30$ (1.4 d)	(Z)
2019nrb	00:58:09.874	-26:13:18.06	0.8292	58711.32899	0.20750±0.02660 (PS1)	$z=-20.82\pm0.24$ (1.4 d)	(Z)
2019nrc	01:29:33.236	-32:26:23.70	0.7715	58711.35100	0.41923±0.22188 (LDR8)	$z=-21.13\pm0.30$ (1.5 d)	(Z)

Table 5 continued

Table 5 (continued)

Name	α (J2000)	δ (J2000)	Cumulative LVC Prob. ^a	Discovery Date (MJD)	Redshift ^b	Absolute Magnitude ^c (AB mag)	Note ^d
2019nrd	00:46:07.284	-26:25:25.99	0.9053	58711.31500	0.24716±0.00033 (s)	$r=-20.35\pm0.30$ (1.4 d)	(Z)
2019nre	01:27:47.085	-31:45:18.56	0.7676	58711.28600	–	$r=-17.01\pm0.30$ (1.4 d)	$\Delta_z=-1.54\pm0.15$ mag)
2019nrf	00:53:06.283	-25:22:59.52	0.1930	58711.31899	0.26791±0.15589 (PS1)	$z=-20.42\pm0.30$ (1.4 d)	(Z)
2019nrg	01:28:22.218	-31:12:30.38	0.8713	58711.29300	0.42341±0.00000 (PS1)	$z=-22.00\pm0.30$ (1.4 d)	(Z)
2019nrh	01:32:58.426	-31:17:06.17	0.9325	58711.29500	0.39881±0.13875 (LDR8)	$z=-21.08\pm0.30$ (1.4 d)	(Z)
2019nri	00:46:41.737	-24:26:08.84	0.3895	58712.27899	–	–	(MP) 2008 SD335
2019nro	01:30:44.285	-32:36:09.19	0.8101	58711.34999	0.24795±0.05842 (LDR8)	$z=-19.66\pm0.30$ (1.5 d)	(Z)
2019nrp	01:37:16.351	-32:09:33.76	0.9522	58711.30100	0.25509±0.02762 (LDR8)	$z=-20.69\pm0.30$ (1.4 d)	(Z)
2019nrq	00:50:57.481	-22:22:20.06	0.9667	58712.23600	–	–	(MP) 2005 OL33
2019nrs	01:40:46.165	-32:36:57.92	0.9836	58711.30100	0.34916±0.02637 (LDR8)	$r=-20.94\pm0.30$ (1.4 d)	(Z)
2019nrt	00:54:19.821	-23:05:03.93	0.9536	58712.23600	–	–	(MP) 2014 UL252
2019nru	01:31:16.167	-34:02:32.37	0.9744	58711.35600	0.18847±0.01724 (LDR8)	$z=-19.28\pm0.30$ (1.5 d)	(Z)
2019nrv	01:30:50.152	-31:40:24.50	0.8384	58712.24500	0.11850±0.01784 (LDR8)	$r=-19.78\pm0.30$ (2.4 d)	(Z)
2019nrw	00:47:55.814	-21:49:52.87	0.9786	58712.31000	0.36754±0.13300 (LDR8)	$z=-20.77\pm0.30$ (2.4 d)	(Z)
2019nrx	00:57:08.123	-26:15:44.11	0.7619	58711.32899	0.38697±0.21990 (PS1)	$z=-20.88\pm0.30$ (1.4 d)	(Z)
2019nsc	00:44:37.598	-23:35:16.51	0.6856	58711.31000	0.31059±0.16121 (LDR8)	$z=-21.27\pm0.30$ (1.4 d)	(Z)
2019nsd	00:49:15.718	-21:57:42.23	0.9866	58712.31199	–	–	(MP) 2014 WR28
2019nse	00:42:15.009	-25:10:44.50	0.9611	58712.27899	0.45301±0.09298 (PS1)	$z=-22.62\pm0.30$ (2.4 d)	(Z)
2019nsf	00:41:01.541	-22:54:01.92	0.9421	58712.30399	0.45782±0.14586 (PS1)	$i=-21.44\pm0.30$ (2.4 d)	(Z)
2019nsi	01:34:31.208	-33:02:16.94	0.9107	58711.34999	0.30067±0.21282 (LDR8)	$r=-19.37\pm0.30$ (1.5 d)	(Z)
2019nsj	00:53:41.120	-25:26:14.18	0.2826	58711.31899	0.39582±0.14126 (PS1)	$r=-20.62\pm0.30$ (1.4 d)	(Z)
2019nsk	00:41:25.930	-22:02:29.23	0.9460	58712.30800	0.47463±0.14531 (LDR8)	$z=-23.55\pm0.23$ (0.5 d)	(Z)
2019nsl	00:45:40.343	-23:18:07.85	0.6781	58712.20699	–	–	(MP) 2012 AA29
2019nsm	00:43:30.111	-22:43:29.46	0.8421	58712.30600	0.24807±0.03582 (PS1)	$z=-23.48\pm0.23$ (0.5 d)	(Z)
2019nsn	00:41:48.270	-23:42:42.43	0.8797	58712.30399	–	–	(MP) 2019 PX19
2019nsr	00:57:27.726	-26:16:42.85	0.7746	58711.25100	0.05791±0.00024 (s)	$i=-17.48\pm0.10$ (1.4 d)	(PHOT; bright)
2019nte	01:34:13.766	-31:43:18.12	0.9252	58711.29699	0.07061±0.00005 (s)	$r=-18.24\pm0.26$ (0.4 d)	(Z)
2019ntm	00:48:04.438	-23:47:50.91	0.4220	58712.20699	0.26206±0.03879 (LDR8)	$r=-23.30\pm0.43$ (0.6 d)	(Z)
2019ntn	01:34:53.352	-31:22:49.74	0.9642	58711.35100	0.10006±0.00017 (s)	$i=-16.82\pm0.22$ (1.4 d)	(SN) Ia-CSM
2019nto	00:42:03.349	-24:48:20.45	0.9425	58711.23100	0.22218±0.07694 (PS1)	$z=-19.48\pm0.30$ (1.3 d)	(VAR; PS1 DR2)
2019ntp	00:50:12.071	-26:11:52.63	0.6137	58711.31600	0.11415±0.00005 (s)	$r=-17.61\pm0.30$ (1.4 d)	(SN) Ia
2019ntr	01:00:01.879	-26:42:51.65	0.9540	58711.32899	0.21845±0.00010 (s)	$z=-19.06\pm0.27$ (1.4 d)	(SN) II
2019nts	00:48:31.378	-23:06:39.24	0.7119	58712.28499	0.49280±0.15836 (LDR8)	$z=-21.44\pm0.30$ (2.4 d)	(Z)
2019ntt	00:46:32.894	-26:46:00.89	0.9524	58710.29199	0.07410±0.00021 (s)	$i=-17.87\pm0.30$ (0.4 d)	(Z)
2019nui	00:42:23.018	-21:51:48.19	0.9650	58712.31000	–	$z=-19.56\pm0.23$ (0.5 d)	(PHOT; bright)
2019nuj	00:49:01.738	-23:14:04.93	0.6897	58711.31199	0.35959±0.07251 (PS1)	$z=-24.08\pm0.43$ (0.6 d)	(Z)
2019nuk	00:54:57.827	-26:08:04.61	0.6196	58712.22399	0.07570±0.00030 (s)	$r=-18.77\pm0.30$ (2.3 d)	(Z)
2019nul	00:55:16.443	-26:56:34.57	0.8376	58711.32899	0.09848±0.00021 (s)	$r=-18.05\pm0.30$ (1.4 d)	(Z)
2019num	00:55:31.602	-22:58:08.48	0.9832	58713.27899	0.12744±0.00009 (s)	$i=-17.92\pm0.30$ (3.4 d)	(SN) IIb
2019nun	00:56:48.599	-24:54:30.48	0.8269	58713.26199	0.13190±0.00021 (s)	$r=-19.83\pm0.24$ (1.3 d)	(Z)
2019nuo	00:56:03.820	-23:18:14.42	0.9699	58713.26199	0.08881±0.00794 (PS1)	$r=-18.04\pm0.30$ (3.4 d)	(Z)
2019nup	00:55:04.382	-26:46:12.59	0.7800	58713.34899	0.03664±0.00014 (s)	$i=-17.48\pm0.22$ (2.5 d)	(VAR; ASAS-SN)
2019nuq	01:32:36.497	-33:55:01.88	0.9435	58712.32699	0.10620±0.00030 (s)	$r=-18.04\pm0.30$ (2.4 d)	(Z)
2019nur	00:44:51.630	-24:07:40.60	0.6268	58713.24699	0.13935±0.00021 (s)	$z=-20.20\pm0.23$ (1.4 d)	(Z)
2019nus	00:44:34.557	-22:01:44.62	0.9451	58713.27600	–	$z=-18.56\pm0.43$ (0.5 d)	(PHOT; bright)
2019nut	00:41:47.054	-24:18:01.45	0.8743	58713.27100	0.19920±0.13574 (LDR8)	$i=-18.33\pm0.30$ (3.4 d)	(PHOT; bright)
2019nuu	00:43:53.923	-23:39:23.88	0.7233	58711.31199	0.21065±0.00020 (s)	$z=-19.21\pm0.30$ (1.4 d)	(Z)
2019nuw	00:50:26.340	-25:52:57.83	0.3832	58713.54100	0.32323±0.01040 (LDR8)	$z=-19.38\pm0.33$ (3.7 d)	(Z)
2019nux	00:50:21.019	-23:42:46.79	0.5399	58713.54100	0.40005±0.14810 (PS1)	$z=-24.35\pm0.43$ (0.6 d)	(Z)
2019nuy	00:50:50.397	-25:29:29.55	0.1110	58713.54100	0.26399±0.23968 (LDR8)	$z=-19.71\pm0.25$ (3.7 d)	(PHOT; bright)
2019nuz	00:49:52.264	-25:31:25.62	0.2694	58713.54100	–	$z=-15.03\pm0.31$ (3.7 d)	(PHOT; $\Delta_z < -0.07$ mag)
2019nva	00:52:43.395	-23:37:54.01	0.7925	58713.54100	–	$z=-19.69\pm0.43$ (0.6 d)	(PHOT; bright)
2019nvb	00:46:51.168	-25:25:39.31	0.5585	58713.54100	0.00081±0.00001 (s)	$z=-6.08\pm0.31$ (3.7 d)	(Z; Sculptor Galaxy)

Table 5 continued

Table 5 (continued)

Name	α (J2000)	δ (J2000)	Cumulative LVC Prob. ^a	Discovery Date (MJD)	Redshift ^b	Absolute Magnitude ^c (AB mag)	Note ^d
2019nvc	00:52:18.326	-26:19:42.07	0.5834	58713.54300	0.42176±0.09255 (PS1)	$z=-20.59\pm 0.29$ (3.7 d)	(Z)
2019nvd	00:55:42.309	-24:41:50.28	0.7156	58713.54100	0.32070±0.20355 (PS1)	$z=-24.00\pm 0.43$ (0.6 d)	(Z)
2019nve	00:56:05.510	-24:38:26.40	0.7758	58713.54100	0.34634±0.16662 (PS1)	$z=-24.20\pm 0.43$ (0.6 d)	(Z)
2019nvr	00:48:16.088	-25:28:14.99	0.4418	58713.53899	0.15648±0.04068 (LDR8)	$z=-19.04\pm 0.25$ (3.4 d)	(Z)
2019nvs	00:52:37.759	-26:11:41.40	0.5394	58713.54899	0.40516±0.14138 (PS1)	$z=-20.36\pm 0.33$ (3.7 d)	(Z)
2019nwt	00:46:09.886	-22:57:37.49	0.7696	58710.27800	0.24584±0.00030 (s)	$z=-19.46\pm 0.22$ (0.4 d)	(Z)
2019nxd	00:42:44.598	-24:57:20.34	0.9239	58712.20300	0.26237±0.14280 (LDR8)	$z=-18.89\pm 0.23$ (2.3 d)	(Z)
2019nxe	00:46:16.814	-24:22:21.19	0.4584	58711.31199	0.07770±0.00010 (s)	$z=-20.56\pm 0.43$ (0.6 d)	(SN) Ia
2019nys	00:57:56.903	-24:34:00.56	0.9168	58711.24699	0.36814±0.08607 (PS1)	$z=-19.77\pm 0.23$ (1.4 d)	(Z)
2019nyt	00:53:00.429	-26:36:15.39	0.6998	58710.29500	0.42840±0.00000 (PS1)	$i=-22.06\pm 0.22$ (0.4 d)	(Z)
2019nyv	00:46:59.451	-23:05:59.50	0.7291	58713.25100	0.45830±0.07601 (PS1)	$z=-21.49\pm 0.30$ (3.4 d)	(Z)
2019nyw	00:48:37.038	-23:58:48.09	0.3197	58713.32800	0.49551±0.39476 (PS1)	$z=-24.91\pm 0.43$ (0.6 d)	(Z)
2019nyx	00:58:58.757	-23:56:35.06	0.9895	58713.26199	0.39586±0.35165 (PS1)	$r=-20.73\pm 0.30$ (3.4 d)	(PHOT; bright)
2019nyy	00:48:16.652	-26:38:26.97	0.8880	58713.25600	0.47304±0.08623 (LDR8)	$z=-20.96\pm 0.30$ (3.4 d)	(Z)
2019nyz	00:50:29.424	-26:14:04.06	0.5910	58713.33300	0.41460±0.00021 (s)	$i=-20.57\pm 0.30$ (3.5 d)	(Z)
2019nza	00:49:16.952	-23:15:03.22	0.7039	58713.27899	0.38622±0.03542 (PS1)	$r=-24.28\pm 0.43$ (0.6 d)	(Z)
2019nzb	01:01:06.066	-26:58:17.85	0.9672	58713.26699	0.49256±0.39074 (PS1)	$r=-20.91\pm 0.30$ (3.4 d)	(Z)
2019nzc	00:44:28.531	-21:58:45.38	0.9493	58713.27500	0.45462±0.13519 (LDR8)	$z=-23.70\pm 0.43$ (0.5 d)	(Z)
2019nzd	00:58:06.435	-24:50:14.35	0.9026	58716.19100	0.44524±0.06301 (LDR8)	$i=-19.94\pm 0.30$ (6.3 d)	(Z)
2019nze	00:58:43.637	-27:31:49.76	0.9728	58713.26699	0.44258±0.10620 (LDR8)	$z=-20.59\pm 0.30$ (3.4 d)	(Z)
2019nzf	00:38:01.308	-23:02:31.86	0.9692	58712.30600	-	$r=-16.37\pm 0.30$ (2.4 d)	(PHOT; $\Delta_z < -1.01$ mag)
2019nzg	00:51:28.250	-27:06:53.53	0.9015	58711.31600	0.21323±0.00021 (s)	$z=-21.27\pm 0.24$ (1.3 d)	(Z)
2019nzh	01:29:35.346	-32:50:26.45	0.8015	58713.28800	0.33844±0.09418 (LDR8)	$i=-19.90\pm 0.30$ (3.4 d)	(Z)
2019nzi	00:52:05.294	-26:11:03.46	0.5312	58713.25600	0.36789±0.11529 (LDR8)	$z=-20.58\pm 0.30$ (3.4 d)	(Z)
2019nzj	00:52:31.799	-25:47:35.64	0.2530	58713.33800	0.34142±0.05076 (PS1)	$i=-19.85\pm 0.30$ (3.5 d)	(Z)
2019nzk	00:48:04.598	-25:00:04.23	0.2666	58713.26000	0.10372±0.02667 (LDR8)	$z=-16.68\pm 0.30$ (3.4 d)	(Z)
2019nzm	00:57:23.849	-23:56:53.54	0.9547	58713.34300	0.21432±0.00021 (s)	$z=-19.00\pm 0.30$ (3.5 d)	(Z)
2019nzn	00:55:19.968	-24:09:33.35	0.8001	58716.19100	0.17160±0.00011 (s)	$i=-17.36\pm 0.30$ (6.3 d)	(Z)
2019nzo	00:47:21.410	-24:34:36.58	0.2894	58711.23399	0.25488±0.00024 (s)	$z=-23.37\pm 0.43$ (0.6 d)	(Z)
2019nzs	00:58:23.518	-24:33:29.53	0.9428	58711.24699	0.22500±0.00100 (s)	$z=-21.01\pm 0.25$ (1.3 d)	(Z)
2019oab	00:58:59.398	-25:46:12.66	0.8919	58711.34600	0.30585±0.09350 (LDR8)	$z=-19.46\pm 0.23$ (1.5 d)	(Z)
2019oad	01:31:56.010	-33:05:50.38	0.8749	58711.34999	0.01650±0.00030 (s)	$i=-12.86\pm 0.30$ (1.5 d)	(Z)
2019oae	00:49:16.395	-23:51:40.61	0.3957	58716.17699	0.29461±0.26818 (PS1)	$z=-23.58\pm 0.43$ (0.6 d)	(PHOT; bright)
2019oaf	00:46:48.782	-26:05:48.43	0.7516	58716.17000	0.49536±0.24849 (LDR8)	$i=-20.07\pm 0.30$ (6.3 d)	(Z)
2019oag	00:47:22.389	-25:27:54.75	0.5281	58716.17000	0.13648±0.04893 (PS1)	$i=-17.29\pm 0.30$ (6.3 d)	(Z)
2019oah	00:41:27.855	-23:23:03.92	0.9082	58713.35399	0.41845±0.05560 (LDR8)	$z=-20.28\pm 0.30$ (3.5 d)	(Z)
2019oai	00:54:02.025	-23:28:44.03	0.8688	58713.34300	0.24787±0.11938 (PS1)	$z=-21.27\pm 0.24$ (0.5 d)	(Z)
2019oaj	00:46:17.652	-26:10:39.94	0.8320	58716.18000	0.20171±0.05081 (PS1)	$i=-17.56\pm 0.30$ (6.3 d)	(Z)
2019oak	00:46:49.037	-23:22:40.82	0.6405	58713.25100	0.48219±0.04492 (LDR8)	$z=-21.07\pm 0.30$ (3.4 d)	(Z)
2019oal	00:46:22.813	-26:39:41.70	0.9468	58713.25600	0.30034±0.01839 (LDR8)	$z=-19.76\pm 0.30$ (3.4 d)	(Z)
2019oam	00:45:25.354	-25:53:42.52	0.8632	58712.27899	0.48028±0.15028 (LDR8)	$r=-21.94\pm 0.30$ (2.4 d)	(Z)
2019oan	00:51:31.134	-23:29:56.38	0.7104	58711.31199	0.19870±0.00029 (s)	$z=-22.84\pm 0.43$ (0.6 d)	(Z)
2019oao	00:57:44.079	-25:40:15.52	0.7991	58711.26699	0.31574±0.00016 (s)	$i=-20.79\pm 0.22$ (1.4 d)	(Z)
2019oap	00:58:16.023	-24:08:23.18	0.9580	58713.26199	0.21600±0.00050 (s)	$r=-18.60\pm 0.22$ (3.4 d)	(SN) Ia
2019oaq	01:36:24.905	-33:39:18.29	0.9525	58713.29199	0.35566±0.12268 (LDR8)	$r=-19.82\pm 0.30$ (3.4 d)	(Z)
2019oar	00:38:07.178	-23:03:03.14	0.9692	58712.30600	-	$z=-15.60\pm 0.30$ (2.4 d)	(PHOT; $\Delta_z < -0.26$ mag)
2019oas	01:00:11.488	-25:53:20.51	0.9552	58712.24199	0.04040±0.00030 (s)	$i=-17.23\pm 0.30$ (2.4 d)	(PHOT; $\Delta_z < -2.52$ mag)
2019oat	01:32:47.844	-31:27:58.23	0.9086	58711.37500	0.07050±0.00030 (s)	$i=-16.58\pm 0.30$ (1.5 d)	(Z)
2019oau	01:34:47.473	-31:37:09.96	0.9443	58711.35100	0.06800±0.00041 (s)	$z=-18.17\pm 0.24$ (1.4 d)	(Z)
2019oav	01:37:05.812	-32:13:48.07	0.9522	58712.27399	0.11060±0.00030 (s)	$i=-17.91\pm 0.30$ (2.4 d)	(Z)
2019oaw	00:46:01.689	-25:27:32.94	0.6629	58712.20300	0.05513±0.00017 (s)	$i=-15.48\pm 0.22$ (2.3 d)	(PHOT; $\Delta_z < -0.03$ mag)
2019oax	00:47:28.032	-25:26:14.68	0.4990	58711.31600	0.15731±0.00219 (PS1)	$z=-17.64\pm 0.23$ (1.4 d)	(Z)
2019oay	00:55:19.237	-26:11:50.77	0.6670	58716.54199	0.11853±0.00005 (s)	$z=-18.87\pm 0.24$ (3.4 d)	(Z)

Table 5 continued

Table 5 (continued)

Name	α (J2000)	δ (J2000)	Cumulative LVC Prob. ^a	Discovery Date (MJD)	Redshift ^b	Absolute Magnitude ^c (AB mag)	Note ^d
2019okr	00:47:23.696	-25:27:30.78	0.5281	58712.21300	0.13648±0.04893 (PS1)	$i=-16.42\pm0.23$ (2.3 d)	(Z)
2019omt	00:59:26.742	-25:59:41.28	0.9340	58713.26800	0.26082±0.08430 (PS1)	$z=-18.28\pm0.23$ (3.4 d)	(Z)
2019omu	01:33:58.890	-34:20:20.01	0.9827	58711.27600	0.01269±0.00015 (2MPZ)	$i=-12.46\pm0.22$ (1.4 d)	(Z)
2019omv	01:39:54.812	-33:23:01.39	0.9559	58711.27699	0.45430±0.08074 (LDR8)	$z=-20.10\pm0.23$ (1.4 d)	(Z)
2019omw	00:48:56.255	-23:10:12.49	0.7187	58713.25100	0.04690±0.00017 (s)	$i=-14.07\pm0.23$ (3.4 d)	(PHOT; $\Delta_z=0.01\pm0.06$ mag)
2019omx	01:36:44.246	-33:18:09.64	0.9377	58711.30100	0.21420±0.07773 (LDR8)	$i=-17.68\pm0.23$ (1.4 d)	(Z)
2019oni	00:45:26.226	-24:10:01.20	0.5676	58712.20500	–	$z=-19.71\pm0.43$ (0.6 d)	(PHOT; bright)
2019onj	00:47:26.006	-25:26:55.13	0.5281	58712.20500	0.06647±0.00011 (s)	$z=-15.73\pm0.23$ (2.3 d)	(PHOT; $\Delta_z < 0.02$ mag)
2019opp	00:57:38.254	-25:16:45.00	0.7884	58712.24199	0.38828±0.15777 (PS1)	$z=-19.22\pm0.30$ (2.4 d)	(Z)
2019ore	00:55:45.505	-26:20:06.35	0.7254	58719.57300	0.11725±0.00019 (s)	$r=-19.94\pm0.24$ (3.4 d)	(Z)
2019osy	00:55:47.000	-27:04:33.00	0.8850	58718.57291	0.07380±0.00030 (s)	–	(Z)
2019paa	00:55:13.778	-24:07:08.44	0.8001	58716.19100	0.33287±0.15298 (PS1)	$r=-19.00\pm0.30$ (6.3 d)	(Z)
2019pag	00:44:53.217	-24:17:17.52	0.6504	58716.17499	0.20828±0.02082 (PS1)	$r=-22.91\pm0.43$ (0.6 d)	(Z)
2019paw	00:48:34.270	-25:05:25.81	0.2425	58716.25000	0.31681±0.11891 (PS1)	$i=-18.95\pm0.30$ (6.4 d)	(Z)
2019pax	01:02:02.994	-25:28:58.33	0.9852	58716.34699	–	$i=-14.96\pm0.30$ (6.5 d)	(PHOT; $\Delta_i < 0.01$ mag)
2019pay	00:48:40.759	-25:14:54.40	0.3112	58716.17000	0.36073±0.01926 (PS1)	$i=-19.10\pm0.30$ (6.3 d)	(Z)
2019paz	00:46:24.035	-22:05:43.25	0.9483	58716.20699	0.25885±0.07726 (LDR8)	$r=-22.29\pm0.43$ (0.6 d)	(Z)
2019pbb	00:52:37.634	-26:07:47.60	0.4879	58716.18600	0.46159±0.10016 (PS1)	$i=-19.83\pm0.30$ (6.3 d)	(Z)
2019pbc	00:51:37.416	-26:26:04.28	0.6341	58716.30899	0.29718±0.19215 (LDR8)	$i=-19.05\pm0.30$ (6.4 d)	(Z)
2019pbv	00:59:59.211	-25:49:27.35	0.9545	58716.28199	0.16838±0.07629 (PS1)	$i=-17.86\pm0.30$ (6.4 d)	(Z)
2019pbw	00:46:43.393	-25:24:02.01	0.5628	58713.24699	0.14820±0.02326 (PS1)	$i=-17.90\pm0.30$ (3.4 d)	(Z)
2019pcf	01:33:11.048	-33:24:49.27	0.9021	58716.28800	0.34614±0.09647 (LDR8)	$i=-19.19\pm0.30$ (6.4 d)	(Z)
2019pck	00:47:24.344	-25:13:33.80	0.4540	58713.32399	0.20887±0.10457 (PS1)	$z=-19.16\pm0.30$ (3.4 d)	(Z)
2019pcm	00:49:17.545	-22:01:06.09	0.9850	58716.21199	0.40167±0.12097 (PS1)	$r=-23.61\pm0.43$ (0.6 d)	(Z)
2019pfn	00:57:23.242	-25:15:38.50	0.7884	58713.28300	0.17875±0.07322 (PS1)	$r=-20.04\pm0.24$ (3.3 d)	(Z)
2019qbu	00:51:09.173	-22:17:40.69	0.9824	58715.15808	0.40611±0.12653 (LDR8)	$r=-22.44\pm0.43$ (0.6 d)	(Z)
2019qby	00:44:14.334	-25:07:44.32	0.8267	58711.27500	0.02271±0.00015 (2MPZ)	$r=-13.74\pm0.22$ (1.4 d)	(Z)
2019qbz	00:56:53.980	-27:59:21.37	0.9840	58711.29899	–	$r=-15.98\pm0.23$ (1.4 d)	(PHOT; $\Delta_r=0.04\pm0.05$ mag ^e)
2019qca	00:45:48.540	-26:49:39.01	0.9828	58717.16800	0.37932±0.07406 (LDR8)	$r=-19.81\pm0.25$ (7.3 d)	(Z)
2019qcb	00:46:19.062	-26:08:43.19	0.8320	58711.23000	0.23079±0.07951 (PS1)	$r=-18.81\pm0.23$ (1.3 d)	(Z)
2019qcc	00:53:49.820	-24:45:49.58	0.4113	58715.17800	0.46644±0.14625 (PS1)	$r=-24.96\pm0.43$ (0.6 d)	(Z)
2019thm	00:47:56.625	-26:54:02.80	0.9544	58710.29199	0.42976±0.13566 (PS1)	–	(Z)
2019tig	00:58:04.296	-26:04:58.71	0.7952	58716.21800	0.17492±0.12570 (PS1)	$r=-17.77\pm0.30$ (6.3 d)	(PHOT; bright)
2019tii	00:49:35.203	-27:02:09.33	0.9479	58716.24500	0.08666±0.04046 (PS1)	$i=-16.16\pm0.30$ (6.4 d)	(PHOT; $\Delta_i < -0.01$ mag)
2019tix	00:48:45.678	-24:38:50.59	0.1972	58716.17490	0.35875±0.23938 (PS1)	$z=-18.59\pm0.25$ (6.3 d)	(Z)
2019ufp	00:45:45.479	-24:40:06.83	0.5615	58716.53699	0.47474±0.05693 (LDR8)	$z=-24.94\pm0.43$ (0.6 d)	(Z)
2019zza	00:46:10.914	-25:35:18.12	0.6871	58716.57100	–	$i=-14.93\pm0.29$ (6.7 d)	(PHOT; $\Delta_r=-0.19\pm0.22$ mag)
2019zzb	00:55:06.381	-26:12:49.74	0.6400	58716.57699	0.13631±0.04225 (PS1)	$r=-20.40\pm0.23$ (0.4 d)	(Z)
2019zzc	00:55:16.380	-25:59:45.90	0.5861	58716.57300	0.13344±0.06499 (PS1)	$r=-18.96\pm0.23$ (5.4 d)	(Z)
2019zzd	00:50:08.848	-25:57:43.92	0.4764	58716.57300	0.20432±0.17289 (LDR8)	$i=-18.64\pm0.24$ (6.7 d)	(PHOT; bright)
2019aaah	00:45:31.718	-24:43:47.11	0.5821	58712.20300	0.11332±0.02029 (LDR8)	$r=-21.44\pm0.43$ (0.6 d)	(Z)
2019aabz	00:54:31.457	-24:17:10.53	0.6906	58713.28300	0.11246±0.04555 (PS1)	$r=-21.48\pm0.43$ (0.6 d)	(Z)
2019aacd	00:54:11.280	-24:56:17.66	0.4162	58713.52735	0.22609±0.06227 (PS1)	$r=-23.14\pm0.43$ (0.6 d)	(Z)
2019aakm	00:43:07.938	-23:29:58.77	0.7972	58716.34964	0.13135±0.13129 (PS1)	$r=-18.15\pm0.29$ (6.5 d)	(PHOT; bright)
2019aakn	00:46:43.351	-23:22:19.58	0.6405	58720.33419	0.48253±0.33798 (LDR8)	$r=-21.17\pm0.26$ (10.5 d)	(Z)
2019aako	00:51:45.074	-27:14:46.06	0.9464	58719.30922	–	$r=-15.80\pm0.25$ (9.4 d)	(PHOT; $\Delta_r=-0.04\pm0.05$ mag)
2019aakp	00:48:03.306	-21:46:06.51	0.9786	58718.20368	–	$r=-16.50\pm0.24$ (8.3 d)	(PHOT; $\Delta_r=0.01\pm0.05$ mag)
2019aakq	01:33:39.426	-31:10:57.06	0.9671	58720.38197	–	$r=-16.22\pm0.24$ (10.5 d)	(PHOT; $\Delta_r=-0.04\pm0.04$ mag)
2019aakr	00:51:39.446	-26:11:54.41	0.5230	58711.49086	0.39331±0.12816 (PS1)	$r=-23.14\pm0.30$ (1.6 d)	(Z)
2019aaks	00:48:11.960	-24:43:45.82	0.1977	58723.43052	–	$r=-17.38\pm0.27$ (13.5 d)	(PHOT; bright)

Table 5 continued

Table 5 (continued)

Name	α	δ	Cumulative LVC Prob. ^a	Discovery Date	Redshift ^b	Absolute Magnitude ^c	Note ^d
	(J2000)	(J2000)		(MJD)		(AB mag)	

^a Cumulative probability within the GW190814_sky map provided by Abbott et al. (2020a).

^b Redshifts are identified as spectroscopic (s) or photometric (by source) as described in Section 3.

^c We indicate absolute magnitude at the earliest detection epoch (given in parentheses in observer-frame days relative to the GW190814 merger).

^d We rule out each source based on classification as likely minor planets (MP), supernovae (SN), pre-merger variability (VAR), a redshift inconsistent with the GW190814 volume (Z), or photometric evolution (PHOT) as described in Section 3. For minor planets we give the identified minor planet, and for supernovae we give the type described in Section 3.2.

^e The photometry used to rule out 2019qzb is presented in Ackley et al. (2020). 2019qzb has a relatively flat light curve across ≈ 6 days of follow up as shown in Figure 5.

Table 6. Photometry of Candidate Electromagnetic Counterparts to GW190814

Name	MJD	Filter	m	σ_m	Source
		(mag)	(mag)		
2019noq	58713.2883	<i>r</i>	20.12	0.10	Swope
2019noq	58714.2699	<i>r</i>	20.39	0.10	Swope
2019noq	58715.2022	<i>r</i>	20.44	0.09	Swope
2019noq	58716.3051	<i>r</i>	20.46	0.06	Swope
2019noq	58720.3270	<i>r</i>	20.42	0.04	Swope
2019noq	58725.2115	<i>r</i>	20.42	0.04	Swope
2019noq	58737.3559	<i>r</i>	20.57	0.08	Swope
2019npd	58723.4640	<i>r</i>	19.67	0.11	Thacher
2019npd	58734.1757	<i>r</i>	19.76	0.03	Swope
2019npe	58713.2936	<i>r</i>	19.10	0.05	Swope
2019npe	58714.2747	<i>r</i>	19.17	0.06	Swope
2019npe	58715.1228	<i>r</i>	19.34	0.05	Swope
2019nph	58713.1804	<i>r</i>	20.01	0.10	Swope
2019npp	58718.2653	<i>r</i>	20.62	0.07	Swope
2019npp	58734.2729	<i>r</i>	20.91	0.05	Swope
2019npw	58716.3444	<i>r</i>	21.01	0.10	Swope
2019npy	58726.3109	<i>r</i>	21.26	0.06	Swope
2019nqq	58718.2688	<i>r</i>	20.81	0.07	Swope
2019nqq	58719.3726	<i>r</i>	21.01	0.14	Swope
2019nqt	58716.3607	<i>r</i>	20.26	0.06	Swope
2019nqy	58716.3555	<i>r</i>	21.25	0.12	Swope
2019nra	58712.1556	<i>r</i>	19.54	0.10	Swope
2019nra	58713.1781	<i>r</i>	19.60	0.07	Swope
2019nra	58715.2524	<i>r</i>	19.87	0.07	Swope
2019nra	58720.3748	<i>r</i>	19.80	0.16	Swope
2019nre	58713.1898	<i>r</i>	19.94	0.08	Swope
2019nre	58716.2295	<i>r</i>	20.18	0.06	Swope
2019nre	58718.2856	<i>r</i>	20.15	0.04	Swope
2019nrf	58716.3271	<i>r</i>	20.22	0.06	Swope
2019nrf	58718.3524	<i>r</i>	20.32	0.05	Swope
2019nrf	58726.2689	<i>r</i>	20.38	0.02	Swope
2019nri	58712.1620	<i>r</i>	19.19	0.08	Swope
2019nrp	58712.3401	<i>r</i>	19.29	0.06	Swope
2019nrp	58713.3356	<i>r</i>	19.28	0.05	Swope
2019nrp	58714.3396	<i>r</i>	19.31	0.09	Swope
2019nrp	58715.4032	<i>r</i>	19.34	0.06	Swope

Table 6 continued**Table 6** (continued)

Name	MJD	Filter	m	σ_m	Source
			(mag)	(mag)	
2019nrs	58734.3562	<i>r</i>	21.11	0.07	Swope
2019nrw	58715.2450	<i>r</i>	20.42	0.11	Swope
2019nrw	58716.1418	<i>r</i>	20.40	0.06	Swope
2019nrw	58718.2037	<i>r</i>	20.33	0.05	Swope
2019nrx	58715.2548	<i>r</i>	20.28	0.07	Swope
2019nrx	58716.3387	<i>r</i>	20.26	0.06	Swope
2019nrx	58720.3771	<i>r</i>	20.53	0.06	Swope
2019nrx	58726.3549	<i>r</i>	20.59	0.04	Swope
2019ntm	58710.4672	<i>r</i>	17.42	0.36	Thacher
2019ntm	58718.1860	<i>r</i>	20.48	0.05	Swope
2019ntm	58719.3415	<i>r</i>	20.68	0.06	Swope
2019ntm	58720.3422	<i>r</i>	20.62	0.06	Swope
2019ntn	58720.3820	<i>r</i>	20.79	0.07	Swope
2019nuj	58710.4672	<i>r</i>	17.42	0.36	Thacher
2019nuj	58720.3443	<i>r</i>	20.92	0.07	Swope
2019nux	58726.2652	<i>r</i>	21.61	0.07	Swope
2019nva	58719.3280	<i>r</i>	21.03	0.08	Swope
2019nva	58726.3072	<i>r</i>	21.11	0.05	Swope
2019nvd	58716.3555	<i>r</i>	21.08	0.11	Swope
2019nve	58716.3555	<i>r</i>	20.60	0.07	Swope
2019nve	58718.2231	<i>r</i>	20.61	0.06	Swope
2019nve	58719.3213	<i>r</i>	20.64	0.05	Swope
2019nve	58720.3541	<i>r</i>	20.79	0.06	Swope
2019nve	58726.3191	<i>r</i>	20.81	0.04	Swope
2019nyx	58718.2593	<i>r</i>	20.86	0.09	Swope
2019nze	58726.2919	<i>r</i>	21.68	0.07	Swope
2019nzf	58718.1233	<i>r</i>	20.89	0.08	Swope
2019oab	58734.2408	<i>r</i>	21.11	0.09	Swope
2019oav	58719.3394	<i>r</i>	21.05	0.07	Swope
2019oav	58734.2037	<i>r</i>	21.20	0.10	Swope
2019oay	58725.1983	<i>r</i>	21.25	0.09	Swope
2019zza	58710.2946	<i>r</i>	20.28	0.21	Swope
2019zza	58719.3543	<i>r</i>	21.52	0.10	Swope
2019aakm	58716.3496	<i>r</i>	20.92	0.18	Swope
2019aakn	58720.3342	<i>r</i>	21.10	0.14	Swope
2019aako	58719.3092	<i>r</i>	21.14	0.12	Swope
2019aakp	58718.2037	<i>r</i>	20.65	0.08	Swope
2019aakq	58720.3820	<i>r</i>	20.74	0.09	Swope
2019aakr	58711.4909	<i>r</i>	18.60	0.20	Thacher
2019aaks	58723.4305	<i>r</i>	19.62	0.16	Thacher

Table 6 continued

Table 6 (*continued*)

Name	MJD	Filter	m	σ_m	Source
			(mag)	(mag)	

NOTE—All photometry of candidate counterparts (Table 5) to GW190814 from follow up and search observations presented in this paper. We use these data along with photometry presented in [Andreoni et al. \(2020\)](#), [Ackley et al. \(2020\)](#), and [Morgan et al. \(2020\)](#) to classify all candidates.